Fabrication and Characterization of Polyimide-based Mixed Matrix Membranes for Gas Separations

By

Todd W. Pechar

Dissertation submitted to the Faculty of the Virginia Polytechnic and State University in partial fulfillment of the requirements for the degree of

Doctor of Philosophy

in

Chemical Engineering

Approved by:

_____

Dr. Eva Marand, Chair

_____ _____

Dr. Richey Davis Dr. William Ducker

_____ _____

Dr. S. Ted Oyama Dr. Judy Riffle

July 14, 2004

Blacksburg, VA

Keywords: polyimide, mixed matrix membrane, permeability, carbon nanotubes, poly(imide siloxane)

Fabrication and Characterization of Polyimide-based Mixed Matrix Membranes for Gas Separations

Todd W. Pechar

(Abstract)

A series of mixed matrix membranes based on zeolites incorporated into fluorinated polyimides were fabricated and characterized in this study. The first system consisted of a polyimide (6FDA-6FpDA-DABA) with carboxylic acid groups incorporated into its backbone and amine-functionalized zeolite particles (ZSM-2). FTIR indicated that these functional groups interacted with each other through hydrogen bonding. Both SEM and TEM images revealed good contact between the polyimide and the zeolite. Permeability studies showed a drop in He permeability suggesting there were no voids between the two components. While simple gases such as O_2 and N_2 followed effective permeabilities predicted by mixing theories, polar gases such as CO_2 did not.

The second system fabricated used the same polyimide with amine-functionalized zeolite L. This zeolite differs from ZSM-2 in that zeolite L's pores are not clogged with an organic template, and it possesses 1-D pores as opposed to ZSM-2's 3-D pore structure. XPS and zeta potential experiments were performed to verify the presence of amine groups on the zeolite surfaces. FTIR data showed that after a heat treatment, amide linkages were created between the amine group on the zeolite and the carboxylic acid group of the polyimide. SEM images showed a good distribution of zeolite L throughout the polymer matrix, and no indication of voids between the two components. Permeability experiments were performed to determine if the addition of zeolite L to the polyimide improved its separation performance. He permeability was unchanged between the pure polyimide membrane and the mixed matrix membrane, suggesting there were no voids present within the matrix. Permeability results of larger gases followed a Maxwell Model.

A third system was prepared using a poly(imide siloxane) (6FDA-6FpDA-PDMS) and untreated zeolite L. The primary focus of this investigation was to determine if the addition of the flexible segment would promote direct contact with the zeolite surface and remove the need to amine-functionalize the zeolite. Poly(imide siloxane)s were synthesized at 0, 22, and 41 wt % PDMS as verified using ^{1}H-NMR. FTIR was employed to qualitatively verify the successful imidization of the polymers. SAXS patterns and TEM images did not reveal distinct phases indicative of phase separation, however, AFM images did show the presence of phase separation of the surfaces of the poly(imide siloxane)s. Permeability results showed a decrease in selectivity and an increase in permeability as the wt % of PDMS was increased. Permeabilities and selectivities dropped as the zeolite loading was increased from 0 to 20 wt %. Upon increasing the zeolite loading from 20 to 30 wt %, increases in permeability were observed, but both the permeability and selectivity were still below that of the pure polymer.

The final system studied employed the 41 wt % PDMS poly(imide siloxane) as the polymer matrix and either closed-ended or open-ended carbon nanotubes as the filler. SEM images showed regions of agglomeration for both types of nanotubes. Helium permeability dropped in both types MMMs, but more so in closed-ended carbon nanotubes MMM. Nitrogen permeability was unchanged for the closed-ended carbon nanotubes MMM, and dropped slightly in the open-ended carbon-nanotube MMM.

Acknowledgments

The work I have accomplished in close to five years at Virginia Tech would not have been possible without the help and generosity of many individuals.

I would like to extend my greatest thanks and gratitude to my adviser Eva Marand for her guidance and patience in my endeavor. I also am deeply grateful for the advice and guidance from my committee members Rick Davis, William Ducker, Ted Oyama, and Judy Riffle.

I would like to thank Steve McCartney (microscopy), Tom Glass (NMR), Frank Cromer (XPS), and Dr. Shobha (GPC) for their efforts in training me and characterizing some of my materials.

I wish to offer my sincere gratitude to Dr. Michael Tsapatsis, Dr. Vladimiros Nikolakis, Dr. Ravishankar Raman, and Dr. Hae-Kwon Jeong for providing the zeolites used in this study, as well as their helpful input concerning the results of this study.

My current and former lab mates were always helpful and supportive during my stay at Virginia Tech. I would like to thank Chris Cornelius and Christelle Laot for the training and support they gave me during my first summer here. I thank Will James and Ben Vaughan for being supportive lab mates and good friends. I would especially like to thank Chris Hibshman not only for the training and support he provided for me while he was here, but for being an outstanding friend while he was here, and now that he has left.

I would like to thank the following graduate students for their help in various aspects of my research: Ann Fornof, Vince Baranauskas, Paolo Scardina, Jignesh Sheth, Pankaj Gupta, and Derek Klinedinst.

I would like to extend my appreciation to all of my friends who were supportive and cheerful towards me even when I didn't return it. I especially would like to thank Lon Weber, Jean Miller and Mike Fisher, Sandra Case, Earl Kline, Jon Gotow and Eric Scribben for the fun and stress-relief they provided when I mountain biked with them. I am thankful for the support and friendships I was offered by Jean Huie, Jignesh Sheth, Tregei Starr, Wade DePolo, Phillip Doerpinghaus, and Ashish Aneja. I would also like to

thank Elliot Wolf and Jamie Gramz whose discussions of attending graduate school encouraged me to consider it.

My parents receive my warmest thanks and love for their unending support, help and guidance in each endeavor I pursue. I also am deeply grateful to my brother Justin, and both of my grandmothers for their love and support.

Finally, there are many people I have never met that I owe more thanks and gratitude than anyone else. I could only pursue my interests in chemical engineering, because I was fortunate enough to be born in a prosperous stable country that respects and values freedom. I am not responsible for these conditions; other people are. There are individuals who unselfishly died at Normandy, or at Saratoga, or some other place and never benefited from their sacrifices like I have. There are individuals who spent their entire life working excessive hours under deplorable conditions and never benefited from the large and robust economy in this country as well as the high standard of living they helped create. To you and the others that have allowed me the opportunity to devote my life to research rather than survival, I am more grateful than I know how to express in words.

List of Abbreviations

Abbreviation	Name
6FDA	2,2'-Bis(3,4-dicarboxyphenyl)hexafluoroporpane dianhydride
6FpDA	4, 4' – hexaflouroisopropylidene dianiline
APTES	3-aminopropyltriethoxysilane
BTDA	3,3',4,4'-benzophenone tetracarboxylic dianhydride
CNT	carbon nanotube
D	diffusion coefficient
DABA	3,5-diaminobenzoic acid
DMAC	dimethylacetamide
DMTA	dynamic mechanical thermal analysis
DSC	differential Scanning Calorimetry
DSDA	diphenylsulfonetetracarboxylic dianhydride
FESEM	field emission scanning electron microscope
FFV	fractional free volume
FTIR	fourier transform infrared spectroscopy
IPDA	isopropylidenedianiline
MDA	methylenedianiline
MMM	mixed matrix membrane
M_n	number average molecular weight
mPD	m-phenylene diaminel
MPDA	meta-phenylene diamine
M_w	weight average molecular weight
MWNT	multiwalled carbon nanotube
NMP	N-methylpyrrolidinone
ODA	4,4'-oxydianiline
P_2O_5	phosphorus pentoxide
PDMS	polydimethylsiloxane
PFDNB	2-(perfluorohexyl)ethyl-3,5-dinitrobenzoate
PMDA	pryomellitic dianhydride
S	solubility cofficient
SWNT	singlewalled carbon nanotube
tan δ	loss tangent
TEM	transmission electron microscopy
THF	tetrahydrofuran
WAXS	wide angle x-ray scattering
XPS	x-ray photoelectron spectroscopy
T_C	critical temperature

Table of Contents

List of Figures

Chapter 1

Chapter 2

Chapter 3

Chapter 4

Chapter 5

Chapter 6

List of Tables

Chapter 1

Chapter 2

Chapter 3

Chapter 4

Chapter 5

Chapter 6

Chapter 1 Introduction

1.1 Motivations for Research

The existence of the gas industry revolves around the ability to produce gases without impurities in a cost efficient manner. Due to the current limits of chemistry and chemical reaction technology, the desired product is often in a mixture of several byproducts, which must be removed in order for the product to have any chance of profitability in the market. As the cost of traditional methods of separation, such as cryogenic distillation and pressure-swing absorption, become increasingly expensive due to rising energy costs, and environmental regulations become more stringent, traditional separation methods will become economically unacceptable. Alternative separation methods, such as membranes can offer better and more modern approaches to separate chemical species.

Since the first commercial plant was put into operation in 1979, membranes have made large strides in increasing their share of performing gas separations.[1] As of 2002 membrane based gas separations have grown to a $150 million/year industry and prognosticators have anticipated the market to reach $760 million/year by 2020.[2] Some current gas separation applications of membranes are listed in Table 1-1.[1]

Table 1-1. Applications of gas permeation membranes adapted from reference 1.

Recovered Gas	Application
H_2	Removal from petrochemical (H_2, N_2, CH_4, CO) and refinery purge streams (H_2, C_nH_m)
	Removal during methanol synthesis
CO_2	Removal from natural gas and landfills
	Elimination from fuel cells,
H_2S	Removal from hydrocarbon gases
	Sour gas treatment
N_2	Removal from air for applications in food preservation and inert blanketing
O_2	Removal from air for combustion, medical gases, and oxidative applications
He	Removal from hydrocarbon gases
Hydrocarbons	Removal from air for pollution control

Membranes can offer several advantages over traditional unit operations employed for the purpose of separating gaseous mixtures. Examples of these advantages for separating H_2 from a refinery gas stream are listed in Table 1-2.[1] The initial investment cost for installing a membrane separation system is less than half of that for cryogenic distillation and pressure swing adsorption. The operating cost of using a membrane based separation system is competitive to that of the others, and the purity of the recovered H_2 is competitive with the two other technologies.

Table 1-2. Comparison of the separations for hydrogen recovery from a refinery gas stream. The data was taken from reference 1.

	Membrane	Adsorption	Cryogenic
Hydrogen Recovered (%)	91	73	90
Hydrogen Purity (%)	96	98	96
Hydrogen Gas Flow Rate (MMscfd)	2.86	2.24	2.86
Investment ($ Millions)	0.91	2.03	2.66
Instillation Area (ft^2)	52	651	1292

Despite strong performances for some H_2 separations, membranes are often not the first choice of industry for other gas separations. Currently, despite hundreds of polymers that have been developed and targeted for gas separations, 90% of the total gas separated using a membrane was separated from one of nine polymers.[2] This can be attributed to the inability of many membranes to offer the permeability and the selectivity under industrial conditions. Research efforts focusing on altering the chemical structure of the polymers used to compose these membranes have offered little improvement, and are now reaching the point of diminishing returns.

This limit of polymeric membrane performance was best presented in 1991 by Lloyd Robeson in his trade-off curve, which showed an upper bound for several common gas separations.[3] Robeson gathered all available permeation data for membranes at the time, and plotted each membrane's permeability of a gas against its selectivity for that gas. The plot revealed that there is an upper bound that membranes have difficulty operating above. Since then, very few attempts at developing membranes which operate above this upper bound have been successful. Unfortunately, the area above the upper bound is where the membranes need to perform in order to become more commercially

attractive. In Figure 1-1 the trade off of permeability of O_2 against O_2 / N_2 selectivity is shown for the air separation.

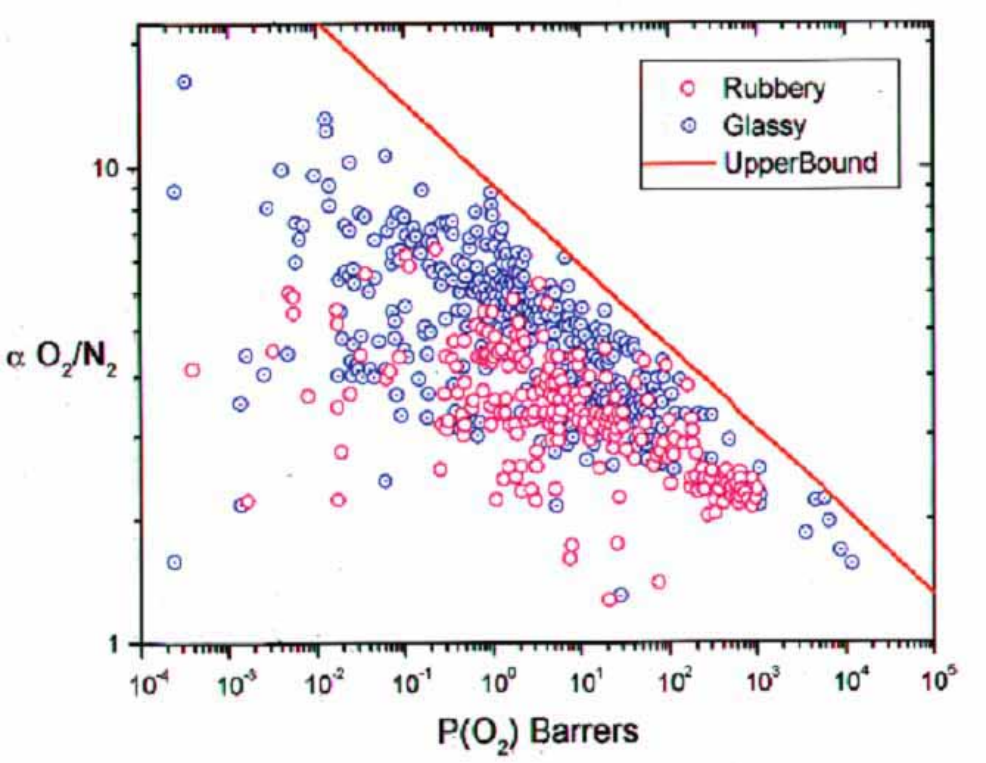

Figure 1-1. Trade off curve between permeability and selectivity for polymeric membranes.

Recent work by Freeman resulted in a theory which explains the upper bound displayed by polymeric materials.[4] In his work, he was able to show that the slope of the trade-off curves is dictated by the penetrant size ratios, and is not influenced by the polymer structure. Freeman also goes on to suggest that there is an asymptotic end point in the performance of purely polymeric membranes. His work is reviewed more thourougly in the Literature Review section.

To further impede the incorporation of membranes into wider use, polymeric membranes often can not tolerate the operating conditions present in industrial feed streams. Membranes often operate with reduced selectivity at higher temperatures, and may fracture at high pressures. Even more detrimental to their inclusion is their inability

to be chemically resistant to plasticizing feeds. Feeds rich in CO_2 or highly soluble organic vapors can often plasticize the polymer, increasing it segmental mobility and reducing its selectivity.[5,6] This hinders the ability of the membrane to discriminate by size among the feed components and leads to a poorer quality separation. Until these limitations can be overcome, purely polymeric membranes will continue to be limited to niche gas separation applications.

Zeolites are the inorganic counterpart to polymeric membranes, and they outperform polymeric membranes in many areas. Unlike polymeric membranes, these crystalline aluminosilicates possess a rigid repeatable pattern of uniformly sized pores.[7] These pores may separate different species based on factors such as size, shape, polarity, or degree of unsaturation. For example, zeolites can efficiently separate species which are very similar, for instance, benzene and cyclohexane.[8] Furthermore, these inorganic membranes can tolerate high temperature and high pressure environments, as well as operate effectively in chemically aggressive streams.[9]

While defect-free zeolite membranes offer these impressive properties, fabricating them without defects can be difficult. Often, cracks and pinholes within the membrane which are larger than the size of the pores will reduce the selectivity of the membrane. This often leads to zeolite membranes having lower production cost efficiency than polymeric membranes, and thus eliminating their usefulness.[10]

Recent efforts focused on developing the next generation of membranes have concentrated on combining polymer and zeolite into mixed matrix membranes. Mixed matrix membranes (MMMs) offer the potential to combine the processability and low cost of the polymer with the high selectivity and both chemical and thermal resistance of the zeolite. This could lead to a high performance membrane and thus more efficient gas separations.

MMMs already have been successfully fabricated using rubbery polymers and zeolites.[11-14] Some of these membranes resulted in improvements for targeted separations, as will be extensively discussed in the Literature Review section. MMMs incorporating glassy polymers and zeolites have only recently been investigated[15-18], and much of the work has involved simulations as opposed to actual experimental data.[19,20]

Koros et al., recently conducted a simulation study for one such MMM. Their study looked at a composite membrane of Ultem and zeolite 4A. The simulation looked at the separation performance of the membrane at different volume percents of zeolite. Their results predicted that these membranes would operate above the upper bound at certain zeolite loadings. Their predicted results are shown in Figure 1-2 which was adapted from Mahajan et al.[12]

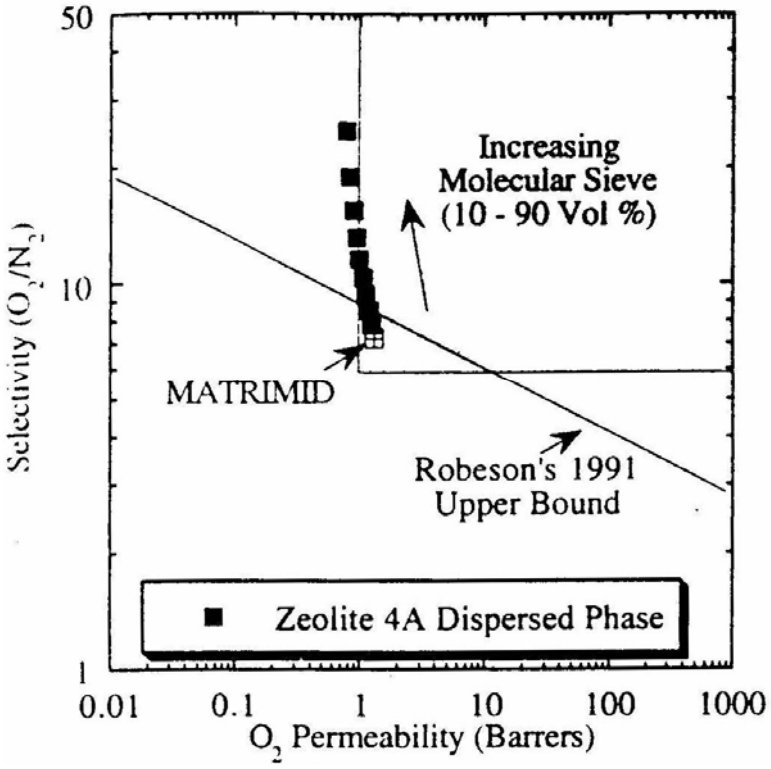

Figure 1-2. Predicted zeolite 4A-Matrimid mixed matrix membrane performance as a function of zeolite loading for the O_2 / N_2 separation. The upper right boxed-in area is the commercially attractive region.

Along the lines of polymer-zeolite mixed matrix membranes, different fillers could be used to develop better performing membranes. Carbon nanotubes (CNT's) are one such filler.[21,22] These graphite tubes with diameters on the order of a few nanometers would not likely offer any improvement in selectivity. However, theoretical simulations of CNT's have predicted their diffusion coefficients to be on the order of 1 x 10^{-1} cm^2/s,

whereas polymers typically have diffusion coefficients on the order of 1 x 10^{-9} cm^2/s.[23] Using this type of filler in a MMM could increase the permeability to the point that it breaks the upper bound. Additionally, the addition of CNT's to polymers have led to improved mechanical properties.[24-26]

The addition of inorganic fillers such as MMMs and CNT's into polymers appears to offer outstanding potential to improve the gas separation abilities of membranes. This is the primary motiviation of this investigation. In this work we look at adding zeolites to polyimides and to polyimide based copolymers for the purpose of improving their separation efficiency. Additionally, we study the incorporation of CNT's into a polyimide copolymer matrix to determine the feasibility of producing a MMM which operates above the upper bound.

1.2 Research Studies

The research studies in this investigation are briefly described below.

1. Properties of a polyimide-ZSM-2 mixed matrix membrane – The fabrication and characterization of a 6FDA-6FpDA-DABA polyimide and amine-functionalized ZSM-2 zeolite MMM is studied. The goals of this investigation are to determine if defect free MMMs can be fabricated using these two components, what interactions are present between the two components, and to determine the permeation properties of the MMM.

2. Properties of a polyimide-zeolite L mixed matrix membrane - The fabrication and characterization of a 6FDA-6FpDA-DABA polyimide and amine-functionalized zeolite L MMM is studied. The goals of this investigation are to determine if the zeolite L was functionalized with amine groups, to determine if defect free MMMs can be fabricated using these two components, to determine what interactions are present between the two components, and to determine the permeation properties of the MMM and how they change at different feed pressures.

3. Properties of polyimide-*b*-polydimethylsiloxane-Zeolite L mixed matrix membranes - The fabrication and characterization of a random block copolymer of 6FDA-6FpDA and polydimethylsiloxane (PDMS) is studied. This investigation looks at developing MMMs without the need to amine-functionalize the zeolite. The permeation properties of the MMMs as the mol % of PDMS changes in the copolymer is studied.

4. Fabrication and permeation properties of a polyimide-*b*-polydimethylsiloxane-CNT mixed matrix membrane – The fabrication and permeation properties of a poly(imide siloxane) copolymer and single walled carbon nanotubes is investigated. The purpose of this investigation is to determine the feasibility of fabricating MMMs using these two components and characterize their permeabilities to various gases.

1.3 Outline of Chapters

Chapter 2 is devoted to an extensive literature review for membranes designed for gas separations. The first part of the literature review focuses on the fundamental equations and parameters governing and describing the performance of membranes. The second section is a recount of the historical development of polymeric membranes. A subsection of this part reviews literature studying copolymeric membranes. A separate section provides background on the development of zeolites and their properties. The section on mixed matrix membranes is divided into two sections: one for rubbery MMMs, and one for glassy MMMs. Finally, a brief section on carbon nanotubes and their properties is included. Within this section polymer-CNT composites and polymer-CNT MMMs are reviewed.

Chapter 3 is devoted to the investigation of a mixed matrix membrane composed of 6FDA-6FpDA-DABA and amine-functionalized ZSM-2. In this investigation we describe a fabrication procedure for developing pinhole free MMMs. SEM and TEM were used to study the surface, cross-section, and bulk of the membranes, and FTIR was employed to determine if any secondary forces existed between the two components.

Additionally, permeabilities for He, O_2, N_2, CH_4, and CO_2 were determined for both the pure polyimide and the MMM.

Chapter 4 recounts the study of a mixed matrix membrane composed of 6FDA-6FpDA-DABA and amine-functionalized zeolite L. Zeolite L differs from ZSM-2 in that it is not synthesized with the aide of an organic template. Therefore, it's pores are not clogged with the template, as is the case for most of the pores in a ZSM-2 crystal. In this investigation we describe a new fabrication procedure for developing pinhole free MMMs. Zeta potential and XPS were used to characterize the zeolite. SEM was used to study the surface and cross-section of the membranes, and FTIR was employed to determine if any secondary forces existed between the two components. Additionally, permeabilities for He, O_2, N_2, CH_4, and CO_2 were determined for both the pure polyimide and the MMM. Finally, a study of the effects of varying feed pressure for a polar gas (i.e. CO_2) and a non-polar gas (i.e. CH_4) was performed to determine if the zeolite enhanced transport of either gas as the feed pressure was increased.

Chapter 5 describes the study of a series of mixed matrix membranes using unfunctionalized zeolite L and a copolymer of composed of a polyimide and PDMS. The polyimide block was composed of the 6FDA and 6FpDA monomers, and the DABA monomer was replaced with PDMS. Because MMMs composed of PDMS and zeolite do not require any functionalization of the zeolite, it was hoped that adding a small amount of PDMS to the polymer would remove the need to treat the zeolite. In this investigation we describe a new fabrication procedure for developing pinhole free MMMs. We synthesize pure 6FDA-6FpDA, and we synthesize 6FDA-6FpDA-PDMS at varying weight percent of PDMS. AFM and SEM were used to study the membrane surfaces, and TEM was used to study bulk of the pure copolymer films. All three techniques were employed to verify the presence of phase separation between the hard and soft segment of the copolymer. FTIR was employed to verify the presence of functional groups in the copolymers, and ^{1}H-NMR was used to determine the weight percent of PDMS in the copolymers' backbones. Additionally, permeabilities for He, O_2, N_2, CH_4, and CO_2 were determined for both the pure polyimide and the MMM.

Chapter 6 describes the fabrication and characterization of a MMM composed of a 6FDA-6FpDA-PDMS block copolymer and single walled carbon nanotubes (SWNT's).

A fabrication procedure to prepare this type of MMM is described. SEM is used to study the surfaces and cross sections of the MMMs, as well as inspect the adhesion between the two components. TEM and AFM are used to investigate the presence of phase separation in the copolymers. Permeation studies were performed as well.

Finally, **Chapter 7** discusses future work based on the conclusions found in this investigation.

1.4 References

1 Scott, K. *Handbook of Industrial Membranes*, 2 ed.; Elsevier Science Publishers, 1998.

2 Baker, R. W. *Industrial Engineering and Chemistry Research* 2002, *41*, 1393-1411.

3 Robeson, L. M. *Journal of Membranes Science* 1991, *61*, 165-185.

4 Freeman, B. *Macromolecules* 1999, *32*, 375-380.

5 Wessling, M.; Strathmann, H.; Bos, A.; Punt, I. G. M. *Journal of Membrane Science* 1999, *155*, 67-78.

6 Chenoweth, M. B. *Synthetic Membranes*, 1 ed.; Harwood Academic Publishers: New York, 1986.

7 Breck, D. *Zeolite Molecular Sieves*, 1 ed.; John Wiley & Sons: New York, 1974.

8 Nikolakis, V.; Xomeritakis, G.; Abibi, A.; Dickson, M.; Tsapatsis, M.; Vlachos, D. *Journal of Membrane Science* 2001, *184*, 209-219.

9 Tavolarao, A.; Drioli, E. *Adv. Mater.* 1999, *11*, 975-996.

10 Burganos, V. *Materials Reseach Society Bulletin* 1999.

11 Fraenkel, D.; Levin, G.; Goldman, M. *Journal of Applied Polymer Science* 1989, *37*, 1791-1800.

12 Koros, W. J.; Mahajan, R. *Industrial Engineering and Chemistry Research* 2000, *39*, 2692-2696.

13 Smolders, C. A.; Duval, J. M.; Folkers, B.; Mulder, M. H. V.; Desgrandchamps, G. *Journal of Membrane Science* 1993, *80*, 189-198.

14 Tantekin-Ersolmaz, S. B.; Atalay-Oral, C.; Tather, M.; Erdem-Senatalar, A.; Schoeman, B.; Sterte, J. *Journal of Membrane Science* 2000, *175*, 285-288.

15 Koros, W. J.; Mahajan, R. *Polymer Engineering and Science* 2002, *42*, 1420-1431.

16 Koros, W. J.; Mahajan, R. *Polymer Engineering and Science* 2002, *42*, 1432-1441.

17 Mulder, M. H.; Duval, J. M.; J. B. Kemperman; Folkers, B.; Desgrandchamps, G.; Smolders, C. A. *Journal of Applied Polymer Science* 1994, *54*, 409-418.

18 Pechar, T.; Marand, E.; Davis, R.; Tsapatsis, M. *Desalination* 2002, *146*, 3-9.

19 Koros, W. J.; Zimmerman, C. M.; Singh, A. *Journal of Membranes Science* 1997, *137*, 145-154.

20 Mahajan, R.; Koros, W. J. *Industrial Engineering and Chemical Research* 2000, *39*, 2692-2696.

21 Iijima, S. *Nature* 1991, *354*, 56-58.

22 Popov, V. *Materials Science and Engineering* 2004, *43*, 61-102.

23 Ackerman, D. M.; Skoulidas, A. I.; Sholl, D. S.; Johnson, J. K. *Molecular Simulation* 2003, *29*, 677-684.

24 Thostenson, E.; Chou, T. *JOURNAL OF PHYSICS D-APPLIED PHYSICS* 2003, *36*, 573-582.

25 Weisenberger, M.; Grulke, E.; Jacques, D.; Rantell, T.; Andrews, R. *JOURNAL OF NANOSCIENCE AND NANOTECHNOLOGY* 2003, *3*, 535-539.

26 Wong, M.; Paramsothy, M.; Xu, X.; Ren, Y.; Li, S.; Liao, K. *Polymer* 2003, *44*, 7757-7764.

Chapter 2 Literature Review

2.1 Introduction

This chapter contains several sections which intend to give a broad overview of membrane fundamentals, and to provide a review of the literature for membranes. The theory and equations governing gas transport through membranes are covered first. This chapter then discusses the history and development of polymeric membranes. Subsections devoted to copolymer systems and polyimide membranes are also introduced due to their significance to this investigation. The development of mixed matrix membranes will be covered in two sections: one for rubbery MMMs which were developed first, then one for glassy MMMs. Finally, a section on carbon nanotubes and their incorporation into polymer matrices will be presented.

2.2 Brief Overview

Membranes are thin films which are used to separate at least two different chemical species. Membranes are used to separate components of a feed stream as shown in Figure 2-1. A feed stream will come into contact with a membrane, and one or more components of the feed stream will not be able to permeate through the selective barrier. These components leave the membrane in the retentate stream. Other

components which are capable of traversing the membrane exit the system in the permeate stream.

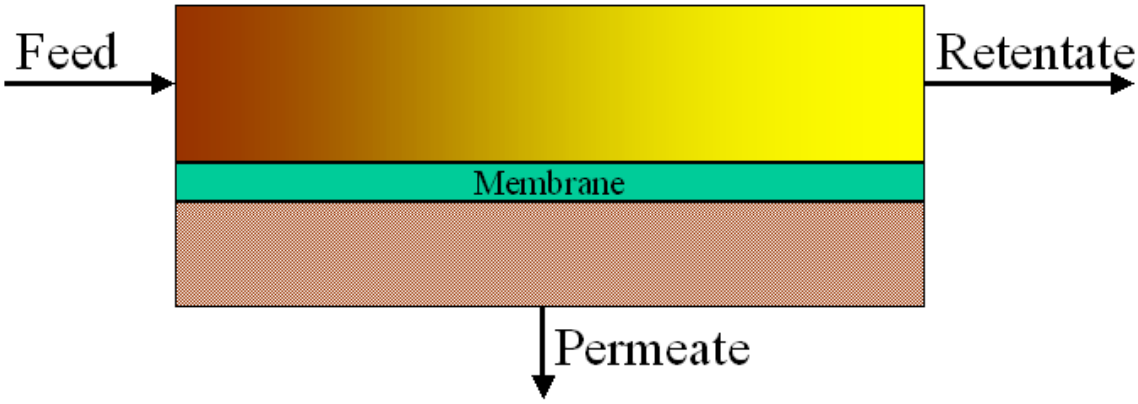

Figure 2-1. Illustration of a simple membrane process.

The components which are desired to be purified can be left in the retentate stream, or they can leave the system through the permeate stream. The user may work with a membrane that is permeable to those components needing purification, in which case the permeate stream would be the product stream. In turn, the user may choose to work with a membrane that is nonpermeable to the components needing purification, in which case the retentate stream becomes the product stream. The choice of membrane type depends on the components in the feed stream and will be discussed later in this chapter.

A more detailed schematic of how a membrane separates different components is shown in Figure 2-2.

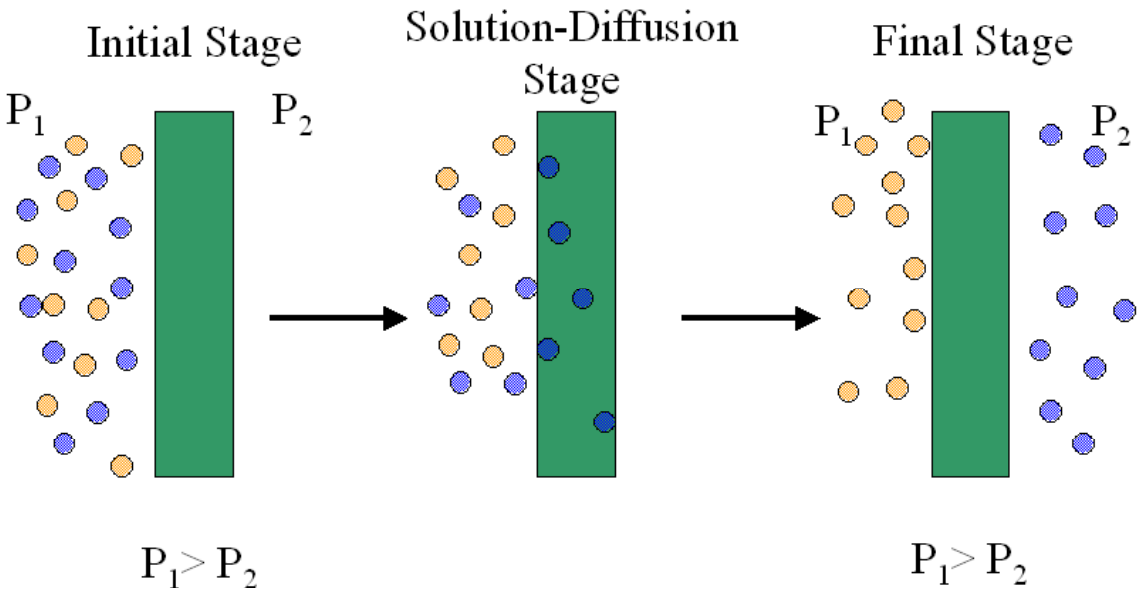

Figure 2-2. Schematic of how a membrane separates two different gases.

In this schematic the rectangle is the membrane, and the two different colored circles represent to two different gas molecules which need to be separated from each other. Typically, this type of gas mixture will come into contact with a membrane at a high pressure side (P_1). The membrane will separate the components using a solution-diffusion mechanism.[1] In this mechanism, a component will sorp into the upstream face of the membrane, and then diffuse across it to the low pressure (P_2) downstream face. At this face it will desorb into the permeate stream. One of the species will sorp into the membrane and diffuse through it faster than the other, and this leads to the separation of the components. The rate at which a species sorps and diffuses into a membrane can be altered by changing the chemical structure of the membrane. The solution-diffusion mechanism and the effects of a membrane's chemical structure on permeability will be discussed in detail later within this chapter. The next section will describe three parameters that are used to model this mechanism and that are related to a membrane's chemical structure.

2.3 Fundamental Parameters of Membranes

The rate of gas transport through a membrane is referred to as permeability. Maximizing the permeability is often a primary goal in the development of new membranes.

Gas transport through a polymeric membrane is considered to be a multi- step process called the solution-diffusion mechanism. This process was first proposed by Sir Thomas Graham in 1866.[2] Graham proposed that a gas that permeates through a nonporous polymer does so via three steps: sorption, diffusion, desorptoin. Sorption involves the penetrant dissolving into the membrane surface from the gas phase of the high pressure feed side. Once on the membrane surface the penetrant diffuses into and through the membrane. This diffusion step is the rate-controlling step of the process, as the penetrant must wait for the polymer chains to make a sufficiently sized gap for it to "jump" into. The penetrant makes a series of these "jumps" until it reaches the low pressure face of the membrane. Here it desorps into the permeate stream.

There are three fundamental parameters used to describe the capability of a membrane to transport a gas. The first is the permeability coefficient (P), or permeability. The permeability is the flux of a gas through the membrane after it has been normalized for the thickness of and the pressure gradient across the membrane. One can look at it as a flow rate of a gas through the membrane. The second is the diffusion coefficient (D), and it describes how easily a penetrant can migrate through a membrane. The third is the solubility parameter (S), and it describes how much of a penetrant can be held by the membrane at one time.

The three parameters form the fundamental equation modeling the performance of a polymeric membrane. This equation is shown below:

$$P = D \cdot S \qquad \text{Eq (2.1)}$$

These parameters will be described in detail in the following sections.

2.3.1 The Permeability Coefficient (*P*)

The permeability coefficient (*P*) is a measure of the rate that a penetrant can pass through a membrane. It often just referred to as the permeability. The permeability can be calculated easily for an individual component (P_i) using the equation below:

$$P_i = \frac{J_i}{(p_f - p_p)} \cdot l \qquad \text{Eq (2.2)}$$

where J_i is the steady-state flux of the component through the membrane, l is the membrane thickness, and p_f and p_p are the partial pressure of component i in the feed stream and the permeate stream. In cases dealing with nonideal gaseous mixtures (e.g. high pressure) the partial pressures of a component are replaced with the fugacity of that component (f_i).

Permeability in polymers is most commonly reported in Barrers. A barrer can be defined as follows:

$$1\,\text{Barrer} = 1 \text{ x } 10^{-10}\,\frac{\text{cm}^3\,(\text{STP}) \cdot \text{cm}}{\text{cm}^2 \cdot \text{sec} \cdot \text{cm Hg}} \qquad \text{Eq (2.3)}$$

2.3.2 The Diffusivity Coefficient (D)

The diffusivity coefficient (D) is a measure of how easily a penetrant can diffuse once inside the membrane. It is often reported in units of cm^2/s. The diffusion coefficient of a penetrant within a polymer is a kinetic parameter, and it is function of the properties of the penetrant and the polymer which composes the membrane.

The properties of the penetrant affect the diffusion coefficient in several ways. Larger sized particles have more difficulty moving than smaller sized particles, and as such, the larger the size of a particle the smaller its diffusion coefficient will be. Studies have been published which show there is an inversely related trend between D and the van der Waals volume of a penetrant.[3]

Park measured the diffusion coefficients for a series of noble gases in polyethylmethacrylate.[4] His results show clearly that D decreases as the size of the penetrant increases within this family. The trend is shown in Table 2-1.[4]

Table 2-1. Diffusion coefficients of various noble gases in polyethylmethacrylate.

Noble Gas	Kinetic Diameter (nm)	D (cm^2/s)
Helium	0.26	0.5×10^{-4}
Neon	0.32	1×10^{-6}
Argon	0.34	1×10^{-8}
Krypton	0.40	0.5×10^{-8}

The shape of a penetrant also influences the diffusion coefficient. D of linear molecules such as CO_2 are higher than those of spherical molecules for the same van der Waals volume, for example CH_4.[5,6] Berns et al. believed this was due to the ability of linear or "flattened" molecules to diffuse along their linear axis, which is not an option for the spherical molecules. The kinetic diameter of a molecule captures this aspect of a molecule's ability to diffuse much better than the van der Waals volume of the molecule. The kinetic diameter of a molecule is strongly related to the smallest sized zeolite pore that will permit the molecule to enter. For spherical molecules the kinetic diameter and the Lennard-Jones diameter are essentially equal. However, for asymmetric molecules the kinetic diameter is closer in value to the minimum diameter of the molecule. When one looks at the sizes of these molecules in terms of their kinetic diameter, it becomes more apparent that CO_2 should diffuse more easily. The kinetic diameter of the gases used in this study have been listed in Table 2-2.[7] Additionally, it is believed that the individual jump lengths may be only fractions of the total length of the molecule.[8]

Table 2-2. Kinetic diameter of various gases.

Molecule	Kinetic Diameter (nm)
He	0.26
CO_2	0.33
O_2	0.346
N_2	0.364
CH_4	0.38
Ar	0.34

Sever researchers have focused on characterizing the nature of a gas molecule's jumps through a polymeric material. Pace et al used pulsed-field NMR to determine the root-mean-square displacement between jumps of various simple gases in polyethylene.[9] Their results indicated that a the jump length can range from 2.5 – 20 nm, and we consistent with the statistical theory equation of Chandrasekhar.[10]

Gusev et al used transition-state theory to study the dynamics of light gases dissolved in glassy polycarbonate and rubbery polyisobutylene.[11] To estimate the properties of and behavior of dissolved molecules in the polymers, the authors employed the rigid-matrix approximation. However, their results indicated that this approach did not adequately describe the dynamics of gases in polymer, except for helium. Later work by this group focused on using experimental and simulation data on helium transport in glassy polycarbonate to elucidate the influence of molecular motions on transport.[12] In this study the authors based their simulations on the transition state approach, which assumes that small molecules move in polymer matrices by thermally activated jumps, and that on relevant time scales for this process only the elastically fluctuating polymer atom movements are significant. The authors compared experimental permeation and diffusion activation energies to simulated permeation and diffusion activation energies and found good agreement between the two. From this they concluded that it is the fast elastic vibration of the polymer atoms which are relevant to

He transport, and that all other motions in glassy polycarbonate appear to be too slow to affect transport.

The diffusion coefficient is a function of the chemical structure of the polymer as well. In order for a penetrant to diffuse across a membrane, its movement must coincide with the polymer chains' intersegmental motions. These intersegmental motions must result in a gap large enough for a penetrant to move into as shown in Figure 2-3. As such, the chemical structure of the polymer plays an important role in the value of D. The incorporation of flexible linkages, such as -O-, allow for easy intrasegmental motion. Rigid units in the polymer's backbone, such as aromatic groups, can reduce the polymer flexibility, and thus the diffusion coefficient of a penetrant.

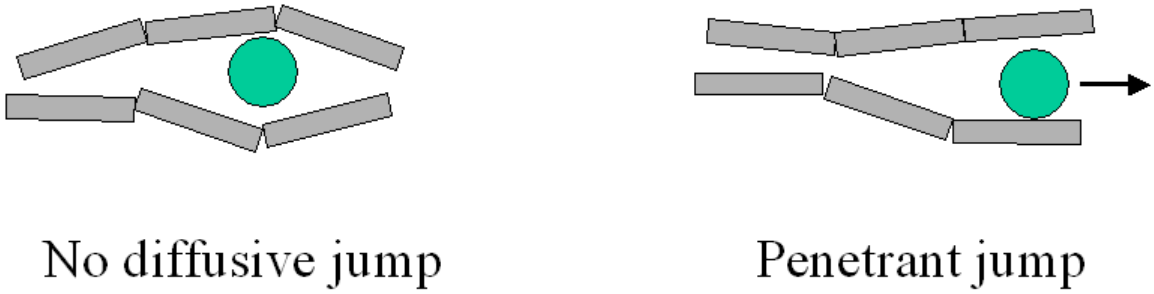

Figure 2-3. Illustration showing that the intersegmental motions must result in a gap larger than the size of the penetrant in order for it to make a jump and diffuse through the membrane.

With polymer structure strongly influencing the diffusivity of a component, it follows that there will be drastic differences in the diffusion values for a gas between glassy and rubbery membranes. Indeed, this is the case. Rubbery polymers are known to have diffusion coefficients that are much higher than glassy polymers for the same gas. For example, natural rubber has a D_{O2} of 158 x 10^{-8} cm^2/s, while glassy polycarbonate has a D_{O2} value of 5.1 x 10^{-8} cm^2/s.[13] Work done by Crist et al. highlighted the differences of diffusion coefficient values in rubbery and glassy polymers.[14] In their work, they studied natural rubber and glassy poly(vinyl chloride) for a series of gases.

They determined the diffusion coefficients and van der Waals volumes for each gas and plotted their results. Their results are shown in Figure 2-4.[14]

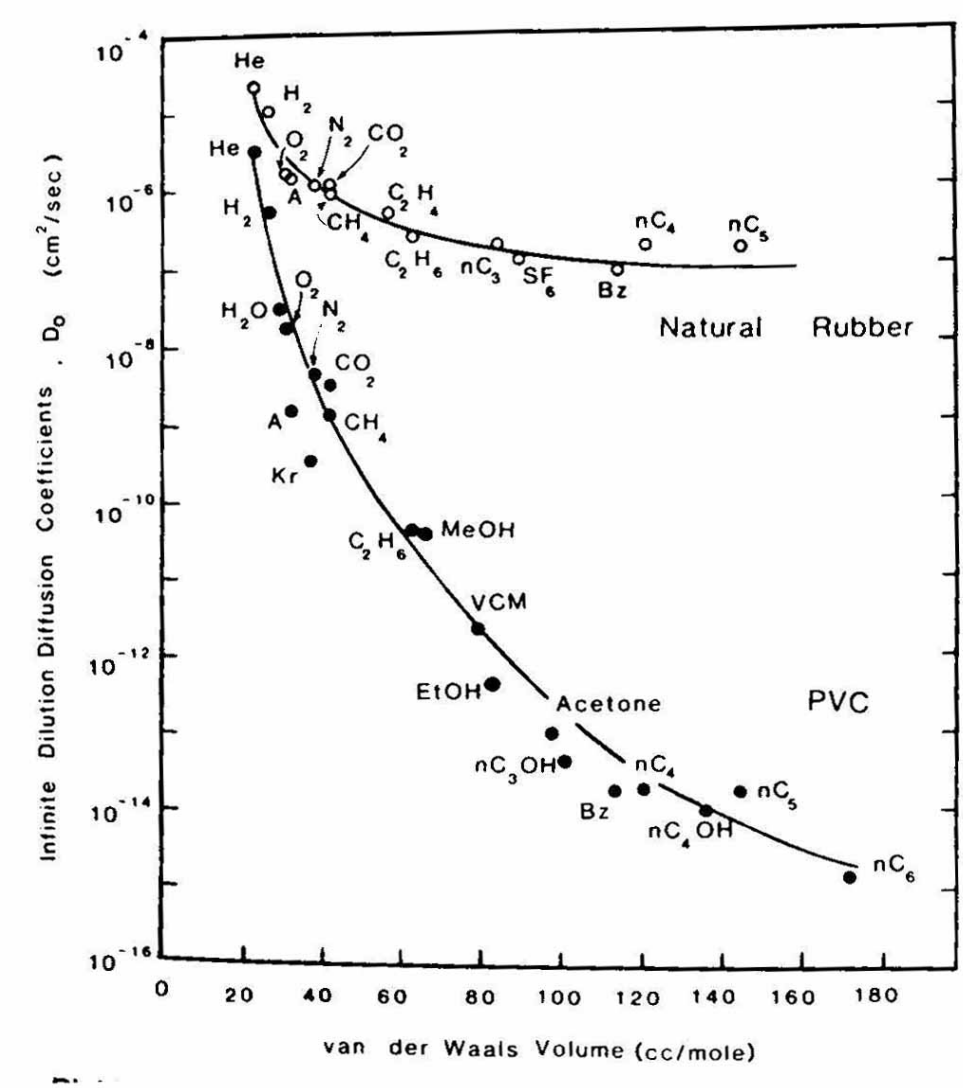

Figure 2-4. Diffusion coefficients of various molecules in natural rubber and glassy poly(vinyl chloride). The figure was adapted from reference 14.

The amount of free volume trapped within a polymer will effect the diffusivity of a penetrant, and is often referred to as the fractional free volume (FFV). The FFV is the amount of space which is not occupied by the polymer chain. As it consists of empty

space, it scales exponentially with the diffusivity coefficient. The FFV can be determined using the relationship below:

$$FFV = \frac{V - V_o}{V} \qquad \text{Eq (2.4)}$$

here, FFV is the fractional free volume, V is the specific volume of the polymer, and V_o is the volume which is occupied by the polymer, which is equal to 1.3 times the van der Waals volume of the polymer.

D and FFV can be related through the Doolittle expression:[15]

$$D = D_o \cdot \exp\left(\frac{-B}{FFV}\right) \qquad \text{Eq (2.5)}$$

where D is the diffusivity coefficient, FFV is the fractional free volume, and D_o and B are constants characteristic of the polymer-penetrant system. D_o is equal to (RT A_f) where A_f depends on the size and shape of the gas molecule, and B is a measure of the minimum local free volume necessary to allow a diffusive jump.[16] This relationship shows that as the FFV increases, the diffusion coefficient will increase exponentially with it. This trend was highlighted in a publication by Ghosal et al. and is shown in Figure 2-5.[17]

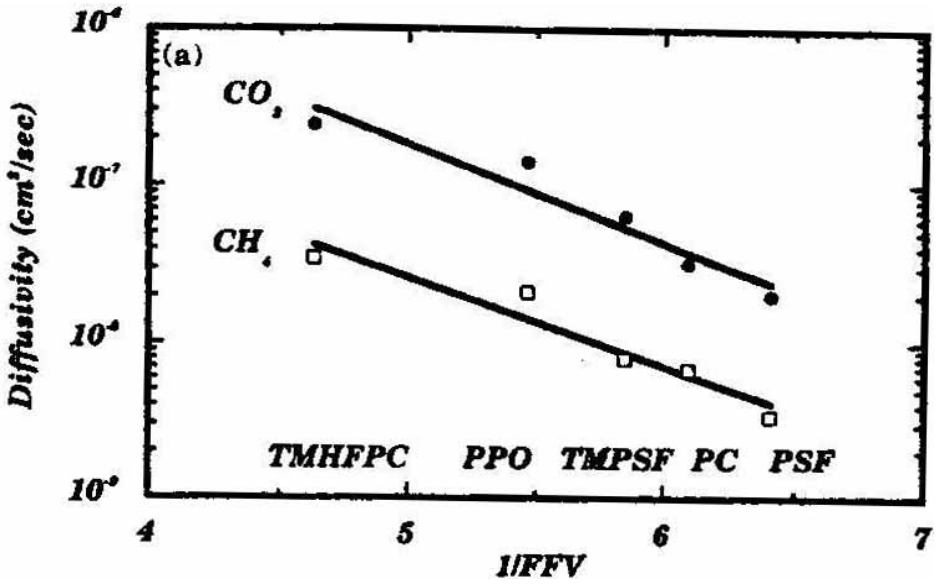

Figure 2-5. The diffusion coefficient and fractional free volume for a series of glassy polymers. The image was adapted from reference 17.

The temperature of the system will also influence the value of the diffusion coefficient. The temperature will increase the segmental motions of the polymer chains and lead to the development of more gaps large enough for a gas molecule to fit into. Additionally, it will impart more kinetic energy to the penetrant allowing it to diffuse faster. The relationship between temperature and D is typically modeled by an Arrhenius-type relationship and can be expressed as follows:

$$D = D_o \cdot \exp\left(\frac{-E_d}{RT}\right) \qquad \text{Eq (2.6)}$$

where E_d is the activation energy of diffusion, D_o is a constant, and R is the ideal gas constant.[18]

The diffusion coefficient usually increases sharply with temperature, provided the polymer does not undergo crystallization or other morphological changes as the temperature increase. Crystals act as impenetrable barriers to gas molecules and lower the permeability. Additionally, molecules cannot sorp or diffuse into a crystal. The temperature increases the thermal motions of a polymer chain allowing easier diffusion for a gas penetrant.

2.3.3 The Solubility Coefficient (S)

A membrane possesses a thermodynamic maximum amount of gas it can hold at a given pressure. This amount is called the solubility and is represented by S. The equation used to calculate the solubility coefficient is given below:

$$S_i = \frac{C_i}{P_i} \qquad \text{Eq (2.7)}$$

here, S_i is the solubility of component i, C_i is the concentration of i in the membrane, and P_i is the partial pressure of i in the feed stream. S is often reported in units of cm^3 (STP)/($cm^3_{polymer}$ cmH).

The value of the solubility coefficient depends partly on the properties of the gas molecule. A gas molecule with a high critical temperature (T_c) generally will have a higher S than a similar molecule with a lower T_c.[3] The size of the gas molecule influences S as well. As the size increases, generally the solubility will increase too.

Solubility also tends to correlate well with the gas molecules' boiling point (T_b) and Lennard-Jones force constant.[3,19]

S is a coefficient that is a function of the interactions between the penetrant and the polymer. Gases which are polar can have favorable interactions with polymer functional groups. CO_2 has a quadrupole moment which increases it solubility in polar polymers relative to a nonpolar molecule. For example, Koros et al, performed a study in which the Henry's constant ratio of CO_2 to CH_4 (i.e. k_{CO2}/k_{CH4}) was reported for a series of polymers.[20] These polymers contained different amounts of polar functional groups. The series of ratios began with polyethylene, which contains no polar groups, and went on to include polymers such as cellulose acetate, and poly (methyl methacrylate). The data is shown in Figure 2-6 which was adapted from Koros et al.[20]

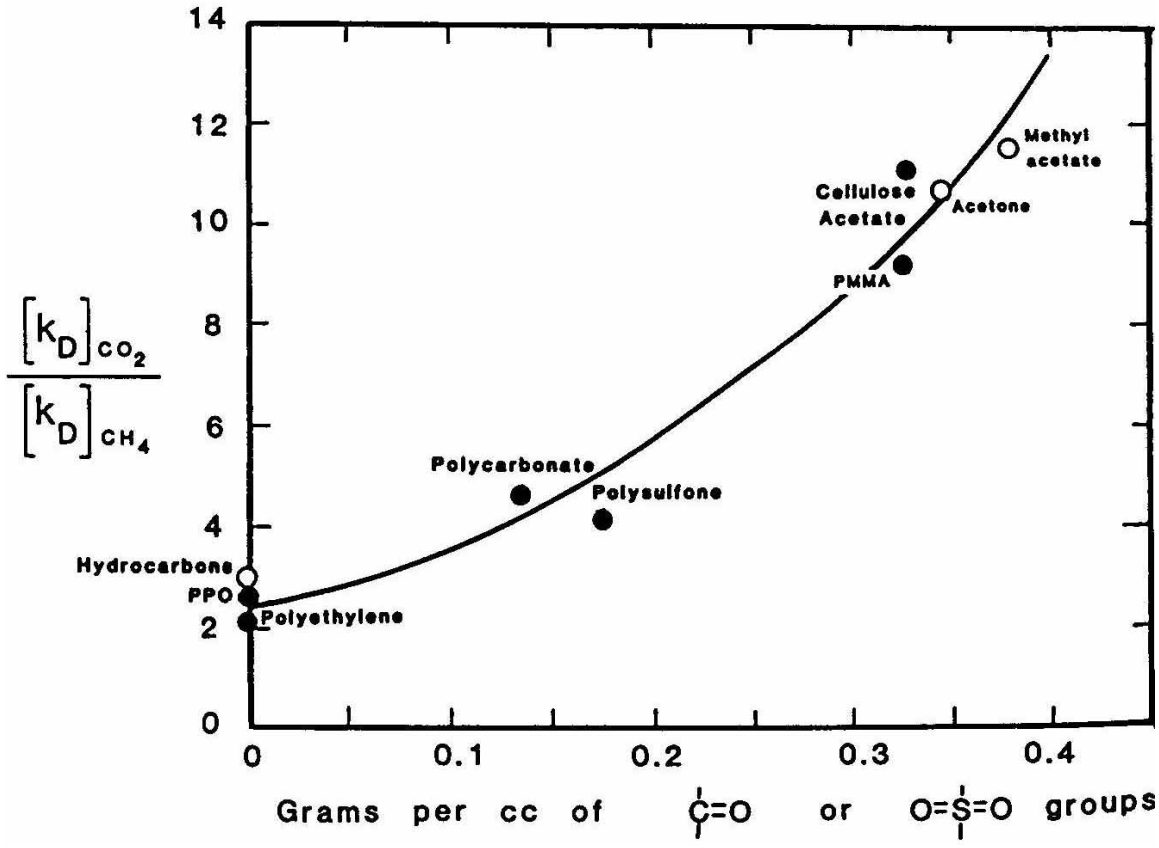

Figure 2-6. Solubility selectivity of CO2 and CH4 for various polymers as the number of functional groups increasese. The figure was adapted from reference 20.

Temperature can increase or decrease the solubility coefficient depending on the interactions between the condensate and the polymer. Solubility in polymers can be expressed as:

$$S = S_o \cdot \exp\left(\frac{-\Delta H_s}{RT}\right) \qquad \text{Eq (2.8)}$$

here, S_o is a constant, R is the ideal gas constant, T is the temperature , and ΔH_s is the partial molar enthalpy of sorption. ΔH_s can be calculated as follows:

$$\Delta H_s = \Delta H_{cond} + \Delta H_{mix} \qquad \text{Eq (2.9)}$$

here, ΔH_{cond} is the enthalpy change of the penetrant from a gaseous penetrant to a condensed density, and ΔH_{mix} is the enthalpy change associated with creating a gap in the polymer of sufficient size to accommodate the penetrant molecule.[21] For gases such as H_2 and He which have low molecular weight and very low T_c's, ΔH_{cond} is very small and ΔH_s is dominated by ΔH_{mix}. If the interactions between the gas and polymer are weak, then ΔH_{mix} is positive, and S will increase with temperature. For cases in which the gas in condensable (e.g. CO_2) or capable of interacting with the polymer, ΔH_{cond} may be large, leading to a positive value of ΔH_s. In this case, S will decrease with temperature.[17]

The solubility can be affected by the amount of free volume when working with glassy polymers. Free volume in a glassy polymer results from the polymer chains' inability to undergo conformational rearrangement fast enough to attain equilibrium once the temperature falls below the polymer's T_g. This excess volume becomes a sorption site for gas molecules. However, these sites can become saturated as the pressure increases, resulting in diminishing increases in concentration as the pressure is raised. This lowers the value of the solubility parameter. A publication by Ghosal et al. illustrated this relationship and is shown in Figure 2-7.[17] This phenomenon will be covered more extensively in the Solution Diffusion Model section.

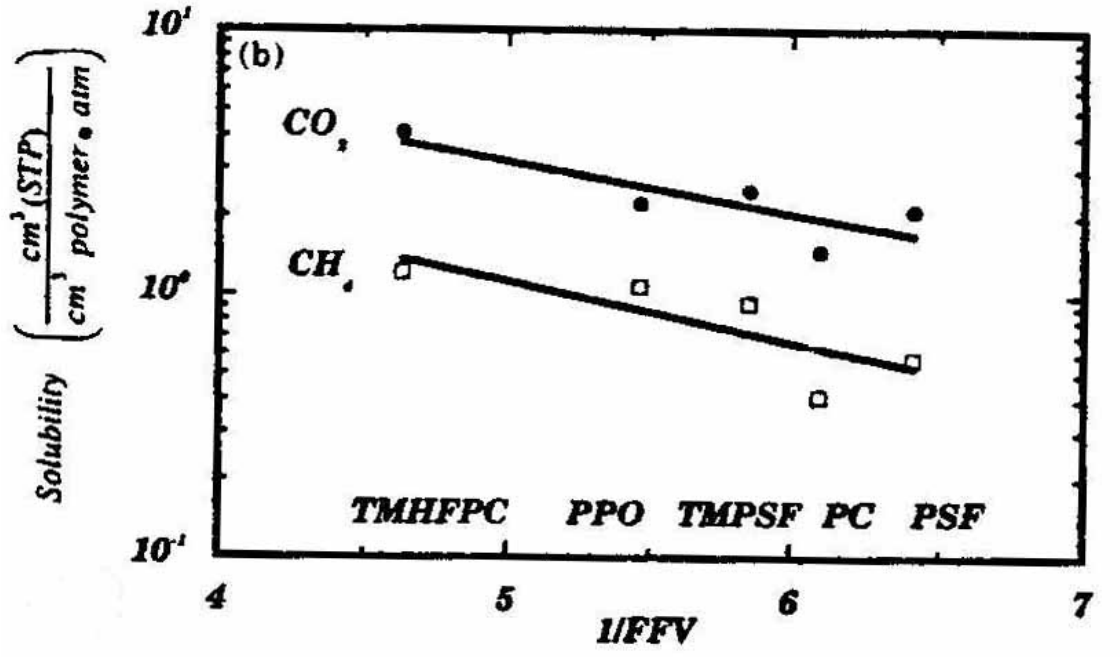

Figure 2-7. Relationship between solubility and fractional free volume for a series of glassy polymers. The figure was adapted from reference 17.

2.4 Gas Transport through a Rubbery Polymeric Membrane

Rubbery polymers are relatively easy to model when there are no strong interactions between the penetrant and the membrane. When this is the case, the concentration of the gas within in the rubbery polymer will obey Henry's Law, which is shown below:[22]

$$C = k_D P \qquad \text{Eq (2.10)}$$

here, C is the concentration of the penetrant in the membrane, k_D is the Henry's constant, and P is the pressure. Substituting Eq (2.7) into Eq (2.10), it becomes evident that the solubility of a component in a rubbery polymer is equal to the Henry's constant.

When there is no crystallization, diffusion of gases in rubbery polymer's follow Fick's law.[19] Fick's law is shown below:

$$J = - D \frac{\partial C}{\partial x} \qquad \text{Eq (2.11)}$$

substituting Eq (2.10) into Eq (2.11), replacing x with l (i.e. membrane thickness), and recalling the definition of permeability from Eq. (2.2), the equation below is derived for describing the permeability (*P*) of a gas through a rubber membrane:

$$P = k_D \cdot D \qquad \text{Eq (2.12)}$$

Permeabilities through rubbery polymers are typically much higher than their glassy counterparts. This is a result of the increased backbone mobility present in a rubber polymer, particularly the loss of restrictions on rotations due to bulky side groups or due to interactions among chains. However, the these factors which increase *P* of rubbery materials, also lead to lower selectivity, as the material's ability to separate based on size becomes impaired.[16] Examples of the performance of rubbery polymers will be discussed in the History of Membranes section.

2.5 Gas Transport through a Glassy Polymeric Membrane

Glassy polymers are more complicated to model than their rubbery polymer counterparts due to the introduction of excess volume. This excess volume within the polymer matrix is a result of the loss of large scale movement in the polymer once it crosses its T_g. This loss of movement prevents the chains from rearranging quickly enough to reach equilibrium. Once below T_g the polymer chains possess extraordinarily long relaxation times. As a result, excess volume is trapped inside the polymer, however, the polymer will slowly drift towards this equilibrium and thus reduce this volume through a process known as physical aging.[16,17,23,24]

The excess volume, also referred to as holes, offers a new sorption site for penetrants which is not available in rubbery polymers. The concentration of penetrant in these sites is expressed as a Langmuir isotherm:[25]

$$C_H = \frac{C_H' \cdot b \cdot P}{1 + b \cdot P} \qquad \text{Eq (2.13)}$$

where C_H is the concentration of the penetrant in the holes, C_H' is the hole saturation constant or Langmuir sorption capacity, b is the Langmuir affinity parameter, and P is the pressure. C_H' has been related to the excess volume through the following equation:[26]

$$C'_H = \left(\frac{V_g - V_l}{V_g} \right) \rho^* \qquad \text{Eq (2.14)}$$

where V_g is the specific volume of the glassy polymer, V_l is the specific volume of the hypothetical rubbery polymer, and ρ^* is the molar density of the penetrant.

The hole saturation constant is temperature dependant, as the unrelaxed volume in a glassy polymer can be reduced, if not eliminated. As a glassy polymer is heated to its T_g, the polymer chains acquire more thermal energy to overcome rotational restrictions, and thus can adopt more conformations. When at or above its T_g, the chains have enough energy to pack differently, specifically, more efficiently, and reduce the excess volume within the polymer matrix. From Eq (2.14), it is evident that this phenomenon will force the value of V_g to approach that of V_l, and thus, C'_H will go to zero. Work by Koros et. al, looked at this in a study of poly(ethylene terephthalate) (PET) and CO_2.[27] The group determined the hole saturation constant of PET at different temperatures above and below PET's T_g. Their results showed a clear inverse relationship between C'_H and temperature; C'_H would go to zero as T_g was attained. A sample of their results is shown in Figure 2-8 which was taken from reference 17.[27] Studies by Toi et al. have verified that the relationship between C'_H and T_g is linear with an intercept at zero at a temperature equal to the T_g.[28]

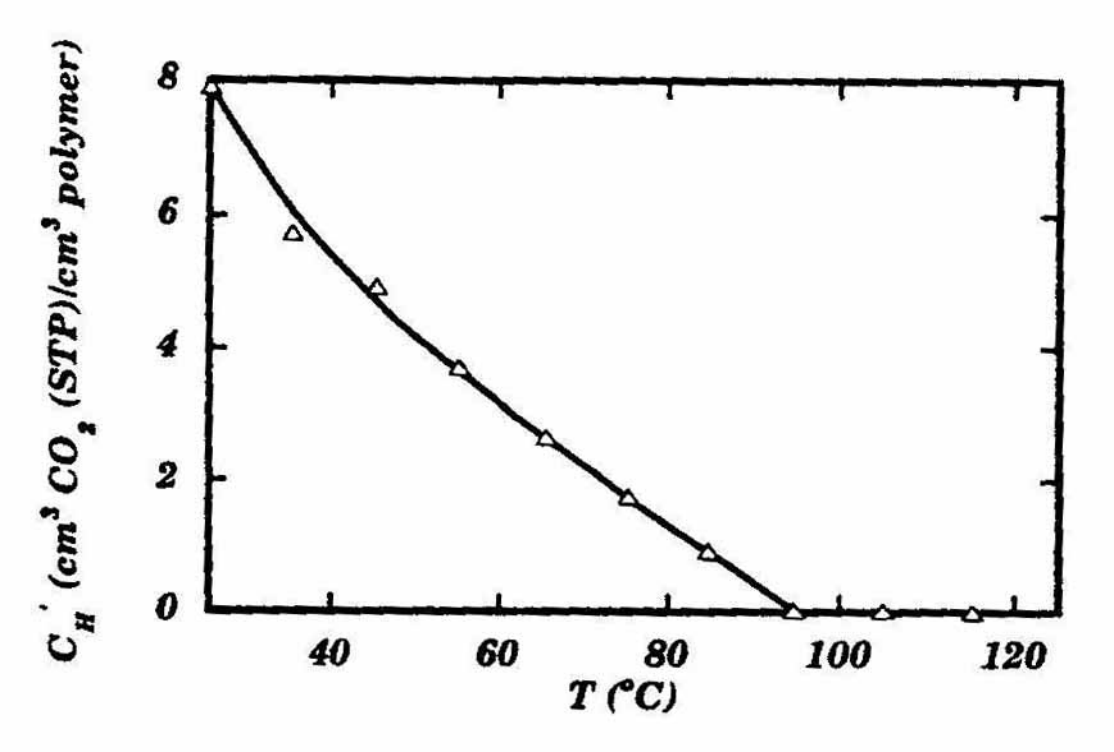

Figure 2-8. The effect of temperature on the Langmuir capacity constant for CO_2 in PET.

With a way to describe the concentration of a condensate in the free volume of an amorphous glassy polymer, we can now look at describing the permeability through it when it contains sorption in between the chains and in the holes. This model is called the Dual Mode Sorption model, and is outlined in the next section.

2.5.1 Dual Mode Sorption Model

The Dual Mode Sorption (DMS) model was introduced in 1981 and since then has become the primary model for analysis of permeation through glassy membranes.[26] This model takes into account the two modes of sorption in glassy polymers: sorption in between the polymer chains called the dissolved mode (C_D), and sorption in Langmuir sites referred to as the hole-filling mode (C_H).

The total concentration of penetrant (C) within a glassy amorphous polymer can be expressed as:

$$C = C_D + C_H \qquad \text{Eq (2.15)}$$

C_D can be expressed using Henry's law (Eq 2.10), and C_H can be expressed using Eq (2.13). Substituting those equations into Eq (2.15) leads to the DMS model:

$$C = k_d P + \frac{C_H' \cdot b \cdot P}{1 + b \cdot P} \qquad \text{Eq (2.16)}$$

typically, C carries units of cm^3 (STP)/$cm^3_{polymer}$, k_d has units of cm^3 (STP)/$cm^3_{polymer}$ atm, C_H' is in cm^3 (STP)/$cm^3_{polymer}$, b is in atm^{-1}, P is in atm.

From the DMS model, it is evident that the equilibrium concentration of a gas in a glassy polymer behaves very differently than that of a rubbery polymer. In rubbery polymers, the concentration was directly proportional to the applied pressure. However, in glassy membranes, the equilibrium concentration typically is non linear and begins to approach an asymptotic value as the pressure is increased. This is a result of the holes becoming saturated, and not being able to accommodate any more gas molecules

From the DMS model, it is also evident that at high P, Eq (2.16) will reduce to:

$$C = k_d P + C_H' \qquad \text{Eq (2.17)}$$

which is a linear relationship between the amount of gas sorbed and the applied pressure. In the limit of low pressure, Eq (2.16) reduces to:

$$C = \left(k_d + C_H' \cdot b\right) \cdot P \qquad \text{Eq (2.18)}$$

which once again shows a linear relationship between the concentration of sorbed gas and the applied pressure.

The DMS model is nonlinear in the intermediate range. In this range it is concave to the pressure axis. Work by Ghosal et al. illustrates this behavior well. Their work looked at polysulfone for N_2, O_2, CH_4, and CO_2 and their corresponding concentration in polysulfone at different pressures. Their work shown in Figure 2-9 clearly shows linear behavior at low and high pressures, and concave behavior in between.[29]

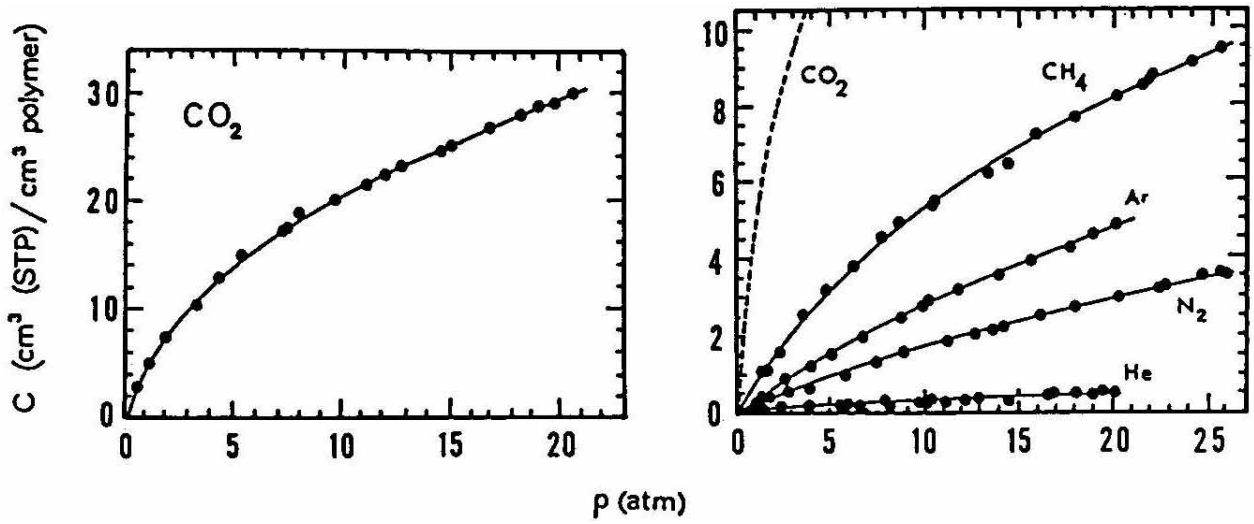

Figure 2-9. Gas sorptions isotherms for polysulfone at 35 °C which were adapted from reference 17.

2.5.2 The Time Lag Method

This section outlines the method used in this study to determine the diffusion coefficient and the solubility coefficient for the membranes tested. The method used is called the Time Lag Method.

The time lag is the amount of time required for a gas or vapor to permeate through a membrane. It can be calculated using a two chambered closed volume-variable pressure. The upstream chamber simply contains the feed gas and a pressure transducer to to record the feed gas pressure. This chamber is separated from the downstream chamber by a membrane, which is degassed before testing. At the beginning of the test, a feed gas is introduced into the system and the permeate pressure is recorded as a function of time. The Time Lag is defined where the pressure is zero on the time axis, when a line is extrapolated to the time axis from the linear part of the response curve. The pressure data can be divided into two regions: and unsteady state region and steady state region. The unsteady state region exists at shorter times, and includes portions where the permeate pressure is zero. The steady state region is the area of interest in the Time Lag Method, and consists of a linear relation between permeate pressure and time. Figure 2-10 shows

the location of the Time Lag Θ, and the unsteady state and steady state regions for gas permeation.

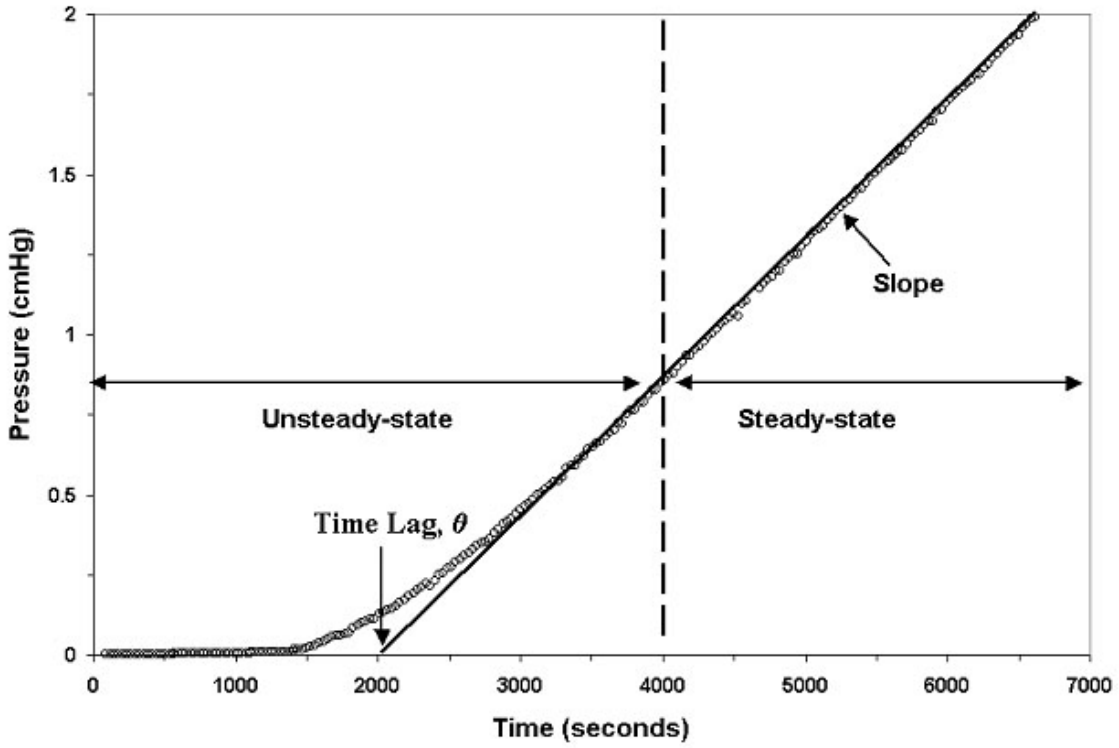

Figure 2-10. Typical permeation experiment data analyzed using Time Lag Method.

To define the Time Lag method, one must recall Fick's second law of diffusion. This law can be used to model the permeation process, which is shown below.

$$\frac{\partial C}{\partial t} = D\frac{\partial^2 C}{\partial x^2} \qquad \text{Eq (2.19)}$$

In order to solve for the Time Lag using the previous equation, the following boundary conditions are imposed.

$t < 0$	$0 \le x \le l$	$C = 0$
$t \ge 0$	$x = 0$	$C = C_{2,m} = S p_2$
$t \ge 0$	$x = l$	$C = \partial C / \partial t = 0$

Applying these boundary conditions results in the numerical solution shown in Eq 2.19. This solution is for one-dimensional flow through the membrane, with the assumption that the diffusion coefficient D is a constant. This statement implies that D is independent of temperature and concentration.

$$\frac{Q}{l C_2} = \frac{Dt}{l^2} - \frac{1}{6} - \frac{2}{\pi^2} \sum_{n=1}^{\infty} \frac{(-1)^n}{n^2} exp\left(- \frac{D n^2 \pi^2 t}{l^2} \right) \qquad \text{Eq (2.20)}$$

In Eq 2.20, Q is the total permeant passing through the membrane, and l is the thickness of the film. The other variables in this equation are the concentration in the film at the feed side C_2, the diffusion coefficient D, and the time t. It is possible to reduce Eq 2.20 when time t is allowed to approach infinity. When t is allowed to approach infinity, the summation element in goes to zero, and the following equation is obtained.

$$\frac{2}{\pi^2} \sum_{n=1}^{\infty} \frac{(-1)^n}{n^2} exp\left(- \frac{D n^2 \pi^2 t}{l^2} \right) \Bigg|_{t \to \infty} = 0 \qquad \text{Eq (2.21)}$$

The steady-state region of the pressure response curve, shown in (Figure 1), implies that t has gone to infinity. This steady-state region also signifies that $\partial C / \partial t = 0$. When Equation 2.21 is substituted into Equation 2.20, then the reduced equation becomes

$$\frac{Q}{l C_2} = \frac{Dt}{l^2} - \frac{1}{6} \qquad \text{Eq 2.22}$$

Rearranging this in terms of Q reveals the Time Lag Θ shown in Equation 2.23. Equation 2.23 indicates that the total gas passing through the membrane, Q, is zero until a

time t has elapsed, which is greater than the Time Lag Θ. Q is also commonly referred to as the accumulation term, since the gas permeate is trapped within a fixed volume.

$$Q = \frac{DC_2 t}{l} - \frac{lC_2}{6} = \frac{DC_2}{l}\left(t - \frac{l^2}{6D}\right) = \frac{DC_2}{l}(t - \theta) \qquad \text{Eq (2.23)}$$

$$\theta = \frac{l^2}{6D} \qquad \text{Eq (2.24)}$$

Obtaining the Time Lag Θ shown in equation 2.23 provides a direct route for calculating the diffusion coefficient D.

The permeability coefficient P is calculated from the slope found in (Figure 1) within the steady-state region. Solving for the flux J, is the starting point for the solution of the permeability coefficient P. The solution for the flux J, through the membrane is given by the following expression.

$$J = \frac{Slope}{RT} \cdot \frac{V}{A}\left(\frac{22414\, cm^3 (STP)}{mol}\right) \qquad \text{Eq (2.25)}$$

The solution for the flux J is converted to STP conditions, and the slope is obtained during a permeation experiment, within the steady-state region shown in Figure 2-10. In Equation 2.25, V is the volume of the evacuated chamber into which gas permeates, and A is the cross-sectional area of the membrane. The temperature of the experiment is T, R is the ideal gas constant, and l is the membrane thickness. Because the downstream pressure p_1 is much smaller than the feed pressure p_2, the pressure difference Δp can be replaced with p_2, shown with Equation 2.26.

$$J = P\frac{\Delta p}{l} \cong P\frac{p_2}{l} \qquad \text{Eq (2.26)}$$

This can be rearranged to give equation 2.27

$$P \cong J \frac{l}{p_2} \qquad \text{Eq (2.27)}$$

Using the Time Lag and its relationship with the permeability coefficient *P*, the diffusion and solubility coefficients are then given by the following expressions.

$$D_{eff} = \frac{l^2}{6\theta} \qquad \text{Eq (2.24)}$$

$$S_{eff} = \frac{P}{D} \qquad \text{Eq (2.28)}$$

2.6 Polymeric Membranes

This section of the literature review is intended to recapitulate the major events and publications concerning membranes that are relevant to this study. The section devoted to polymeric membranes contains several subsections. The first is devoted to the history of polymeric membranes, in which the major events in developing gas separation membranes are recounted. This section is followed up with a section which details the observed and theoretical limits of polymeric membranes. The last two sections are more narrowly focused to provide some background on the literature related to polyimide and poly(imide siloxanes), both of which were employed in this work.

2.6.1 Major Events in the History of Gas Separation Membranes

The first recorded study devoted to a membrane was in 1748 by Abbe Nollet. Nollet placed "spirits of wine" in a vessel, and sealed the vessel's mouth with an animal bladder which was then immersed in water.[30] The bladder was more permeable to water than to wine, and as a result swelled and on occasion burst.

In 1855 Fick published his laws of diffusion which would aide in describing and modeling diffusion through a membrane.[31] Fick would also publish that same year studies on synthetic membranes. These membranes were made from an ether-alcohol solution of cellulose nitrate called collodion.[32]

Thomas Graham is considered the father of gas separations using membranes. In 1866, Graham published work in which he documents his discovery that rubber exhibits different permeabilities to different gases.[33] Graham would go on to develop Graham's law of diffusion in gases.

From this point, work on membranes appears to have been limited in scope, focusing primarily on liquid separations. Even in the 1960's membrane processes for gas separations were still primarily limited to laboratory scale studies. At this time the only commercially competitive membrane available was an asymmetric membrane made from cellulose acetate.[34] This membrane was used for water desalination via reverse osmosis. This asymmetric membrane was an industrial breakthrough as it drastically increased the permeability of cellulose acetate without sacrificing its selectivity. This asymmetric membrane consisted of a very thin dense top layer with thickness < 0.5 μm supported by a porous sublayer with thickness between 50 -200 μm.

This design would become the standard for gas separation membranes used by industry today. The design was adapted for gas separations by Henis and Tripodi; they would go on to publish a model for describing transport behavior in hollow fibre asymmetric membranes.[35] An image of an asymmetric membrane is shown below in Figure 2-11.[16]

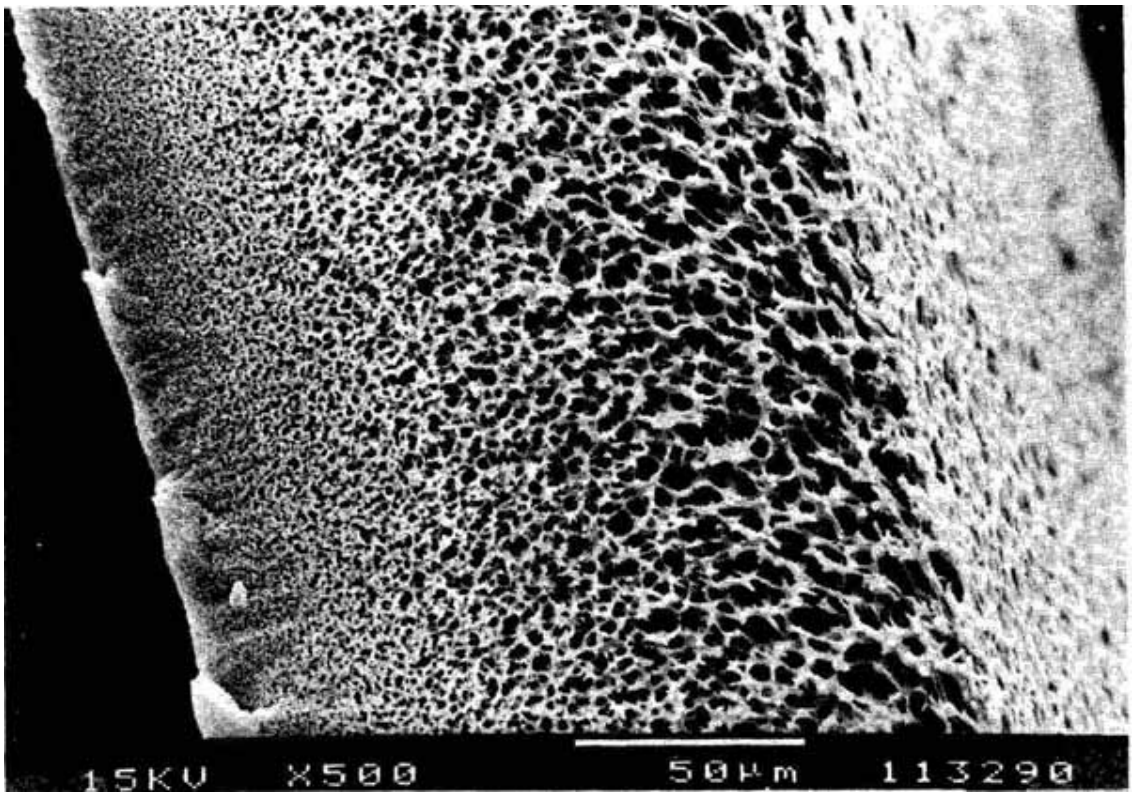

Figure 2-11. Cross-sectional image of an asymmetric polysulfone membrane. The left side of the membrane is the dense selective layer. The right side is the microporous sublayer. The image was adapted from reference 16.

Up until the 1970's, membranes failed to make an impact in the industrial sector. In his review of the progress of membranes through the early 1980's, Lonsdale attributed this lack of progress by membranes to four factors:[36]

- When compared to other separation processes such as distillation, the early membranes did not offer enough flux to perform an economical separation
- When compared to other separation processes such as distillation, the early membranes were not highly selective
- No efficient and inexpensive method of modularizing membranes existed. Prior to 1960 mostly plate-and-frame modules were used which were expensive and cumbersome
- Energy was exceedingly cheap as compared to present day energy costs.

In the 1970's membrane development was given a big push by the energy crisis. Membranes were looked at as a potential solution to replace energy intensive separation units, because membranes did not separate species using heat or cooling, and did not have any moving parts. Rather, when operating ideally, they would only require pumps to produce the pressure gradient across the membrane.

In 1979 Permea, which is now a division of Air Products, released its first hydrogen separating Prism membrane. This was the first large scale industrial application of gas separation membranes, and was targeted towards the recovery of hydrogen from the purge streams of ammonia plants.[37]

With the success of Permea, other companies began to sprout. Cynara, Separaex, and GMX all developed cellulose acetate membranes to remove carbon dioxide from natural gas. Additionally, membranes to produce nitrogen from air were released in this time. This nitrogen selective membrane was made by Generon and was based on poly(4-methyl-1-pentene).[38] These membranes displayed an oxygen/nitrogen selectivity around 4, and produced nitrogen with roughly 95% purity.

In the 1990's new membranes were developed to separate nitrogen from air. These membranes had oxygen/nitrogen selectivity of 6 – 8, and could produce nitrogen with 99% purity. With these advances, membranes could now be economically competitive in the production of liquid nitrogen for small users. This application has grown to account for one-third of nitrogen production, and currently, there are 5000 - 10,000 nitrogen systems operating world wide.[38] Also in the 1990's, the first propylene/N_2 plant and medal-polyimide hollow-fiber membrane for CO_2/CH_4 separation were installed.

As of 2002, membrane gas separation equipment has grown into a $150 million/year market. The majority of the separations for which membranes are employed involve the separation of condensable gases, such as N_2 from air, CO_2 from CH_4, and H_2 from N_2, Ar or CH_4. Currently, efforts are underway to open up the market of separations involving noncondensable gases, such as butane from CH_4, propylene from propane, and n-butane from isobutene.

2.6.2 Performance Limits of Polymeric Membranes

An ideal membrane will possess very high permeability, yet still retain very high selectivity in order to effectively separate a gas pair. During the 1980's many research efforts to developing a polymeric membrane with these qualities reached the same result: The selectivity of a membrane towards a gas pair varies inversely with the permeability of the most permeable gas in the pair.

In 1991 Robeson developed a model which would define membrane performance.[39] Robeson gathered permeation data from over 300 references for a series of gas mixtures. Each gas mixture, every membrane's permeability to more permeable component was plotted against the membrane's selectivity. The data points were also coded to distinguish between rubbery polymers and glassy polymers.

The resulting graphs illustrated the recognized trade off between permeability and selectivity. Furthermore, there appeared to be an upper bound to membrane performance, which denotes the limit of the separating ability of polymers. Robeson designated this line as a solid black curve. The trade-off curve for the O_2/N_2 separation is shown below in Figure 2-12.[39]

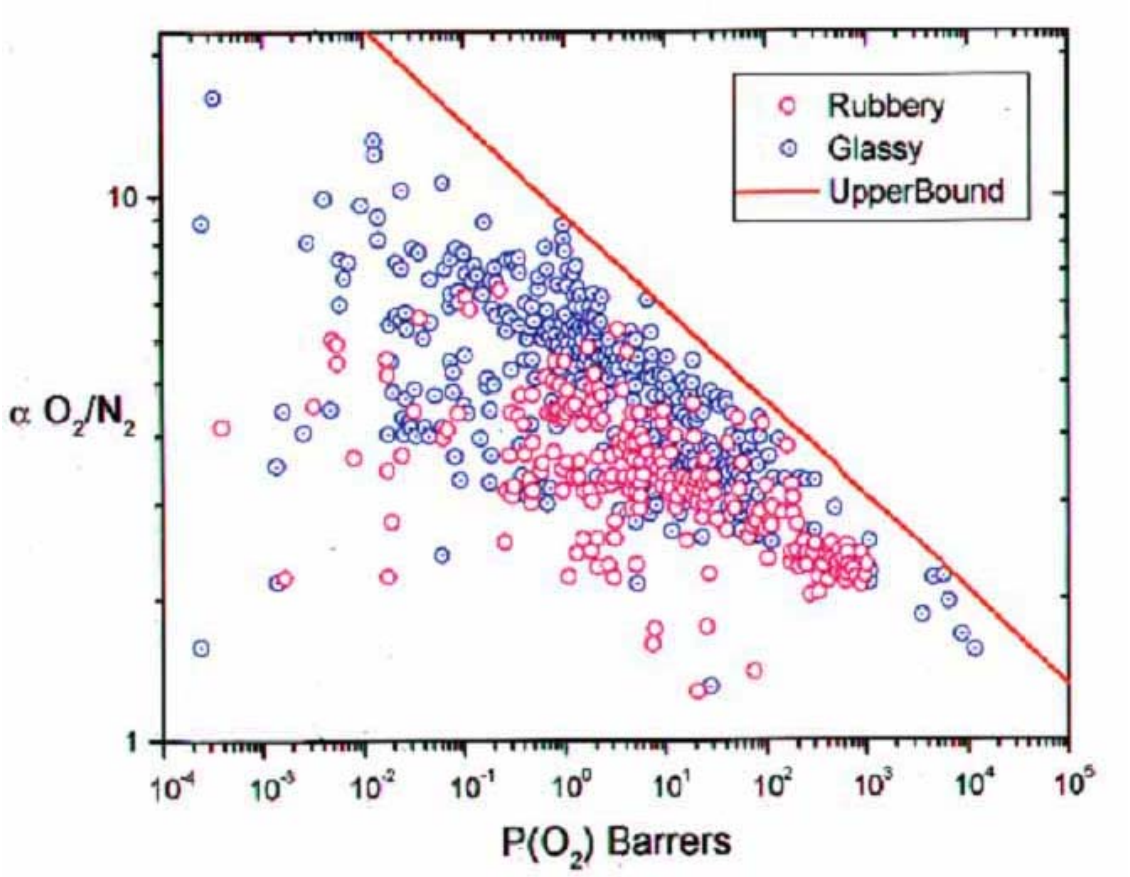

Figure 2-12. Trade off curve between permeability and selectivity for polymeric membranes.

As is evident from the figure, plotting the variables as log-log data leads to a linear upper bound. The author analyzed the slope of the line and was able to describe it with the following equation:

$$\alpha_{ij} = k^{-1/n} P_i^{1/n} \qquad \text{Eq (2.29)}$$

in this equation, α_{ij} is the separation factor for the gas pair ij, P_i is the permeability of the more permeable component, k and n are constants specific to each gas pair; k has units of barrer and n is unitless. Robeson determined the values of these constants for each gas pair he studied. The results for gas pairs that are relevant to this study are listed below in Table 2-3.[39]

Table 2-3. The trade off curve k and n values for selected gas pairs.

Gas Pair	k (Barrer)	n
He/N_2	12500	-1.0242
He/CH_4	5002	-0.7857
He/O_2	4600	-1.295
O_2/N_2	389,224	-5.800
CO_2/CH_4	1,073,700	-2.6264

Robeson was able to correlate a trend between 1/n and the differences in the kinetic diameters' of the gas pair. He noted that kinetic diameter offered the best correlation compared to other dimensional measures (e.g. van der Waals volume, molar volume). The author noted that the correlation passed through the origin, which he believed verified his analysis. The trend is shown below in Figure 2-13 which was adapted from the Robeson's publication.[39]

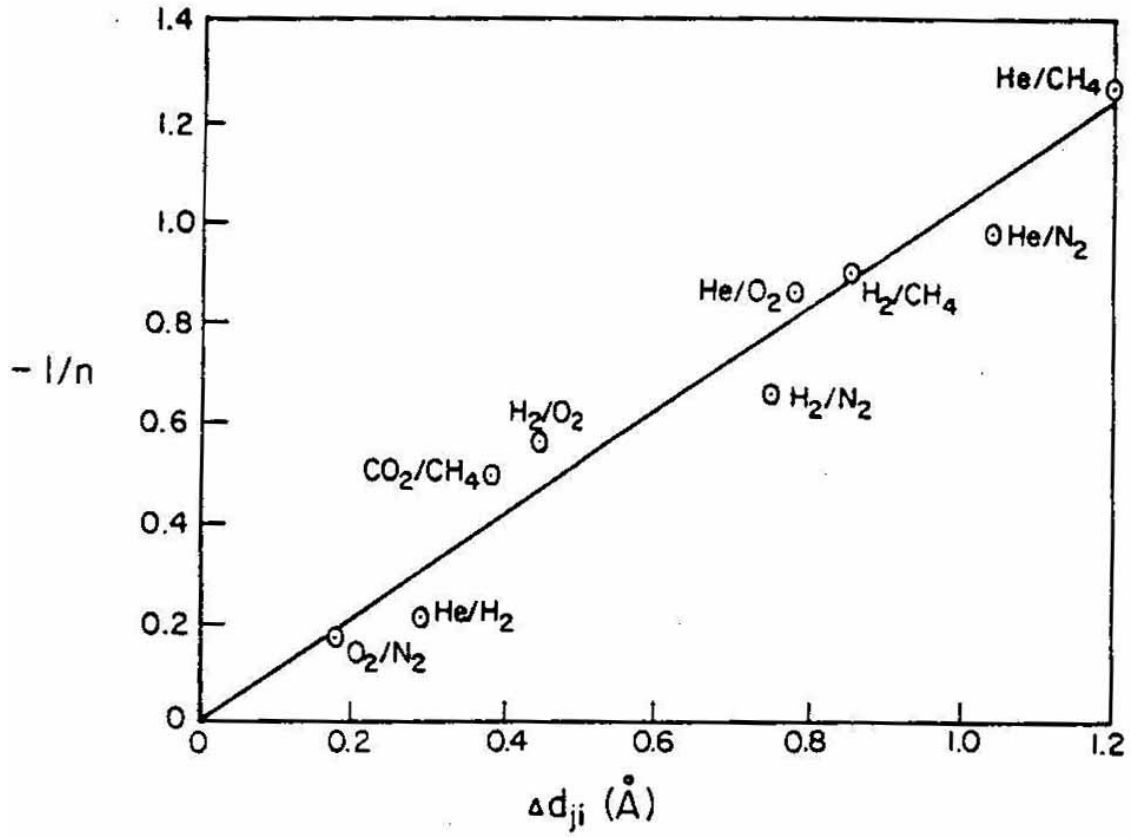

Figure 2-13. Relationship between n and the difference in kinetic diameter of a gas pair.

Robeson also noted that the large amount of recent data in his analysis resulted in a slight change in the position of the upper bound. When he removed the data from the most recent three years from his analysis, the upper bounds were all slightly lower. However, the slope of the upper bounds remained constant.

Work by Freeman expanded on that of Robeson, and looked to develop a theoretical justification for the presence and location of the observed upper bounds.[40] Freeman began with the equations Robeson developed, particularly Eq (2.29) and used models developed by others as outlined in the paper to modify them. His conclusions were that the separation factor of a polymer for a given gas pair (α_{AB}) can be expressed as:

$$\ln\alpha_{A/B} = -\lambda_{A/B}\ln D_A + \left\{\ln\left(\frac{S_A}{S_B}\right) - \lambda_{A/B}\left(b - f\left(\frac{1-a}{RT}\right)\right)\right\} \qquad \text{Eq (2.30)}$$

here, $\lambda_{A/B}$ is a parameter that depends only on the size ratio of the two gas species, D_A is the diffusion coefficient of gas A in the polymer, S_A is the solubility of A in the polymer (the notation is the same for B),a is a constant, b is a constant with units of cm^2/s, f is a constant which depends on the polymer and has units of cal/mol, R is the gas constant, and T is the temperature. The constant a was determined to have a value of 0.64, and is independent of polymer type.[41] The constant b has a value of 9.2 for rubbery polymers and 11.5 for glassy polymers.[42] The constant f varies in value from 0 for rubbery polymers and low performance glassy polymers to near 14,000 cal/mol for some polyimides.

Equation 2.30 highlights the impact of the diffusion coefficient on the separation factor. The solubility ratio will vary little from polymer to polymer, and $\lambda_{A/B}$, b, and a are constants for a given gas pair and polymer type. From this Freeman concluded that the diffusivity plays a more influential role in determining the location of the upper bound than the solubility.

The author also noted that his theory explained the presence of the same type of polymers near the upper bound. These polymers were typically designed with a high degree of backbone stiffness, possessed a high T_g, but also were designed to disrupt interchain packing and carried a large fractional free volume. This would increase the diffusivity and in turn the permeability. Specifically, the best polymers will have a large interchain distance so that the permeability is high, but not so large that the interchain distance grows to a point that the diffusion coefficients are no longer governed by thermally stimulated polymer segmental motions. One must recall that when a gas molecule diffuses through a polymeric membrane, it does so by a series of jumps. The jumps occur when the interchain distance between two polymer chains becomes temporarily larger than the size of the particle due to the thermally induced segmental motion of the polymer. This allows the gas molecule to jump through the opening. A series of jumps allows the polymer to reach the downstream face of the membrane. As the interchain distance becomes larger, a point will be reached where the interchain distance is larger than the size of the molecule. At this point, the gas molecule can diffuse between two chains without waiting for a thermal induced backbone motion to

open the distance between them more. At this point, the diffusion coefficients are no longer governed by thermally induced segmental motions of the polymer.

While adjusting the polymer structure may move the upper bound higher, the author noted that his results conclude that the slope will not be changed by characteristics of the polymer. The slope of the upper bound is determined by $\lambda_{A/B}$. This parameter is strictly a function of the size ratio of the two gases being separated.

Freeman mentions that unless methods to significantly enhance the solubility selectivities of polymers are discovered there is a limit to the gas separation performance of polymeric membranes. The point where the interchain distance between polymer segments grow so great that penetrants do not need segmental motion to diffuse will mark this limit. This threshold on interchain distance would depend on the sizes of the gas molecules one is attempting to separate. As stated earlier the slope of the upper bounds will not be affected by polymer structure. Therefore, to achieve more desirable permeability and selectivity in membranes, new materials which do not follow these rules will need to be developed.

2.6.3 Aromatic Polyimide Membranes

Aromatic polyimides have long been known for their impressive array of properties. As a whole, these types of polyimides have the ability to operate continuously at temperatures as high as 200 ^{o}C.[43,44] Additionally, these polymers can retain their excellent mechanical properties over a broad temperature range. These characteristics match those which are desirable in a gas separation membrane. As such, aromatic polyimides designed for gas separations have become the focus of many recent research efforts.[45-53]

When developing his upper bound for gas separations, Robeson noted that the membranes which lie near it are from the aromatic polyimide family.[39] It was observed by Kim et al. that unlike most polymers, polyimides are more permeable to N_2 than to CH_4.[54] This makes them ideal candidates for separating N_2 from natural gas streams. Freemen noted in his theoretical justification for the upper bound that polymers with rigid backbones and poor packing would provide the most selective and permeable membranes

when working with amorphous polymers.[40] These observations have become the driving motivation to develop new aromatic polyimides for gas separation applications.

Wind et al. developed polyimide membranes to perform important natural gas separations at high pressures.[55] The primary focus was on the CO_2/CH_4 separation, as some natural gas fields contain as much as 70% CO_2 and pressures up to 5000 psia. Furthermore, while most membranes have CO_2/CH_4 selectivities of 12-15, selectivities of 40 are needed for membranes to compete with other technologies such as amine scrubbing. The investigators looked to use polyimide membranes to meet these requirements. Polyimides offer good mechanical strength which should help in deal with high pressure environments. Furthermore, they are known to have good selectivity.

The authors looked at two polyimides: 6FDA-6FpDA-DABA, and 6FDA-DAM-DABA. In addition, these two systems were crosslinked separately using different diol compounds. This was done to investigate the effects of crosslinking on the permeability, selectivity and resistance to plasticization. The diols would react with the carboxylic groups in the DABA moiety to produce the network. An illustration of the repeat structures and the diol compounds is shown in Figure 2-14.[55]

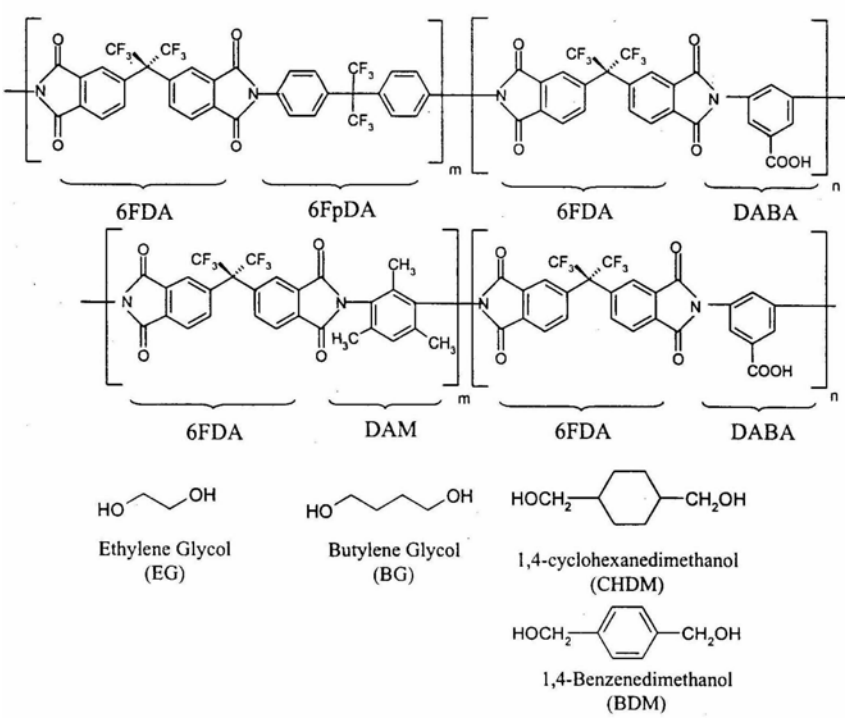

Figure 2-14. Repeat structure and the chemical structure of the diols adapted from [15].

The authors looked at 50/50 mixtures of CO_2 and CH_4 in order to determine the separation abilities of these membranes. A trend was noticed between the temperature at which cross-linking was performed and CO_2 permeability. The membranes cross-linked at 295 ^oC saw close to a four fold increase in permeability compared to the membranes which were cross-linked at 220 ^oC. The separation factor at 10 atm feed pressure of the higher temperature cross-linked membrane was much higher than its lower temperature cross-linked membrane counterpart (i.e. 39 to 31, respectively). However, as the feed pressure was increased up to 30 atm, the 295 ^oC membrane displayed a sharp linear decrease in separation factor eventually dropping to 30 at 30 atm. This was in stark contrast to constant separation factor of the 220 ^oC membrane over the same temperature range. The authors believed that cross-linking at 295 ^oC created more free volume due to the elimination of pendant diol groups, or by inhibiting chain packing.

The effects of annealing on 6FDA-DAM-DABA were also studied. Membranes were annealed at 130, 220, and 295 ^oC. Pure CO_2 permeabilities showed a drastic drop in the permeability with increasing annealing temperature. This was attributed to the reduction of free volume during annealing as the polymer chains were given more thermal energy to reorganize. The separation factors for a 50/50 CO_2/CH_4 stream were not very different at lower pressures. However, as the pressure was increased, the membrane annealed at 130 ^oC displayed a linear drop in selectivity. The membranes at annealed at higher temperatures showed a diminishing drops in selectivity as the pressure was increased. The authors believed this was a result of plasticization occurring in the lower temperature annealed membrane. This membrane would have a higher free volume, which would increase its CO_2 solubility. Based on the pure CO_2 permeation tests, the 130 ^oC membrane appeared to plasticize above 11 atm, while the higher temperature annealed membranes didn't show any signs of plasticization up to 25 atm.

The 6FDA-DAM-DABA polymer was exposed to mixed gas feeds of CO_2, CH_4, and either toluene or n-butane, in order to observe how this membrane would operate in an environment more representative of that found in natural gas fields. The focus was on the separation factor for CO_2/CH_4 at different pressures with these feed streams. The CO_2 permeability dropped slightly when comparing the pure gas permeability to that of the 50/50 CO_2/CH_4 mixture. However, when toluene or n-butane saturated the feed

streams, there was a dramatic drop in CO_2 permeability, roughly 20% at 4 atm feed pressure and becoming more severe at 11 atm (~60%). Drops in the selectivity of CO_2/CH_4 were present in toluene and n-butane feeds compared to the pure 50/50 feed. However, these were more linear with pressure, always showing ~10% decreases for n-butane and ~20% for toluene.

Matsumoto et al. performed an extensive investigation into the effect of the chemical structure on the gas permeation performance of aromatic polyimide membranes.[49,56] The authors prepared 17 different aromatic polyimides and characterized them using permeability studies, WAXS, and TMA. Several series of polyimides in which the same dianhydride monomer was used in the synthesis but the diamine was varied and vice-cersa were created to study the effects of the structure on the properties.

The dianhydride structures along with the structure of the amine they were reacted with are shown in Figure 2-15, which was taken from Matsumoto et al.[49] The authors noted that polyimides with the 6FDA monomer had higher permeability and selectivity than those using ODA, and diphenylsulfonetetracarboxylic dianhydride (DSDA). This was attributed to the $–CF_3$ groups in 6FDA which are not present in the other anhydride monomers. These groups break-up interchain interactions (i.e. charge transfer complexes) associated with aromatic polyimides, which leads to an increase in the free volume, and thus a higher permeability. WAXS studies also showed the polyimides with $–CF_3$ groups in their structure had larger intersegmental spacings than their nonfluorinated counterparts. The incorporation of these groups also increases the solubility of the polyimide. Fluorinated carbons in the polyimide's backbone increase the selectivity by hindering rotation. The $–CF_3$ groups are bulky compared to a $–CH_3$ group or an -O- linkage, and have a larger energetic barrier to rotation that the smaller groups. This adds more sieve like character to the polymer, reducing the size of the transient gaps it can create as a result of thermal energy. This mobility reduction is reflected in the T_g's of polymers as the 6FDA polyimides displayed higher T_g's than their ODA or DSDA counterparts.

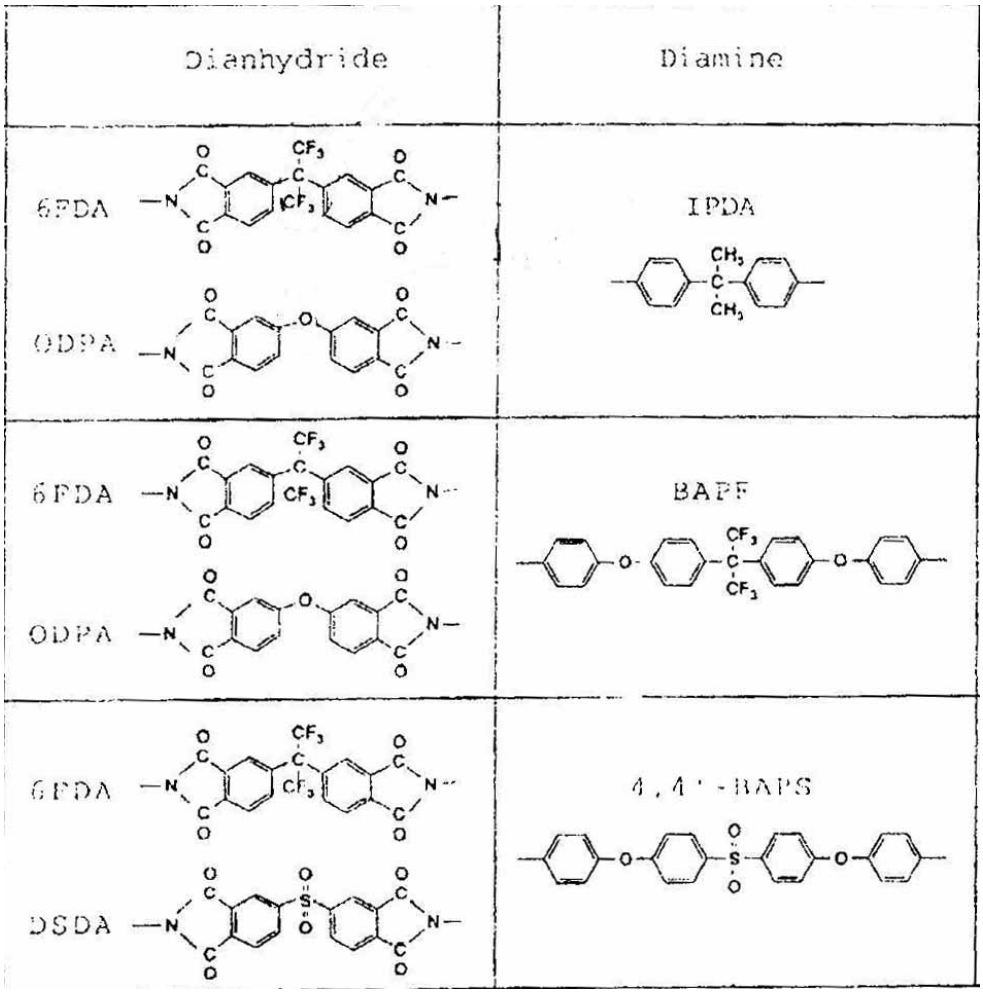

Figure 2-15. Dianhydrides and diamines used by Matsumoto et al; image adapted from reference 49.

The investigators repeated this type of experiment in which the diamine monomer used in the synthesis was varied while the anhydride was kept constant. The results were the same as those of the anhydrides: the addition of $-CF_3$ groups increased permeability. However, the permeability of these polyimides was lower than those of the 6FDA polyimides in which the diamine portion did not contain any $-CF_3$ groups. The authors concluded from this that the introduction of fluorine groups into the anhydride is more effective for permeability increases than introduction into the diamine part.

The authors also noted at trend between meta and para connected polyimides. Polyimides containing meta connections showed higher selectivity and lower

permeability than their para counterparts. This was explained by the inability of meta linkages to rotate about their primary axis, unlike para connections which can.

A similar study was conducted by Stern et al. in which series of polyimides were synthesized using 6FDA and pyromellitic dianhydride (PMDA) with varying aromatic diamines.[52] The structures of the monomers used in this study are shown below in , which was taken from Stern et al Figure 2-16.[52]

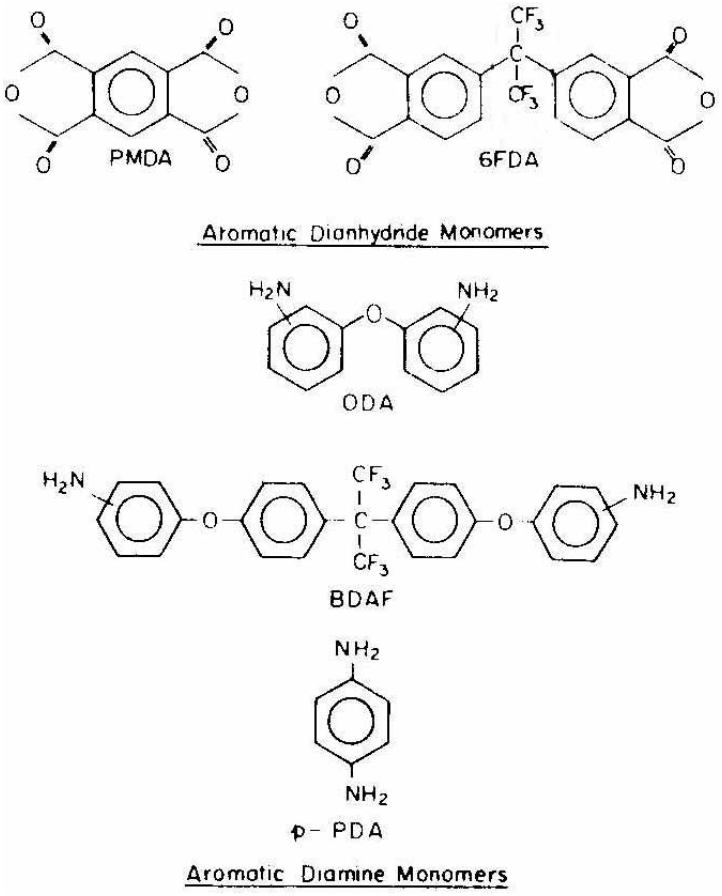

Figure 2-16. Monomers used by Stern et al; image from reference 51.

Permeability studies on the CO_2/CH_4 separation were performed for the 6FDA and PMDA polyimides; the selectivity factors were calculated from the pure gas permeabilities. The authors noted that the polyimides they tested outperformed many common polymers (e.g. polysulfone, polycarbonate, cellulose acetate) in terms of both permeability and selectivity. Additionally, they noted that the 6FDA polyimides

outperformed the PMDA polyimides as well. The authors attributed the better performance of 6FDA to several factors:

- The segmental mobility of 6FDA polyimides is likely lower than that of PMDA polyimides with the same diamines. The 6FDA monomer has –CF3 groups which inhibit chain mobility. Furthermore, the polyimides with 6FDA will possess a lower concentration of flexible -O- linkages compared to the PMDA. This lower concentration would lead to a higher selectivity
- The mean interchain distance (d) in 6FDA polyimides is larger than that of PMDA polyimides with the same diamines. The authors were able to determine this using WAXS. The larger d in 6FDA polyimides was attributed to the bulky $–CF_3$ groups its backbone. These groups also break-up interchain interactions (i.e. charge transfer complexes), which raises d. This would lead to an increase in permeability.
- The polar $–CF_3$ groups in the 6FDA polyimide backbones may induce specific interactions with some gas molecules, such as CO_2. This would lead to a solubility selectivity increase in these polyimides.

Within the same dianhydride family, the authors observed some trends that occurred with changes in the diamine monomer. For both dianhydride families the inclusion of a diamine which increased permeability also lowered the selectivity of the resulting polyimide. The authors noted that the permeability of polymers containing the same diamine chemical structure, but in which the diamine is changed from meta to para, increases. For example, WAXS studies of PMDA-m-ODA and PMDA-p-ODA showed no difference in d between the two polyimides. However, PMDA-p-ODA has a permeability about twice that of PMDA-m-ODA. The authors believed that the diamine moiety in the para connected polyimide could rotate around its -O- linkage, whereas the meta linkage could not. This flexibility around the oxygen linkage increased the permeability. The authors also cited work by Pavlova et al. which showed that para connected aromatic rings can rotate freely, while meta connected aromatic rings can not.[57]

T.H. Kim et al. performed a similar investigation on aromatic polyimide structure and its affects on permeability.[58] Their investigation involved synthesizing aromatic

polyimides using the PMDA and 6FDA anhydrides. These anhydrides were reacted with several different diamines to study the effects of structural changes on the separation properties of the membranes. The diamines employed were ODA, methylenedianiline (MDA), and isopropylidenedianiline (IPDA). The resulting structures and the names of the repeat units are shown below in Figure 2-17, which was taken from Kim et al.[58]

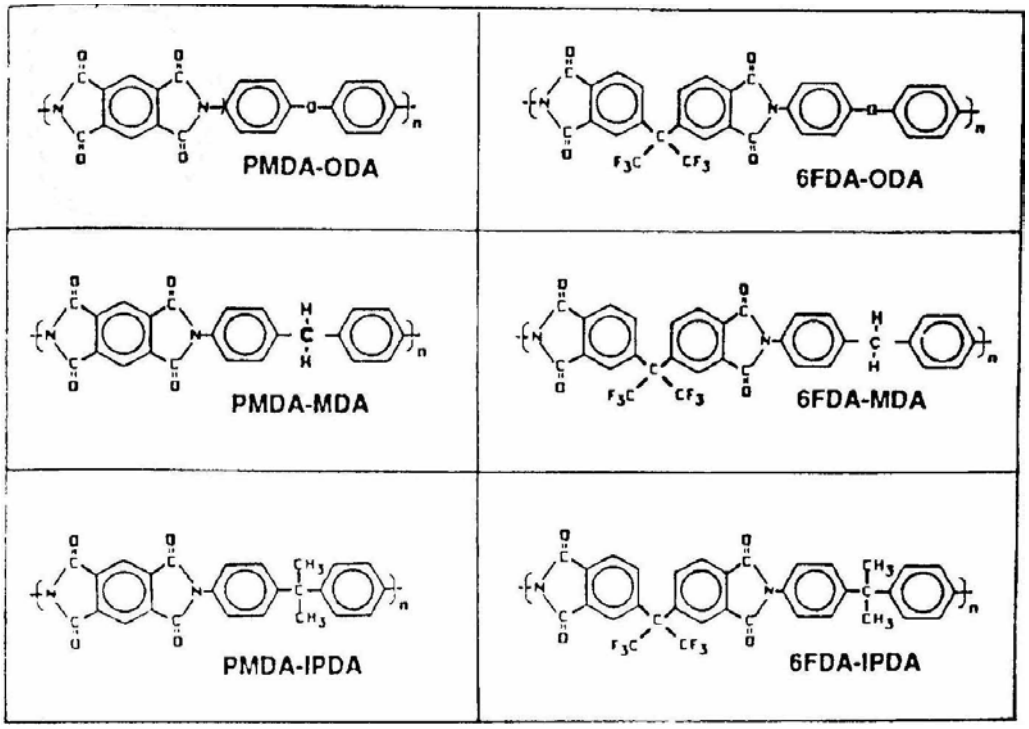

Figure 2-17. Repeat structures of the polyimides used by Kim et al; image from [58].

The authors noted within the PMDA series of polyimides, the general trend of higher permeability at the expense of lower selectivity was realized. They also noted that the separation of gases in this series depends strongly on diffusivity selectivity and is not strongly related to solubility selectivity. As the central moiety of the diamines was varied from -O- to $–CH_2-$ to $–C-(CH_3)_2-$, intersegmental packing and intrasegmental mobility were restricted. The measured densities and intersegmental spacings (obtained from WAXS) correlated well with the permeability results. PMDA-ODA had the highest density, smallest d-spacing, and the lowest permeability. PMDA-IPDA had the lowest density, largest d-spacing and the highest permeability. The authors observed that

changing the diamine moiety was more effective in effecting the permeability of the larger penetrants (e.g. N_2, CH_4) than it was for effecting the permeability of the smaller components (e.g. He, CO_2). For example, the permeability of CO_2 increased 990% within the polyimide series, but the CO_2/CH_4 selectivity fell 35%.

The investigators compared each member of the PMDA series to its corresponding 6FDA polyimide. 6FDA-ODA showed increases in permeation of roughly 600% for He and CO_2 with approximately the same separation factor for CH_4 when compared to PMDA-ODA. Because PMDA is flat and rigid unlike 6FDA, it was believed the neighboring PMDA chain segments should pack more efficiently, resulting in a poorer ability to execute motions leading to gas molecule diffusion. The introduction of 6FDA is believed to cause increases in packing. WAXS studies supported this, as the d-spacing increased when PMDA was replaced with 6FDA. The selectivity increases are believed to be a consequence of two factors. First, $-CF_3$ groups are bulky and believed to reduce the mobility of the polyimide backbone. Secondly, for a given molecular weight of polymer, when 6FDA replaces PMDA, the flexible linkage in the diamine (e.g. –O-) is decreased. For example, comparing 6FDA-ODA to PMDA-ODA, there is a reduction of 40% per volume in the number of flexible –O-linkages. This makes the 6FDA polyimides more selective while the increased d-spacings improve the permeability.

The permeability results of the 6FDA polyimides were promising. This series of polymers showed an increase in permeability of small penetrants like He and CO_2, with no loss or an improvement in selectivity from CH_4, when compared to the PMDA series. In some cases the 6FDA series saw decreases in the permeabilities of N_2 and CH_4. From these experiments the authors concluded that the structural changes in a polymer's backbone which include adding groups which open the polymer matrix while restricting segmental mobility may be the most effective route for developing highly permeably and selective membranes.

J.H. Kim et al, added fluorinated alkyl side groups into a series of polyimide and compared their permeation properties with those of the polyimides without the side groups.[59] A series of four polyimides including were synthesized; each series contained a polyimide with a fluorinated alkyl side chain and one without the side chain. The monomers used were PMDA, 6FDA, ODA, and 3,3',4,4'-benzophenone tetracarboxylic

dianhydride (BTDA). Two diamines were used: 2-(perfluorohexyl)ethyl-3,5-dinitrobenzoate (PFDNB) and m-phenylene diamine (m-PDA). The structures of these monomers are shown below in Figure 2-18, which was taken from Kim et al.[59]

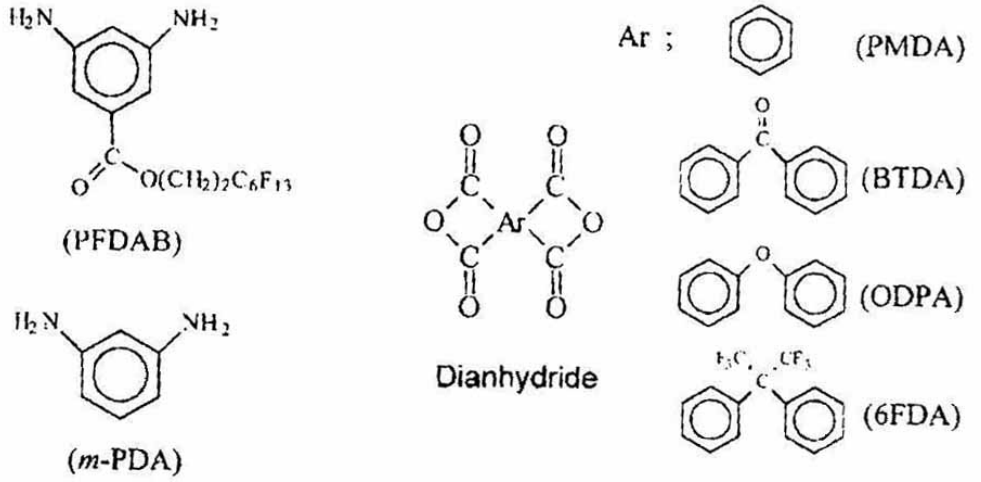

Figure 2-18. Monomers used by Kim et al in a second study of aromatic polyimide membranes. The image was adapted from reference 59.

The permeability studies on these polyimides showed the general trend of the smaller the penetrant size, the higher its permeability. Between fluorinated side chain and nonflourinated side chain membranes, the fluorinated side chain membranes displayed large increases in permeability, in some cases up to ~250%, but these gains were mitigated with losses in selectivity.

The authors performed other characterization experiments to help explain the observed permeation results. Differential scanning calorimetry (DSC) was used to determine the T_g's of the polyimides. In all cases the incorporation of the fluorinated side chain led to a drastic decrease in the observed T_g value, typically between a 85-100 ^oC drop. The fractional free volume (FFV) of each polymer was calculated as well. In this case, the fluorinated polymers always had a higher FFV than their nonfluorinated counterparts. The authors believed that the fluorinated side groups disrupted pakcing due to their bulky nature, thus resulting in a higher FFV, lower T_g, and higher permeability.

Moe et al. studied the effects of film history on the gas separation performance of a fluorinated aromatic polyimide.[60] The authors studied a rigid polyimide chain composed of the 6FDA dianhydride and 1,5-diaminophthalene. Membranes were made from a 20 wt % polyimide in dimethyl acetamide (DMAC) which was cast onto a hot plate at 100 ^{o}C and drawn with a doctor knife. Some of the membranes were taken through an addition step involving annealing step which involved being heated to a temperature of 240 ^{o}C for 6 hours.

Pure gas permeability experiments were performed on both types of membranes. Interestingly, the helium permeability was roughly 50% higher in the annealed membrane compared to the unannealed membrane. However, CO_2 permeability was roughly 50% lower in the annealed membrane compared to the unannealed membrane.

Fourier transform infrared spectroscopy (FTIR) was used to determine if any residual DMAC was present in the membranes. Spectra of the unannealed membrane showed a peak at 2950 cm^{-1} which was not present in the annealed film's spectrum. The spectrum of DMAC shows a peak in this area, suggesting some was still present in this film. DSC scans were taken of the two films as well. The unannealed scan showed a broad peak in the region of 80-100 ^{o}C; this peak was visible as well in the annealed sample, but it was much smaller. For each sample, after the first heating cycle, the films were cooled and reheated two more times. The peak never reappeared, suggesting that it may have been the result of residual solvent being driven off.

The authors believed these results could be explained by an antiplasticization effect driven by the presence of residual solvent. At low levels (i.e. post annealing) solvent molecules may actually stiffen the polymer chain and retard segmental motions. In addition, they have been observed to decrease solubility. However, as the concentration of solvent is increased (i.e. pre annealing), the amount of solvent is sufficient enough to plasticize the polymer, resulting in an increase in permeability.

2.6.4 6FDA-6FpDA and 6FDA-6FpDA-DABA Polyimide Membranes

Rigid aromatic polyimides have offered the best separation performance of polymeric membranes as reported by Robeson and Freeman.[39,40] Within this group of

polymers, polyimides synthesized from 2,2'-Bis(3,4-dicarboxyphenyl)hexafluoroporpane dianhydride (6FDA) have shown both high permeability and high selectivity relative to other polyimides. These improvements in performance were discussed in the Aromatic Polyimide Membrane section.

The monomer 6FDA can be reacted with 4, 4' – hexaflouroisopropylidene dianiline (6FpDA) and heated to form a fluorinated aromatic polyimide called 6FDA-6FpDA.[44,61,62] The repeat unit's structure of this polyimide is shown below in Figure 2-19.

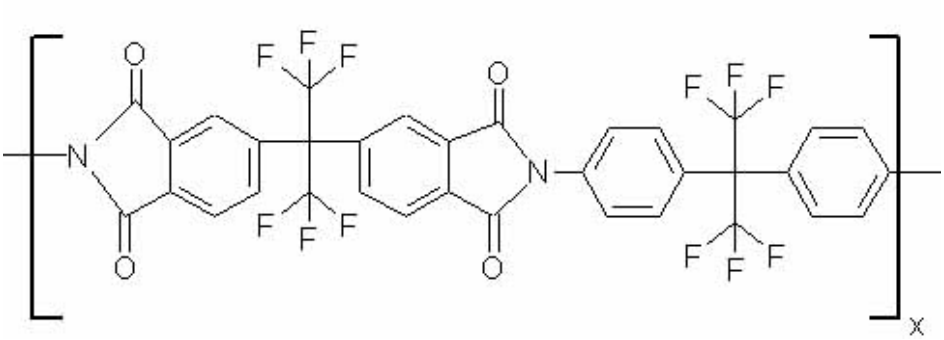

Figure 2-19. 6FDA-6FpDA Repeat Unit.

The stoichometry of the reaction can be controlled such that the ends of this polyimide are anhydride terminated. When this is the case, the anhydride ends can react with 3,5-diaminobenzoic acid (DABA). This has the effect of linking 6FDA-6FpDA chains together and thus achieves a higher molecular weight. This polyimide is referred to as 6FDA-6FpDA-DABA; its repeat structure is shown in (Figure 2-21). Additionally, the resulting polyimide had carboxylic functional groups integrated into its backbone, which can be used in a variety of reactions which will be discussed shortly. The repeat structure of the polyimide is shown below in Figure 2-20.

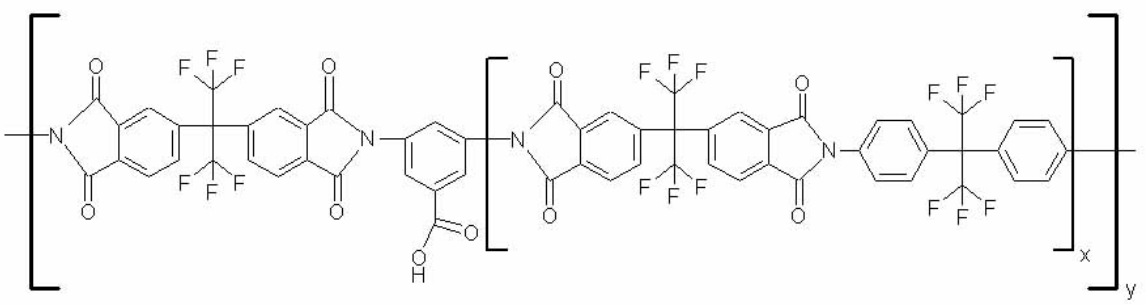

Figure 2-21. 6FDA-6FpDA-DABA Repeat Unit.

This section is devoted to reviewing publications in which 6FDA-6FpDA and 6FDA-6FpDA-DABA were studied.

Kawakami et al. developed an asymmetric membrane with an ultrathin and dense selective surface skin layer composed of 6FDA-6FpDA.[63] The membrane was created using a dry-wet-phase inversion process. In this process 6FDA-6FpDA was dissolved in a trisolvent system including methylenechloride, 1,1,2-trichloroethane, and butanol. The solution was cast onto a glass plate and smoothed with a doctor blade with the gap set to 250 μm. The film was allowed to air dry for ~ 10 minutes. Then it was coagulated in methanol, allowed to air dry, and dried under vacuum at 150 ^{o}C for 15 hours to remove residual solvent. Using this process the authors were able to fabricate asymmetric membranes with skin layer thicknesses varying from 10 – 200 nm.

The permeation results for the CO_2/CH_4 separation showed that the selectivity increased as the skin layer thickness decreased. At a skin thickness of ~150 nm the selectivity for this separation was 34, but as the thickness was decreased the selectivity increased, eventually reaching 43 at a thickness of 30 nm. The authors believed that during annealing thinner skin layers may form more packed structures easier than thicker ones, leading to a more selective layer.

Niwa et al. performed research which was an extension of this work.[64] In this study the effects of the shear rate resulting from the speed at which the doctor blade was pushed across the polymer solution were investigated. Four membranes were fabricated, each at a different shear rate using the same method as Kawakami. SEM and AFM were employed to determine if shear rate influenced the surface morphology and structure of each membrane. Cross sectional SEM images of the asymmetric membranes were taken

and showed that as the shear rate was increased, the membrane structure changed from sponge-like structure to a structure with a thin skin layer supported by a sponge-like structure with finger-like voids. The skin layer thickness decreased as the shear rate increased. AFM surface images of the membranes at low shear rates showed surfaces covered by nodular aggregates, while at higher shear rates the surfaces were covered by nodules. The authors attributed these results to the exchange rate of solvent and nonsolvent in the phase separation process which is affected by shear rate.

To determine if there was any orientation induced by the shear rate, FTIR spectra of each membrane were gathered. Two spectra were gathered per membrane, and they were taken at angles perpendicular to each other. The differences in absorbance of band would indicate an orientation. The lower shear rate membranes showed no difference in their two spectra. However, at the highest shear rate, there was an absorption difference between the two, indicating the skin layer was oriented. The authors believed the high shear rate was enough to orient the chains, resulting in this absorption difference.

Permeation experiments were conducted, and showed increasing permeability with shear rate. Additionally, the selectivity increased for both the O_2/N_2 and CO_2/CH_4 separation as the skin layer thickness decreased. The authors believed that the permeability increased with shear rate, because of the introduction of finger–like voids and the thinning of the dense selective layer were associated with the shear rate. The selectivity increase with shear rate was thought to be a result of the orientation that accompanies the skin layer as the shear rate was increased.

Mikawa et al. performed studies to determine the effects of molecular weight on separation performance of these membranes.[65] Additionally, they wanted to observe this material's gas permeation stability over longer periods of time. The membranes were prepared using the same procedure as Kawakami.[63]

To study the permeation stability of 6FDA-6FpDA membranes, four membranes of this material were prepared with different skin thicknesses. The M_w for all membranes was 200,000 g/mol. The investigators gathered pure O_2 permeability data for each membrane 20 times at one pressure, then increased the pressure and performed the experiment again. They did not observe a change in permeability at a pressure

throughout the 20 runs, regardless of skin layer thickness. The same results were reached for pure N_2 and pure CH_4 permeation experiments.

Carbon dioxide permeability measurements were gathered for the four membranes as well. For skin thicknesses greater than 1000 nm, no changes in CO_2 permeability with pressure observed. However at the thinner thicknesses, plasticization effects were observed at 10 atm feed pressure. The authors believed that CO_2 swelled the dense skin layer and enhanced its permeability. To study any changes in confirmation solid state ^{13}C-NMR spectroscopy was employed. The results indicated that there were conformational changes centered on the sp^3-carbons which are connected to the $–CF_3$ groups. The authors also suggested that these results indicated that plasticization only occurs in 6FDA-6FpDA when enough CO2 absorbs into the polymer to create large motions of the $-CF_3$ groups.

Lastly, the authors looked at the effect of M_w on the permeation of the membranes. Pure CO_2 permeability measurements at a range of feed pressures showed that permeability was inversely related to the Mw of the polyimide. However, the lower molecular weight membranes plasticized, whereas the higher molecular weights did not. Density measurements on these membranes showed indicated that the density scaled with the molecular weight. From this it was concluded that the side groups in the higher molecular weight 6FDA-6FpDA membranes are unable to undergo large molecular motions due to the presence of a more packed structure.

Staudt-Bikel et al., studied the ability of 6FDA-6FpDA membranes to separate olefins/paraffin mixtures.[66] The authors looked at the ability of this polyimide to separate ethane/ethylene mixtures and propane/propylene mixtures. For both gas pairs the olefin was more permeable than the paraffin across the pressure range tested (i.e. 2-15 atm). While no plasticization effects were observed for ethane and ethylene, propylene began to plasticize the membrane at a feed pressure of 5 atm; propane plasticized the membrane at a slightly higher pressure.

Sorption experiments for all gases in 6FDA-6FpDA were performed. For both pairs, the paraffin sorped more strongly than the olefin, however the differences were small, except at higher pressures for ethane/ethylene. From this the authors concluded that 6FDA-6FpDA separates mainly on diffusivity selectivity.

The investigators gathered mixed gas permeation data for the mixtures. The feed streams were composed of 50:50 olefin:paraffin. For the ethylene/ethane mixture a constant selectivity of 3.2 was observed across the feed pressure range, which was ~20% lower than the ideal selectivity values. For the propylene/propane mixture, the idea selectivity was constant at 16, but the selectivity was ~20% below this, and dropped drastically as the feed pressure was increased. This was a consequence of the plasticaztion by the feed stream.

Finally, the authors looked at how 6FDA-6FpDA performed at two different temperatures: 298 K and 308 K. For the ethylene/ethane separation the pure gas permeabilities experiments showed that the permeability and ideal selectivity were increased. However, for the propylene/propane pure gase permeation tests, there is a loss in selectivity with no change in permeability. The authors had difficulty explaining these results. They noted that they were not entirely in agreement with reports from other groups. They suggested that the discrepancies may be attributable to the differences in preparation of the membranes between the studies.

The authors performed a separate investigation studying the effects of crosslinking polyimdes.[67] It was hoped that by adding crosslinks to the polymer matrix, resistance to plasticization and an increase in selectivity would be achieved without a sacrifice in permeability. This investigation looked at substituting DABA groups into the polymer backbone. These groups were added for their ability to be crosslinked through their –COOH groups with ethylene glycol. The targeted separation was the CO_2/CH_4 separation. Additionally, m-phenylene diaminel (mPD) was substituted for 6FpDA as the diamine used in the synthesis of the polyimide.

The authors synthesized several polyimides: 6FDA-mPD, 6FDA-mPD/DABA with a 9:1 ratio of mPD/DABA, and 6FDA-DABA. The T_g's of the polyimides were 578 K, 643 K, and 727 K, respectively. It was presumed that the addition of DABA introduced hydrogen bonding into the systems. As the amount of DABA increased, the affect on T_g became more pronounced.

Pure gas permeation studies showed that there was a drastic drop for both CO_2 and CH_4 with the introduction of DABA into the polymer's backbone. The authors believed due to hydrogen bonding, the matrix became "tighter", thus reducing diffusion

of gas molecules. Both pure gas permeabilities fell by ~40%, but CH_4 slightly more than CO_2. This lead to an increase in ideal selectivity from 58 to 65. Interestingly, as the 6FDA-mPD/DABA was crosslinked with ethylene glycol, the permeability rose for both gases by ~30. The ideal selectivity dropped slightly from 65 to 63. The authors attributed this to the introduction of "space" between the polyimide chains due to the ethylene glycol. This provided an increase in free volume to produce the higher permeability. The 6FDA-DABA polyimide was crosslinked and its permeation was determined as well. It offered the highest permeability, except for the pure 6FDA-mPD, and outperformed every membrane in terms of selectivity with a value of 87. The authors attempted to explain this by claiming the removal of mPD and the high degree of crosslinking in this system, provided an increase in free volume relative to the other polymers. However, the distribution of the free volume was in sizes that favored smaller molecules such as CO_2 and not CH_4.

These membranes were subjected to CO_2 at elevated pressures to determine their resistance to plasticization. 6FDA-mPA plasticized at a feed pressure of 5 atm, while 6FDA-mPA/DABA plasticized at a pressure of 15 atm. The elevated plasticization pressure was attributed to the hydrogen bonding. When the 6FDA-mPDA/DABA was crosslinked, no sign of plasticization was observed at pressures up to 35 atm; the same was true for the crosslinked 6FDA-DABA membrane. From this the authors concluded that crosslinking rigid aromatic polyimide's can lead to more durable membranes with better selectivity and roughly the same permeability as their noncrosslinked counterparts.

Wind et al. followed up this work by investigating the effects of crosslinking on a different system.[68] The investigators looked at an aromatic polyimide with two repeat units. One was 6FDA-DABA, the second repeat unit was formed from the reaction of 6FDA and diaminomesitylene (DAM). The resulting polymer was named 6FDA-DAM:DABA and possessed a 2:1 ratio of DAM:DABA. This polymer was crosslinked using three different linkers: ethylene glycol, butylenes glycol, 1,4-cyclohexanedimethanol.

Pure CO_2 permeability experiments were taken to determine if crosslinking altered the plasticization pressure, and if the crosslinker influenced this point. The uncrosslinked 6FDA-DAM:DABA polymer had the highest permeability, but it

plasticized at a feed pressure near 26 atm. When this polymer was crosslinked using any of the crosslinkers, the plasticization pressure increased to ~37 atm, and the permeability decreased. When ethylene glycol was employed, the permeability relative to the uncrosslinked polymer dropped by roughly 20%. Butylene glycol and cyclohexanedimethanol crosslinking resulted in drops of 66% and 80%. When 50:50 CO_2/CH_4 feeds were used, the crosslinked membranes showed small increases in selectivity relative to the uncrosslinked 6FDA-DAM:DABA, but again showed large drops in permeability.

The authors determined the dual mode sorption parameters to help explain what were the driving factors for these changes. A 6FDA-DAM:DABA membrane was crosslinked with butylene glycol at two temperatures: 100 ^oC, and 295 ^oC. At 100 ^oC there is almost no crosslinking, however, at 295 ^oC there is significant crosslinking. From sorption measurements, it was discovered that crosslinking leads to higher sorption. When the dual mode adsorption parameters were determined, it was shown that as the polymer was crosslinked, its Henry's constant decreased, but its Langmuir capacity constant increased. Physically, this means that crosslinking lead to an increase in unrelaxed free volume, however, the segment packing wasn't increased. With these results the authors concluded that a key step to controlling plasticization is not to control the sorption, but the swelling.

Wind et al. performed a second study focusing on crosslinking 6FDA-6FpDA-DABA to prevent plasticization from CO_2.[69] Ethylene glycol was used as the crosslinking agent. Without crosslinking this polyimide plasticized at a pressure near 150 psia, however, when crosslinked the plasticization pressure was raised to ~450 psia. Pure CO2 sorption isotherms were gathered for the two membranes. At pressures below 150 psia, the two isotherms were very similar. However, above this pressure the two isotherms deviated as the uncrosslinked membrane showed a higher concentration of sorped CO_2. Determining the dual-mode sorption parameters showed the same relationship as the authors found in their previous work. The Henry's constant dropped with crosslinking, but the Langmuir capacity constant increased.

When a 50:50 CO_2/CH_4 mixed gas feed was applied, the crosslinked membrane displayed a higher selectivity. This was true across a broad range of pressures. The

selectivity did decrease with increasing feed pressure for both membranes. The rate of decline of selectivity was the same for both membranes.

Cornelius et al developed and characterized a series of 6FDA-6FpDA polyimides that differed by their molecular weights.[70] The M_ws of the polyimides ranged from 39,000 – 82,000 g/mol. The researchers noticed that the permeability of all gases tested increased as the molecular weight increased. Additionally, the larger molecule the larger the increase in permeability. Analysis of D and S showed they both increased with molecular weight as well. The authors suggested that because these trends increased with molecular weight they could be due to packing defects. Additionally, the free volume of these polyimides was expected to increase with molecular weight, and would explain the increases in D and S.

2.6.5 Poly(imide siloxane) Block Copolymer Membranes

Polyimides exhibit many desirable properties as discussed earlier, however, polyimides still possess disadvantages that can limit their usefulness. Some polyimides become insoluble upon imidization drastically reducing their processability. More specific to gas separation applications, polyimides typically possess a high modulus and a low permeability to many gases. Additionally, the flexibility of a polyimide is often less than that of other polymer families.

To address these and other issues, polyimides have been synthesized which include siloxane blocks in their backbone. These copolymers are referred to as poly (imide siloxanes). Polydimethylsiloxane (PDMS) is likely the most often used siloxane oligomer for the construction of these copolymers. PDMS offers several attractive properties:[44]

- Low temperature flexibility
- Ultraviolet radiation resistance
- High permeability
- Low viscosity for a given molecular weight
- High compressibility
- Broad service temperature range due to its low T_g

- Thermal and oxidative stability

Typically, the addition of siloxane oligomers into the polyimide's backbone offers improvements in processability, toughness, flexibility, adhesion, and permeability. The drawbacks are some losses in thermal and thermooxidative stability relative to the pure polyimide.

This section of the Literature Review focuses on poly(imide siloxanes). A review of the studies most closely related to the work done in this investigation will be discussed. Due to how broad a topic this is, it is not practical to attempt to cover all aspects of this subject. The reader is referred to other references for further information on this subject.[71-73]

Nagase et al, investigated the permeability properties of poly(imide siloxane) copolymer membranes, in which the PDMS segment was grafted onto the polyimide backbone.[74] The investigators reacted pyromellitic dianhydride (PMDA) with 2-(3,5-diaminophenyl)ethyl-terminated dimethylsiloxane. The degree of polymerization of the PDMS branch was varied in this study from 4.5 up to 22. This block was combined with a second block synthesized from (PMDA) and one of six different aromatic diamines. The resulting copolymers varied in PDMS wt % from 40-74%. These copolymers retained the polyimide's insolubility in organic solvents such as THF despite the wt % of PDMS. Additionally, DSC studies showed only one T_g for the series of grafted copolymers, except when the degree of polymerization of the PDMS chain was 22.

Permeation studies revealed that the copolymer permeabilities were far higher than that of the pure polyimide, and on the same order of magnitude as PDMS. Furthermore, while the order of permeability in the pure polyimide was $P_{H2} > P_{CO2} > P_{O2} > P_{N2} > P_{CH4}$, the order in the copolymer membranes was $P_{CO2} > P_{H2} \sim P_{CH4} > P_{O2} > P_{N2}$. In particular, the methane permeability increased five orders of magnitude from the polyimide to the copolymers. PDMS is knows to have a high permeability for CH_4 unlike most polyimides. The authors suggested this may be evidence of a continuous PDMS phase.

Nagase et al. also investigated the performance of one copolymer in pervaporation applications. Looking at mixtures of water and common organic solvents, such as THF, acetone, and ethanol, the compositions of the feed stream and permeate stream were

measured. The selectivity (solvent/water) of the copolymer was 5.14 for ethanol, 12.4 for acetone, 15.7 for acetonitrile, and 56.5 for THF. The copolymer did not swell during the experiments, which would be typical of a PDMS membrane. The authors concluded that these poly(imide siloxane) graft copolymers could be used as highly durable membrane material to separate different kinds of organic liquid mixtures.

Lai et al. studied the physical properties of poly(siloxane imide) membranes that were synthesized by a step growth reaction using PMDA, 4,4'-oxydianiline (ODA), and amine-terminated PDMS.[75] The wt % of PDMS in the copolymer was varied from 0 – 92.0%. Additionally, the copolymers were synthesized using different M_n's of the PDMS block including 720, 1130, and 2130 g/mol.

The authors then characterized the morphology and mechanical properties of these membranes. Their results showed that at 15 wt % loading of PDMS, no matter what its length, the WAXS patterns were very similar to that of the pure polyimide. However, as the PDMS content increased, a crystal peak began to appear at 35 wt % PDMS. The authors offered a possible explanation. They suggested that the polyimide had a lower interchain distance (d) than the PDMS. When PDMS was incorporated into the backbone, it behaved as a spacer and increased d. This also increased the flexibility of the backbone, and allowed it to organize to form a regular structure. As a result, this regular arrangement of PDMS in the copolymer increased the crystallinity.

The investigaters performed tensile strength measurements on the polyimide and copolymers. They found that the elongations increased, and the tensile strength decreased as the PDMS content increased. This was a consequence of the flexible nature of PDMS. Furthermore, at the same wt % PDMS, the shortest siloxane length had the highest elongation and lowest tensile strength when compared to the longer siloxane lengths.

To determine the ability of these membranes to operate in a high temperature environment, thermogravimetric curves were gathered for the polyimide and the copolymers. The results indicated that the initial decomposition temperature of the copolymers decreased with increasing PDMS content. The authors attributed this to the dissociation of the Si-C bond which links the PDMS oligomer to the aromatic polyimide. The weight loss of the initial decomposition also increased with increasing PDMS

content. From this the authors concluded that the lower the PDMS content, the higher the thermal stability.

The thermal stability tests also was performed on copolymers with the same wt % PDMS, but with different PDMS oligomer lengths. These results showed that the longer the PDMS oligomer, the higher its thermal stability. This can be accounted for in that the lower temperature dissociating Si-C bonds will be reduced in number as the oligomer size is increased.

For all copolymers and the pure polyimide, the first onset of thermal degradation began above 400 ^{o}C in a N_2 atmosphere. The authors believed this made the copolymeric membranes suitable for high temperature gas separations.

In a separate publication, Chen et al. investigated the effect of PDMS content and the length of the incorporated PDMS on the microstructure and gas permeability of the poly(imide siloxane) copolymers.[76] The investigators synthesized their copolymer through a step growth reaction using PMDA, ODA, and amine-terminated PDMS; for this study, the PDMS oligomer was used with two M_n of 900 and 1680 g/mol. The films were made in the same manner as before. [75]

In all cases, the gas permeabilities of O_2 and N_2 were higher in the polyimidesiloxanes than in the polyimides. Additionally, in all cases the selectivities of the copolymers were lower than the polyimides. By determining the diffusion coefficients and solubility coefficients for each gas in each polymer, the authors were able to show that polymers were diffusivity selective rather than solubility selective.

Permeation experiments were also performed at elevated temperatures, up to 125 ^{o}C, and elevated pressures, up to 9 atm. A trend of decreasing selectivity and increasing permeability as the temperature was raised was observed. There was no changer in permeability with feed pressure for any of the membranes.

Tsujita et al. performed a study on poly(imide siloxane) membranes with varying PDMS contents which looked at permeability and dynamic viscoelasticity and CO2 sorption.[77] The general reaction used to synthesize the copolymers is shown in Figure 2-22; image taken from [77].[77] Copolymers of 10, 20 and 20 wt % PDMS were synthesized, and the average degree of polymerization of the PDMS oligomer was 7.6.

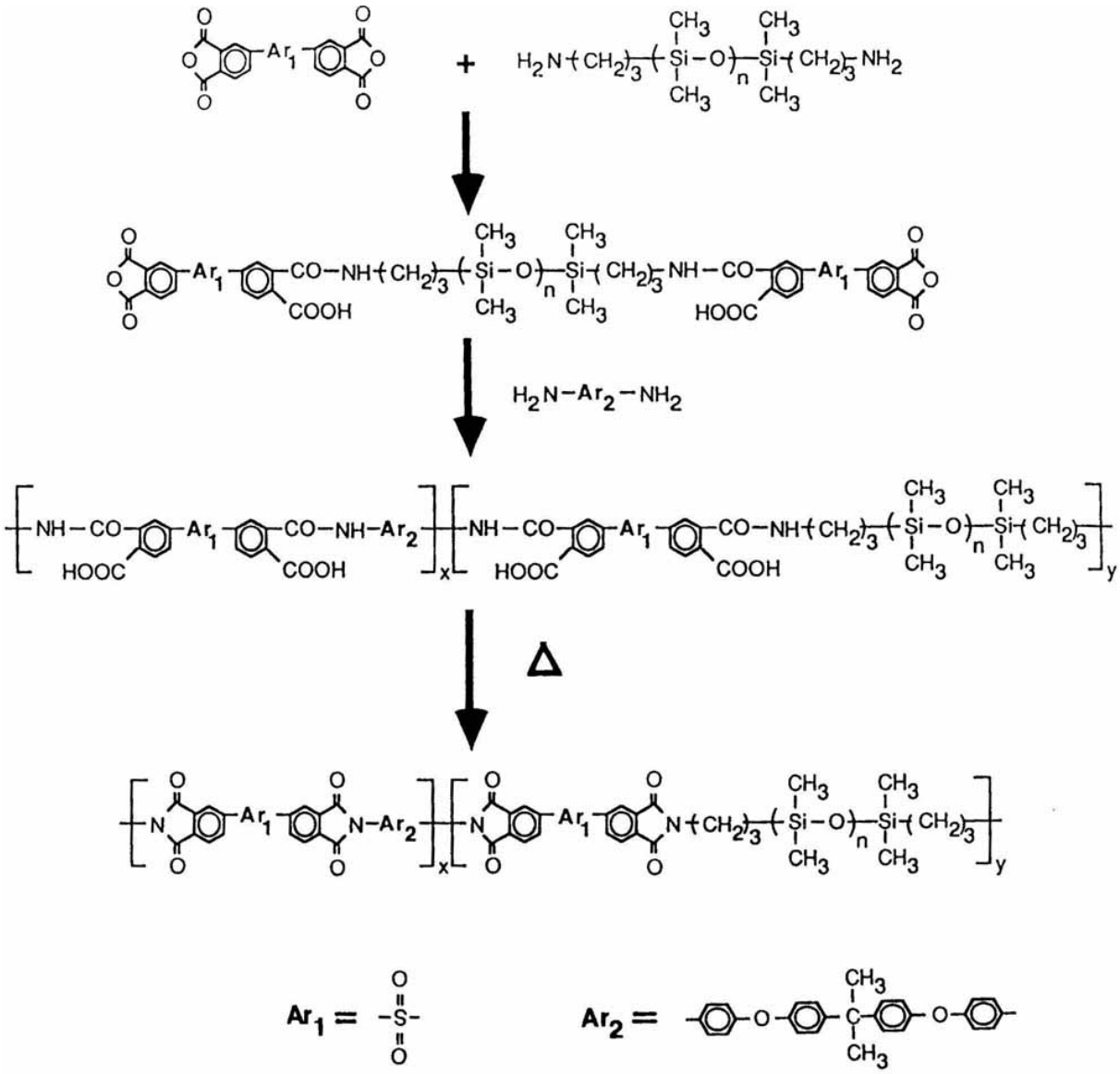

Figure 2-22. Synthesis scheme for the poly(imide siloxanes) performed by Tsujita et al.

The authors measured the shear modulus (G') and the loss tangent (tan δ) for the polymers. Two peaks in tan δ were observed in the copolymers, while only one peak was observed in the pure polyimide. These tests were also performed on the polyamic-acid precursors of the polyimide film. The presence of two peaks At 20 wt % PDMS indicated to the authors that the copolymers possessed microphase separated structures. The observed T_g's for the films are listed below in Table 2-4.[77]

Table 2-4. Glass transition temperatures of the polyamides, the polyimides, and the poly(imide siloxanes) used in the study by Tsujita et al.

Polymer	T_g (^oC)
Polyamic Acid	132.5
Polyimide	268.4
20 wt % PDMS- Polyamic Acid	-118.0, 133.7
20 wt % PDMS- Polyimide	-106.6 217.5

CO_2 sorption experiments at 25 ^oC were also performed on all the polymers in the study. The authors reported a clear trend that CO_2 sorption increases with imidization, and decreases with PDMS content. This observation is consistent with the dual-mode sorption theory as outlined in Solubility Section of the Literature Review. The equation to calculate the concentration of a gas in a membrane was shown in Eq (2.16). In that equation a parameter C'_H referred to as the Langmuir capacity parameter was present, and the concentration of the gas was directly proportional to this parameter. C'_H was shown to go to zero at a polymer's T_g, thus reducing the sorption capacity of the membrane for a gas at this temperature. With the inclusion of PDMS into the copolymer's backbone micro-domains of the membrane lost their sorption capacity at the experimental temperature, thus lowering the CO_2 sorption. The data for this work is shown in Figure 2-23.[77] The image was adapted from reference 77.

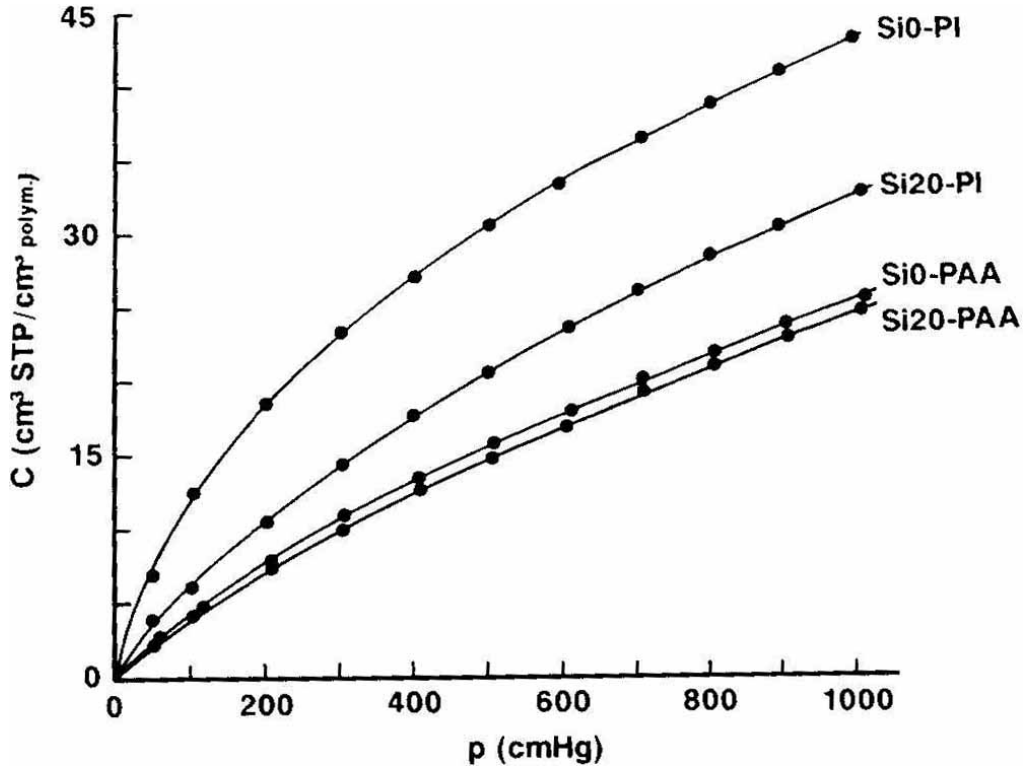

Figure 2-23. CO_2 sorption isotherms for the pure polyimide (PI), poly(amic acid) (PA), and their corresponding PDMS copolymers (Si) at 20 wt % PDMS. The label Si0 means no PDMS was included in the polymer, and Si20 means that copolymer contains 20 wt % PDMS.

Permeation experiments for O_2 and N_2 were performed on all the polymers as well. The results showed the permeabilities of both gases increased with increasing PDMS content. Furthermore, the selectivity dropped significantly as the PDMS content was increased.

Nakagawa et al. developed at a new series of poly(imide siloxanes) and studied their morphologies and gas permeability behaviors.[78] The copolymers were synthesized using a condensation reaction of 2,3,5-tricaboxy cyclopentyl acetic dianhydride with diamino diphenyl ether and bis(aminopropyl)polydimethylsiloxane with differing chain lengths. The resulting amic-acids were imidized in solution.

The authors used ^{1}H-NMR to determine the percent of imidization for the polymers. In every case, the percent imidization was greater than 95%. This was based

on the peaks at 11.7 and 10 ppm, which corresponded to the carboxylic acid and acid-amid, respectively. The ^{1}H-NMR spectrum is shown below in Figure 2-24.[78]

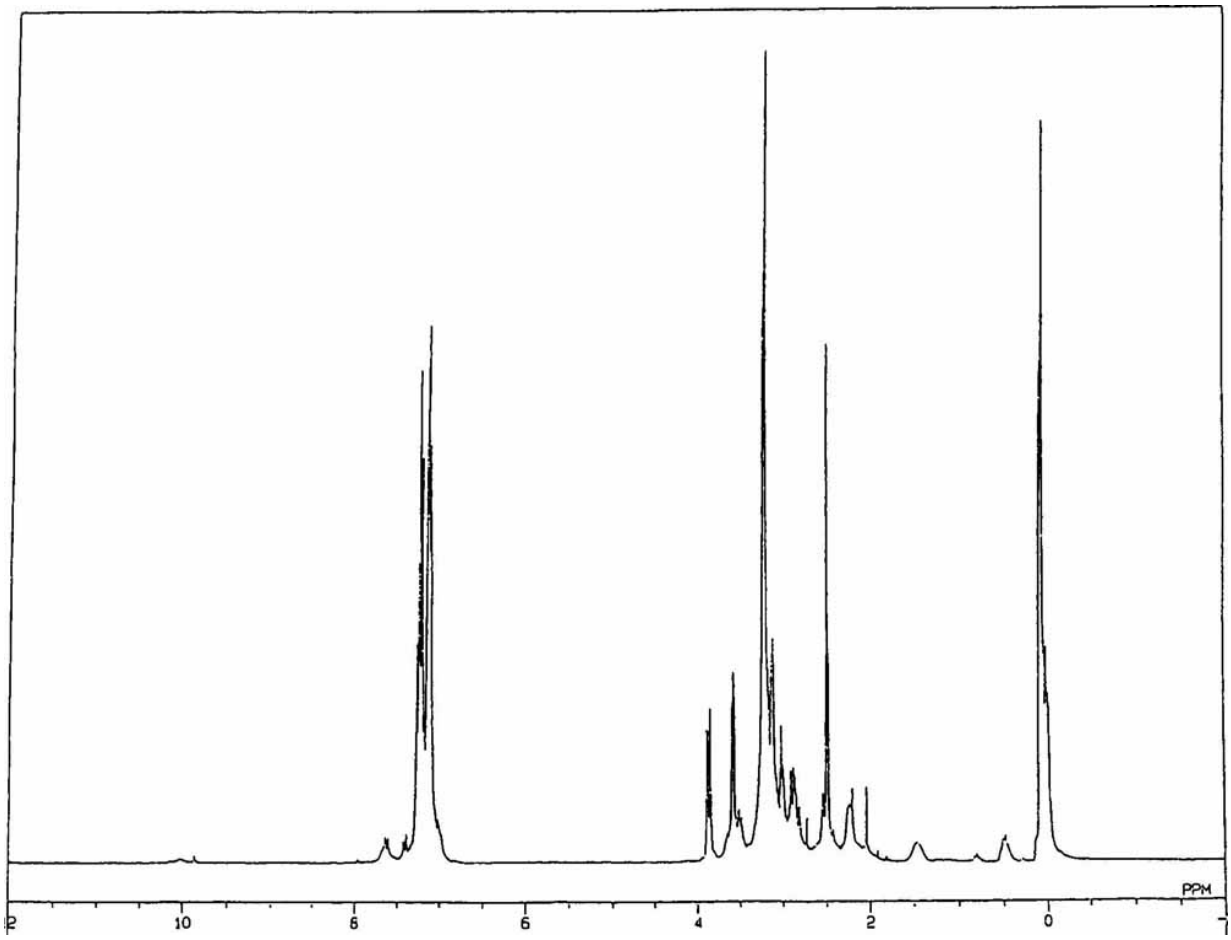

Figure 2-24. The 1H-NMR spectrum of a poly(imide siloxane) synthesized by Nakagawa et al. The copolymer was ~12 wt % PDMS. The image was adapted from reference 78.

WAXS studies of the pure polyimide and copolymer indicated that the polyimide was amorphous, as its scattering pattern consisted only of a broad halo. This pattern changed very little with the addition of different amounts of PDMS. The authors attributed this to the copolymers retaining an amorphous structure.

DSC studies were performed on all the polymers as well. The T_g of the pure polyimide was determined to be ~325 ^{o}C. As the PDMS content was increased, the T_g dropped, eventually falling below 300 ^{o}C when the longer chain PDMS oligomers were

incorporated into the polymer's backbone. When the PDMS block had a degree of polymerization of 5 or higher, two T_g's were observed, indicating the presence of phase separation within these copolymers. The DSC curve of pure PDMS showed an increase in heat capacity with temperature at -123 ^oC, while the copolymers showed this change at -116 ^oC for a n=9 and, -102 ^oC for n=5. This shift up in the PDMS T_g was a consequence of the segment's ends being restricted by the rigid polyimide. The DCS curves for the polymers is shown below in Figure 2-25.[78]

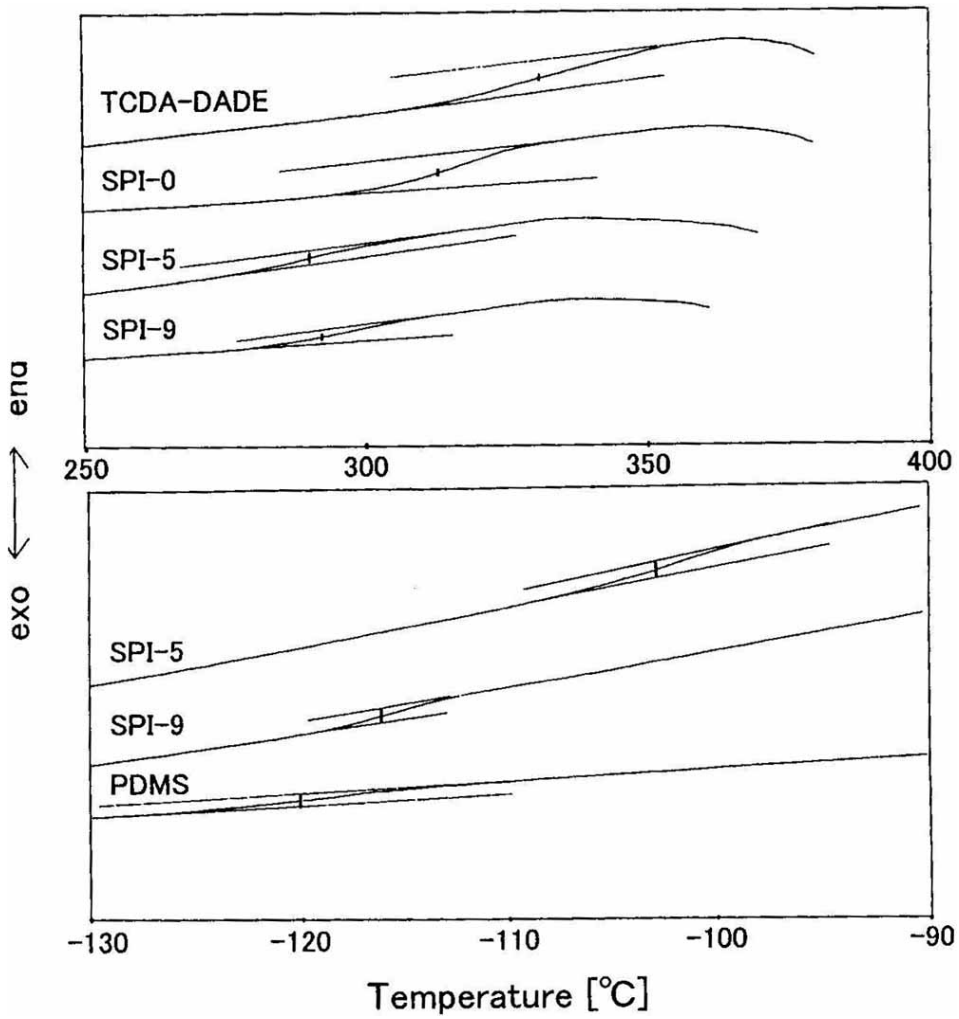

Figure 2-25. DSC curves for the polymers used in the study by Nakagawa et al. Here TCDA-DADE is the pure polyimide, SPI-X corresponds to a poly(imide siloxane) composed of TCDA-DADE and PDMS. X is the degree of polymerization of the PDMS oligimer. The image was adapted from reference 78.

The permeability of CO_2, O_2, N_2, and CH_4 were determined for all the polymers included in the study. The general trend of increasing permeability with increasing PDMS content was again observed. The diffusion coefficients of the gases also increased with PDMS content, while the solubility of the gases declined. The effect of temperature was also investigated on the permeability of these gases from a range of 40 – 110 ^{o}C. As the temperature increased, so did the permeability of all gases. However, as the PDMS content was increased, temperature less strongly influenced the permeability of CO_2; pure PDMS has a constant CO_2 permeability over this range of temperature.

The authors expanded the permeation study to include high pressure permeability studies for both pure and 50/50 mixes of CO_2 and CH_4. This part of the study only included the pure polyimide and the copolymer with the longest PDMS segment. The pressure range was from 2 – 20 atm. The results showed that the permeability of CO_2 at a given pressure was the highest for both membranes when the feed stream was pure. However, the plasticization pressure for the copolymer (5 atm) was slightly lower than that of the pure polyimide (7 atm). The authors believed this was due to fewer Langmuir sites in the copolymer, as it was of a less glassy nature with the addition of PDMS. As a result of fewer sites, it would become saturated faster by CO_2. Methane's permeability was higher with a mixed feed when compared to a pure feed for both membranes. The investigators believed that the absorbed CO_2 in the membranes enhanced the CH_4 diffusivity.

Arnold et al. investigated the synthesis and structure-property relationships for a series of poly(imide siloxanes).[79,80] The majority of the results reported were for poly(imide siloxanes) composed of benzophenone tetracarboxylic dianhydride (BTDA), 3,3'-diaminodiphenyl sulfone (DDS), and PDMS oligomer; the poly(imide siloxanes) synthesized from these monomers are referred to as BTDA-DDS. The investigators looked at incorporating PDMS oligomers ranging in M_n from 800 – 10,000 g/mol into the polyimide's backbone to make poly(imide siloxanes) of 5 – 70 wt % PMDS. Cosolvent mixtures of tetrahydrofuran (THF) and either N-methylpyrrolidinone (NMP) or dimethylacetamide (DMAC) were employed for the step growth synthesis. The authors noted as a general rule that the larger the PDMS oligomer, or the higher the percent PDMS in the final copolymer, the more the cosolvent ratio had to favor THF.

To achieve high molecular weight copolymers, the authors first dissolved dianhydride into the cosolvent, and then slowly added the PDMS oligomer, effectively capping the siloxane oligomer through the reaction of its amine end-groups with dianhydride. Later, the aromatic diamine was slowly added to this solution of anhydride-capped PDMS and free anhydride to react and form a poly(amic acid).

Poly(amic acids) were imidized using one of two methods. The first method was referred to as the bulk imidization method and involved casting the poly(amic acid) film onto a glass plate. The glass plate was placed under vacuum at 100 ^{o}C for several hours to remove the solvent. Then it was placed into a forced air oven for one hour at 100 ^{o}C, one hour at 200 ^{o}C, and one hour at 300 ^{o}C to complete the cyclodehydration.

The second method was referred to as the solution imidization technique. In this technique a cosolvent system of 80% NMP and 20% cyclohexylpyrrolidinone was emplyed. The poly(amic acid) in this solution was heated to 160 ^{o}C for 24 hours during which it cyclodehydrated to a polyimide. The authors noted both methods led to tough, transparent, flexible films.

The investigators employed ^{1}H-NMR and FTIR to verify that the imidization process was successful for the copolymers. The authors noted that the nmr spectrum of BTDA-DSS with 38 wt% PDMS had no peaks above 10 ppm. Peaks in that range would have been due to the presence of carboxylic acid groups, indicating the presence of unreacted poly(amic acid). The authors were able to verify the PDMS content of the copolymers by ratioing the integrated peak areas of the aromatic proton region and the silicon methyls. The ^{1}H-NMR spectrum is shown in Figure 2-26.[79]

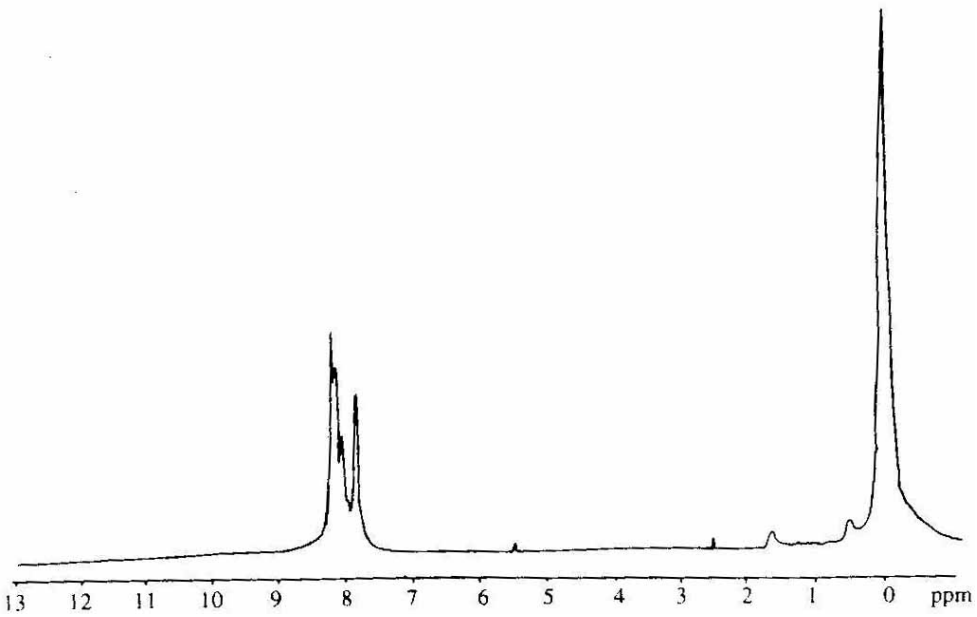

Figure 2-26. ^{1}H-NMR of solution-imidized BTDA-DDS based poly(imide siloxane) with 40 wt % PDMS synthesized by Arnold et al. The figure was adapted from reference 79.

FTIR offered a qualitative measure of the success of the imidization processes. Imides display strong bands at 1778 and 725 cm-1, while the amic acid displays a band at 1546 cm-1. The absorbances of these bands both before and after the imidization process were used as measures of the success of the imidization process. The FTIR spectra are shown in Figure 2-27.[79] The figure was adapted from reference 79.

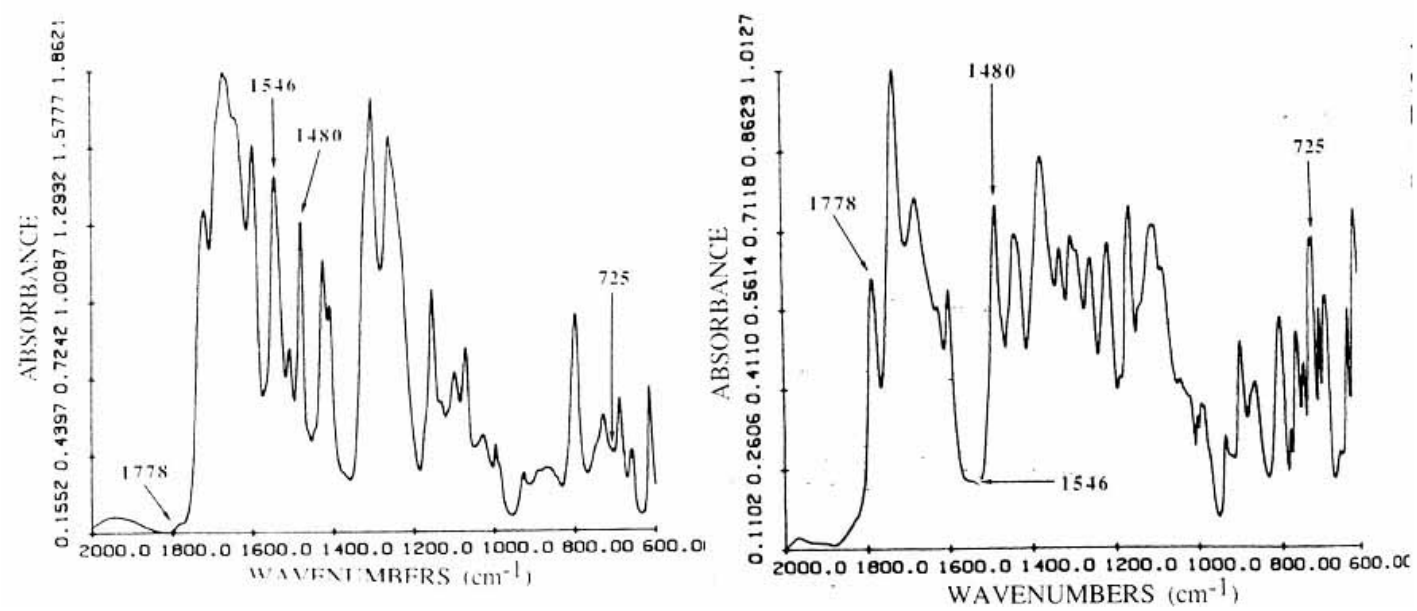

Figure 2-27. FTIR spectra of BTDA-DDS with 10 wt% siloxane. The left is the spectrum of the polyamic acid form BTDA-DDS, and the right spectrum is of the imidized BTDA-DDS.

Studies using DSC showed the presence of two T_g's indicating microphase separation occurred between the polyimide and the siloxane segments. Generally, the upper transition temperature increased with greater siloxane oligomer molecular weight, and with decreasing siloxane loading. Often, the upper T_g was only depressed slightly when compared to the pure polyimide, suggesting strong and distinct microphases existed. The authors noted that the lower T_g associated with the PDMS segments was difficult to detect when the loading was less than 20 wt %. Only when the loading was increased did transitions begin to appear between -123 and -117 ^oC.

The presence of phase separation was further investigated using transmission electron microscopy (TEM). TEM images revealed siloxane domains forming with as little as 10 wt % PMDS when the oligimer size had a M_n of 2000 g/mol. The domain size was estimated to be near 5.0 nm. The domain size increased to ~ 16 nm when the oligimer size was increased to 10, 000 g/mol.

Stress-strain measurements were gathered for pure BTDA-DDS, and its copolymer counterpart at different PDMS loadings. The general trend of lower modulus

as the PDMS loading was increased was observed. However, large changes in the modulus were not observed until the loading reached 40 wt %.

Park et al. fabricated composite membranes made up of poly(imide siloxane) block copolymers covalently bonded to silica domains.[81] They varied the wt % of silica in the membranes using 0, 30, and 50%. Additionally, the copolymer was synthesized with varying wt % of PDMS (i.e. 2, 5, 8, 15). The investigators synthesized the polyimide block by dissolving PMDA into a solution of NMP and THF, which was in a 3:1 volume ratio. Then ODA which was dissolved in NMP was added drop wise over a 3 hour period under an N_2 atmosphere. Aminopropyltriethoxysilane (APTES) was added and allowed to react with the anhydride ends of the poly(amic acid) for 6 hours. After this time period water and triethylsiloxane were added to the solution to hydrolyise the ATPES, and in order to form the silica network. This solution was mixed for 24 hours, then cast and dried at 40 $_{o}$C for 24 days. This scheme is shown in Figure 2-28.[81] The figure was adapted from reference 81.

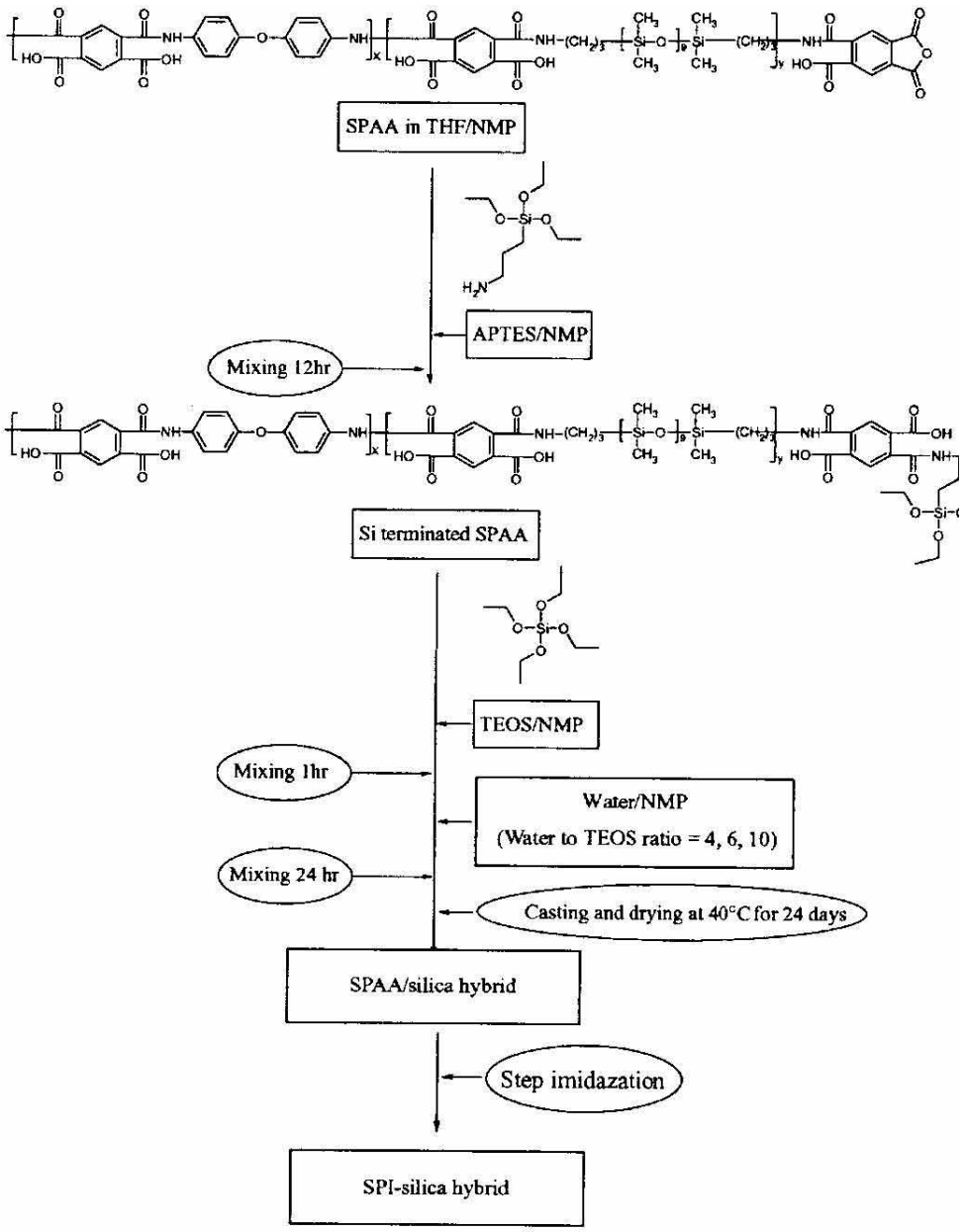

Figure 2-28. Reaction scheme used by Park et al to fabricate Poly(imide siloxane)-silica composite membranes.

Park et al characterized the composite membranes using several methods. The intersegmental spacing was studied using WAXS. The authors noted the presence of two peaks, both of which were broad indicating the composite was amorphous. The first and smaller peak occurred at $2\theta \sim 7^{o}$ and was attributed to the intramolecular chain order. The second peak occurred at $2\theta \sim 18.5\text{-}22^{o}$; it shifted to a larger angle with higher silica

content. This peak was attributed to poor molecular packing combined with the amorphous halo. This shift was believed to be a consequence of of the restriction on chain mobility leading to a smaller interchain segmental distance due to the presence of silica.

Permeation studies of these composite membranes were performed on composite membranes with 50 wt % silica, but with varying wt % of PDMS. The results showed increases in the permeation of all gases as the PDMS content increased. The authors stated this indicated that the gas transport occurred dominantly through the PDMS phase. Selectivity decreased slightly with PDMS content, but not as large as selectivity losses in these copolymers without silica. For example, one pure copolymer offered an O_2/N_2 selectivity of 2.5 where its silica counterpart offered a selectivity of 7.65; the pure polyimide offered 10. The authors submitted that the presence of silica may have restricted the chain mobility of the PDMS. They also suggested that the presence of APTES could enhance the interaction between the polymer and the silica, further reducing chain mobility.

Similar experiments were performed on composite membranes with constant PDMS content, but varying silica loading (10, 30, 50 wt %). The permeability increased with silica content, but there was an accompanying decrease in selectivity. The authors noted that the permeability values of these membranes were lower than those of the membranes in which the PDMS content was varied. They concluded that the effect of the polymer phase was greater than that of the inorganic phase on the gas transport.

Ha et al. also performed permeation studies using similar block copolymers.[82] This investigation focused on a poly(amideimide siloxane) synthesized from amine-terminated PDMS (M_n = 900 g/mol) and ODA linked together using trimelltiic anhydride chloride. The details of the synthesis are described in a separate paper by the authors.[83] The repeat structure of this block copolymer is shown below in Figure 2-29.[83] The figure was adapted from reference 83.

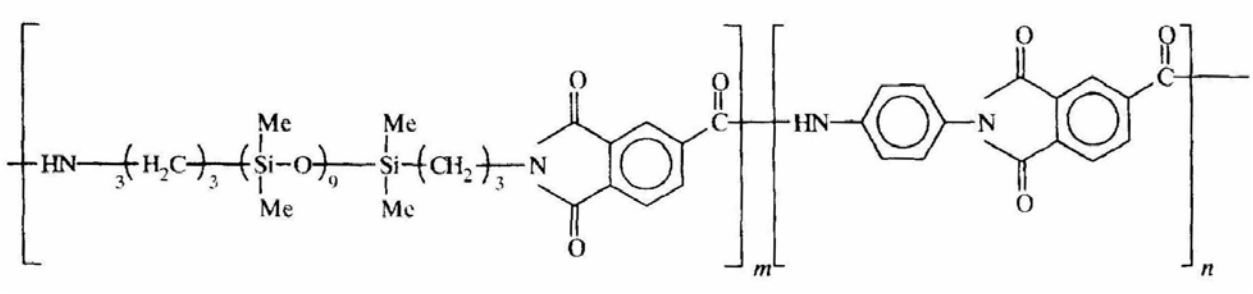

Figure 2-29. Repeat Units of the block copolymer synthesized by Ha et al.

The investigators wanted to determine what volume fraction of PDMS was present at the percolation threshold. The percolation threshold is the volume fraction of a minor component which needs to be added in order to observe drastic changes in the permeability of a membrane. Typically, the minor component forms a continuous phase at the percolation threshold, providing a high permeability channel for a penetrant to pass through. Ha offered in a illustration of this which is shown in Figure 2-30.[82]

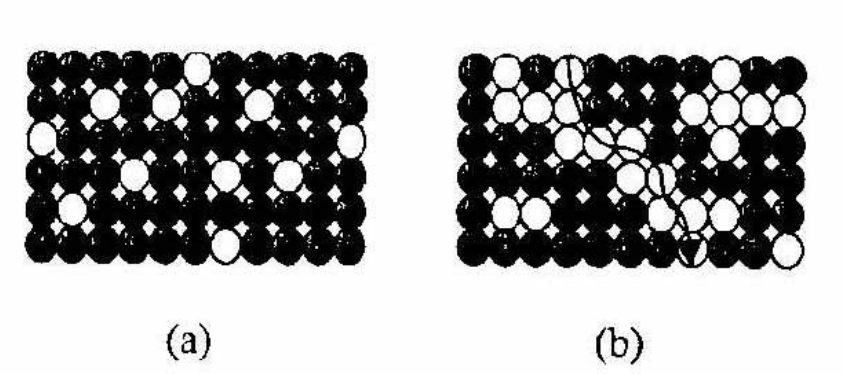

Figure 2-30. Illustration taken from Ha et al. of the morphology required for the percolation effect to occur. If the low permeability phase (dark blocks) prevent a continous path through the high permeability phase (light block) the effect does not occur (A). If the high permeability phase can reach both sides of the membrane, the percolation effect can occur (B). This figure was adapted from reference 82.

In (a) the low permeability poly(amideimide siloxane) is present in such a large volume fraction of the membrane that the high permeability siloxane phases are isolated

from each other. If the siloxane phase' volume fraction is continually increased, eventually a continuous path across the membrane will be created providing a high permeability channel for gas transport. This is easily observed through permeability studies and is called the percolation effect. The recorded data in Ha's work shows that this threshold was near a PDMS volume fraction of 0.2. Their recorded data is shown below in Figure 2-31.[82] The figure was adapted from reference 82.

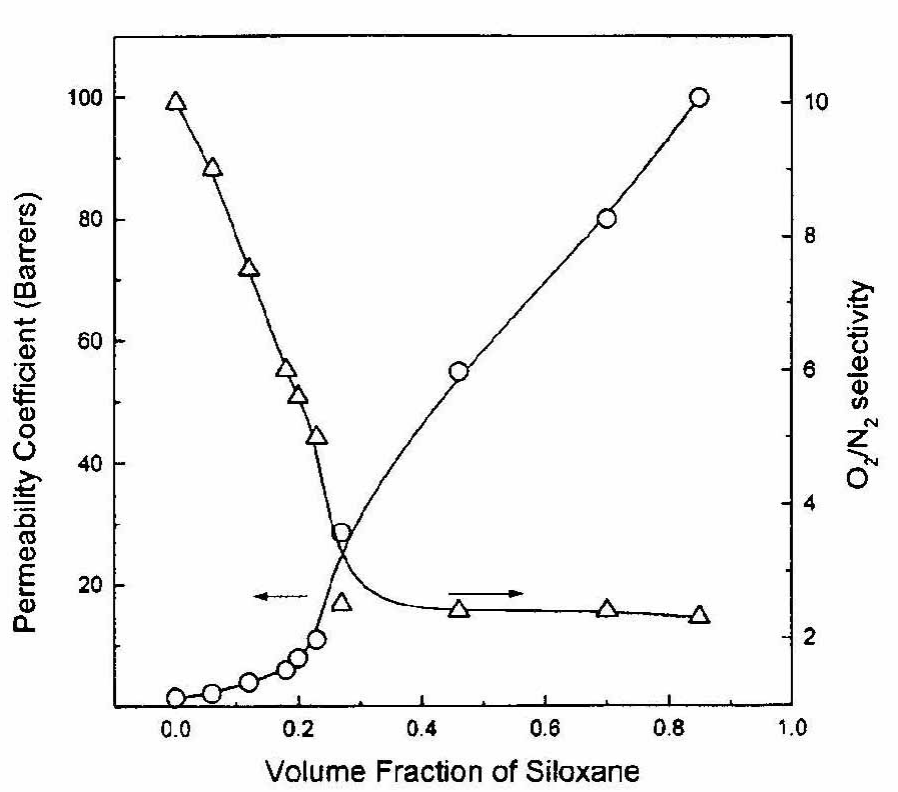

Figure 2-31. Permeation data taken Ha et al. Near 20 vol % PDMS the membrane displays an exponential increase in permeability.

Bowens et al investigated poly(imide siloxane) block copolymers in order to investigate their usefulness as in controlling interfacial properties between silicon substrates layered with thin films for microelectronic applications.[84] Their materials were synthesized from 6FDA and meta-phenylene diamine (MPDA) to form the polyimide block, and amine-terminated PDMS was used for the siloxane block. These materials showed microphase separation when analyzed using TEM. A strength of these materials

was their thermal stabilities as indicated in TGA measurements. The block copolymers showed thermal stability well above 400 ^{o}C.

The investigators analyzed the surfaces of different poly(imide siloxane) copolymers as well. Using angle-dependent x-ray photoelectron spectroscopy (XPS), it was shown that the surface becomes enriched with PDMS segments relative to the bulk. This was attributed to the low surface free energy of PDMS. These results were complimented with water contact angle measurements gathered from the surfaces of these block copolymers. The contact angle analyses indicated a more hydrophobic low energy surface. In fact, these measurements showed that at 5% loading of PDMS, an increase of 25% in the water contact angles was realized. When the surfaces were characterized using tapping-mode AFM, it was apparent that the phase separation on the surface existed. Additionally, AFM surface topographic images indicated that the surface roughness of the polymers increased with larger PDMS loadings.

2.7 Zeolites

Zeolites are the major inorganic component of the mixed matrix membranes used in this work. The zeolites were synthesized and characterized for us by Dr. Michael Tsapatsis' group. His group is now at the University of Minnesota.

This section of the Literature Review is devoted to discussion of zeolites. A very broad overview of what constitutes a zeolite, how zeolites were discovered, and what role they play in research and industry today will be addressed. Characteristics of zeolites will also be discussed. Finally, the two zeolites used in this study, ZSM-2 and zeolite L, will be examined.

2.7.1 Introduction

Zeolites are porous crystalline aluminosilicates that display a repeatable three dimensional structure. These repeatable structures often include channels with openings of a few angstroms. With their pore sizes corresponding to the dimensions of various

gases, zeolites can be used to separate chemical species based on the gases' sizes and shapes. In addition to acting as molecular sieves, these channels give zeolites large surface area to volume ratios. Because of this, zeolites find uses in separations, catalysis, drying and adsorption processes.[7]

The first zeolite, stilbite, was discovered by the Swedish mineralogist A. Cronstedt in 1756. Cronstedt found the zeolite in the small cavities in rocks of volcanic origin. He noted that the mineral lost water rapidly upon heating and thus seems to boil.[85] Seeing this, Cronstedt named the mineral "zeolite", which comes from the Greek words "zeo", which means to boil, and "lithos", which means stone. Today there are about 40 known natural zeolites.

Although the existence of naturally occurring zeolites was known since Cronstedt's discovery, only in the 1950's did research on zeolites begin to expand. In the 1950's Union Carbide developed large-scale industrial synthesis methods for zeolites. This made zeolites available in large amounts for industrial applications, and thus, research on their properties and developing new zeolites gathered momentum.

Today there are approximately 152 recognized zeolite structures according the International Zeolite Association (IZA). These zeolites find applications in separations, catalysis, adsorption, ion exchanging, sensors, and medical applications.[86,87] Some of these applications are listed below in Table 2-5.

Table 2-5. Applications of Zeolites.

Recovered Gas	Application
CO_2	Removal from natural gas, or flue gas
H_2S	Removal from natural gas and liquefied petroleum gas
O_2	Removal from air
Unsaturated hydrocarbons	Separating benzene from cyclohexane Separating propylene from propane
H_2O	Removal from petroleum
Ammonium ions	Removal from sewage treatment plants Removal agricultural waste streams

Zeolite membranes and other inorganic membranes make up about 15% of the total sales in the membrane market. In terms of sales they are far out performed by their polymer counterparts. However, this is not to say that inorganic membranes are less capable of separating gases, rather they have different strengths and weaknesses when compared to polymeric membranes. Some of these advantages and disadvantages are outlined in Table 2-6.[88]

Table 2-6. Advantages and disadvantages of zeolite membranes.

Advantages of Zeolite Membranes	Disadvantages of Zeolite Membranes
Long-term stability at high temperature	High cost
Chemical stability	Brittleness
Resistance to high pressure drops	Low surface area per module volume
Easy cleaned to remove fouling	Dense membranes have low permeability at medium temperatures
Easy catalytic activation	Difficulty achieving high selectivity in large scale membranes (e.g. cracks)

The amount of research devoted to further understanding zeolites has grown dramatically in the last few decades. Figure 2-32 shows the number of publications and patents on zeolites from the 1980's through the 1990's.[87] Furthermore, computer simulations predict that there are six million conceivable zeolite structures, so the list of recognized structures is likely to grow in the future.[89] Clearly from this information, zeolites are viewed as a valuable tool with potential to help industrial processes.

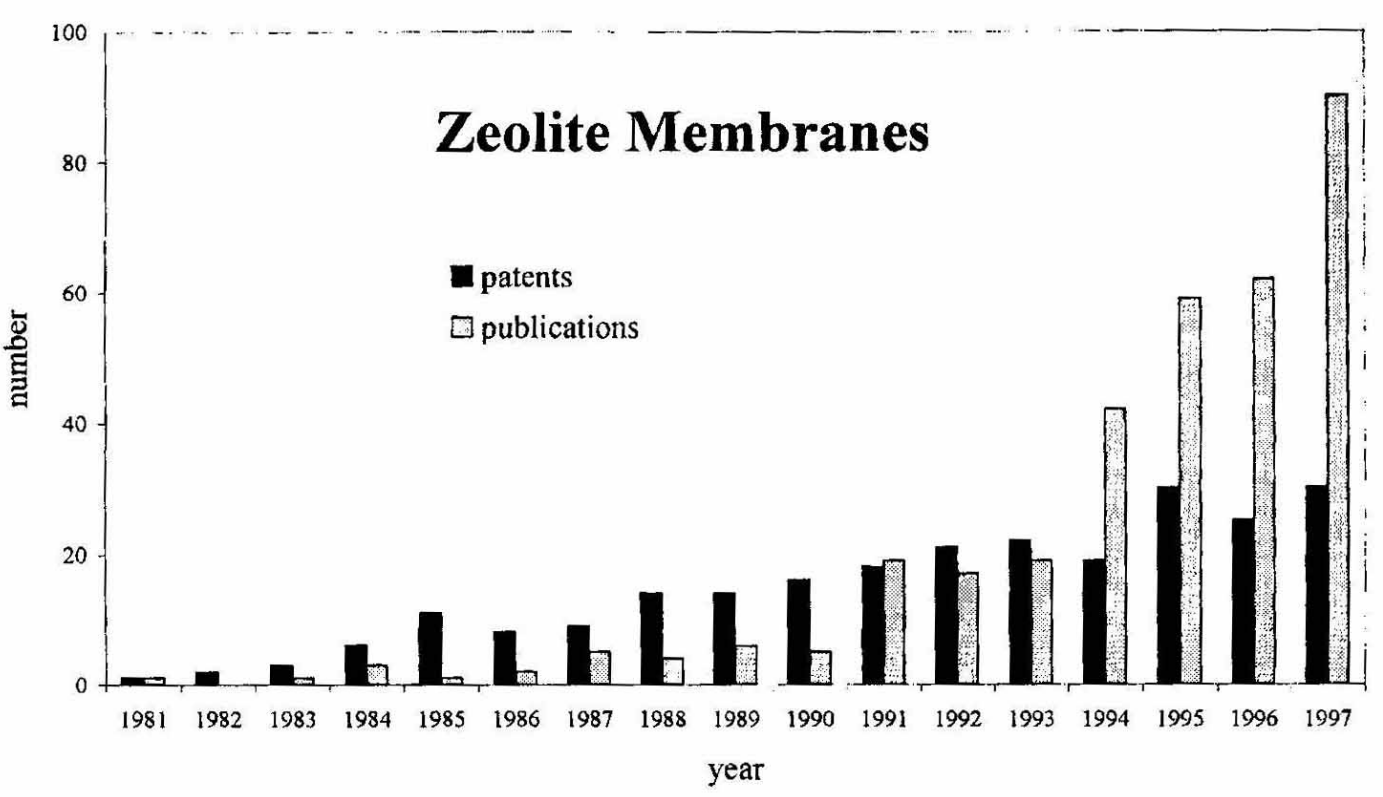

Figure 2-32. The number of patents and publications on zeolite membranes per year from 1981 to 1997. This figure was adapted from reference 87.

2.7.2 Zeolite Structure

The principle component, or primary building unit (PBU) of all zeolites is the TO4 tetrahedral, where T can be silicon or aluminum, but more often it is silicon.[90] Each tetrahedral forms a network with other tetrahedra through the connection of its four oxygen atoms. This leads to a three dimensional structure containing channels and cavities at repeatable intervals.

The most common PBU is SiO_4, but if aluminum is present during the synthesis it can be incorporated into the zeolite structure as well. When aluminum is included, a building block of AlO_4^- is utilized to build the zeolite. This PBU's negative charge must be counterbalanced with a cation which will reside in the channels; the cations are not part of the framework. Cations can be from Group I (e.g. Li^+, K^+)or from Group II (e.g. Ca^{2+}, Mg^{2+}), or they can be organic cations.

With all of this in mind, the zeolite composition can be described as

$$M_{n/m}^{m+} \bullet \left[Si_{1-n}Al_nO_2\right] \bullet nH_2O$$

here, M is a cation, the center bracketed term represents the framework composition, and the water term is the sorbed phase. It must be noted that in this formula n can equal zero, and there will be no cation, aluminum or water in the zeolite. An example of this would be the zeolite ZSM-5.[91]

The PBU is the fundamental building block of a zeolite, but by itself doesn't offer much to explain differences among different zeolite properties. This issue is better addressed through secondary building units (SBU's), which are specific geometric groupings of the PBU's. There are currently 20 IZA recognized SBU's, which can be used to describe all of the known zeolite structures. SBU's can consist of 4, 6, and 8 member single rings, 4-4, 6-6, and 8-8 double rings, and 4-1, 5-1, 4-4-1 branched rings. Although not a complete list of all known SBU's, some of these units are shown below in Figure 2-33:[92] The figure was adapted from reference 92.

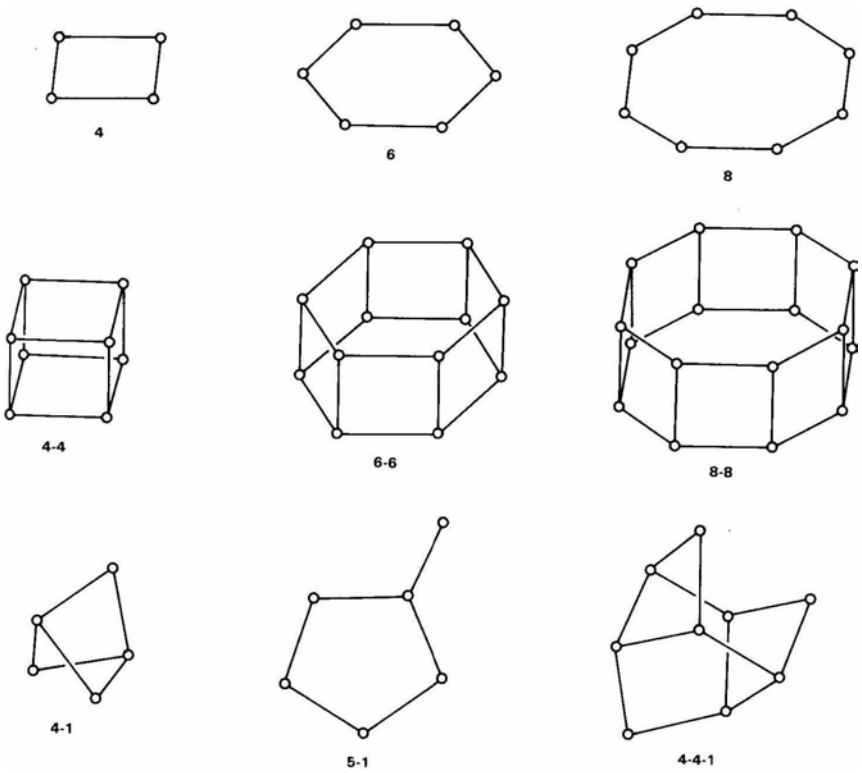

Figure 2-33. Example of secondary building units of zeolites.

Here, each ° represents the center of a PBU. Oxygen linkages are not shown in the units, but can be considered to be in the center of the lines connecting each °. It must be noted that these structures only show the aluminosilicate skeleton, and neglect the presence and influence of cations and water present within the pores. Additionally, it must be noted that rings composed of more than 8 T-atoms do exist, however, they do not have their own individual SBU. They can be created by joining together the SBU's shown above in unique manners.

2.7.3 Classifying Zeolites

Zeolites are classified according to an identification code created by the International Zeolite Association.[93,94] This code creates three letter categories for the zeolites (e.g. FAU, VPI). Each code refers to a specific category of zeolite that is defined by a specific framework symmetry. While the symmetry of the framework within a category is constant for all zeolites, the chemical composition of the zeolites may vary within a category.

The three letter code is often an acronym for those responsible for creating the zeolite. For example, zeolite L is in the LTL category. LTL is an acronym for Linde Type L. Linde is the name of a chemical company that created the structure, but was later bought out by Union Carbide. VPI refers to another category of zeolites, and it was coined by Mark Davis when he was employed at Virginia Tech.

Details of the framework types are published in the *Atlas of Zeolite Framework Types*.[95] The WAXS patterns for each zeolite are recorded here, as well as the synthesis conditions and characteristics of the pore and framework.

2.7.4 Zeolite Pores

A zeolite pore is a 3 dimensional channel that runs from one side of a zeolite to another. These pores can separate gases, or be used as catalysts in reactions. Zeolite pores can be described by three characteristics: pore size, dimensionality, and shape.

All three of these parameters will be described in its own section.

2.7.4.1. Pore Size

A pore in a zeolite is created by a ring composed of at least four tetrahedra all of which are connected through shared oxygen atoms. The tetrahedra can contain either Si, or Al, as long as the obey Lowenstein's rule which is described in detail later in this section. The number of T-atoms (i.e. the center atom of the tetrahedra) can be used to describe and classify the pore size.

Generally, zeolites are classified by pore size into four categories: small, medium, large, and ultralarge. Small pores are pores that composed of six, eight, or nine T-atoms, while medium pores have ten T-atoms. Large pores contain 12 T-atoms, and ultralarge pores possess 14, 18, or 20 T-atoms.

It must be stressed when considering this classification system that no information about the width of the pore can be inferred. For example, both zeolite A and erionite have 8 member rings. Zeolite A's pore has a uniform radius of 0.43nm. However, the pore of erionite is nonuniform in size with the shortest dimension measuring 0.35nm and the longest dimension measuring 0.52nm. An illustration of this is shown in Figure 2-34.[96]

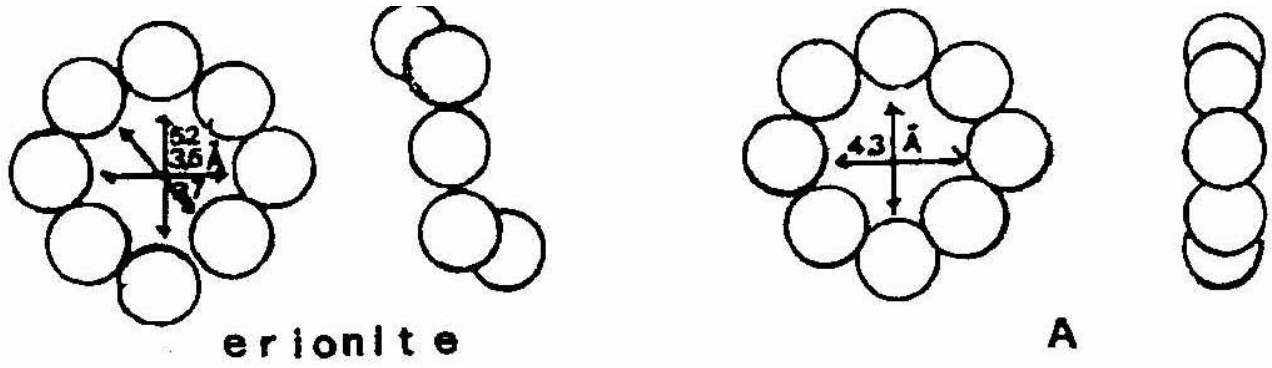

Figure 2-34. Pore opening structures of erionite and zeolite A. Each zeolite has 8 T-atoms in its pore structure, however, the sizes of the two pores are different due to the arrangement of the T-atoms. The figure was adapted from reference 96.

Additionally, whether the pore is 1-D, 2-D or 3-D can not be determined from the pore size classification.

The significance of a zeolite's pore size can best be shown through an example involving catalysis. Both H-mordenite and HZSM-5 are used as catalysts in a process to convert methanol to a higher hydrocarbon. HZSM-5 has a 10 member ring, and selectively converts methanol to hydrocarbons in the octane range. H-mordenite possesses a 12 member ring, and leads to a product skewed toward the production of C_{11} hydrocarbons. This difference can be attributed to their differing pore size, and the ability of a molecule to diffuse into and out of a pore.[92]

The zeolites used in this study, ZSM-2 and zeolite L, both contain 12 member rings.

2.7.4.2 Pore Dimensionality

Zeolite pores also can be distinguished from each other in terms of how they traverse the interior of the zeolite. Specifically, the pores' dimensionality can be one dimensional, two dimensional, or three dimensional.

Zeolites such as zeolite L, which was used in this study, have a 1-D pore that runs along the thinnest dimension of this flat plate structure. Its 1-D channel is a consequence of its structure in which its 12 member rings connect to each other in the form of a cylindrical tube.

ZSM-2, the other zeolite used in this study, possesses 3-D pores. In this zeolite, all the channels are composed of 12 member rings.

Zeolites can have 2-D pores as well. Mordenite has a 2-D pore system, in which 8 member rings connect large 12 member rings together.

2.7.4.3 Pore Shape

Even though two different zeolites may have the same number of T-atoms in their pore size, they may have drastically different separation capabilities. This can be to the

two zeolites having differently shaped pores. The shape of the pore opening is a function of five variables:[92]

- Configuration of the T and O atoms relative to each other
- Si/Al ratio
- Size of the cation
- Location of the cation
- Temperature

The configuration of the T and O atoms has already been shown to effect the pore size as shown in (Figure 2-34). Additionally, the configuration of the T and O atoms in the framework will influence the pore shape. Essentially, the structure of the zeolite can determine the shape of the pore of the mouth.

The presence of cations can strongly influence the shape of a pore. Each cation has its own spatial requirement, therefore its size as well as how many cations are present in the channel will effect the final size of the pore. For example, zeolite A can be synthesized such that sodium ions will fill its pores. When Na^+ is cation exchanged with the larger K+ the zeolite becomes impermeable to all but very small and polar molecules as the pore size has now been drastically reduced. When K^+ is cation exchanged with Ca^{2+}, the pore opening becomes much larger. This is because of the cations divalent nature, which lowers the number of cations required in the channel to balance the charge. Additionally, the Ca^{2+} ions reside in different parts of the channel were they will not block the pore.[92]

Along these lines, the Si/Al ratio dictates how many cations are needed to balance the framework charge, therefore it plays an important role in determining the pore shape. The Si/Al ratio will be discussed more extensively later in the Literature Review.

Finally, the temperature plays an important role in the size of the pore opening. As the temperature increases, the atoms in the ring begin to vibrate more. This can lead to small increases in the size of the pore.

An excellent example of how significantly temperature can change the pore size and thus the selectivity of a zeolite is shown in Figure 2-35.[92] Zeolite NaA will exclude N_2 but not O_2 at very low temperatures (i.e. -200 ^oC). This can be measured from the amount of gas adsorbed in the zeolite. As the temperature is increased, the lattice

vibrations increase as well, and N_2 can now enter the zeolite. Continued increases in temperature will eventually reduce the adsorption of all gases within the zeolite.

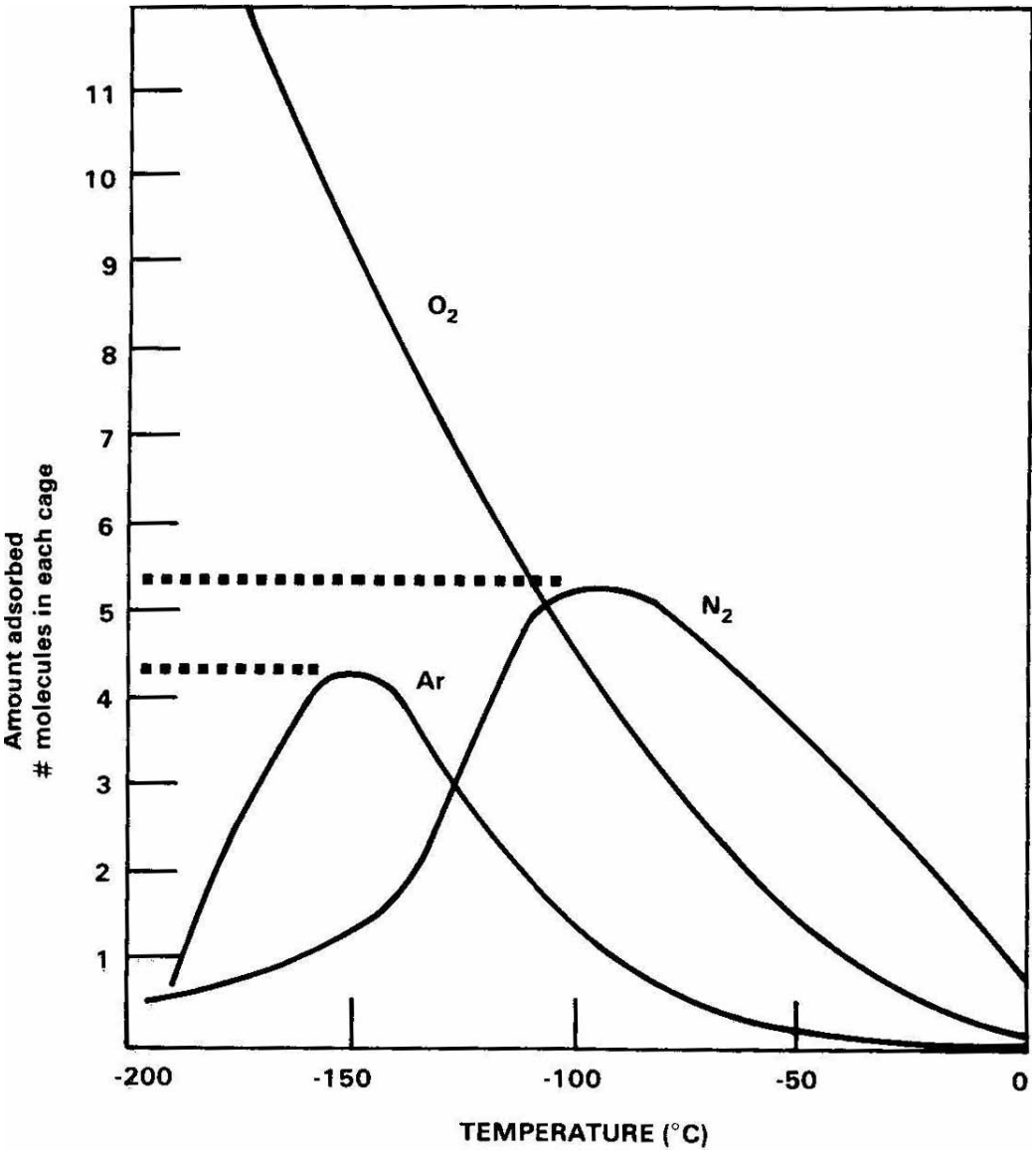

Figure 2-35. Gas adsorptoin in isobars on zeolilte NaA for O2, N2, and Ar as a function of temperature. This figure was adapted from reference 92.

2.7.5 The Silica-Alumina Ratio

The components present at the beginning of the synthesis, and their ratios can play an important role in the final zeolite structure. The Si/Al ratio which is the ratio of Si to Al in a zeolite's framework after the synthesis plays a monumental role in determining sorption properties, the inclusion of cations in the zeolite channels, and the thermal stability of the zeolite.

The amount of Si and Al present at the beginning of the synthesis will dictate the final framework composition. Typically, all of the aluminum present in the synthesis will be incorporated into the zeolite's structure. However, it must be stressed that merely adjusting the Si/Al ratio in the reacting composition will not necessarily translate to the Si/Al ration of the final zeolite framework with no other changes. As if often the case, adjusting the initial Si/Al ratio will change which framework structure will crystalize[97].

Altering the Si/Al ration will directly affect the number of cations that reside in the pores of the zeolite. The presence of Al in the framework is through AlO_4^- tetrahedral. The negative charge of these group must be balanced, which is normally attained through the introduction of a cation in the channel. The cations are introduced in the synthesis. Because of this, as the aluminum content drops, the presence of cations in the channel will diminish.

The Si/Al ratio plays a strong role in determining the affinity of the zeolite towards polar and unsaturated molecules. These molecules interact with cation within the channel, and as stated above, as the aluminum content decreases, the cation decreases with it. It should also be noted that zeolites with low Si/Al ratios are hydrophilic, while those with high Si/Al ratios are hydrophobic.

Finally, the stability of the zeolites varies with the Si/Al ratio. The decomposition temperature of low Si/Al ratio zeolites is typically around 700 ^oC, while zeolites with a high Si/Al ratio can be stable up to 1300 ^oC. The resistance to acid will decrease as the Si/Al ratio decreases, while the acid resistivity will climb with the Si/Al ratio. High-silica zeolites can be stable in boiling mineral acids, however, they typically are unstable in a very basic solution.

There is a lower limit on this ratio that has been described by Loewenstein's Rule.[98] Loewenstein developed rules that governed how tetrahedral may be linked together. He stated that how the tetrahedral connect in a zeolite is not entirely random. His rule is listed below:

- When two tetrahedra are linked together through one oxygen atom, only one center of the two tetrahedra may be occupied by Al; the other center must be occupied by Si, or by another small ion of electrovalence 4 or more (e.g phosphorous).

From this rule, it becomes evident that the minimum in the Si/Al ratio is one for zeolites. To date, no zeolite has been discovered that does not obey this rule.

2.7.6 ZSM-2

ZSM-2 was used in our first study presented on MMMs. The zeolite was synthesized and supplied to us from Dr. Michael Tsapatsis' group currently at the University of Minnesota. This section describes some of ZSM-2's physical characteristics, separation properties as well as its synthesis.

2.7.6.1 Background

ZSM-2 is a zeolite which falls into the faugasite category. It's name comes from a two part acronym meaning Synthetic Zeolite and Mobil, the latter part being the company that synthesized it. Its basic building blocks are the cubic FAU and hexagonal EMT structure types. ZSM-2 contains both aluminum and silicon in a ratio of 1 – 1.5 silicon atoms per aluminum atom. Because of the inclusion of aluminum in the framework, cations must reside in the zeolite's channels to balance the charge. For ZSM-2, the cation is lithium.

ZSM-2 crystals are plate like with the two largest faces adopting a hexagonal shape. An image of the ZSM-2 crystals used in this work are shown in Figure 2-36.

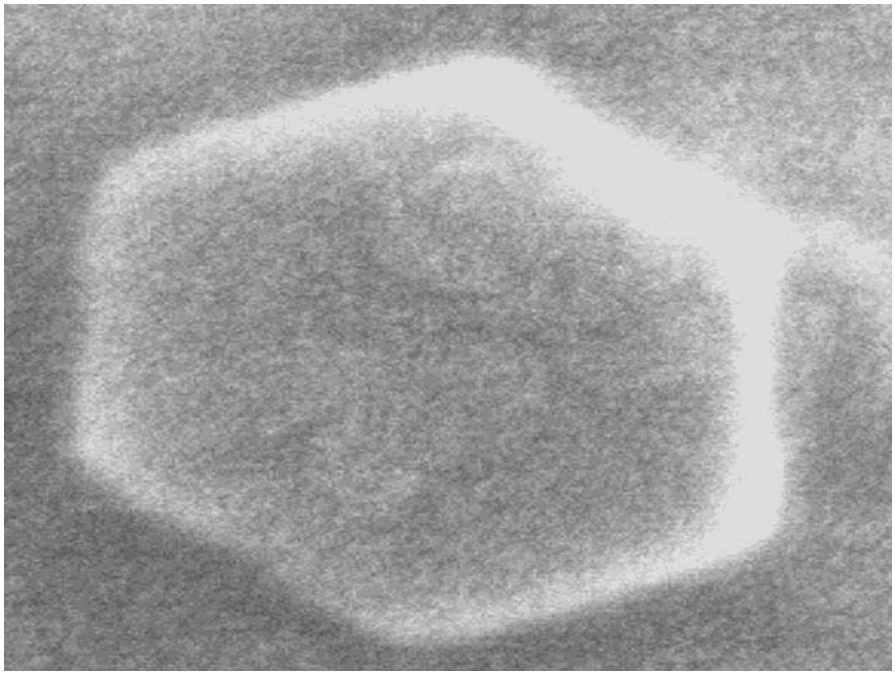

Figure 2-36. FESEM image of a ZSM-2 crystal. The length of the hexagonal face measures roughly 250 nm.

The longest length on the hexagonal face is ~250 nm. ZSM-2 possesses channels which measure .74 nm in diameter. However, due to the presence of lithium cations in the pores, the actual open space within the pore is drastically reduced. ZSM-2 has a density of 1.31 g/cm^3.

Because of the cations within the channel, ZSM-2 can separate using a selective adsorption mechanism. Molecules that more strongly adsorb onto the pore walls will receive enhanced transport through access to surface diffusion rather than being limited to Knudsen diffusion. Furthermore, the selective adsorption will enhance the selectivity of the zeolite. When one component sorps to the pore wall, the channel size is reduced, thus making it inaccessible to other nonadsorbing species. Species that sorb onto the zeolite pore walls are typically polar molecues (e.g. H_2O, ammonia), quadrupolar (e.g. CO_2, N_2), or are capable of π-layer interactions (e.g. aromatic hydrocarbons).[99] Because of this, ZSM-2 is typically targeted to remove CO_2 or unsaturated hydrocarbons from mixtures.

Nikolakis et al., performed a study on the synthesis and permeation capabilities of ZSM-2.[100] The zeolite membrane was fabricated using a new two step technique called the secondary growth method. A more detailed recount of the synthesis is available in the paper. Briefly stated, in this method ZSM-2 nanocrystals are first synthesized by mixing tetraethylorthosilicate, lithium hydroxide, and tetramethylammonium hydroxide (TMAOH) in distilled water.

Aluminum foil was dissolved into TMAOH and distilled water. This solution was slowly added to the lithium-TMA-silicate solution. The resulting mixture has a molar composition of 0.53 Li2O:1 Al_2O_3:6 TMAOH:3.4 SiO_2:315 H_2O. This mixture is then placed into a Teflon lined stainless steel cylinder and sealed. The cylinder is rotated in an oven (~30 rpm) at 140 ^oC for 12 hours. This led to uniformly sized ZSM-2 nanocrystals, or seeds.

2.7.6.2 Secondary Seeded Growth of ZSM-2 Nanocrystals:

The seeds by themselves do not make a zeolite membrane. Rather, they must combine to form a continuous network in order to operate as a membrane. Because zeolite membranes often are very thin (i.e. 5-30 μm), they are very brittle. To help overcome this, they are often fabricated on a microporous support to aid the mechanical properties of the zeolite membrane. This is typically performed by depositing the seeds onto the support and applying conditions in which they combing to form a membrane. This section outlines this process for ZSM-2 seeds (i.e. nanocrystals) called secondary seeded growth.

A suspension of ZSM-2 seeds in distilled water with concentration of 2-5 g/l was poured into a Petri-dish, and this dish was placed on an adjustable height jack. An Al_2O_3 support disk was suspended above the dish, and the dish was slowly raised until the disk was immersed in it. The support was left in the suspension for ~15 seconds, after which it was removed tangentially, and allowed to dry for 24 hours. This process was performed three times to ensure good coverage of the seeds.

To ensure growth of the ZSM-2 membranes, the seeded disks were treated with a mixture that was known to result in the nucleation and growth of the crystals.[101] This

mixture was created by dissolving tetraethylorthosilicate (TEOS) in NaOH and triethylamine (TEA). A second mixture was created by dissolving aluminum foil into NaOH. These two mixtures were added together, and resulted in a molar composition of 4.17 Na_2O:1.0 Al_2O_3:10 TEA:1.87 SiO_2:460 H_2O.

The seed aluminum support was placed vertically in Teflon lined stainless steel cylinders and treated with the above mixture at 85 ^oC. After the growth of the membrane was complete, the membranes were cooled and washed several times with distilled water. The membranes were then heated in air at 450 ^oC to remove any residual TEA in the pores. They were heated in the following manner to prevent cracking of the membrane: 30 ^oC/h until reaching 350 ^oC, remain at 350 ^oC for 5 hours, then at the same rate heat up to 450 ^oC for several days. Several images showing the aluminum support, the ZSM-2 seeds (i.e. nanocrystals), and the growth of these seeds into a zeolite membrane are shown in Figure 2-37.[100] This figure was adapted from reference 100.

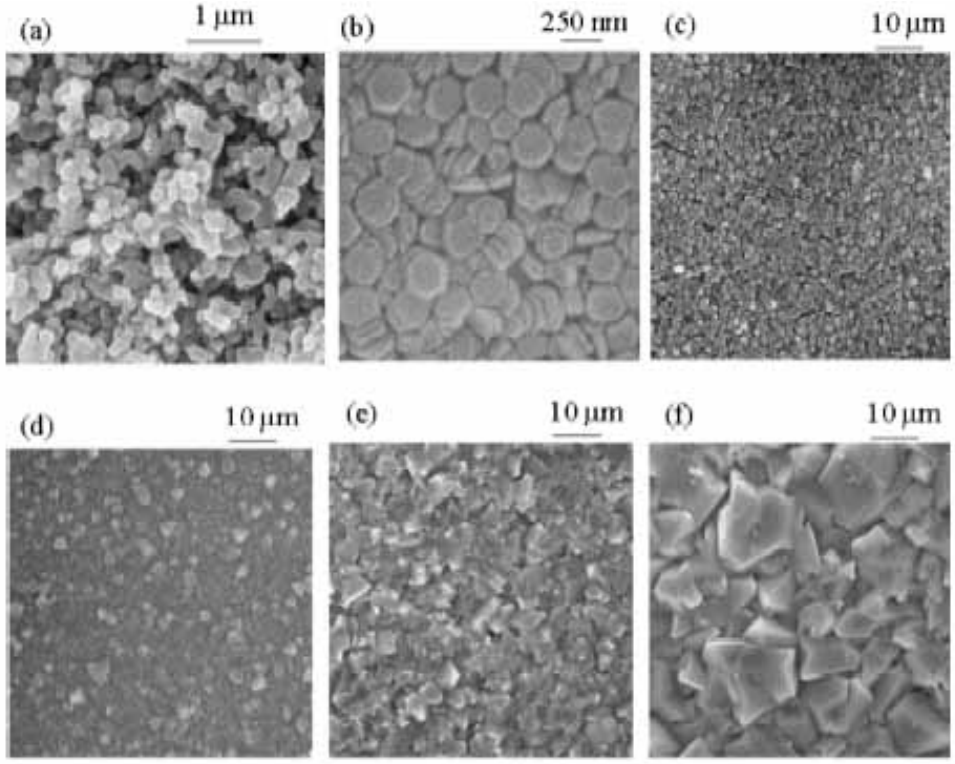

Figure 2-37. SEM images of the growth of ZSM-2 seeds into a ZSM-2 inorganic membrane. The images include (a) the alumina support, (b) the ZSM-2 seeds, the surface of the membrane after (c) 14.4, (d) 40.8, (e) 112.8, and (f)504 hours of thermal treatment.

2.7.6.3 Permeation Properties of ZSM-2 Membranes:

Nikolakis et al., studied the separation efficiency of ZSM-2 membranes for separations such as benzene/cyclohexane which are difficult using traditional methods.[102] These two components have nearly identical boiling points over a broad range of compositions. The mixture is known to azeotrope at 45 vol % cyclohexane. Furthermore, the two have very similar kinetic diameters. Benzene has a kinetic diameter of 0.585, and that of cyclohexane is 0.6 nm.

Nikolakis et al., examined the ability of ZSM-2 membranes to separate this mixture at equimolar feeds. Additionally, they investigated the effects of feed pressure on the separation properties of the membrane. Their results showed that their membranes produced using the secondary growth method gave high fluxes (i.e. 0.70 mmol/m^{2}s) and a high separation factor of 68.5. Figure 2-38 shows the effect of equimolar feed pressure on the separation factor at 100 ^{o}C for this membrane.[100]

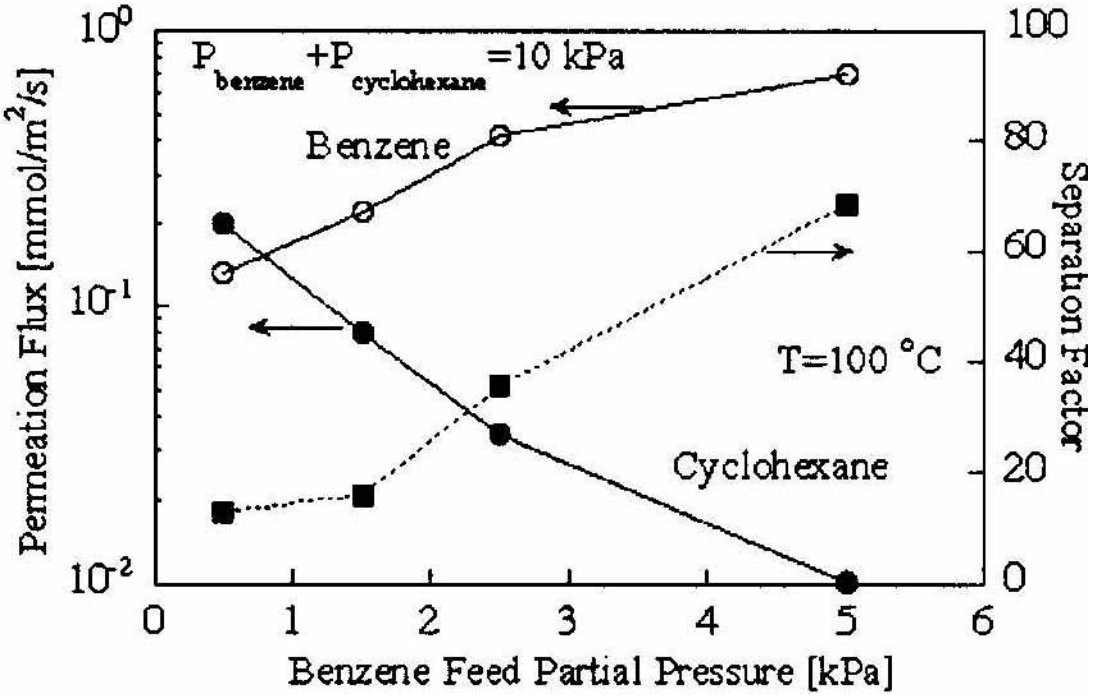

Figure 2-38. Permeation rates and selectivity of a ZSM-2 inorganic membrane with an equimolar feed of benzene and cyclohexane. The image was taken from [100].

The investigators also looked at other saturated/unsaturated mixtures with equimolar feeds. In every case, the membranes were unsaturated hydrocarbon permselective. The results of the study are shown in Table 2-7.[100]

Table 2-7. Fluxes and separation factors of different equimolar mixtures through ZSM-2 membranes.

Mixture A/B	Temperature (^oC)	Flux of A ($mmol/m^2s$)	Separation Factor
Benzene/n-hexane	65	0.14	144
Toluene/n-heptane	60	0.6	45
Propylene/propane	40	1.4	6.2
Ethylene/methane	40	2.5	8.4

The authors attributed the ability of the membrane to be selective towards unsaturated hydrocarbons due the presence of the cations within the channels. Unsaturated hydrocarbons have stronger affinity to the cations of the zeolite, resulting in stronger adsorption in the zeolite pores.[103] This stronger adsorption of benzene effectively blocks out the cyclohexane, essentially making the zeolite channel a clogged pore. This would explain the poorer separation factor at lower feed pressures, because there would be less benzene coverage.

2.7.7 Zeolite L

Zeolite L was used in our second and third study of MMMs. The zeolite was synthesized and supplied to us from Dr. Michael Tsapatsis' group currently at the

University of Minnesota. This section describes some of zeolite L's physical characteristics, separation properties as well as its synthesis.

2.7.7.1 Background

Zeolite L is zeolite with one a one dimensional pore structure which runs along its c-axis. The minimum constricting ring in its channels measures 0.71 nm, however, because of the presence of aluminum in its framework, potassium cations reside in its pores to balance the negative framework charge. This reduces the size of the pore. The unit cell has 36 tetrahedrally coordinated T-atoms (i.e. Si and Al). Zeolite L's has a Si/Al ratio of 3 and a composition of $K_9[AL_9Si_{27}O_{72}]\cdot H_2O$.

Zeolite L can be synthesized in a variety of shapes and sizes. Sizes of zeolite L can range from particles as small as 30 nm to long flat plates with aspect ratios near 100. In the latter case, the channels will run through the thickness of the zeolite (i.e. its shortest dimension).[104,105] An image of a cluster of zeolite L particles is shown in Figure 2-39.

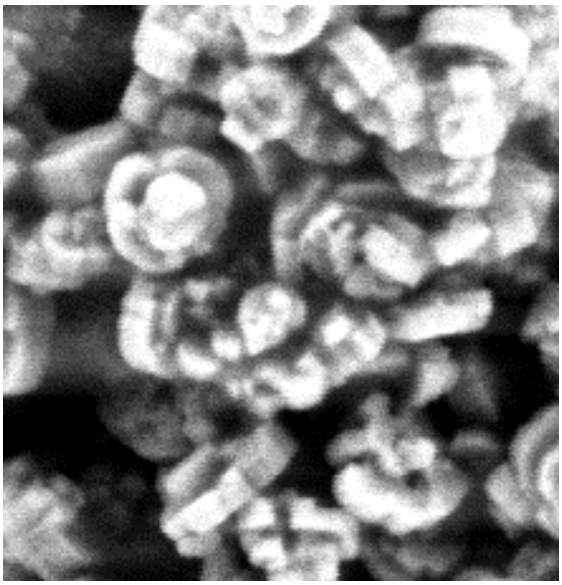

Figure 2-39. Image of a cluster of zeolite L particles. The particles are ~100 nm across their longest dimension.

Zeolite L was synthesized by Union Carbide in . It is also referred to Linde Type L, because it was first synthesized at the Linde division of Union Carbide.

Zeolite L can be synthesized using any one many techniques.[104,106-108] Different synthesis routes often lead to different sized nanocrystals, and in some cases, involve the aid of an organic template which will reside in the pores after the synthesis.

The zeolite L nanocrystals used in this study were synthesized by Dr. Michael Tsapatsis group. Because of this, his method will be the only one discussed.[104,105,109]

2.7.7.2 Synthesis of Zeolite L

3.6 g of aluminum foil was added to 150 mL of 3 M aqueous potassium hydroxide (KOH). Once the aluminum was dissolved the solution was filtered to remove the presence of iron impurities in the foil.

A separate mixture was prepared by adding 80 g of fumed silica in 300 mL of 3 M KOH and mixed at 80 ^{o}C for 12 hours. After this time period the solution was allowed to cool to room temperature. The aluminum solution was slowly added to the cooled silica solution. The resulting mixture was poured into several Teflon lined stainless steel cylindrical vessels.

These vessels were placed into an oven and the temperature was raised 175 ^{o}C. The cylinders were rotated in the oven (30 rpm) at this temperature for 8 hours. After this time, the cylinders were removed from the oven and allowed to cool to room temperature.

The contents of the vessels were transferred to centrifuge tubes. They were centrifuged, and washed several times until the pH was below 8. The solids (i.e. zeolites) were then removed from the tubes, and allowed to dry at 110 ^{o}C in an oven. Samples were taken to be analyzed using WAXS for the purpose of verifying the structure of zeolites.

Currently, there are no publications which document the separation capabilities of zeolite L.

2.8 Functionalization of Zeolite Surfaces

Zeolites surfaces have been chemically modified using silane coupling agents for the purpose of enhancing interactions between, or chemically linking the zeolite to an external surface. Silane coupling agents have a general formula $YSi(OR)_3$, where R and Y stand for a hydrosable group (e.g. methyl or ethyl) and a non-hydrolysable organofunctional group (e.g. amino) which are capable of interacting with fillers and polymers, respectively. In this section, some of the publications involving functionalizing zeolite surfaces are discussed.

Choi et al., functionalized zeolite A with amine groups for the purpose of connecting the zeolite to a modified glass substrate.[110] Their intent was to develop a method to assemble small particles in to highly ordered arrays on a substrate. They choose to work with developing ordered arrays of zeolite A on a glass substrate. The authors' work shows that some zeolites can be amine functionalized, and that this amine groups can still react with other functional groups once on the surface, essentially connecting the zeolite to the substrate. In this work zeolite A was mixed with 3-aminopropyltriethoxysilane (APTES) in boiling toluene. The mixture was allowed to reflux for 1 hour at 110 ^{o}C under argon flow (Scheme 1).

A similar treatment was given to glass substrates. Glass plates were sealed in an incubation chamber. The glass plates measured 18 x 18 mm^2, and for each plate, 0.3 mL APTES was added to the chamber. The chamber was placed under vacuum and kept at a temperature of 100 ^{o}C for 15 minutes. The chamber was allowed to cool to room temperature and the plates were removed and washed with ethanol and finally deionized water. The amine-functionalized plates were allowed to dry under N_2 flow (Scheme 2).

A dried amine-functionalized plate and 1 mg of fullerene were added to a round-bottom flask filled with toluene. This mixture was refluxed for 24 hours under argon flow. After this time, the mixture was allowed to cool to room temperature and the plate was removed, and washed with chlorobenzene to remove unreacted fullerene (Scheme 3). Schemes 1-3 are shown in Figure 2-40.[110]

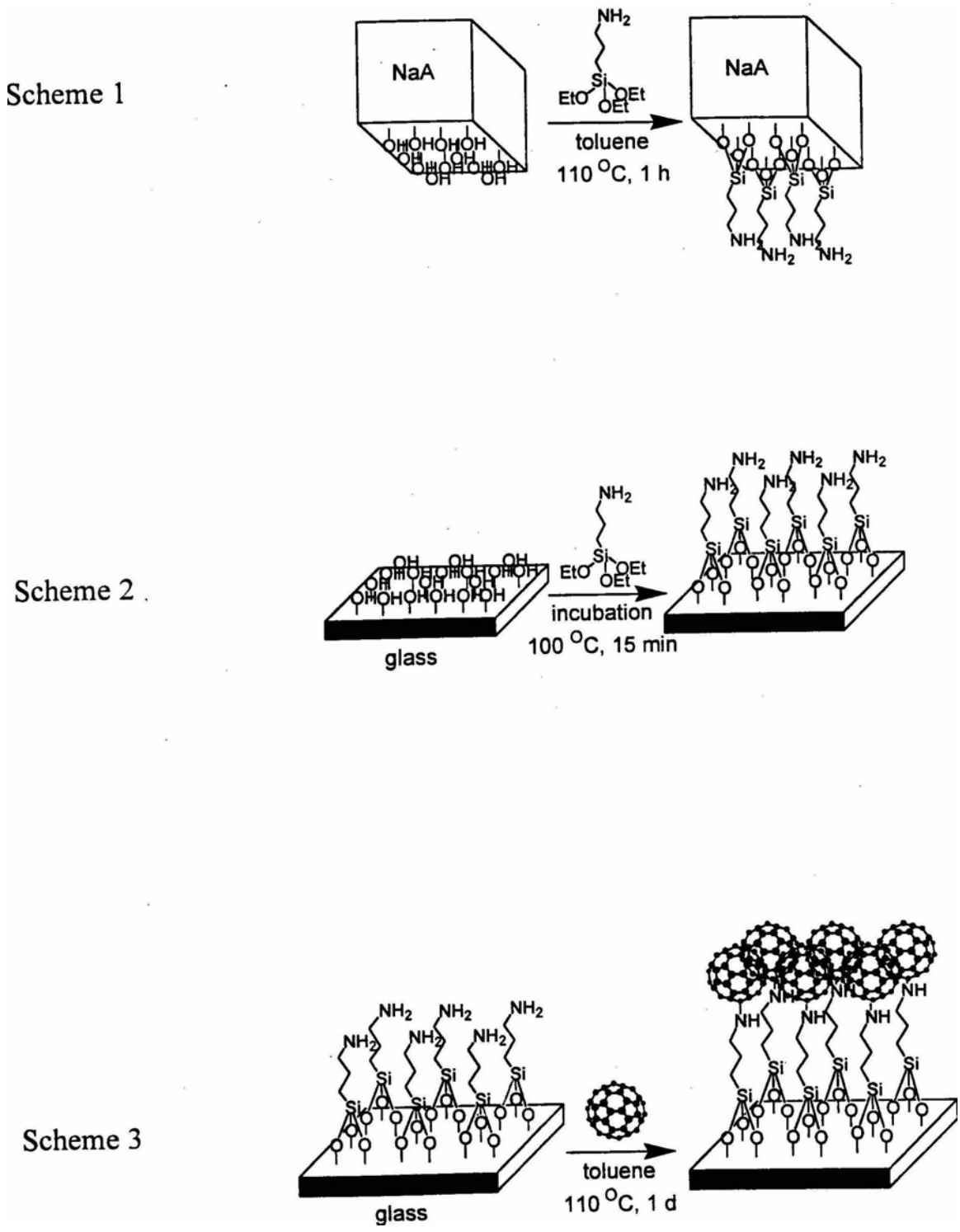

Figure 2-40. Reaction schemes employed Choi et al., to amine-functionalize zeolite A and fullerene-functionalize glass plates. This figure was adapted from reference 110.

To covalently link the amine-functionalized zeolite A with the fullerene functionalized plate, the two components were mixed in a ratio of 50 mg zeolite for one plate. The reaction was performed in a round-bottomed flask with toluene at 110 ^{o}C for 5 hours under argon flow. After this time the plates were removed and sonicated to remove physisorbed zeolite crystals (Scheme 4). Scheme 4 is shown below in Figure 2-41.[110]

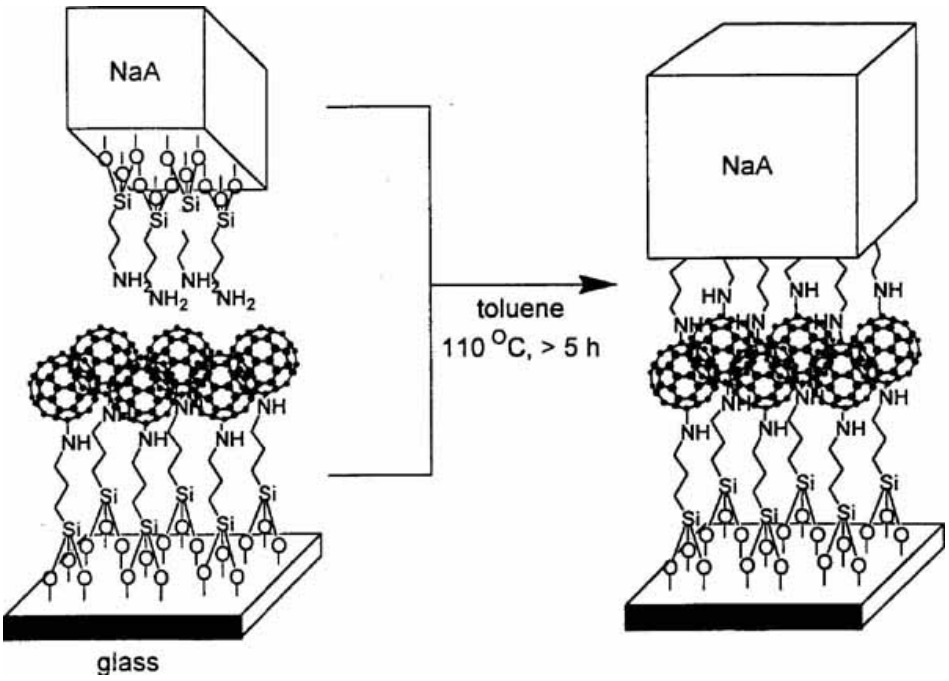

Figure 2-41. Reaction scheme employed by Choi et al., to link amine-functionalized zeolite A to fullerene-functionalized glass plates. The figure was adapted from [110].

Ha et al., investigated fabricating zeolite monolayers on functionalized glass. Glass plates were micropatterned with inert octadecyl (OD) groups using a PDMS stamp. Areas of the glass which were not coated with (OD) were treated with 3-chloropropyltrimethoxysilane in toluene and refluxed at 110 ^{o}C. This treatment resulted in a chlorine group becoming covalently attached to the glass surface.

The functionalized glass plates were reacted with ZSM-5 in toluene. The chlorine group reacted with the proton on the zeolite's –OH group to form HCl and the glass plate was then connected to the plate as shown in Figure 2-42.[111] The reaction was performed

in toluene at 110 ^{o}C for 3 hours. After this time, the mixture was allowed to cool to room temperature, and the plates were then removed, placed in fresh toluene.

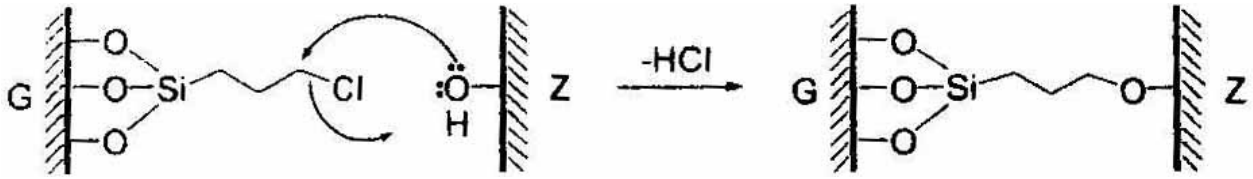

Figure 2-42. Linking zeolite crystals to chloro-functionalized glass plates in order to produce oriented zeolite monolayers. This was adapted from Ha et al [111].

The plates were sonicated for 1 minute to remove physisorbed zeolite crystals from the glass. An image of the resulting glass-zeolite composite is shown in Figure 2-43.[111]

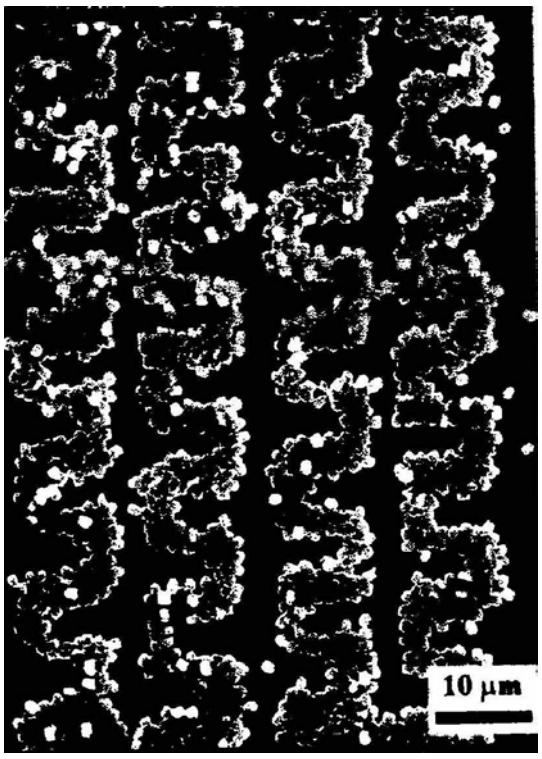

Figure 2-43. SEM images of an area of a glass plate which was micropatterned with a ZSM-5 monolayer. Image taken from Ha et al [111].

Kulak et al., developed a novel technique aimed at strengthening the bond between each zeolite crystal and the modified glass.[112] In order for the method reported by Ha et al., to work, the distance between the functional groups can not be shorter than the peaks and valleys on each surface. Unlike the other methods discussed to this point, the method by Kulak et al., does not require a smooth glass surface; in fact, it was designed specifically to be used under this condition.

In this method the authors used polyethlenimine as a long flexible linker between the zeolite and the glass. Zeolite A crystals were tethered with epoxypropoxyproplytrimethoxysilane (EPP) in toluene at 110 ^{o}C under argon for 1 hour. Glass plates (18 x 18 mm^2) were prepared similarily. The EPP functionalized glass plates were treated with polytheyleneimine (M_w = 25000 g/mol) in toluene and the unreacted polymer was removed by repeated reflux and sonication in ethanol. These plates were then allowed to react with the EPP tethered zeolite A crystals in boiling toluene for 2 hours. After this time, the plates were immersed in fresh toluene and and sonicated for 1 minute to remove physisorbed zeolite.

This technique led to a zeolite monolayer which was covalently attached to the glass plate. An illustration of this concept is shown in Figure 2-44.[112]

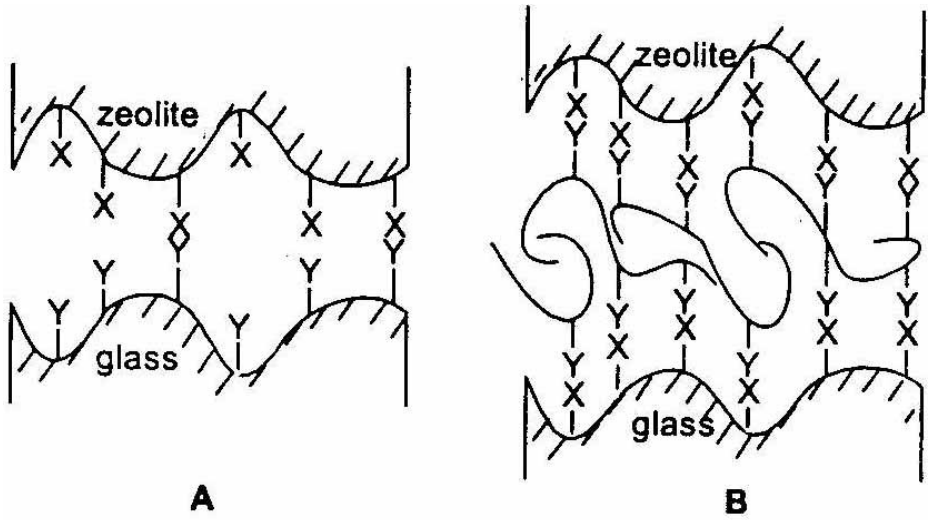

Figure 2-44. Illustration of the limited number of possible linkages between the zeolite and glass plate (A). Using a flexible polymeric linker can increase the number of linkages (B). Image taken from Kulak et al [112].

Metin et al., investigated the differences in mechanical properties among polypropylene-zeolite composites in which the zeolites were treated with different silane coupling agents and polyethylene glycol.[113] **Table 2-8** lists each coupling agent and its chemical structure.[113]

Table 2-8. Surface modifers used by Metin et al. in polypropylene-zeolite study.

Surface Modifier	Chemical Formula
Polyethylene glycol	$HO\text{-}(C_2H_4O)_n\text{-}H$
3-Aminopropyltriethoxysilane	$NH_2\text{-}(CH_2)_3\text{-}Si\text{-}(O\text{-}CH_2\text{-}CH_3)_3$
3-mercaptopropyltrimethoxysilane	$SH\text{-}CH_2\text{-}CH_2\text{-}CH_2\text{-}Si\text{-}(O\text{-}CH_3)_3$
Methyltriethoxysilane	$CH_3\text{-}Si\text{--}(O\text{-}CH_2\text{-}CH_3)_3$

In this study the zeolites were functionalized by mixing them with a coupling agent in an aqueous ethanol solution. The slurry was allowed to mix for 2 hours at room temperature. Following this, the slurry was dried in a vacuum oven at 110 ^{o}C and 400 mbar for 4 hours.

The composites were prepared at 2, 4 and 6 wt % treated zeolite, and the same was done for composites using untreated zeolites. To make the composites polypropylene (PP) pellets were mixed with the zeolite. For treated zeolites epoxidised soybean oil was added as a plasticizer. The mixture was extruded at 220 ^{o}C through a thin slit die and onto a water cooled casting drum. The resulting film was then stretched between casting rolls.

Tensile strength measurements of the composite membranes showed that Young's modulus increased with zeolite loading. This was attributed to the restrictions on the mobility of PP within the matrix. The authors reffered to a different study by Pehlivan et al., in which decreases in Young's modulus were observed when no treatment was given to the zeolites.[114] This observation was consistent with the results of Metin et al., which

was a 10-20% increase in the modulus when comparing untreated zeolite composites with treated zeolite composites.

2.9 Mixed Matrix Membranes

Mixed matrix membranes (MMMs) incorporate an inorganic filler into a polymer matrix. The filler typically has better permeation and separation properties than the polymer. The primary motivation for researching MMMs is to develop hybrid membranes which retain the low cost and processability of the polymer, but improve its separation performance with the addition of the zeolite.

Mixed matrix membranes can be composed of either rubbery or glassy polymers. This section of the Literature review devoted to MMMs has two subsections: rubbery MMMs, and glassy MMMs. The rubbery MMMs are discussed first, as they were developed first. Glassy MMMs are discussed more in detail as the are more pertinent to the research outlined in this dissertation.

2.9.1 Rubbery Mixed Matrix Membranes

Mixed matrix membranes were first developed using rubbery polymers and zeolites with the goal of improving membranes for pervaporation applications. Te Hennepe et al, mixed polydimethylsiloxane (PDMS) with silicalite-1 leading to an improved separation of ethanol from water.[115] The separation factor increased almost six fold, and the permeation rates doubled as the zeolite loading approached 70%. Jia et al., looked at the same system, but for gas separation performance.[116] Their membranes showed increased permeability for He, H_2, O_2 and CO_2, while the permeabilities of N_2, CH_4, n-butane, iso-butane, and 1-butene decreased. Furthermore, the PDMS-Silicalite-1 membranes offered better O_2/N_2 selectivity than any organic membrane at the time of the publication. The authors claimed that the silicalite-1 only allowed molecules of a specific dimension or smaller to pass through. Because their membranes were up to 70% in weight zeolite (i.e. over 50% by volume zeolite), molecules too large to enter the

silicalite-1 were essentially limited to diffusion through a membrane with less than half of its volume being permeable to the gas. Later work by these authors aimed at determining ideal fabrication methods for PDMS-silicalite membranes.[117] Common problems encountered when making MMMs were the precipitation of the zeolite from solution (zeolites are not soluble in any organic solvent), and the agglomeration of zeolites in the solution leading to pin hole defects in the final membrane. Furthermore, MMMs in which the zeolites were not thoroughly dispersed did not show improvements relative to the pure polymer membrane. To overcome these problems, the authors fabricated PDMS-silicalite membranes from a suspension of ultra-fine silicalite crystals (i.e. 0.2 – 0.5 μm) and partially polymerized PDMS, which increased the viscosity of the suspension preventing the zeolites from precipitating or sedmenting. A series of membranes of varying thicknesses, PDMS to solvent (i.e. iso-octane) ratio, and silicalite to PDMS ratio were made to find the optimum parameters. MMMs of 3.5-4.0 PDMS to solvent ratio and silicalite to PDMS ratios of 1.5-3.3 delivered the highest selectivity reproducibly of the combinations.

With rubbery MMMs showing promise in the gas separation field Duval et al., broadened the scope of research by investigating the effects of different zeolites on the performance of rubbery MMMs.[118] Using silicalite-1 (S1), zeolite 13X (13X), zeolite KY (KY), and zeolite 5A (5A) four variables of zeolites were considered: pore size, direction of pores (1-d, 2-d, or 3-d), Si/Al ratio, which controls hydrophilicity and adsorption, and the type of cation (its size and valence). Their results indicate that the permeability and selectivity of a component can be enhanced in a membrane if the added zeolite possesses a large sorption capacity for that component. These effects were seen for the CO_2/CH_4 separation for S1, KY, and 13X in ethylene-propylene rubber (EPDM), and the effects were more pronounced until an optimum loading was reached, typically between 45 and 55 percent. The greatest enhancement of performance came from the incorporation of 13X whose pores are about twice the size of CO_2 and CH_4. The 13X-EPDM MMM offered better permeability and selectivity for all loadings relative to its S1 counterpart, despite S1 having a smaller pore size than 13X. While the larger pores size of 13X would explaing the higher permeability relative to S1, it does not explain the increased selectivity. The authors believe this indicated that size exclusion is not the only

mechanism involved in separating gases, rather the affinity of the gas for the zeolite greatly influenced the MMMs properties.

Tantekin-Ersolmaz et al, investigated the relation between particle size and MMM performance for silicalite-PDMS systems.[119] Silicalite sizes were varied from 0.1 μm up to 8 μm, and the resulting MMMs were tested for O_2, N_2 and CO_2 permeability. The data indicated that as the particle size of the zeolite increased, the permeability of the membrane correspondingly increased, while the ideal selectivities remained unchanged. Furthermore, at the same loading differences in permeability were observed between MMMs with well dispersed zeolites and MMMs with agglomerated zeolites; the latter showing a higher permeability. The authors believed this phenomenon could be explained by considering the resistance at the zeolite-polymer interface. There were more interfaces and more interfacial area in the well dispersed systems. Due to this the mass transfer resistance became more pronounced. However, they did not account for the variation in fabrication methods necessary to achieve size variation, which could lead to differences in the inherent separation properties of the zeolites.

More systems were investigated by Koros et al.[120] Poly(vinyl acetate) (PVAC) and zeolite 4A (4A) were combined into a MMM leading to improved ideal separation values for air, but lower permeability values at a loading of 15% by volume. However, when the loading was increased to 25%, the membranes became defective; the authors believed this was due to agglomeration of the zeolites. To overcome this, the zeolites were first primed with a polymer coating. This was achieved by dispersing 4A and "a small amount of polymer" into toluene. Toluene was not a good solvent for the polymer forcing it to coil-up thereby reducing its dimensions and allowing more of it to be adsorbed onto the zeolite surfaces. The coated zeolites were mixed with PVAC to make a MMM. At 25% and 40% volume, the MMMs offered roughly the same permeability for the air separation, but almost double the ideal selectivity.

Despite the promising work performed on rubbery MMMs which has been outlined here, the focus of many research efforts began to shift from rubbery MMMs to glassy MMMs. The reason for this is that rubbery MMMs often have very low selectivity. Furthermore, the permeability of some gases in a rubbery polymer, for example CO_2 in PDMS, is very high (i.e. 3200 Barrer). This can results in the gas

molecules diffusing around the zeolite. Glassy polymers often offer higher selectivity than rubbery polymers. Additionally, the lower permeability of glassy polymers relative to rubbery polymers should help insure that the gas molecules diffuse through the zeolite, and receive the zeolite's enhanced selectivity and permeability. Relevant research in glassy MMMs is outlined in the following section.

2.9.2 Glassy Mixed Matrix Membranes:

With the improvements in separation performance associated with adding zeolites to rubber polymers, focus began to shift to mixing zeolites with glassy polymers. Initial attempts at fabricating MMM using glassy polymers and zeolites resulted in the presence of voids between the polymer and zeolite, thus reducing the separation performance of the composite membrane relative to the pure polymer.[118,120,121] Duval et al, simply mixed several glassy organic polymers with varying glass transition temperatures (T_g's), and one rubbery inorganic polymer all of which resulted in poor adhesion between the two phases. To overcome these defects, several different silane coupling agents were successfully employed to improve adhesion between the polymer and zeolite, however, the resulting permeabilities were slightly lower, and ideal selectivities were largely unchanged when compared to the pure polymer. The authors also fabricated a Poly(4-methyl-1-pentene) - Z-6032 (30% vol) MMM which was solution cast at a temperature of 60 ^{o}C, well above its T_g of 36 ^{o}C. They postulated that this would relieve any stress introduced into the membrane when the solvent evaporates. According to the SEM images of the membrane, the structure of this membrane was improved, but the membranes were still found to be defective from a "separations" perspective.

Other attempts at developing glassy polymer-zeolite composite membranes have focused on fabrication methods without modifying the zeolite surface. Gür combined molecular sieve 13X (13X) and polyethersulfone (PES) through a melt extrusion process.[122] PES pellets and 13X powder were extruded twice in a twin screw extruder at 340^{o}C and then dried in a vacuum oven at 200^{o}C. Finally, the resulting mixture was extruded through a slit die producing thin membranes. This process was repeated to

produce MMMs at 10%, 20%, and 40% vol 13X. However, the resulting membrane's permeation properties did not change significantly relative to the pure PES membrane.

Süer et al simply mixed polyethersulfone with either zeolite 13X or zeolite 4A and cast the mixture in an attempt to study the effects of fabrication on membrane performance.[123] They used three different solution drying and annealing procedures to fabricate the membranes, one of which resulted in improved permeability and selectivity relative to the pure PES. All the procedures involved mixing the polymer with one of the zeolites in dimethylformamide. The mixture was mechanically cast onto a glass plate. The first procedure let the solution dry at room temperature for one day, followed by annealing at 80-100^{o}C for 6-8 hours. The second procedure involved allowing the mixture to dry at barometric pressure under nitrogen flow at 60-80^{o}C for 8-10 hours. The resulting membrane was then quenched in water, and annealed under vacuum at 80-100^{o}C for 16-24 hours. The third procedure involved allowing the mixture to dry under low pressure with nitrogen circulation at 60-80^{o}C for 8-10 hours. This was followed by quenching in water, and annealing at 80-100^{o}C for 16-24 hours at barometric pressure.

The first fabrication procedure lead to a nonselective membrane which allowed all the gases tested to pass through unrestricted. The remaining two procedures lead to workable membranes. However, MMMs produced by the second procedure were much more brittle than those produced by the third procedure, not allowing the researchers to reach a high loading of zeolites. Additionally, the permselectivity of membranes created using the third method were better than those created using the second method. These differences between the two procedures were attributed to the drying rate of the membranes. The second method applied a slow evaporation rate followed by a rapid drying rate under vacuum. The authors postulated that this inhibited relaxation of intersegmental packing leading to a denser membrane, thus resulting in a lower permeability and poorer distribution of zeolites in the matrix. The third procedure, involving a fast evaporation step followed by a slow evaporation step, allowed relaxation of the packing and more homogenously distributed the zeolites within the matrix. This lead to a less dense matrix resulting in higher permeation rates, and separation performance.

For both types of zeolites the permeation first decreased upon loading, then after reaching a minima, began to rise with additional loading along with the selectivity. SEM images revealed that the zeolites were embedded in cavities and possessed very little contact with the polymer. The authors believed that as the zeolites loading increased, a network of void spaces was created leading to a series of low resistance channels for gases to permeate through. This phenomenon would normally lead to lower separation factors, however, due to the resulting increase in free volume near the zeolites, the polymer matrix must have increased its packing density restricting gas flow, and counterbalancing the void effects.

Koros outlined an approach for designing MMMs and presented an equation to predict the separation performance of a MMM based on pure component properties.[121] His approach involved reaching optimum separation performance by choosing a polymer that already has good separation performance. As the polymer often composes most of the MMM, in the absence of any defects, it will set the lower limit of performance. The zeolites chosen must posses separation characteristics superior to that of the polymer if the MMM is to be an improvement. Not only must the zeolite component separate species better, it must posses a higher permeability than the polymeric phase, otherwise, the gas will simply diffuse around the zeolites minimizing separation enhancements.

The equation presented for predicting MMM performance was adopted from work done by Robeson.[39] Robeson described the permeability through a continuous phase containing a dilute suspension of spheres, which Koros et al. adopted for MMM applications. The equation, called the Maxwell equation, is defined below:

$$P_{eff} = P_C\left(\frac{P_D + 2P_C - 2\phi_D\left(P_C - P_D\right)}{P_D + 2P_C + \phi_D\left(P_C - P_D\right)}\right) \qquad \text{Eq (2.31)}$$

where P_{eff} is the permeability through the matrix, P_C the permeability through the continuous phase, P_D is the permeability through the dispersed phase (i.e. spheres), φ_D is the volume fraction of the dispersed phase. Using this equation, Koros et al. predicted the permeability for a polysulfone – zeolites 4A MMM shown in Figure 2-45; the image was taken for their work.[124]

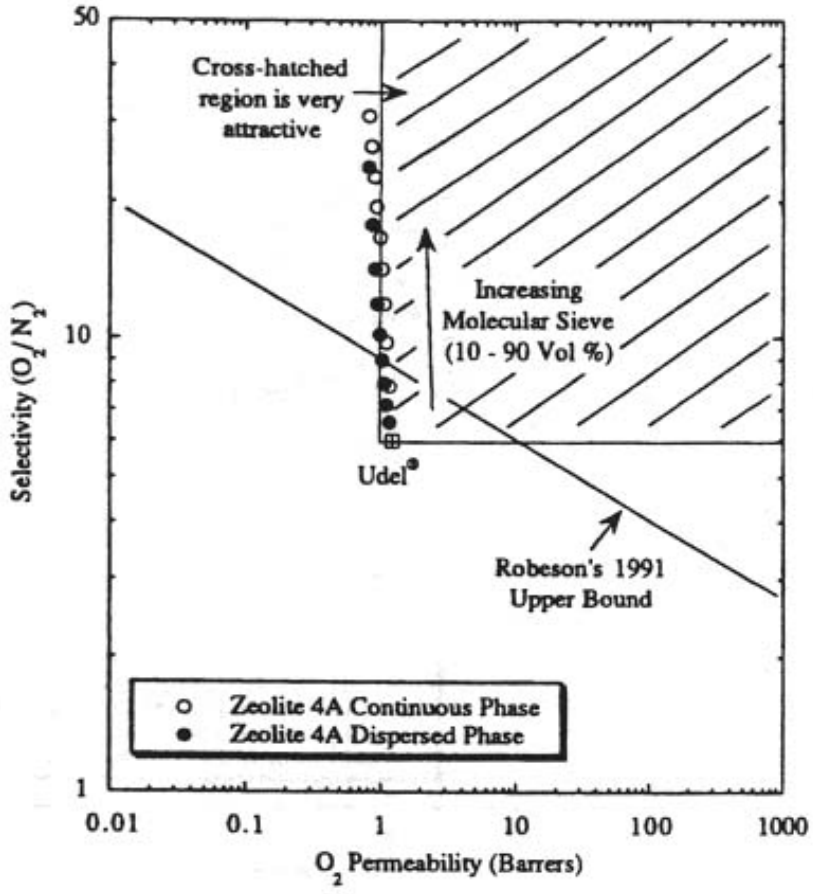

Figure 2-45. Predicted zeolites 4A-Polysulfone (Udel®) MMM performance from Maxwell's equation.

Later work by Koros considered new systems and would compare the Maxwell equation predictions to experimental results of these systems.[120] To help alleviate poor adhesion between the polymer and zeolites, poly(vinyl acetate) (PVAC) was chosen for its low T_g, flexibility, and affinity for alumina (a component of many zeolites). The lower T_g and increased flexibility of PVAC was exploited to overcome any stresses in the polymeric phase upon evaporation of the solvent. The polymer was mixed with unmodified zeolites 4A and solution cast. At 15% loading by volume, the MMM showed improved selectivity, but a 10% decrease in permeability relative to the pure PVAC. The observed selectivity agreed with that predicted by the Maxwell equation, but the observed permeability was roughly 15% lower than the predicted Maxwell value; predicted

selectivities were determined by ratioing the predicted P_{eff} (Eq 2.31) of the two gases. When this system was extended to loadings of 25%, the samples became defective. The authors attributed this to poor zeolites-polymer contact and poor dispersion, both leading to channel of voids within the samples.

To overcome these deficiencies at higher loadings the authors proposed priming the zeolites with a thin coating of polymer to aid in phase contact and dispersal. A mixture of toluene, zeolites 4A and PVAC was used for the priming. Toluene was chosen because it provided an environment where the polymer has a stronger affinity for the zeolites than the solvent, as well as the zeolites possessing a stronger affinity for the polymer than the solvent. Furthermore, toluene is a poor solvent for PVAC, leading it to retract its coil size and allowing more polymer to adsorb onto the zeolites surfaces. Based on the amount of polymer and zeolites added and the surface area of the components, the calculated layer thickness was 400Å.

At 15 vol % loading, this method at lead to similar properties as those produced from solution casting. The priming also allowed the higher loading MMMs to be successfully fabricated. At 25 vol% loading the observed selectivity was slightly less than that predicted by the Maxwell equation, and the observed permeability was almost 30% less than the predicted value. Again, the predicted selectivities were determined by ratioing the predicted gas permeabilities using the Maxwell equation (Eq 2.31). These differences became more pronounced as the loading was increased to 40%. The permeation results of the study have been listed in Table 2-9 directly from their work.[120]

Table 2-9. Permeation results for PVAC - Zeolite 4A membranes.

Vol % Zeolite 4a	Predicted Permeation O_2 (Barrer)	Observed Permeation O_2 (Barrer)	Predicted O_2/N_2	Observed O_2/N_2
0	-	0.5	-	5.9
15	0.53	0.45	7.5	7.3 – 7.6
25	0.55	0.4	8.7	8.3 – 8.5
40	0.55	0.28 – 0.35	10.9	9.7 – 10.4

The authors attributed these deviations to several sources. First, the permeability of pure zeolites 4A may be inaccurate, because a defect frees zeolites 4A membrane whose intrinsic permeability could be effectively measured, has not yet been produced. The permeability was indirectly determined from gas sorption studies.[121] Additionally, it was proposed that the polymer chains at the zeolite surface were restricted in movement, leading to the lower permeation rates. This phenomenon was also observed by others working on composite membranes, and would be come more pronounced as the loading was increased.[125]

Yong et al developed interfacial void free polyimide mixed matrix membranes by using a low molecular weight chain capable of hydrogen bonding with both the polymer and zeolite.[126] This chain essentially enhanced the contact between the two components. The resulting membranes displayed increased permeability without much change in the selectivity. The authors mixed a commercial polyimide (i.e. Matrimid 5218 CH) (PI), 2,4,6-triaminopyrimidine (TAP) as the low molecular weight chain, and one of many zeolites (i.e. 4A, 5A, 13X, NaY) in dimethylsulfoxide, then cast onto a glass plate and leveled the solution with a casting knife. SEM images revealed that there were no voids

between the polymer and zeolites with the inclusion of TAP; voids were present without the presence of TAP. IR spectra taken of the pure PI, the pure TAP, and the mixtures of the two showed the presence of hydrogen bonding between the PI's carbonyl group and the amine groups of TAP. Permeation results indicated that the addition of zeolites to the PI-TAP membrane could alter the permeation rate or selectivity depending on the nature of the zeolites added. When zeolite 4A was added, permeation rates dropped for all gases studied (i.e. He, CO_2, O_2, N_2, CH_4), however the selectivities often improved. The addition of zeolite 13X resulted in much higher permeation rates for the same gases with little, if any, loss in selectivity. Zeolite 13X has a much larger pore size than zeolites 4A (i.e. 7.4Å versus 3.8 Å) allowing a less restricted passage for gas transport through the membrane.

Koros et al focused on the interface region again when they attempted to expand upon their successes using low T_g polymers in MMMs.[127] Despite successfully fabricating defect free MMMs, none of them broke the upper bound. The authors attributed this to the incorporation of a flexible polymer with low selectivity to overcome the defect causing stresses in the matrix. A return to more rigid polymers would likely push the MMMs above the upper bound, if the internal stresses could be alleviated.

Initial attempts using Matrimid, a commercial aromatic polyimide membrane, and zeolite 4A resulted in unchanged selectivity and increased permeability.[127] From these results the authors proposed a possible morphology to account for the experimental data. Dewetting of the polymer chains from the zeolite surface could result in a "sieve in a cage" structure in Figure 2-46 which was taken from their publication.[127] This morphology allows the gas to bypass the sieve avoiding its selectivity enhancements, and increases the gas permeability by providing a nonrestrictive passage.

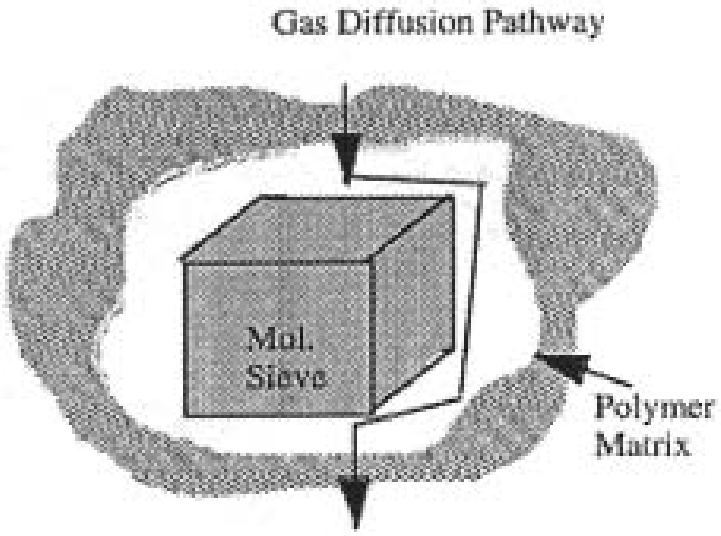

Figure 2-46. Sieve in a cage morphology.

One strategy to remove the voids was to anneal the MMMs above their T_g's. This strategy proved to be unsuccessful judging from SEM images taken before and after the annealing. The images showed the morphology to be unchanged despite reaching an annealing temperature almost 100°C above the polymer's T_g. From this the researchers concluded that to remove the sieve in a cage morphology, steps would have to be taken to prevent the cage from occurring rather than taking steps to remove it.

Earlier work by the same group attempted to form MMMs at temperatures close to the T_g of the polymer in the matrix. However, the common solvents used in fabricating membranes often boil at or below these temperatures. The only polymer that displayed a T_g close to the boiling points of common solvents was Udel®, a commercial polysulfone, and it did not interact favorably with zeolites surfaces.

To address this issue low T_g plasticizers were blended with Matrimide® to lower its T_g, initially 305°C, and increase its flexibility. Furthermore, low volatility solvents (i.e. 1-methyl-2-pyrrolidinone, 2-pyrrolidinone) with boiling temperatures above the blend's T_g were used in the casting of the membrane. The blends were composed of 75% weight Matrimid® and 25 % weight plasticizer, and all displayed a single T_g indicating good compatibility. The resulting T_g's of the blends have been listed in Table 2-10 below which was adapted from their work.[127]

Table 2-10. Glass transition temperatures of Matrimid® and 25% weight plasticizer.

Plasticizer	Blend's T_g (^oC)
RDP Fyroflex®	161
Di-Butyl Phthalate	150
4-Hydroxy Benzophenone	144

The polymeric blends were mixed with zeolite 4A (15% loading by volume) and cast under slight vacuum. Pure polymer membranes composed of Matrimid® and plasticizer were made as well. Permeation results showed that in each case the MMM offered improved selectivity, but lower permeation when compared to the polymer-plasticizer counterpart, with the exception of the MMM with 4-Hydroxy Benzophenone as a plasticizer which could never be successfully produced. The experimental values deviated negatively from the predicted Maxwell's values. When RDP Fyroflex® was used as a plasticizer the selectivity both with and without the addition of zeolites was better than that of pure Matrimid®; the addition of zeolites amplified the improvements. However, this was the only combination that resulted in improved selectivity. All other combinations lead to lower permeability. Further work focused on adjusting the weight % of plasticizer. These results showed the permeation scaled with the amount of plasticizer added to the matrix. The selectivity appeared to reach a maximum near 15% plasticizer.

Koros et al. investigated the use of covalent linkages between the polymer and zeolite for the fabrication of a mixed matrix membrane.[128] Aminopropylsilane was reacted zeolites using the reaction scheme shown in Figure 2-47 which was adapted from their work.[128]

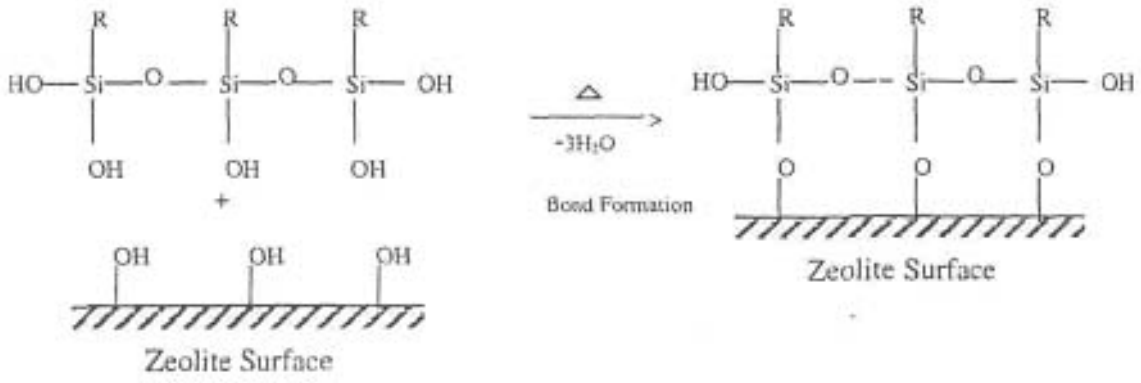

Figure 2-47. Attachment of silane to zeolite surface.

The reaction was carried out by dispersing zeolites into a 95% ethanol/ 5% water solution. The solution was sonicated for 30 minutes and cooled intermittently to avoid boiling off the solvent. The presence of amine groups on the zeolites was detected by XPS analysis.

After attaching the silane to the zeolite, the amine tethered zeolites were reacted with the imide linkage of a polymer in order to chemically bond the two components. This reaction has been outlined in Figure 2-48 which was adapted from the authors' work.[128]

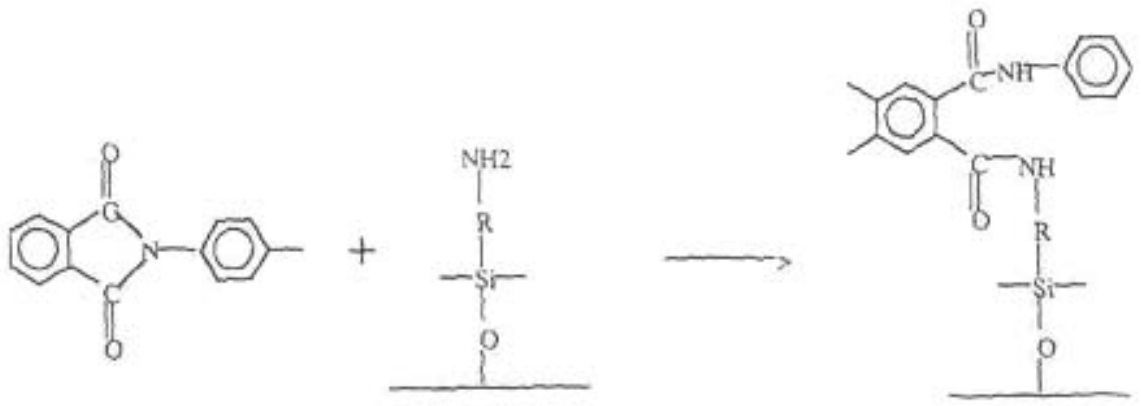

Figure 2-48. Reaction of polyimide with amine treated zeolite to chemically link zeolite 4A to polymer through an amide group.

This reaction was performed using Matrimid® and Zeolite 4A. SEM images indicated that covalently bound MMMs displayed much better adhesion than the MMMs possessed with unmodified zeolites. The MMMs produced from these covalently bonded polymer and zeolites offered lower selectivity and slightly higher permeability than both the pure polymer and the polymer – unmodified zeolite 4A composite for the O_2/N_2 separation. The authors proposed that the voids between the polymer and zeolite have been reduced in size but not eliminated. These smaller voids offer non-selective resistance leading to the loss in permeability. Specifically, the smaller O_2 molecule does not receive much of a boost in permeability, while the larger N_2 molecule receives a relatively larger increase in permeability, thus the loss of selectivity.

After establishing a relationship between retaining polymer flexibility during formation and successful production of MMMs, Koros et al. expanded their research to consider chemical coupling between the polymer and zeolite.[129] Three polymers were chosen based on exhibiting intermediate T_g's and the belief they would have some attractive interaction with Zeolite 4A. The polymers chosen were 2,2'-BAPB + BPADA (BAPB) and MPD/3,5di-t-Bu-APB-124 (3:1) + BPADA (MPD). Ultem was used in addition to these two polymers to provide a high T_g MMM for comparison. The polymers' T_g's and the monomers they were produced from have been listed in Table 2-11 which was adapted from their work.[129]

Table 2-11. Polymer glass transition temperatures and the monomers used in their synthesis.

Polymer	Structure or Constituent Monomers	Tg (°C)
2,2'-BAPB + BPADA (Polymer A)	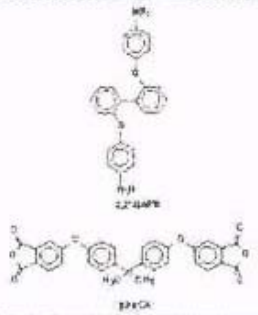	197
MPD/3,5di-t-Bu-APB-124 (3:1) + BPADA (Polymer B)	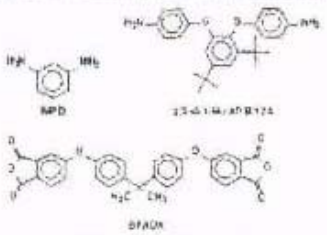	210
Ultem		220

.

MMMs were made using BAPB or MPD and zeolite 4A with 15% loading by volume. For each combination of polymer – zeolite 4A, one MMM was fabricated by mixing pure polymer with zeolite, and another was made by mixing pure polymer with zeolites functionalized with coupling agents that would then be chemically reacted to the polymer to produce a covalent linkage. The coupling agent used was 3-aminopropyldimethylethoxysilane. The silane reaction was performed by using the sonication method outlined previously. The MMMs were fabricated at 200^{o}C to ensure flexibility of the polymer during the removal of the solvent (i.e. NMP).

SEM images of the MMMs fabricated without the aide of coupling agents revealed good dispersion for both MMMs, but only the BAPB MMM had good contact between the polymer and zeolite. Permeation experiments were performed on these membranes and the results have been listed in Table 2-12 which were taken from their

work.[129] In this table, the Maxwell predicted selectivities were determined by ratioing the predicted permeabilities of the gas pair using the Maxwell equation (Eq 2.31).

Table 2-12. Permeation and selectivity results for the O2/N2 separation for polymer and unmodified zeolite mixed matrix membranes developed by Koros et al.

Polymer and Zeolite Loading	O_2 Permeability at 35 ^oC (Barrer)	Maxwell Prediction (Barrer)	O_2/N_2 at 35 ^oC	Maxwell Prediction
BAPB	0.5	-	7.3	-
BAPB + 15% Zeolite 4a	0.5	0.54	8.4	8.9
MPD	0.3	-	7.9	-
MPD + 15% Zeolite 4A	0.55	0.35	7.8	9.9

These results highlighted to the authors the importance of maintaining flexibility during the formation stage, as well as the importance of an attraction between the two components. Apparently, from the BAPB MMM results, one only needs a flexible polymer and one that has an attraction to the zeolites to successfully produce a MMM. The BAPB MMM offered improved selectivity with no loss of permeation, while the MPD MMM offered improved selectivity at a cost of a small decrease in selectivity. The latter was attributed to the unfavorable interaction between MPD and zeolite 4A due to MPD's bulky nonpolar t-butyl groups, which are hydrophobic while the zeolite is hydrophilic. Additionally, the T_g of MPD is higher than that of BAPB, so it had lower flexibility.

The MMMs consisting of a zeolite, coupling agent and polymer gave the results listed below in Table 2-13 which was adapted from the authors' work.[129] Ultem, a high T_g polymer, was added to the study to monitor the importance of polymer flexibility.

Table 2-13. Permeability results for polymeric mixed matrix membranes employing a coupling agent that chemically attached the polymer and zeolite.

Membrane	Zeolite 4A Loading %	Predicted O_2 Permeability (Barrer)	Observed O_2 Permeability (Barrer)	Predicted α O2/N2	Observed α O2/N2
BAPB	0	-	0.5	-	7.1
	20	0.55	0.47	9.4	9.4 - 9.6
	30	0.57	0.4	10.8	10.6 – 10.8
	40	0.6	0.37	12.6	12.4 – 12.5
Ultem®	0	-	0.38	-	7.8
	15	0.42	0.38	9.7	9.7
	35	0.49	0.28	13	12.85
	35-Mixed Gas	-	0.275	-	13.5

The authors looked at one final method of fabricating MMMs. To avoid carrying out a silonation step, a polymer was chosen that was capable of bonding directly to the zeolite. The polymer was reacted from hexafluoro dianhydride, 4, 4'-hexafluoro diamine, m-phenylene diamine, and diamino benzoic acid (DABA). The carboxylic group along the polymer's backbone was reacted with the silanol groups of the zeolite to make a covalent bond. The polymer possesses a high T_g of 368 ^oC. The structure of DABA has been listed in Figure 2-49 which was taken from the authors' work.[129]

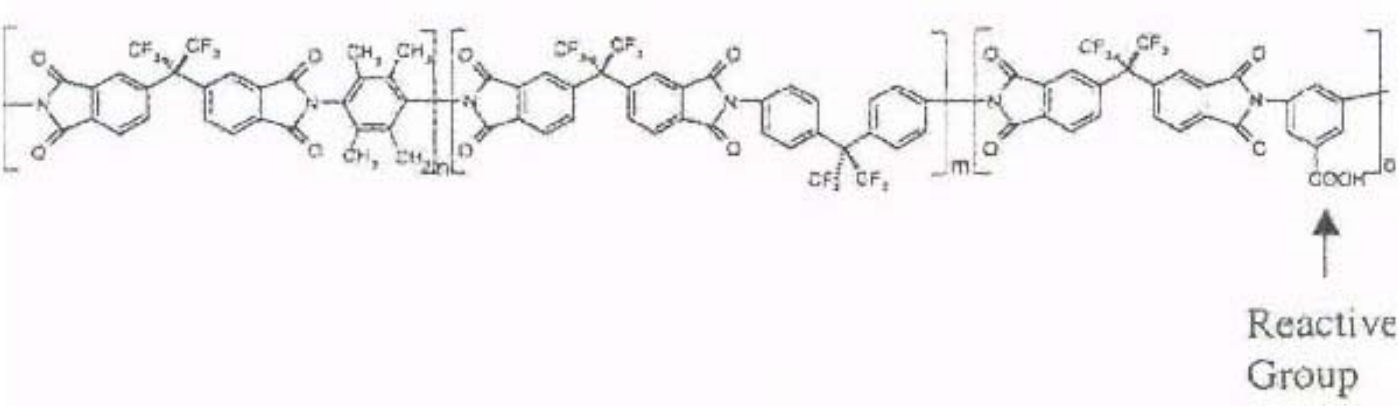

Figure 2-49. Chemical structure of polymer synthesized from hexafluoro dianhydride, 4, 4'-hexafluoro diamine, m-phenylene diamine, and diamino benzoic acid.

To make a DABA MMM zeolite 4A was dispersed into dimethylacetamide. After dispersal the polymer was added and allowed to mix until completely dissolved. The mixture was then heated at 150^{o}C until all of the solvent had evaporated. The remaining solid mixture was dissolved in tetrahydrafuran at room temperature, cast onto a glass surface, and a doctor blade was run over the solution to provide a more constant thickness.

SEM images of these membranes showed good dispersion of the zeolites, and good contact between the two components. The permeation results for this membrane have been listed in Table 2-14 which were taken from the authors' work.[129]

Table 2-14. Permeability results for DABA containing polymers linked to zeolite 4A. These mixed matrix membranes were fabricated with 15% volume zeolite 4A.

Membrane	**Zeolite 4A (Vol %)**	**Predicted O_2 Permeability (Barrer)**	**Observed O_2 Permeability (Barrer)**	**Predicted O_2/N_2**	**Observed O_2/N_2**
DABA	0	-	22	-	4.2
Polymer	15	16	14	4.3	4.5

These results suggested to the investigators that MMMs could be fabricated from rigid polymers without silanation steps, or efforts to maintain polymer flexibility. The authors went on to note that the resulting properties of the DABA MMM were not attractive, and that this may be due to a poor selection of polymer. Additionally, they noted that in order to make an attractive MMM, one must chose components such that the fastest gas to travel through the MMM has nearly identical permeabilities through both components. Otherwise, the gas will diffuse around the zeolite increasing the path length through the membrane and thus lowering the permeability.

2.10 Carbon Nanotubes-Polymer Composites

Carbon nanotubes (CNT's) have become the focus of many research efforts since their discovery in 1991 by Iijima.[130] These graphite tubes have large length to diameter ratios and are predicted to have high Young's modulus and tensile strength. Because of this, CNT's have been used in polymer composites to improve their mechanical properties, as is outlined in this section.

In this section CNT's and their properties relevant to this study are discussed. This section discusses both multiwalled CNT's and singlewalled CNT's. The latter is emphasized more, because it was more relevant to our research. Additionally, studies in which CNT's were added to a polyimide matrix are discussed.

2.10.1 Carbon Nanotubes

Carbon nanotubes were first synthesized by Iijima in 1991.[130] He noticed the seamlessly rolled sheets of hexagonally arrayed carbon atoms with nanometer diamters in a soot of amorphous carbon. Iijima synthesized the needle like graphite tubes using a DC arc-discharge evaporation technique in which the CNT's were grown on the negative end of a carbon electrode. This approach was adopted from the synthesis of fullerenes.[131] Using this technique he was able to synthesize carbon nanotubes ranging from 4 to 30 nm in diameter and up to 1 μm in length. These tubes were multiwalled carbon nanotubes

which consisted of several graphite tubes of varying diameters. Each of these tubes grew along the same axis but with a different diameter such that they were nested inside one another. Typically, the tubes were separated from each other by a distance of 0.34 nm. The smallest diameter in the center of these bundles of tubes was 2.2 nm.

A few years later Iijima and Bethune separately successfully synthesized single walled carbon nanotubes (SWNT's).[132,133] These nanotubes were synthesized by co-evaporation of a metal with graphite in an electric arc. In Iijima's method, the synthesis was conducted in a chamber filled with a gas mixture of 10 Torr methane and 40 Torr argon. The cathode was impregnated with iron prior to the synthesis. When the DC arc was applied to the electrodes the iron and graphite evaporated and condensed to form SWNT's. These SWNT's were several micrometers in length, and typically consisted of 7-14 bundled tubes which were individually ~1 nm in diameter, ranging from 0.7 – 1.65 nm.

Bethune et al employed a slightly different method to obtain SWNT's.[132] In their method the anodes contained bored holes filled with mixtures of pure metal powders (i.e. Fe, Ni, or Co). Under the application of a current in a He atmosphere (i.e. 100-500 torr), SWNT's were synthesized. Only CNT's synthesized using Co as the metal resulted in SWNT's. These tubes had very uniform diameters with a range of 1.1 – 1.3 nm.

2.10.2 Diffusion in Single Walled Carbon Nanotubes

Ackerman et al performed atomistic simulations of diffusion of pure Ar and Ne through SWNT's.[134] For comparison, they also predicted the diffusion of these gases through the zeolite silicalite. These simulations were performed for three different sizes of CNT's, feed pressures of 0 – 100 bar, and a temperature of 25 ^{o}C.

The authors determined self diffusion coefficients using the Einstein relation, which calculates the self diffusion coefficient as a function of time, the number of molecules in the system and the vector position of the molecule. The transport diffusivity was calculated using the equilibrium molecular dynamics method. The bundles of SWNT's were represented as an ideal hexagonal array with an inter-tube gap of 0.32 nm.

Their results predicted that the self diffusivity of Ar in SWNT's was orders of magnitude larger than in silicalite. At low pressures the self diffusivity in the CNTs was predicted to be on the order of 10^{-1} $cm^{-2}s^{-1}$ which was much higher than the 10^{-4} $cm^{-2}s^{-1}$ of silicalite. However, as the pressure was increased to 80 bar, the self diffusivity in the SWNT's dropped to 10^{-3} $cm^{-2}s^{-1}$ while that of zeolite was relatively unchanged. This was attributed to the very smooth surface of the interior of the CNT's. At low pressures the adsorbed Ar is well separated from each other, but as the pressure increases this is no longer true. Therefore, the diffusivity begins to become effected by atom-atom collisions. This same trend was predicted for Ne.

Simulations for the transport diffusivity showed a different trend. Again, the diffusivities of pure Ar in the CNT's were much higher than that of silicalite, $\sim 10^{-1}$ vs $\sim 10^{-4}$ $cm^{-2}s^{-1}$. This same result was obtained for simulations run for Ne. Unlike the self diffusivity, the transport diffusivity the SWNT's and silicalite were largely unchanged up to 80 bar.

With these results the authors looked at predicting the pure gas fluxes through SWNT's and silicalite. For both Ar and Ne, the fluxes were approximately four orders of magnitude higher in the CNT's than in the zeolites.

Cooper et al measured gas permeability through a membrane composed of SWNT's, called "buckypaper."[135] The SWNT's in the membrane were determined to have a pore size distribution ranging from 1-10 nm. SEM images of the membrane revealed that the nanotubes were randomly oriented, and that some impurities such as amorphous carbon and metal catalyst were imbedded in the membrane during its synthesis. The authors studied the permeation of oxygen, nitrogen, and argon. The results indicated that permeation through the nanotube membrane did not follow typical transport models. The diffusion rates were dependent on pressure but not time of operation. Additionally, the membrane showed strong pressure dependence, showing a strong increase in permeability as the pressure was increased. The authors suggested that the membrane could be elastically deforming, resulting in flow between the nanotubes.

To date there is only one publication in which a CNT-polymer MMM was fabricated. In that study, Hinds et al developed a MWNT-polystyrene MMM and measured N_2 permeation as well as the transport of $Ru(NH_3)_6^{3+}$ across the membrane in

aqueous solution.[136] The tubes within this membrane were well aligned during their synthesis on a quartz substrate, and a toluene-polystyrene solution was spin coated over the grown MWNT's. The tubes had diameters ranging from 5-10 nm. To remove the film from the quartz after the solution was dried, hydrofluoric acid was employed. This technique resulted in a MWNT-polystyrene membrane film of 5 to 10 μm in thickness. These films were then put under a plasma oxidation treatment to etch away the surfaces of films. Because polystyrene etches faster the CNT's, this process effectively removed any polymer film covering the pores of the MWNT's.

Permeation experiments of pure N_2 and aqueous $Ru(NH_3)_6^{3+}$ were gathered at room temperature. Nitrogen permeance showed a linear relation with pressure drop across the membrane, with a value of 2.6 μmol $m^{-2}s^{-1}Pa^{-1}$. For an aqueous solution of $Ru(NH_3)_6^{3+}$, another linear relationship with pressure across the membrane was observed. The flux was measured to be 0.9 μmol $cm^{-2}h^{-1}$. In an attempt to control the flow rate of the ion through the CNT membrane, the authors coated the tip of the nanotubes with carboxylic groups, intending the slow the transport of the positive ion through interactions with the anion of the carboxylic groups. This method reduced the flux by a factor of 5.5, suggesting that fluxes of molecules could be controlled through these types of membranes.

2.10.3 Carbon Nanotube-Polyimide Composites

Due to carbon nanotubes high aspect ratio, high mechanical strength, as well as high electrical and thermal conductivity, CNT's have been considered as ideal fillers in polymer nanocomposites.

Wong et al investigated CNT-polystyrene and CNT-epoxy composites to investigate the interactions present between the two phases. Using TEM and SEM as well as mechanical simulations and elasticity calculations the authors were able to quantify some of the critical variables that control interactions. The authors stated that the following physical events all contribute to the interactions on the nanometer scale:

- In the absence of chemical bonding between the two phases, the interactions between CNT's and polymer are electrostatic and van der Waals forces.

- Local non-uniformity of a CNT embedded in polymer matrix may result in nano-mechanical interlocking, similar to the meshing of gears
- Differences in the coefficients of thermal expansion is a significant factor contributing to both non-bond interactions and mechanical interlocking, because compressive thermal residual stress may increase the true contact area between the CNT and the polymer.

Park et al developed a method to fabricate SWNT-polyimide composites using an in situ process. The authors dispersed SWNT in dimethyl formamide with the aid of sonication. To this 1,3-bis(3-aminophenoxy) benzene diamine and 6FDA were added to synthesize a polyimide in the presence of the dispersed nanotubes. Using this technique the authors made a series of composites with CNT loadings from 0.01 – 1.0 vol %. The incorporation of CNT's into the matrix appeared to be well dispersed according to TEM images. The authors also noted there was no indication of voids at the interfaces despite the using of a rigid polyimide. The authors believed that using aromatic polyimides allowed the polymer to favorably interact with the CNT's through π-π overlap interactions.

The T_g of the composites was 10 ^oC higher than that of the pure polyimide determined using DMA. The tan δ peak of the composite was shorter and broader than that of the pure polyimide. Despite large changes in the loading of nanotubes, the T_g of the composites remained at 199 ^oC. The authors performed TGA experiments to determine if the addition of CNT's improved the thermal stability of the polymer. Each increase in loading improved the temperature at which there was a 5 wt % loss in the composite, but this improvement began to level off at 0.5 vol % of CNT; the 1.0 vol % CNT composite lost 5% of its weight at 479 ^oC, while the pure polyimide lost 5% of its weight at 444 ^oC.

Park et al performed a second study using the same polyimide and SWNT's.[137] These composites contained 0.5 wt % CNT. TEM images revealed that the nanotubes were present in the polymer matrix as discrete bundles with diameters near 40 nm. The authors used energy-filtered transmission electron microscop to map nitrogen and determine if the polymer adhered well to the CNT. From the mapping, a good distribution of polymer on the nanotubes was observed. The authors concluded from

their study, that aromatic polyimides can be used to make good CNT composites due to the excellent adhesion promoted by π-π overlap interactions as outlined in their previous work.

Ounaries et al did an extension of Parks work investigating the electrical properties of polyimide-CNT composites.[138] In this work, the authors used the same materials as that of Park, but focused on the conductivity of the composites. The authors created polyimide-CNT composites of up to 1 vol % CNT. Both DC and AC measurement techniques were used in this study. The results indicated that the composites have an apparent percolation threshold at 0.05 vol % CNT, at which dramatic increases in conductivity were observed. The authors concluded that it was possible to tailor the conductivity of the composite over many orders of magnitude by varying the CNT loading.

Ogasawara et al developed crosslinked polyimide systems and mixed them with MWNT's.[139] In their technique, a low molecular weight (M_w=1560 g/mol) polyimide oligimer was first synthesized, and then mixed with MWNT's. The mixing was done in the absence of any solvent and with the aide of a mechanical mixer. This mixture was then compressed between two hot plates at 370 oC. At this temperature the oligomers cured. Using this method, the authors fabricated films with 0, 3.3, 7.7, and 14.3 wt % CNT.

Using SEM, the authors were able to show good dispersion of the CNT within the composites. The authors gathered DMA curves to study the mechanical properties of these composites as well. The pure polyimide showed a T_g at 335 ^oC, and with each increase in CNT loading the T_g would rise eventually reaching 357 ^oC at 14.3 wt % CNT. The storage modulus also increased with CNT loading beginning at 2.84 GPa in the pure polyimide and reaching 3.90 GPa with the highest loading of CNT. However, tensile tests showed there was a decrease in failure strain with each increase in loading of CNT's. The authors believed that their results suggested that the MWNT's were acting as macroscopic crosslinks, and were further immobilizing the polyimide chains at elevated temperatures.

2.11 References

1 Koros, W. J.; Chern, R. T. *Handbook of Separation Process Technology*, 1 ed.; John Wiley & Sons, 1987.

2 Graham, T. *Philos. Mag.* 1866, *32*, 401.

3 Chern, R. T.; Koros, W. J.; Hopfenberf, H. B.; Stannett, V. T. *Material Science of Synthetic Membranes*, 1 ed.; American Chemical Society, 1985.

4 Park, G. S.; Bungay, P. M.; Lonsdale, H. K.; Pinho, d. *Synthetic Membranes: Science, Engineering, and Applications*: Reidel Publishing Company, 1986.

5 Berens, A. R.; Hopfenberg, H. B. *Journal of Membrane Science* 1982, *20*, 283-303.

6 Chern, R. T.; Brown, N. F. *Macromolecules* 1990, *23*, 2370-2375.

7 Breck, D. *Zeolite Molecular Sieves*, 1 ed.; John Wiley & Sons: New York, 1974.

8 Chenoweth, M. B. *Synthetic Membranes*, 1 ed.; Harwood Academic Publishers: New York, 1986.

9 Pace, R. J.; Datyner, A. *Journal of Polymer Science: Polymer Physics Edition* 1980, *18*, 1169-1173.

10 Chandrasekhar, S. *Rev. Mod. Phys.* 1943, *15*, 1.

11 Gusev, A. A.; Suter, U. W.; Arizzi, S.; Moll, D. J. *Journal of Chemical Physics* 1993, *99*, 2221 - 2227.

12 Gusev, A. A.; Suter, U. W.; Moll, D. J. *Macromolecules* 1995, *28*, 2582-2584.

13 Stannett, V. T.; Crank, J. *Diffusion in Polymers*; Academic Press, 1968.

14 Crist, B.; Green, P.; Jones, A.; Kramer, E. *Macromolecules* 1989, *22*, 2857-2858.

15 Fujita, H. *Fortschr. Hochpolymer Forsch* 1961, *3*, 1.

16 Mulder, M. *Basic Principles of Membrane Technology*, 1 ed.; Kluwer Academic Publishers: Boston, 1991.

17 Freeman, B. D.; Ghosal, K. *Polymers for Advanced Technologies* 1994, *5*, 673-697.

18 Koros, W. J.; Hellums, M. W. *Encyclopedia of Polymer Science and Engineering*, 1989.

19 Amerongen, G. J. v. *Rubber Chemical Technology* 1964, *37*, 1065.

20 Koros, W. J.; Paul, D. R. In *Synthetic Membranes*; Chenoweth, M. B., Ed.; Harwood Academic Publishers: New York, 1986.

21 Freemen, B. D. *Comprehensive Polymer Science*; Oxford: Oxford, 1992.

22 Prausnitz, J.; Lichtenthaler, R.; Azevedo, E. G. d. *Molecular Thermodynamics of Fluid-Phase Equilibria*, 3 ed.: Upper Sattle River, NJ, 1999.

23 Stevens, M. *Polymer Chemistry: An Introduction*; Oxford University Press: New York, 1999.

24 Sperling, L. *Introduction to Physical Polymer Science*, 2 ed.; John Wiley & Sons, Inc.: New York, 1992.

25 Chern, R. T.; Koros, W. J.; Sanders, E. S.; Chen, S. H.; Hopfenberg, H. F. *Industrial Gas Separations*, 1 ed.; American Chemical Society, 1983.

26 Koros, W. J.; Chern, R. T.; Stannett, V. T.; Hopfenberg, H. B. *Journal of Polymer Science: Physics Edition* 1981, *19*, 1513-1530.

27 Koros, W. J.; Paul, D. R. *Journal of Polymer Science: Polymer Physics Edition* 1978, *16*, 1947-1963.

28 Toi, K.; Morel, G.; Paul, D. R. *Journal of Applied Polymer Science* 1982, *27*, 2997.

29 Ghosal, K.; Chern, R. T.; Freeman, B. D.; Savariar, R. *Journal of Polymer Science Part B: Polymer Physics* 1995, *33*, 657-666.

30 Nollet, A. *Lecons De Physique Experimentale*; Hippolyte-Louis Guerin and Louis-Francois Delatour: Paris, 1748.

31 Fick, A. *Annalen der Physik und Chemie* 1855, *94*, 59-86.

32 Daubner, P. *Membranfilter in Der Mikrobiologie Des Wassers*; Walter de Gruyter & Co.: Berlin, 1974.

33 Graham, T. *Phil. Trans. Roy. Soc.* 1861, *151*, 1836.

34 Leob, S.; Sourirajan, S.; University of California, Department of Engineering Reports: Los Angeles, 1961.

35 Hennis, J.; Tripodi, M. *Journal of Membrane Science* 1891, *8*.

36 Lonsdale, H. *Journal of Membrane Science* 1982, *10*, 81-181.

37 Scott, K. *Handbook of Industrial Membranes*, 2 ed.; Elsevier Science Publishers, 1998.

38 Baker, R. W. *Industrial Engineering and Chemistry Research* 2002, *41*, 1393-1411.

39 Robeson, L. M. *Journal of Membranes Science* 1991, *61*, 165-185.

40 Freeman, B. *Macromolecules* 1999, *32*, 375-380.

41 Barrer, R.; Skirrow, G. *Journal of Polymer Science* 1948, *39*, 48.

42 Van Krevelen, D. *Properties of Polymers: Their Correlation Wiht Chemical Structure; Their Numerical Estimation and Prediction from Additive Group Contributions*; Elsevier: Amsterdam, 1990.

43 Ohya, H.; Kudryavtsev, V. V.; Semenova, S. I. *Polyimide Membranes: Applications, Fabrications, and Properties*; Gordon and Breach Publishers: Tokyo, 1996.

44 McGrath, J.; Taylor, L.; Ward, T.; Wightman, J. *Cass Review Series Volume 1: Polyimdes: Synthesis, Characterization and Adhesion*; Christiansburg Printing Company: Christiansburg, 1992.

45 Kawakami, H.; Niwa, M.; Kanamori, T.; Shinbo, T.; Kaito, A.; Nagaoka, S. *Macromolecules* 2001, *34*, 9039-9044.

46 Koros, W. J., Ryan L. Burns. *Macromolecules* 2003, *36*, 2374-2381.

47 Lai, J.-Y.; Chen, S.-H.; Lee, M.-H. *European Polymer Journal* 1996, *32*, 1403-1408.

48 Marand, E.; Hibshman, C.; Mager, M. *Journal of Membranes Science* 2003, *229*, 73-80.

49 Matsumoto, K.; Xu, P. *Journal of Membrane Science* 1993, *81*, 23-30.

50 S.A. Stern, R. V. *Journal of Membrane Science* 1990, *49*, 1-14.

51 Sang Youl Kim, J.-H. K., Soo-Bok Lee. *Journal of Applied Polymer Science* 2000, *77*, 2756-2767.

52 Stern, S. A.; Mi, Y.; Yamamoto, H. *Journal of Polymer Science* 1989, *27*, 1887-1909.

53 Tai-Shung Chung, C. C., Rong Wang. *Journal of Membrane Science* 2002, *198*, 259-271.

54 Kim, T.; Koros, W. J.; Husk, G.; O'Brien, K. C. *Journal of Applied Polymer Science* 1987, *34*, 1767-1777.

55 Wind, J.; Paul, D. R.; Koros, W. J. *Journal of Membrane Science* 2004, *228*, 227-236.

56 Matsumoto, K.; Xu, P. *Journal of Membrane Science* 1993, *81*, 15-22.

57 Pavlova, S.; Timofeeva, G.; Ronova, J. *Journal of Polymer Science* 1980, *1175*, 1175.

58 Kim, T. H.; Koros, W. J.; Husk, G. R.; O'Brien, K. C. *Journal of Membrane Science* 1988, *37*, 45-62.

59 Kim, J. H.; Lee, S. B.; S.Y., K. *Journal of Applied Polymer Science* 2000, *77*, 2756-2767.

60 Moe, M.; Koros, W. J.; Hoehn, H.; Husk, G. *Journal of Applied Polymer Science* 1988, *36*, 1833-1846.

61 Husk, G.; Cassidy, P.; Gebert, K. *Macromolecules* 1988, *21*, 1234-1238.

62 Bessonov, M.; Koton, M.; Kudryavtsev, V. V.; Laius, L. *Polyimides: Thermally Stable Polymers*; Pleneum Publishing Corp: New York, 1987.

63 Kawakami, H.; Mikawa, M.; Nagaoka, S. *Macromolecules* 1998, *31*, 6636-6638.

64 Niwa, M.; Kawakami, H.; Kanamori, T.; Shinbo, T.; Kaito, A.; Nagaoka, S. *Macromolecules* 2001, *34*, 9039-9044.

65 Mikawa, M.; Nagaoka, S.; Kawakami, H. *Journal of Membrane Science* 2002, *208*, 405-414.

66 Staudt-Bickel, C.; Koros, W. J. *Journal of Membrane Science* 2000, *170*, 205-214.

67 Staudt-Bickel, C.; Koros, W. J. *Journal of Membrane Science* 1999, *155*, 145-154.

68 Wind, J.; Staudt-Bickel, C.; Paul, D. R.; Koros, W. J. *Macromolecules* 2003, *36*, 1882-1888.

69 Wind, J.; Staudt-Bickel, C.; Paul, D. R.; Koros, W. J. *Industrial Engineering and Chemistry Research* 2002, *41*, 6139-6148.

70 Cornelius, C. J. In *Chemical Engineering*; Virginia Tech: Blacksburgh, 2000.

71 Jonquieres, A.; Clement, R.; Lochon, P. *Progress in Polymer Science* 2002, *27*, 1803-1877.

72 McGrath, J.; Dunson, D.; Mecham, S.; Hedrick, J. *Advances in Polymer Science* 1999, *140*, 61-105.

73 Yilgor, I.; McGrath, J.; Worsfold, D. J.; Herz, H. E.; Heublein. *Polysiloxane Copolymers/Anionic Polymerization*; Springer-Verlag Berlin Heidelberg: New York, 1988.

74 Nagase, Y.; Shigehiro, M.; Masahiko, E.; Kiyohide, M. *Makromol. Chem* 1990, *191*, 2413-2421.

75 Lai, J.-Y.; Lee, M.-H.; Chen, S. H.; Shyu, S. S. *Polymer Journal* 1994, *26*, 1360-1367.

76 Chen, S. H.; Lee, M.-H.; Lai, J.-Y. *European Polymer Journal* 1996, *12*, 1403-1408.

77 Tsujita, Y.; Yoshimura, K.; Yoshimuzu, A.; Kinoshita, T. *Polymer* 1993, *34*, 2597-2601.

78 Nakagawa, T.; Nishimura, T.; Higuchi, A. *Journal of Membrane Science* 2002, *206*, 149-163.

79 McGrath, J. E.; Arnold, C. A.; Summers, J. D.; Chen, Y. P.; Bott, R. H.; Chen, D. 1989.

80 McGrath, J. E.; Summers, J. D.; Arnold, C. A. *Polymer Engineering and Science* 1989, *29*, 1413-1418.

81 Park, H.; Kim, J.; Nam, S.; Y, L. *Journal of Membrane Science* 2003, *220*, 59-73.

82 Ha, S.; Park, H.; Lee, Y. *Macromolecules* 1999, *32*, 2394-2396.

83 Ha, S.; Oh, B. K.; Lee, Y. *Polymer* 1995, *36*, 3549-3553.

84 Bowens, A. In *Synthesis and characterization of poly(siloxane imide) block copolymers and end-functional polyimides for interphase applications*; Virginia Tech: Blacksburg, 1999.

85 Cronstedt, A. *Akad. Handl. Stockholm* 1756, *18*, 120.

86 Auerbach, S.; Carroda, K.; Dutta, P. *Handbook of Zeolite Science and Technology*, 1 ed.; Marcel Dekker, Inc: New York, 2003.

87 Caro, J.; Noack, M.; Kolsch, P.; Schafer, R. *Microporous and Mesoporous Materials* 2000, *38*, 3-24.

88 Saracco, G.; Speccia, V. *Chem. Ind.* 1998, *71*, 463.

89 Dyer, A. *An Introduction to Zeolite Molecular Sieves*, 1 ed.; John Wiley and Sons: New York, 1988.

90 Chuang, S.; Bei, C.; Yawu, C.; Abdelhamjid, S. *CHemical Engineering Education* 2004, *38*, 34-37, 47.

91 Flanigen, E.; Bennett, J.; Grose, R.; Cohen, J.; Patton, R.; Kirchner, R. *Nature* 1978, *271*, 512-516.

92 Szostak, R. *Molecular Sieves: Principles of Synthesis and Identification*, 1 ed.; Van Nostrand Reinhold: New York, 1989.

93 Nagy, B.; Bodart, I.; Hannus, I. *Synthesis, Characterization and Use of Zeolitic Microporous Materials*; Deca Gen, Szeged-Szorg, 1998.

94 McCusker, L. B.; Liebau, F.; Engelhardt, G. *Microporous and Mesoporous Materials* 2003, *58*, 3-13.

95 Baerlocher, C.; Meier, W.; Holson, D. *Atlas of Zeolite Framework Types*; Elsevier: Amsterdam, 2001.

96 Tavolarao, A.; Drioli, E. *Adv. Mater.* 1999, *11*, 975-996.

97 Barrer, R. *Hydrothermal Chemistry of Zeolites*; Academic Press: New York, 1982.

98 Loewenstein, W. *American Mineral* 1954, *39*, 92-96.

99 Ruthven, D. *Chemical Engineering Progress* 1988, 42-50.

100 Nikolakis, V.; Xomeritakis, G.; Abibi, A.; Dickson, M.; Tsapatsis, M.; Vlachos, D. *Journal of Membrane Science* 2001, *184*, 209-219.

101 Qiu, S.; Yu, J.; Zhu, G.; Terasaki, O.; Nozue, Y.; Pang, W.; Xu, R. *Microporous and Mesoporous Materials* 1998, *21*, 245-251.

102 Villaluenga, J.; Tabe-Mohammadi, A. *Journal of Membrane Science* 2000, *169*, 259-174.

103 Barthomeuf, D.; Ha, B. *Journal of the Chemical Society: Faraday Transactions* 1973, *12*, 2147-2157.

104 Tsapatsis, M.; Lovallo, M.; Okubo, T.; Davis, M.; Sadakata, M. *Chem. Mater.* 1995, *7*, 1734-1741.

105 Tsapatsis, M.; Lovallo, M.; Davis, M. *Microporous Materials* 1996, *5*, 381-388.

106 Vaughan, D.; Strohmaier, K.: Canadian Patent Application 2,106,170, 1994.

107 Verduijn, V. P.; Mechilium, J.; De Gruijter, C.; Koetsier, W.; Van Oorschot, C.: USA 5,064,630, 1991.

108 Wortel, T.: US Patent 4,544,539, 1985.

109 Lovallo, M.; Tsapatsis, M.; Okubo, T. *Chem. Mater.* 1996, *8*, 1579-1583.

110 Choi, S.; Lee, Y.; Yong, P.; Ha, K.; Yoon, K. *Journal of the American Chemical Society* 2000, *122*, 5201-5209.

111 Ha, K.; Lee, Y.; Lee, H.; Yoon, K. *Adv. Mater.* 2000, *12*, 1114-1117.

112 Kulak, A.; Lee, Y.; Chun, Y.; Park, Y.; Yoon, K. *Journal of the American Chemical Society* 2000, *122*, 9308-9309.

113 Metin, D.; Tihminlioglu, F.; Balkose, D.; Ulku, S. *Composites Part A: Applied Science and Manufacturing* 2004, *35*, 23-32.

114 Pehlivan, H. In *Chemical Engineering*; Izmir Institute of Technology: Izmir, 2001.

115 Te Hennepe, H.; Bargeman, D.; Mulder, M.; Smolders, C. *Journal of Membrane Science* 1987, *35*, 39-55.

116 Jia, M.; Peinemann, K.-V.; Behling, R.-D. *Journal of Membrane Science* 1991, *57*, 289-292.

117 Jia, M.-D.; Pleinemann, K.-V.; Behling, R.-D. *Journal of Membrane Science* 1992, *73*, 119-128.

118 Duval, J.-M.; Folkers, B.; Mulder, M. H. V.; Desgrandchamps, G.; Smolders, C. A. *Journal of Membrane Science* 1993, *80*, 189-198.

119 Tantekin-Ersolmaz, S. B.; Atalay-Oral, C.; Tather, M.; Erdem-Senatalar, A.; Schoeman, B.; Sterte, J. *Journal of Membrane Science* 2000, *175*, 285-288.

120 Koros, W. J.; Mahajan, R. *Industrial Engineering and Chemistry Research* 2000, *39*, 2692-2696.

121 Koros, W. J.; Zimmerman, C. M.; Singh, A. *Journal of Membranes Science* 1997, *137*, 145-154.

122 Gur, T. M. *Journal of Membranes Science* 1994, *93*, 283-239.

123 Suer, M. G.; Bac, N.; Yilmaz, L. *Journal of Membranes Science* 1994, *91*, 77.

124 Koros, W. J.; Mahajan, R. *Journal of Membranes Science* 2000, *175*, 181-196.

125 Moaddeb, M. In *Chemical Engineering*; University of Texas: Austin, 1997.

126 Park, H. C.; Yong, H. H.; Kang, Y. S.; Won, J.; Kim, W. N. *Journal of Membranes Science* 2001, *188*, 151-163.

127 Koros, W. J.; Mahajan, R.; Burns, R.; Schaeffer, M. *Journal of Applied Polymer Science* 2002, *86*, 881-890.

128 Koros, W. J.; Mahajan, R. *Polymer Engineering and Science* 2002, *42*, 1420-1431.

129 Koros, W. J.; Mahajan, R. *Polymer Engineering and Science* 2002, *42*, 1432-1441.

130 Iijima, S. *Nature* 1991, *354*, 56-58.

131 Kroto, H. W.; Heath, J. R.; O'Brien, S. C.; Curl, R. F.; Smalley, R. E. *Nature* 1985, *318*, 162-163.

132 Bethune, D.; Kiang, H.; de Vries, M.; Gorman, G.; Savoy, R.; Beyers, R. *Nature* 1993, *363*, 605-607.

133 Iijima, S.; Ichihashi, T. *Nature* 1993, *363*, 363-366.

134 Ackerman, D. M.; Skoulidas, A. I.; Sholl, D. S.; Johnson, J. K. *Molecular Simulation* 2003, *29*, 677-684.

135 Cooper, S. M.; Chuang, H. F.; Cinke, M.; Cruden, B. A.; Meyyappan, M. *Nano Letters* 2003, *3*, 189-192.

136 Hinds, B.; Chopra, N.; Rantell, T.; Andrews, R.; Gavalas, V.; Bachas, L. *Science* 2004, *303*.

137 Park, C.; Crooks, R. E.; Siochi, E. J.; Harrison, J. S.; Evans, N.; Kenik, E. *Nanotechnology* 2003, *14*, L11-L14.

138 Ounaies, Z.; Park, C.; Wise, K. E.; Siochi, E. J.; Harrison, J. S. *Composites of Science and Technology* 2003, *63*, 1637-1646.

139 Ogasawara, T.; Ishida, Y.; Ishikawa, T.; Yokota, R. *Composites Part A: Applied Science and Manufacturing* 2004, *35*, 67-74.

Chapter 3: Preparation and Characterization of a 6FDA-6FpDA-DABA Polyimide and Amine-functionalized ZSM-2 Mixed Matrix Membrane

3.1 Abstract

Mixed Matrix membranes of 6FDA-6FpDA-DABA, a glassy polyimide, and amine-modified ZSM-2 zeolites were successfully fabricated using the procedure outlined in this paper. The membranes were cast from solution, and then exposed to different gases for the purpose of determining and comparing the diffusivity coefficients, the solubility coefficients, and the permeation rates of He, O_2, N_2, CH_4 and CO_2 of the pure polyimide and the composite membrane. FTIR spectra were collected from the pure polyimide, the polyimide and untreated zeolite solutions, and the mixed matrix membrane (MMM) solution. To determine if unselective voids were present between the polyimide and zeolite, FESEM images and TEM images were taken. These images also offered insight into the distribution of zeolite throughout the matrix. Finally, comparisons of the performances between the pure polyimide and the mixed matrix membrane for industrially significant gas separations were made.

3.2 Introduction

Many recent efforts to surpass Robeson's 1991 upper bound trade off curve have focused on the development of mixed matrix membranes composed of polymers and zeolites.[1] The goal of these membranes is to utilize the outstanding separation

performance of zeolites, but overcome its weaknesses of high cost and poor mechanical properties by introducing a less expensive and more easily processed polymer as the matrix. Potential applications of these new membranes have been discussed elsewhere.[2]

Mixed Matrix Membranes (MMMs) developed from rubbery polymers and zeolites have been fabricated and characterized already.[3-5] Previous attempts at fabricating MMMs using glassy polymers and zeolites resulted in the presence of voids between the polymer and zeolite, thus reducing the separation of performance of the composite membrane relative to the pure polymer.[3,4] An image of a composite membrane made by Duval et al using polysulfone and silicalite is shown in Figure 3-1.[6] To overcome these defects, several different silane coupling agents were successfully employed to improve adhesion between the polymer and zeolite, however, the resulting permeabilities were slightly lower, and ideal selectivities were largely unchanged when compared to the pure polymer.[6]

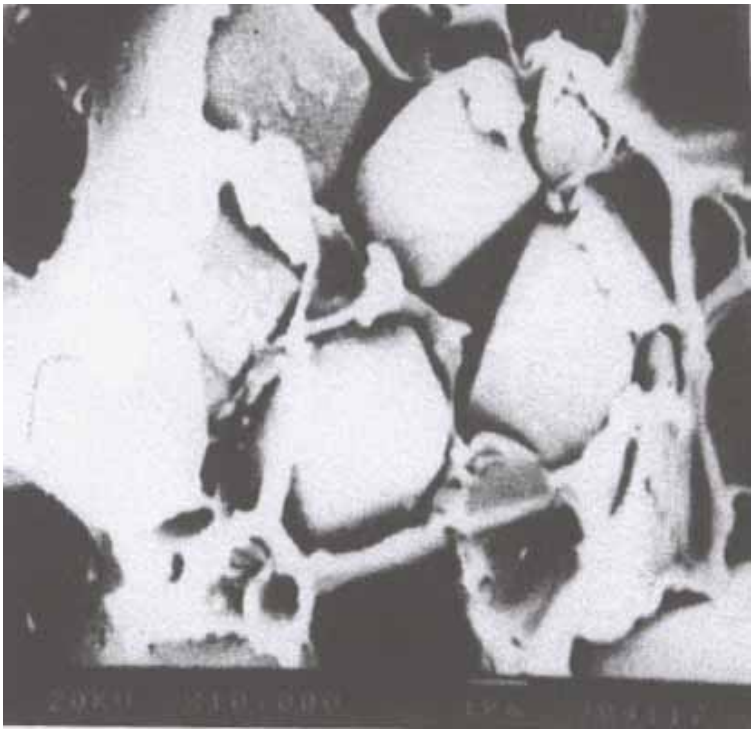

Figure 3-1. Poor adhesion between zeolite and polymer when the two are simply mixed together to make a membrane. The image was taken from reference 6.

Other attempts at developing glassy polymer-zeolite composite membranes have focused on fabrication methods without modifying the zeolite surface. Gür combined molecular sieve 13X and polyethersulfone (PES) through a melt extrusion process.[7] The two components were dried and extruded through a thin slit die to produce defect free membranes. However, the resulting membrane's permeation properties did not change significantly relative to the pure PES membrane. Süer et al simply mixed polyethersulfone with either zeolite 13X or zeolite 4A and solution cast the mixture.[8] However, they used three different solution drying and annealing procedures to fabricate the membranes, one of which resulted in improved permeability and selectivity relative to the pure PES. Yong et al developed interfacial void free polyimide mixed matrix membranes by using a low molecular weight chain capable of hydrogen bonding with both the polymer and zeolite.[9] This chain essentially enhanced the contact between the two components. The resulting membranes displayed increased permeability without much change in the selectivity.

In this paper we present a method to fabricate defect free mixed matrix membranes involving using amine terminated silane coupling agents that are tethered onto zeolite surfaces, and glassy polyimides with hydrogen bonding acidic groups incorporated into their backbone.

3.3 Experimental

This section outlines the materials and what steps, if any, were taken to further purify them. Additionally, the procedures used to synthesize, functionalize, and fabricate materials are discussed.

3.3.1 Materials

The polyimide used in this study was synthesized using a step growth reaction. Step growth reactions require very pure monomers and very dry solvents in order to achieve high molecular weights with narrow polydispersities. All glassware was rinsed with acetone and flame dried before use. This section lists the solvents and monomers

used in the study, and outlines the steps taken to prepare them for use in the step growth reaction synthesis.

3.3.1.1 Solvents

1-Methyl-2-Pyrrolidinone (NMP)

(NMP) was used as the solvent in the synthesis of the 6FDA-6FpDA-DABA polyimide. This solvent was purchased from Fisher Scientific. The solvent was dried over phosphorus pentoxide (P_2O_5) for 24 hours. Because NMP is hydroscopic, it was vacuum distilled immediately before use.

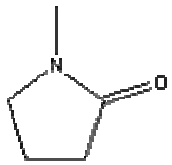

O-Dichlorobenzene (DCB)

DCB was purchased from Fisher Scientific and used in the synthesis of the 6FDA-6FpDA-DABA polyimide. It was added for the purpose of forming an azeotrope with the water produced during the step growth reaction. This azeotrope could be boiled off and help the synthesis achieve a higher molecular weight. DCB was mixed with P_2O_5 for 24 hours and then vacuum distilled immediately before use to avoid exposure to moisture.

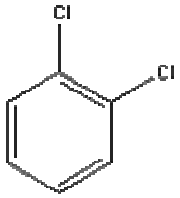

Methanol (MeOH)

Low grade MeOH was purchased from the Virginia Tech Chemistry Stockroom and used as received. This solvent was used to precipitate the polyimide from the NMP and DCB following the synthesis.

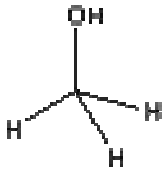

Tetrahydrofuran (THF)

Tetrahydrofuran was purchased from Fisher Scientific and was used as received. The grade purchased was high purity liquid chromatography. It was used in the fabrication of the membranes.

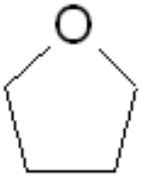

Toluene

Toluene was purchased from Fisher Scientific and used as received. The grade purchased was high purity liquid chromatography. It was used as the solvent in the reaction which covalently added amine groups to the zeolite surfaces.

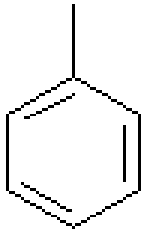

Ethanol

Ethanol was purchased from AAPER Alcohol and Chemical Co. and used in to make ZSM-2 suspensions capable of being centrifuged. It was purchased from Fisher and used as received.

3.3.1.2 Monomers

4,4'-(Hexafluoroisopropylidene)diphthalic Anhydride (6FDA)

6FDA was purchased from Clariant with a purity >99.95%. Prior to use the material was placed under vacuum at a temperature of 150 ^{o}C to ensure compete cyclic anhydride cyclization immediately prior to use.

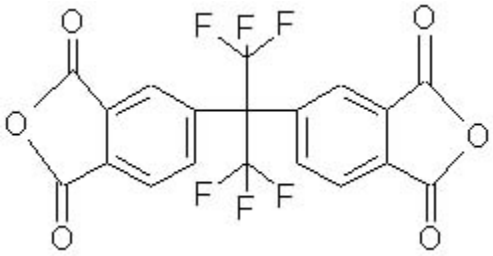

4,4'(Hexafluoroisopropylidene)dianiline (6FpDA)

6FpDA was purchased from SynQuest labs with a purity of >98%. The monomer was sublimed for further purification. After sublimation 6FpDA was kept in a dry box to avoid moisture contact.

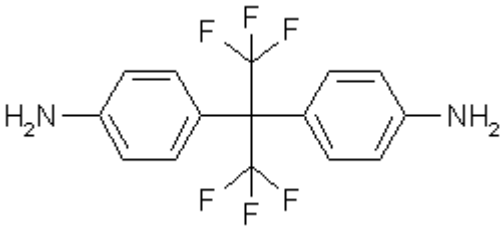

3, 5-Diaminobenzoic Acid (DABA)

DABA was purchased from Aldrich with a purity of >98% and used as received. It was dried under vacuum near 100 ^{o}C prior to use.

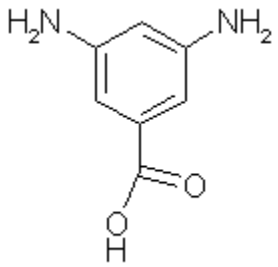

Aminopropyltriethoxysilane (APTES)

APTES was purchased from Gelest with a purity of 99%. It was used as received.

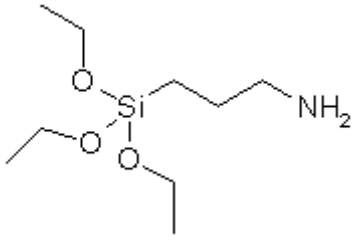

3.3.2 Synthesis of 6FDA-6FpDA-DABA:

A flame dried 1000 mL 3-neck round bottom flask was used as the reaction vessel in this synthesis. The right neck was used as a N_2 inlet and held a thermometer. The center neck of the round bottom was connected to a mechanical stirrer. The left neck led to the condenser and trap to gather condensed DCB and return it round bottom flask. A diagram of the reaction setup is shown below in Figure 3-2.

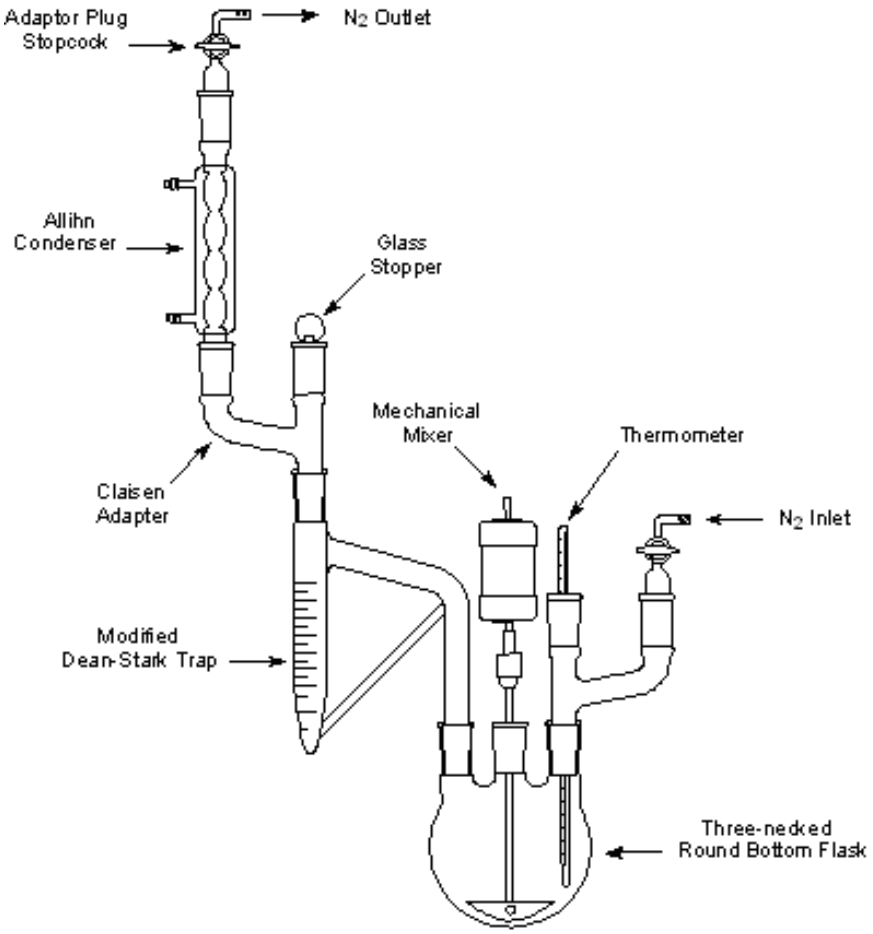

Figure 3-2. Reaction setup for the synthesis of 6FDA-6FpDA-DABA.

4,4'–Hexafluoroisopropylidene dianiline , 4,4'–hexafluoroisopropylidenediphathalic anhydride and 3,5–diaminobenzoic acid were placed under vacuum near 100 ^{o}C to remove water prior to use. 1-Methyl-2-

pyrrolidinone and *o*-dichlorobenzene were dried over phosphorous pentoxide and vacuum distilled.

NMP (485 mL) and DCB (76 mL) were added to a round bottom flask in a 4:1 molar ratio. 6FDA (74.9 g) was added under N_2 flow and allowed to completely dissolved. Following this, the 6FpDA (28 g) was added to the solution and the components were mixed at room temperature for 24 h to form a low molecular weight polyamic acid which was targeted to be end capped with anhydride groups. After 24 h the solution was heated to 180 ^oC for an additional 24 h to imidize the polyamic acid leading to a low molecular weight polyimide. Once the solution cooled to room temperature, DABA (12.7 g) was added, and the mixture was stirred at room temperature for 24 h to form a high molecular weight polyamic acid. After this time, it was heated to 180 ^oC for 24 h to imidize the polyamic acid. Following this step, the polymer solution was allowed to cool to room temperature.

After the synthesis the polyimide solution was purified using 5 μm filters. The filtered solution was poured into a methanol bath to remove the NMP and DCB from the polymer. The precipitated polymer remained in the methanol bath for four days, during which the methanol was changed daily. After the four days, the polymer was removed and allowed to air dry overnight. Once dry, the material was then heated at 110 ^oC for 12 h under vacuum to remove any residual methanol.

The polyimide was then stored in a dessicator until needed.

3.3.3 Synthesis of ZSM-2

ZSM-2 was synthesized by Dr. Michael Tsapatsis' group at the University of Minnesota. They used a technique which has been published before and this recount has been taken from it.[10] In this technique ZSM-2 nanocrystals are synthesized by mixing tetraethylorthosilicate (TEOS), lithium hydroxide (LiOH), and tetramethylammonium hydroxide (TMAOH) in distilled water, resulting in a lithium-TMA-silicate solution. A TMA-aluminate solution was prepared by dissolving aluminum foil in TMAOH. The latter was slowly added to the Lithium-TMA-Silicate solution resulting in a mixture with molar composition: 0.53 Li2O:1 Al_2O_3:6 TMAOH:3.4 SiO_2:315 H_2O. This mixture was

then placed into a Teflon lined stainless steel cylinder and sealed. The cylinder is rotated in an oven (~30 rpm) at 140 ^{o}C for 12 hours. This led to uniformly sized ZSM-2 nanocrystals.

3.3.4 Amine-functionalization of ZSM-2

Once synthesized the zeolites were centrifuged, and their aqueous solution was replaced with ethanol. The resulting mixture was centrifuged six more times, each time replacing the liquid with fresh ethanol. After this cycle, the process was repeating, though ethanol was replaced with toluene. The mixture was added to a round bottom flask, and more toluene was added to provide a zeolite concentration of 6.2 mg/ml toluene. Aminopropyltriethoxysiliane was then added in an amount such that a ratio 0.08 ml APTES/ ml toluene was present in the flask before the reaction began. The mixture was then refluxed under an Argon purge for 3 hours. Upon completion of the reaction, the mixture was centrifuged several times, each time replacing the solvent with tetrahydrafuran.

An amount of 6FDA-6FpDA-DABA required to produce a 20% weight ZSM-2, 80% weight polyimide mixed matrix membrane was added to the zeolite-THF mixture and allowed to mix for 24 hours. The solution was then cast onto a Teflon coated surface and allowed to evaporate over a 2 day period.

3.3.5 Membrane Fabrication

Membranes composed of only 6FDA-6FpDA-DABA were prepared as follows. 6FDA-6FpDA-DABA was synthesized and purified outlined previously in this chapter. Typically, 3 g of the polymer were dissolved in roughly 60 mL of THF in a 100 mL beaker. This gave a solution of 5 wt % solids. This solution was mixed for 24 hours then cast onto a nonstick circular pan with a diameter of 8.25”. Immediately after casting, a flat glass plate was placed over the pan to slow the rate of evaporation. A slow evaporation rate reduces solvent concentrations within the film and curling of the film. The solution was allowed to dry for 2 days.

Upon drying, the membrane was removed and placed under vacuum at room temperature for several hours. After vacuum drying a 2.5" diameter circular sample was cut from the membrane sheet and used for permeation studies. This procedure produced membranes of thicknesses near 0.003".

Mixed matrix membranes were fabricated from the polyimide and the ZSM-2 which had been previously amine functionalized as outlined earlier; MMMs fabricated with non-functionalized ZSM-2 were created in the same manner. For a 20 wt % ZSM-2 MMM, approximately 600 mg of ZSM-2 were dispersed into roughly 60 mL of THF and mixed. After the zeolite was well mixed, 2.2 grams of 6FDA-6FpDA-DABA were added to the suspension, and the mixture was allowed to mix for 24 hours. After mixing, the mixture was cast onto a nonstick circular pan with a diameter of 8.25". Immediately after casting, a flat glass plate was placed over the pan to slow the rate of evaporation. The solution was allowed to dry for 2 days. MMMs composed at 50 wt % ZSM-2 were created in the same manner only differing in the mass of polymer and the mass of zeolite.

Upon drying, the membrane was removed and placed under vacuum at room temperature for several hours. After vacuum drying a 2.5" diameter circular sample was cut from the membrane sheet and used for permeation studies.

3.3.6 Membrane Characterization

The gas permeabilities of the pure polyimide and mixed matrix membrane were measured in a constant volume – variable pressure system. Using the time lag method[11], the permeability, diffusion coefficient, solubility coefficient, and diffusive lag time for both membranes were determined for O_2, N_2, CH_4, and CO_2. The gases were tested in that order for all membranes. The ideal selectivities were calculated by ratioing the pure gas permeabilities.

Fourier Transform Infrared Spectroscopy (FTIR) was used for the purposes of identifying functional groups of the synthesized polymers and studying the interactions between the components of each membrane (e.g. hydrogen bonding). The presence of hydrogen bonding between the zeolite and polymer were determined by observing shifts to lower wavenumbers for interacting groups and noting changes in peak intensity.

The FTIR used in this study was a BIO-RAD FTS-40A. This model was equipped with a liquid nitrogen cooled MCT detector and was capable of gathering spectra in the 4000 – 400 cm^{-1} region. The FTIR was set with a wave number resolution of 1 cm^{-1} and an aperture of 2 cm. The computer software which ran the FTIR was BIO-RAD WinIR Ver. 3.0.

Transmission spectroscopy was used for gathering the spectra of the samples. Samples were prepared from solutions. A pipette was used to transfer a small repeatable amount of solution to the CaF_2 plate which would dry as a thin film. The films would be allowed to air dry, and then placed in the vacuum oven at room temperature to remove any residual solvent. CaF_2 plates were used for investigating the region between 4000 and 1100 cm^{-1}. The sample compartment was continually purged with dry air during the time a spectrum was being gathered from it. Spectral peaks were numbered automatically by the software, and when necessary the software was used to make a baseline to a spectrum. Peaks were assigned to specific groups using two separate books by Alpert and Silverstein.[12,13] Additionally, publications by Husk et al, Becker et al, and Kim et al were used for identifying peaks of the polyimide spectrum.[14-16] Evidence of hydrogen bonding between components was taken as shifts to lower wavenumbers.

Several instruments were employed to characterize the morphology of the composite membrane. Surface and cross sectional images of the composite membrane were gathered using a field emission scanning electron microscope (FESEM). The FESEM used in this study was a LEO 1550. This instrument was equipped with two secondary electron detectors, and a five axis (i.e. x, y, z, θ, φ) sample stage.

Samples used to gather surface images were cut from cast films. These samples were mounted onto a sample holder using a conductive double stick tape. Due to polymers being poor conductors, the samples were coated with a 5 nm gold coating using a Crussington 208HR Sputter Coater. Mounted samples were placed into the sputter coater which was pumped down and flushed with argon several times. The samples would then be put under vacuum and the gold coating was applied.

Samples used to gather cross-sectional images were cut from cast films. These films were embedded in epoxy by Steve McCartney in the Virginia Tech Microscopy

Lab. The embedded samples were ultra-cryomicrotomed by trimming the sample using a razor blade. The sample would then be cut using a 35^{o} diamond knife at -110 ^{o}C.

Each sample was coated with a 5 nm gold coating using a Crussington 208HR Sputter Coater to improve its conductivity. Mounted samples were placed into the sputter coater which was pumped down and flushed with argon several times. The samples would then be put under vacuum and the gold coating was applied.

Additionally, in order to investigate the morphology of these membranes transmission electron microscopy (TEM) was employed. The TEM used in this study was a Philips 420T. TEM offered an excellent method for gathering high magnification and high resolution images of the bulk of the membranes. Samples were prepared as follows. From cast films, samples approximately 2 x 5 mm were taken and embedded were epoxy embedded. The epoxy was allowed to cure at room temperature. The embedded samples were ultramicrotoned with a diamond knife, and pieces with thicknesses of 50 – 70 nm were captured on a 300 mesh copper grid.

3.4 Results and Discussion

3.4.1 Polymer Synthesis

Using the procedure outlined in the Experimental section, 6FDA-6FpDA-DABA was synthesized. The reaction is outlined below, and has been used extensively by others.[15,17,18] In Figure 3-3 the aromatic dianhydride and diamine react to form a low molecular weight polyamic acid. The stoichiometry is controlled such that the ends should be anhydride groups. This polyamic acid is heated to cyclodehydrate the amic acid into a polyimide known as 6FDA-6FpDA.

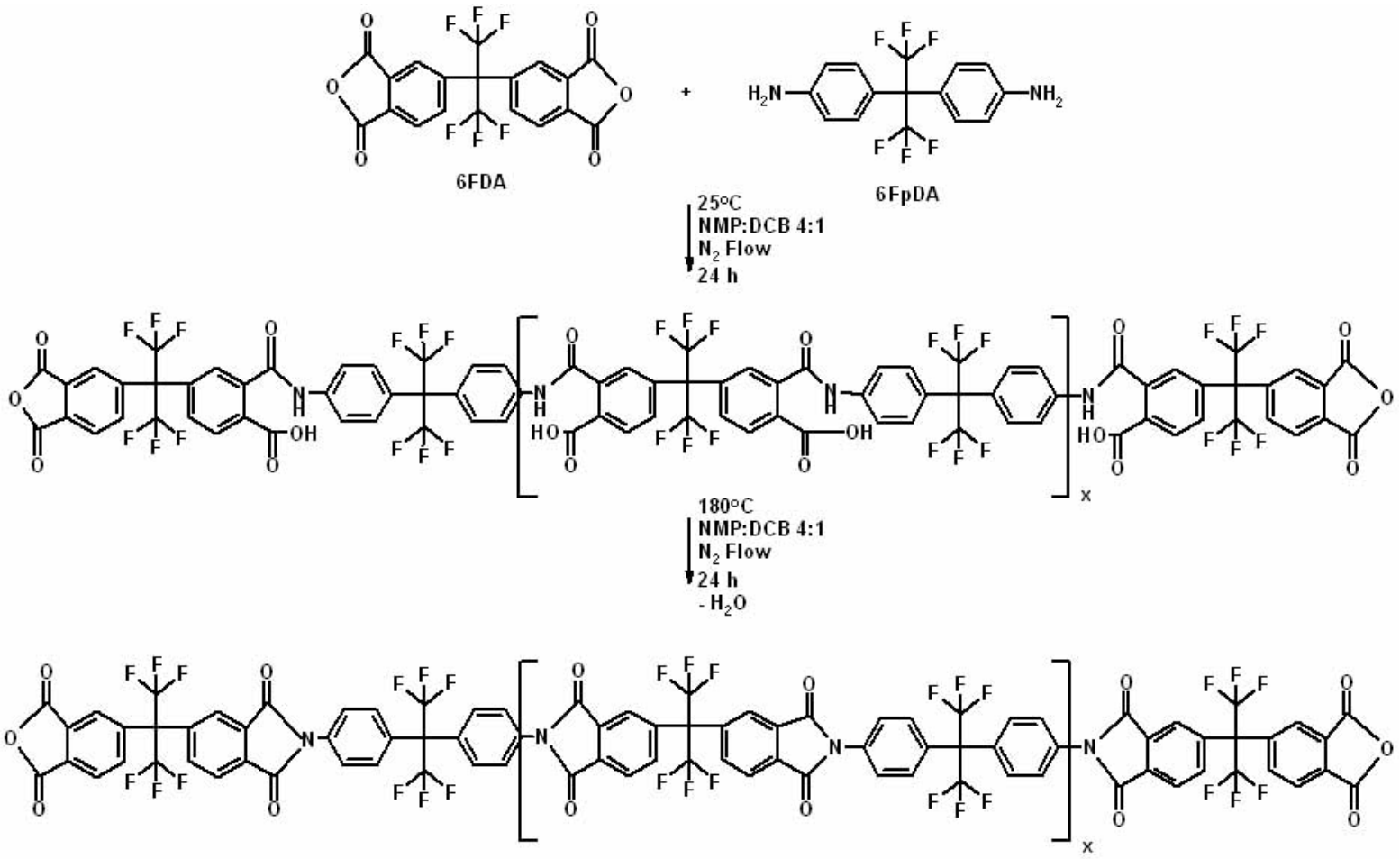

Figure 3-3. Formation of a low molecular weight 6FDA-6FpDA polyimide.

The low molecular weight 6FDA-6FpDA is reacted with 3,5-diaminobenzoic acid. The DABA essentially acts as a linker between the low molecular weight chains to combine them into a high molecular weight polyamic acid as shown below in Figure 3-4.

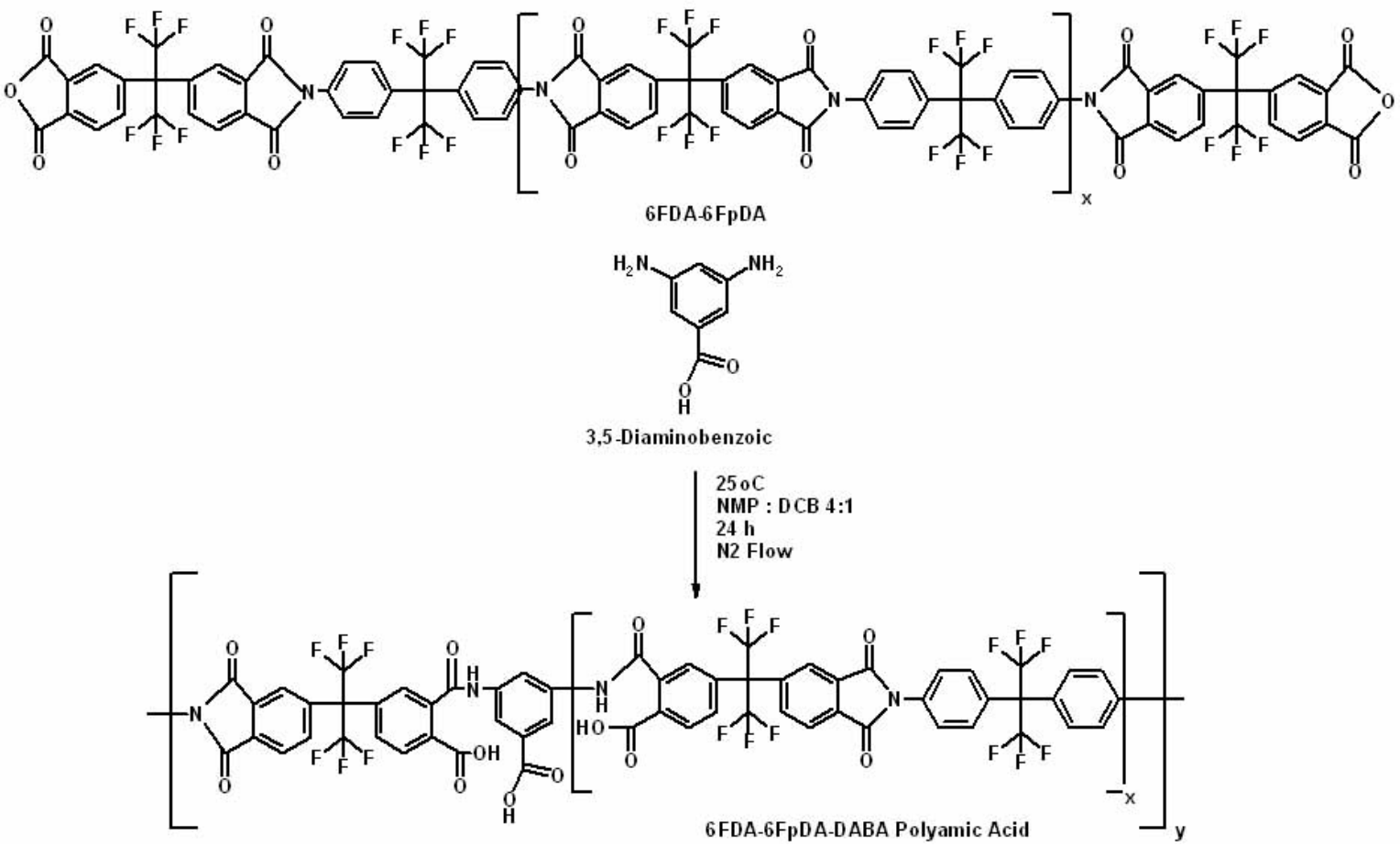

Figure 3-4. Low molecular weight 6FDA-6FpDA reacts with DABA to create a high molecular weight poly(amic acid).

The high molecular weight poly(amic acid) is then heated to 180 ^{o}C to cyclodehydrate the amic acid groups. This step is shown in Figure 3-5. The results a high molecular weight polyimide with carboxylic groups incorporated into its backbone. This polyimide is referred to as 6FDA-6FpDA-DABA.

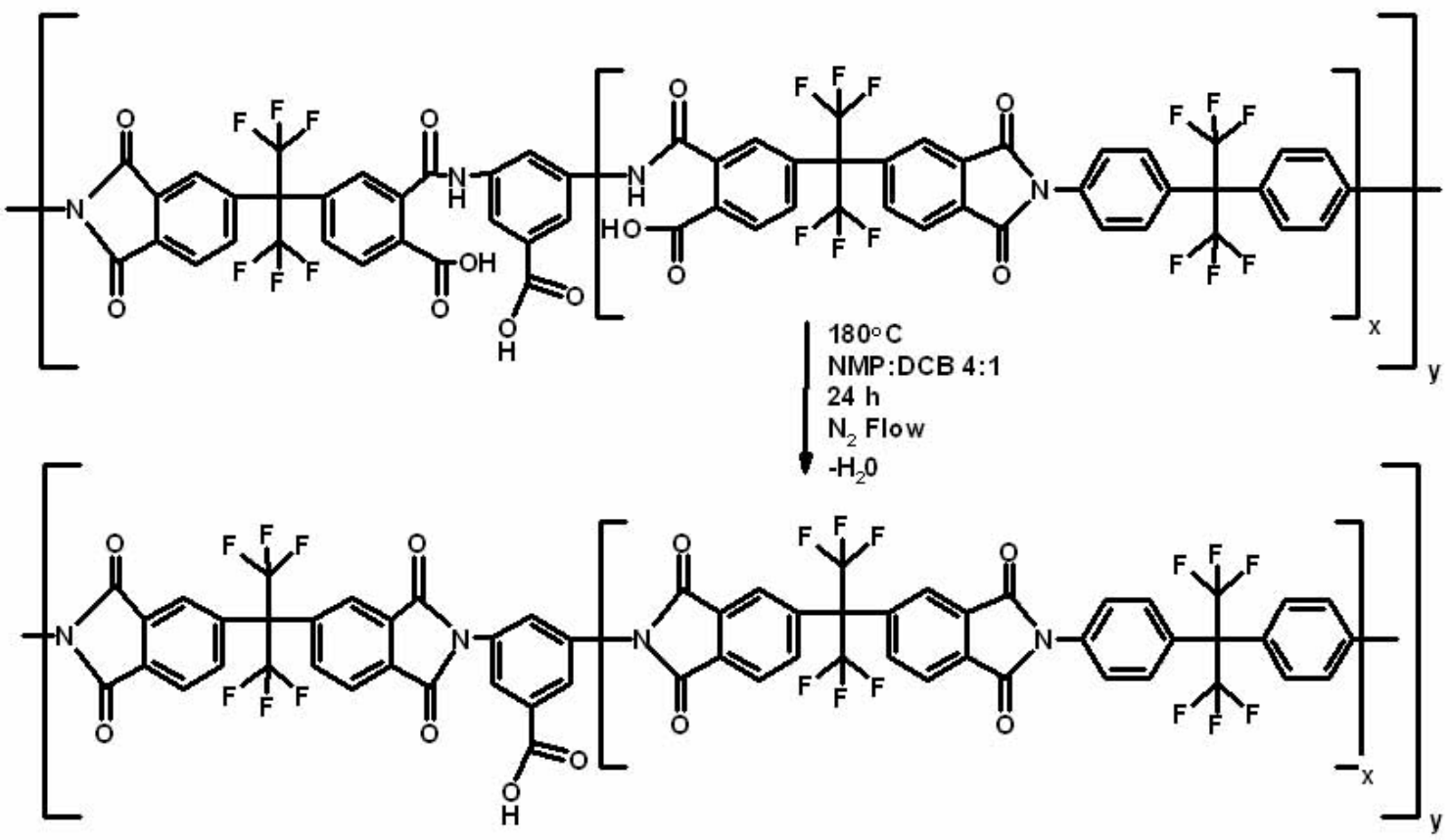

Figure 3-5. Cyclodehydrating high molecular weight poly(amic acid) to produce 6FDA-6FpDA-DABA.

Gel permeation chromatography (GPC) was employed to determine the molecular weight and polydispersity of the polyimide. Three samples were taken from the polymer batch to measure the variability within the synthesized polymer. The results are listed below in Table 3-1.

Table 3-1. GPC data for three samples of the 6FDA-6FpDA-DABA synthesized and used in this study.

Sample #	M_n (g/mol)	M_w (g/mol)	Polydispersity
1	44,600	93,400	2.094
2	39,800	90,100	2.264
3	42,600	94,500	2.218
Average	42,300 ± 2,400	92,700 ± 2,300	2.192 ± 0.088

3.4.2 ZSM-2

ZSM-2 was synthesized and supplied by Prof. Michael Tsapatsis at the University of Minnesota. The synthesis of the zeolites has been outlined in detail by this group elsewhere.[10] ZSM-2 was characterized using WAXS to verify their crystal structure and purity. The product was received in an aqueous suspension and centrifuged. The water was removed and replaced with ethanol. The suspension was centrifuged several more times each time replacing the ethanol. This same procedure was repeated for replacing ethanol with toluene.

The image shown below in Figure3-6 was taken of a single ZSM-2 nanocrystal. ZSM-2 has a density of 1.31 g/cm^3, and the longest length of an individual ZSM-2 crystals measures approximately 250 nm.[19] ZSM-2 possesses channels which measure 0.74 nm in diameter. However, due to the presence of lithium cations in the pores, the actual open space within the pore is drastically reduced.

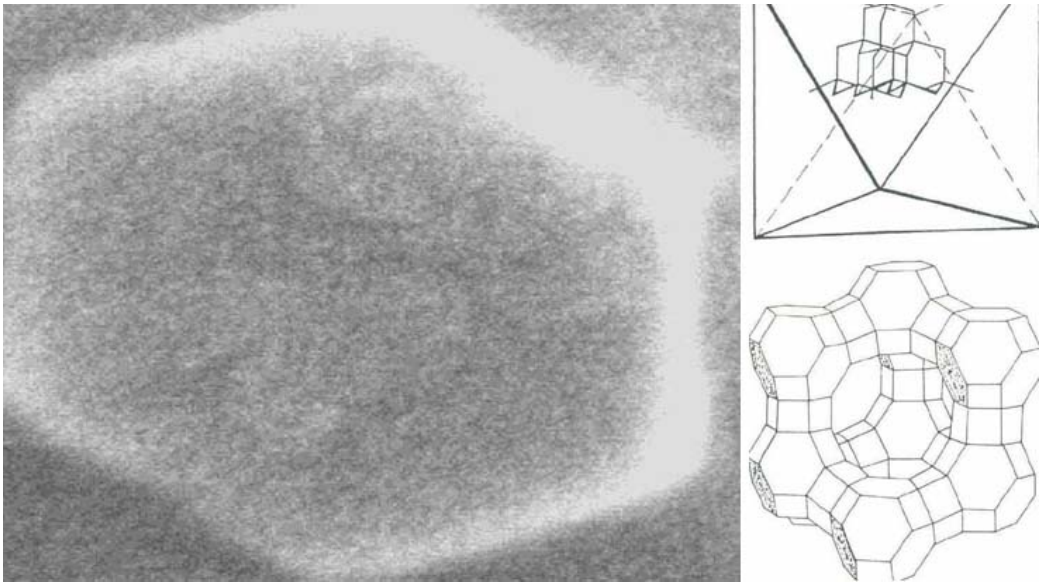

Figure3-6. FESEM image of a ZSM-2 crystal (left) and an illustration of the pore channels with respect to the crystal (top right), and a ZSM-2 pore cage (bottom right). The length of the hexagonal face measures roughly 250 nm and the illustrations were taken from Bekkum et al [19].

Because of the cations within the channel, ZSM-2 can separate using a selective adsorption mechanism. Molecules that more strongly adsorb onto the pore walls will receive enhanced transport through access to surface diffusion rather than being limited to Knudsen diffusion. Furthermore, the selective adsorption will enhance the selectivity of the zeolite. When one component sorps to the pore wall, the channel size is reduced, thus making it inaccessible to other nonadsorbing species. Species that sorb onto the zeolite pore walls are typically polar molecues (e.g. H_2O, ammonia), quadrupolar (e.g. CO_2, N_2), or are capable of π-layer interactions (e.g. aromatic hydrocarbons).[20] Because of this, ZSM-2 is typically targeted to remove CO_2 or unsaturated hydrocarbons from mixtures.

3.4.3 Amine-functionalization of ZSM-2

ZSM-2 nanocrystals were functionalized with APTES for the purpose of covalently attaching amine groups to the zeolite surfaces. This was performed using the reaction illustrated below in Figure 3-7.

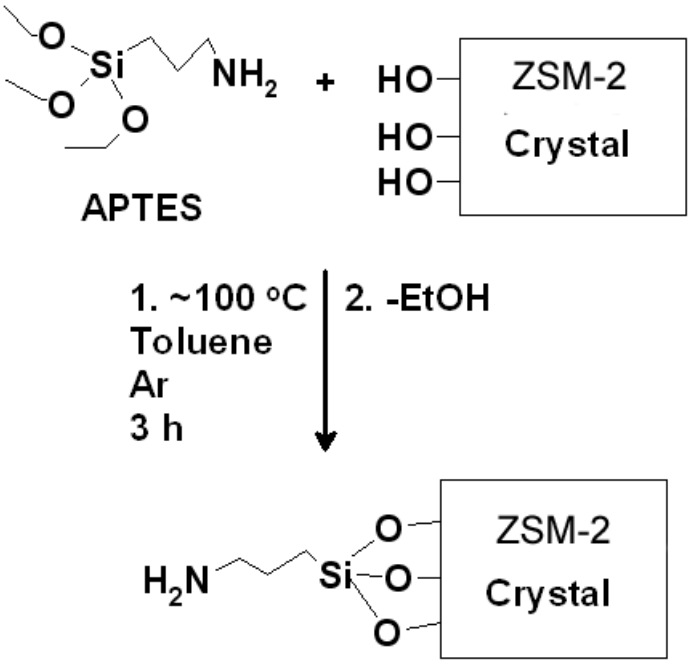

Figure 3-7. Reaction employed to amine-functionalize ZSM-2 using APTES.

With the zeolite amine-functionalized and carboxylic acid groups in the polymer's backbone, hydrogen bonding should be present between the two components Figure 3-8. This would be used to overcome any dewetting of the polymer from the zeolite which would lead to unselective voids.

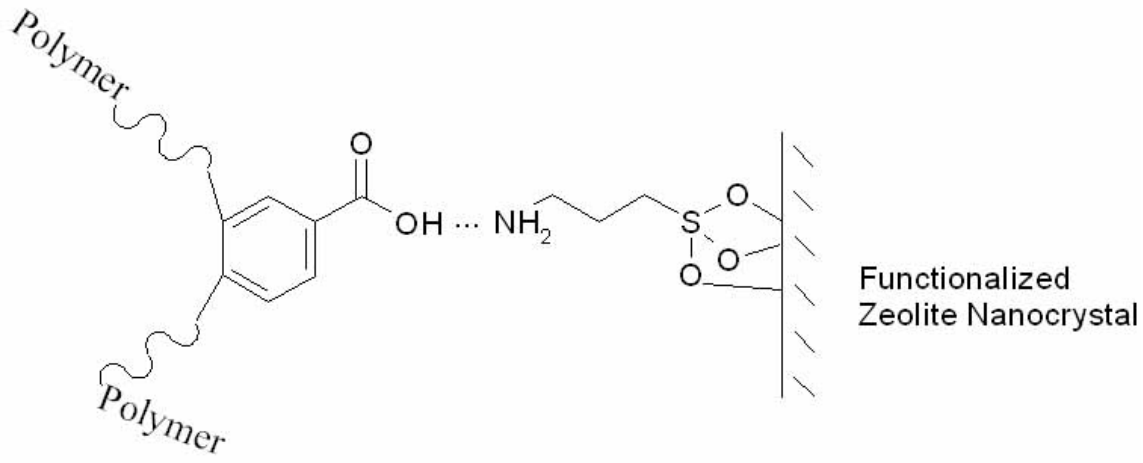

Figure 3-8. The polymer and amine-functionalized zeolite are capable of hydrogen bonding.

3.4.4 Spectroscopic Results:

FTIR spectra were taken in order to investigate the changes in the chemical environment between the polymer and zeolite once the ZSM-2 surface had been functionalized. Spectra were collected from the pure polyimide, the polyimide and untethered zeolite mixture, and the mixed matrix solution. All peaks were identified in this study assigned according to Alpert, Keiser, and Szymanski.[12]

A sample consisting of polyimide, untethered ZSM-2, and APTES was to be prepared using the same concentrations as the other samples. However, immediately after adding APTES to the solution, the solution phase separated. This sample was never made successfully, and no spectrum was gathered for it.

Figure 3-9 shows the FTIR spectra for the three systems in the 3600-2700 cm^{-1} wavenumber range. The pure polyimide is the bottom spectrum, the untreated zeolite-polyimide mixture is the middle spectrum, and the MMM is the top spectrum. Both polymer-zeolite samples contained 20 wt % zeolite. The absorbencies of the spectra were below 1 throughout the entire spectrum. They were normalized to each other by a adjusting the magnitude of the absorbance of the aromatic C-H stretch at 3113 cm^{-1}. This band was chosen because it is a band that is only associated with the polyimide, and is present in each spectrum.

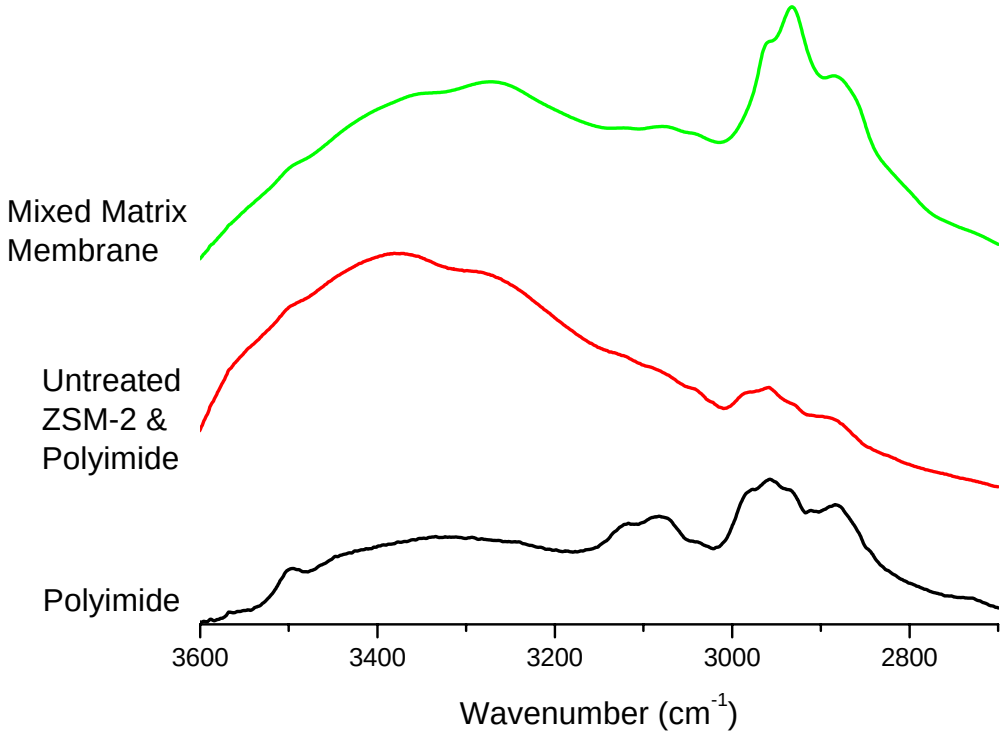

Figure 3-9. FTIR spectra for the pure polyimide, a 20 wt % untreated ZSM-2+polyimide MMM, and a 20 wt % amine-functionalized ZSM-2 MMM.

These three curves appear to support the expected results of the experiment, specifically, successful functionalization of the zeolites with amine groups, and promotion of hydrogen bonding between these amine groups and the carboxylic groups located along the polyimide backbone. The polyimide spectrum displays several bands associated with its functional groups. The carboxylic groups have two bands in this region. The first is the free –OH groups appearing at 3496 cm^{-1}. The second band is from the self associated carboxylic groups. This produces a broad –OH band from 3475 – 3200 cm^{-1}. Peaks below 3200 cm^{-1} are associated with C-H stretches. The two peaks near 3100 cm^{-1} are from the aromatic C-H stretches of the polyimide. Those stretches below 3000 cm^{-1} are from aliphatic C-H stretches, likely due to residual THF.

The incorporation of untreated ZSM-2 into the polymer matrix results in large changes in the spectrum. There is a large increase in absorbance between 3600 – 3200 cm^{-1}. This increase is attributable to the introduction of Si-OH groups from the zeolites which are IR active in this region. This results in a very broad peak that reaches its maximum at 3380 cm^{-1}. These bands are strongly IR active, and drown-out the presence of other bands making inferences of the interactions between the untreated zeolite and polyimide difficult.

The mixed matrix membrane spectrum differs from the other two in a way that suggests the presence of hydrogen bonding between the zeolite and the polyimide. As with the untreated MMM, the absorbance in the region between 3600-3200 cm^{-1} is large due to the presence of silanol groups, and masks any presence of free –OH groups near 3500 cm^{-1}. The N-H stretch of the ATPES amine group is active in this region as well, showing a peak at 3382 cm^{-1}. However, this peak is weakly absorbing and provides only a very small peak in its pure spectra. What should be noted is that the peak in absorbance in this region has been shifted to lower wavenumbers when compared to the untreated zeolite MMM. The MMM system peaks at 3272 cm^{-1}. This would indicate the presence of a hydrogen bonded system, specifically between the APTES amine group attached to the zeolite and the carboxylic group of the polyimide.

The MMM spectrum shows the aromatic C-H stretches present in the other two spectra near 3100 cm^{-1}. Relative to the other two, the MMM spectrum has more activity below 3000 cm^{-1} which is due to aliphatic C-H stretches. This is can be attributed to the propyl and ethyl groups of ATPES.

Investigating the lower region of the IR spectrum also provides some insight into the chemical environments of the membranes. Figure 3-10 shows the FTIR region between 1800-1550 cm^{-1} for all three systems.

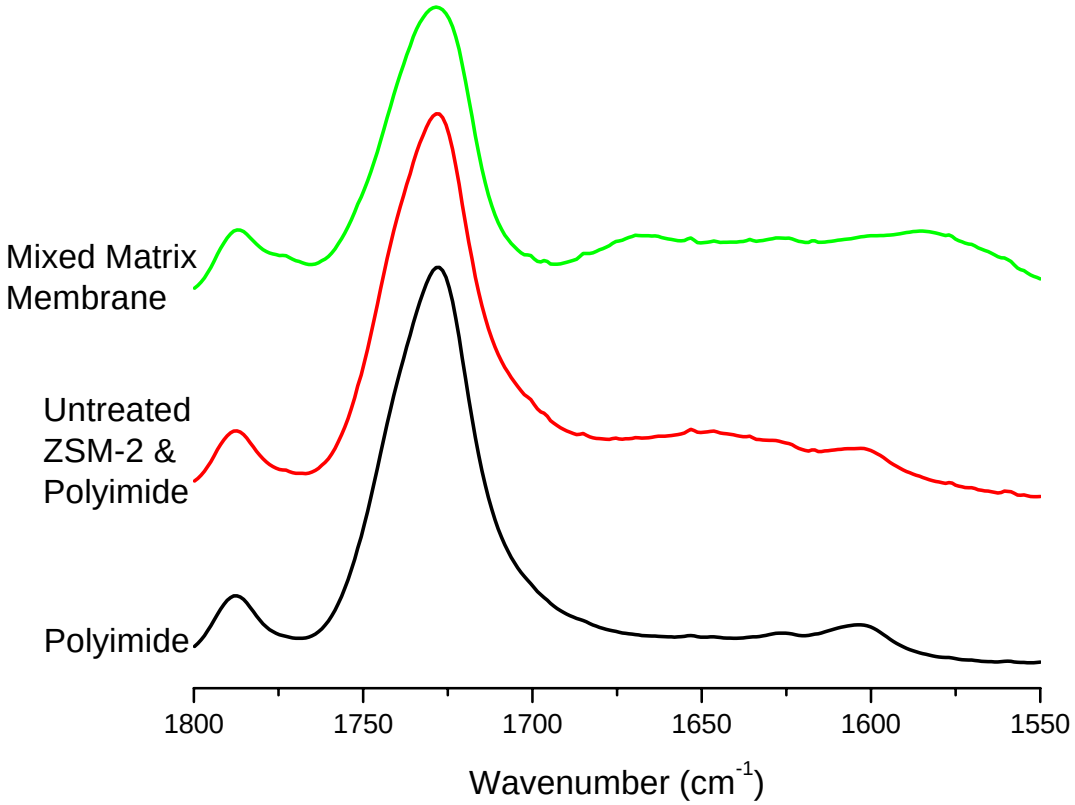

Figure 3-10. FTIR spectra for the polyimide, polyimide and untreated ZSM-2, and the MMM.

All three spectra show the anhydride end peak at 1787 cm^{-1}. Additionally, each spectrum shows the strongly IR active carbonyl stretch at 1728 cm^{-1}, however the height and width of this peak differ among the three systems. The addition of amine-functionalized zeolite has two noticeable effects on the spectrum. First, the carbonyl group band broadens and shortens, indicating there was a change in its chemical environment. Secondly, there is an increase in adsorption between 1675 and 1575 cm^{-1}. This could be due to hydrogen bonding between the carboxylic group of the polyimide and the amine group attached to the ZSM-2 surface. Hydrogen bonded C=O groups would become IR active at lower wavenumbers. This would lower the absorbance of the

nonhydrogen bonded C=O peak as well as broaden it. It could also lead to a new peak. Amine groups are also IR active in this region. Pure APTES displays an IR active N-H stretch at 1617 cm^{-1}. The fact that both the pure polyimide and the polyimide-pure ZSM-2 spectra do not show any absorbance below 1600 cm-1, while the MMM spectra does could be an indication of a hydrogen bonded amine. A third possibility is that there was a reaction between the polyimide's carboxylic group and the zeolite's amine group to create an amide linkage. Amide linkages are IR active in this region as well.

3.4.5 Microscopy Results

Several microscopy instruments provided detailed images of the membrane surface and interior at different magnifications. A field emission scanning electron microscope (FESEM) cross sectional image was taken that revealed a membrane with two distinct regions: a polymer rich region and a zeolite rich region Figure 3-11.

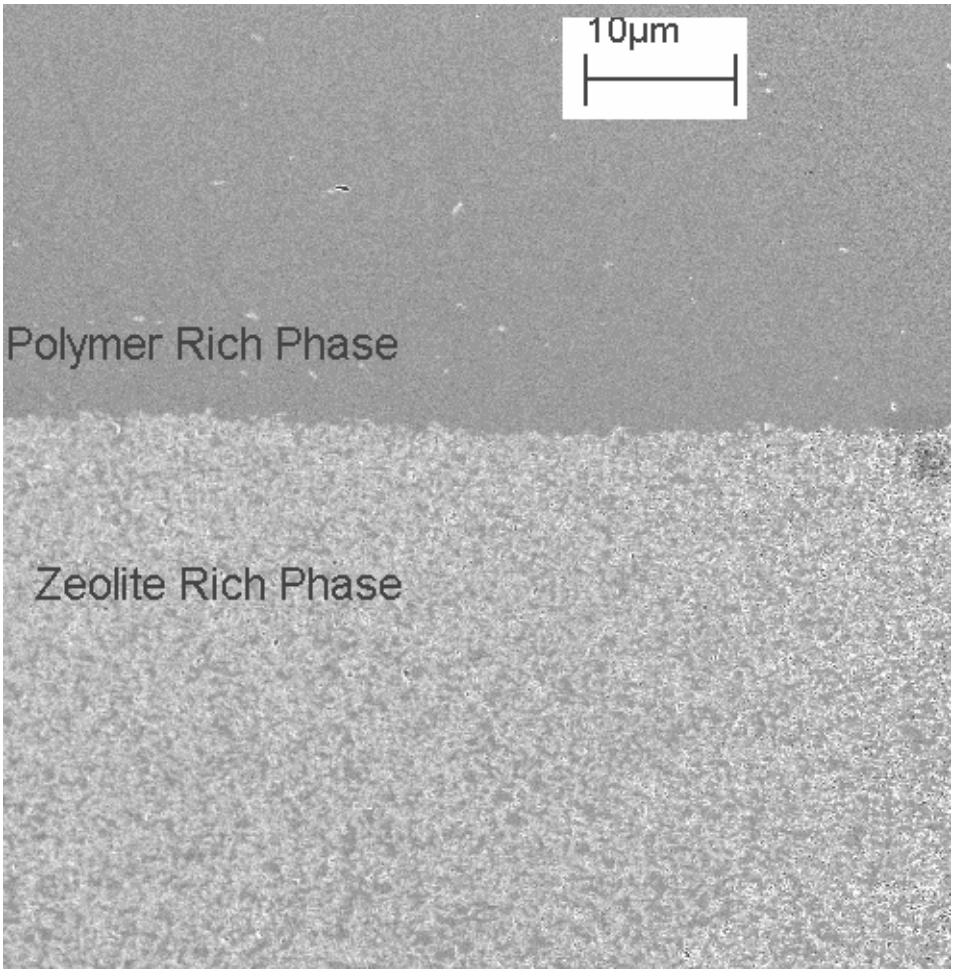

Figure 3-11. Cross sectional FESEM image of a 20% weight surface modified ZSM-2 80% weight 6FDA-6FpDA-DABA membrane.

Exploring both surfaces of the membrane using the FESEM confirmed what the cross sectional shot revealed. One surface contained a miniscule amount of ZMS-2, while the opposite surface carried a high concentration of the zeolite. Presumably, this sedimentation occurred during the membrane fabrication process as a result of the difference in the densities between THF (ρ = .886 g/cm^3) and ZSM-2 (ρ = 1.31 g/cm^3). The surface FESEM images gathered of the zeolite rich surface did not reveal the presence of voids between the polymer and the zeolite as shown below in Figure 3-12:

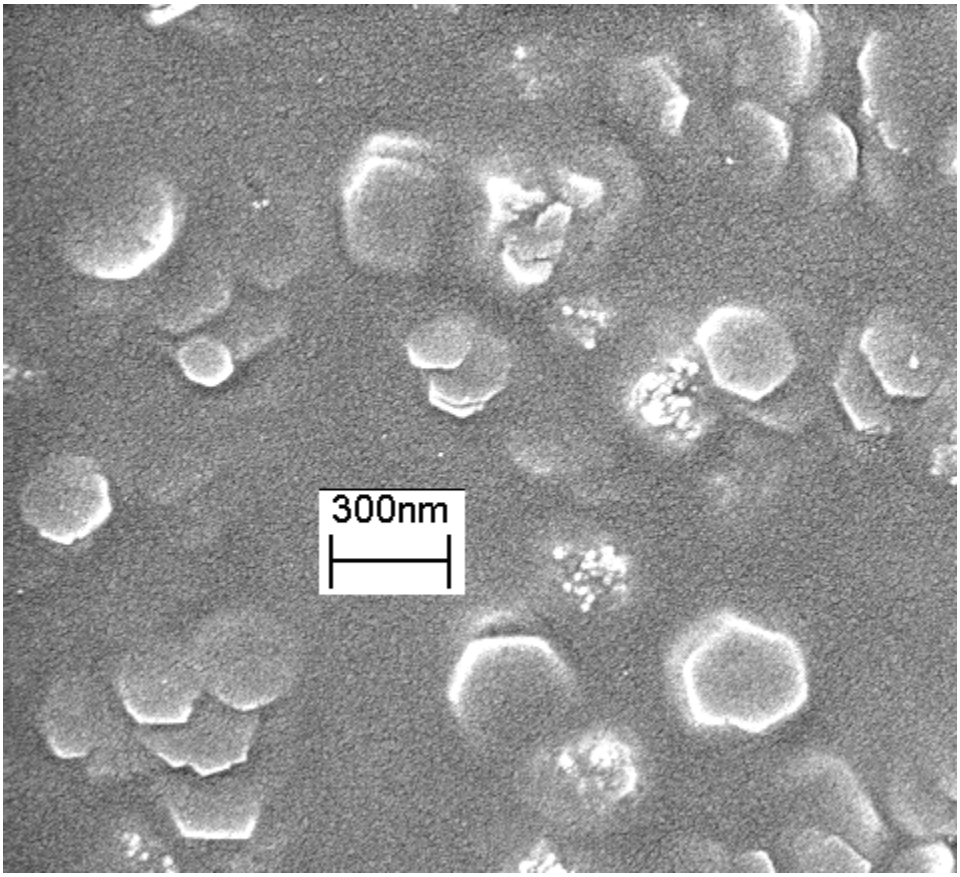

Figure 3-12. Surface FESEM image of the zeolite rich phase of a 20 wt % ZSM-2 zeolite mixed matrix membrane.

Images taken of the same surface at lower magnifications revealed that the zeolite was well distributed across the surface and not agglomerated together, suggesting the modified ZSM-2 has an affinity for the polymer.

Transmission electron microscopy images offered higher powered and higher resolution than those of FESEM. TEM images taken of the cross section of the same membrane indicated that as these zeolites sediment, many of them appear to have a preference to orient themselves such that their largest face (i.e. hexagonal face) becomes parallel to the membrane surface. An example is shown below in Figure 3-13.

Figure 3-13. TEM image of a 20 wt % amine-functionalized ZSM-2 MMM. The ZSM-2 crystals appear to orient themselves during fabrication in a way such that their flat face is oriented perpendicular to the direction of diffusion.

This orientation results in the largest ZSM-2 face being positioned orthogonal to the gas flux, and provides more zeolite surface area for the gas molecules to encounter. This may be due to the hydrodynamic radius of the large zeolite. Although this phenomenon has not been pursued further as of yet, this orientation could yield better separation performance than the same membrane without the zeolite orientation.

3.4.6 Permeation Data

The permeation properties of the pure polyimide and of a 20 wt % amine-functionalized ZSM-2 MMM are summarized below in Table 3-2. Attempts at

fabricating a 20 wt % unfunctionalized ZSM-2 membrane were unsuccessful as they were too brittle and cracked easily. The data reported shows the average value over six runs and the corresponding standard deviation of those runs. The gases tested have been listed from left to right by increasing kinetic diameter. All membranes tested had a thickness around 60 μm. Unfortunately, pure gas data of these gases through a ZSM-2 membrane were not available at the time of this writing. Thus, comparisons cannot be made with the intrinsic permeabilities of the pure zeolite.

Table 3-2. Pure gas permeabilities through pure 6FDA-6FpDA-DABA and 20 wt % amine-functionalized ZSM-2.

Permeability of Pure Gases (Barrer)

Wt % ZSM-2	He	CO_2	O_2	N_2	CH_4
0	30.67 ± 1.21	18.49 ± 0.43	4.22 ± 0.16	0.88 ± 0.02	0.67 ± 0.03
20	25.93 ± 1.85	13.19 ± 0.46	5.28 ± 0.22	1.04 ± 0.07	0.58 ± 0.04

The changes in permeability for gases were mixed, and did not appear to follow a trend with size. Helium saw a large drop in permeability (i.e. 15%). Because He is such a small molecule, it serves as an excellent probing molecule for voids. The presence of unselective voids between the polyimide and zeolite would bolster He's permeability. Since this was not observed, it is likely that voids between the components were prevented during fabrication. One must also recall that ZSM-2 was synthesized with the aide of an organic template. This left its pores clogged with this template after its synthesis. Normally, the template is removed by calcinations, in which the zeolite is given a high temperature treatment (e.g. 600 ^{o}C) to burn off the organics. This treatment would have thermally degraded the polyimide, thus it was avoided, and the template remained in the pores clogging the majority of them.

In discussing our results with our colleagues now at the University of Minnesota, Dr. Michael Tsapatsis believed that He would have a very low solubility in ZSM-2. He believed this because of He's inability to have strong interactions with the cations in ZSM-2's pores. Additionally, He has a very low critical temperature, which would also make it very unsoluble. This too would contribute to a low permeability.

The other gases showed gains and losses in permeability with the addition of ZSM-2. CO_2 and CH_4 saw drops in permeability of 29 and 13%, respectively. O_2 and N_2 saw increases in permeability of 25 and 18 %, respectively. As CO_2 was the smallest and CH_4 was the largest of these four molecules, clearly size did not correlate with the permeability results. In order to provide insight into these results, the diffusion and solubility coefficients were calculated and analyzed.

The diffusion coefficients for the pure gases in both membranes have been listed in Table 3. These values were determined using the Time Lag Method, which is discussed in detail in the Literature Review, and in other sources.[11]

Table 3-3. Pure gas diffusion coefficients in a 6FDA-6FpDA-DABA membrane and a 20 wt % amine-functionalized ZSM-2 MMM.

Pure Gas Diffusion Coefficients ($1 \times 10^{-8} cm^2 s^{-1}$)

Wt % ZSM-2	He	CO_2	O_2	N_2	CH_4
0	-	3.09 ± 0.06	10.74 ± 1.14	4.46 ± 0.58	0.81 ± 0.08
20	-	1.66 ± 0.07	13.33 ± 1.34	6.25 ± 0.13	0.66 ± 0.26

Helium diffusion coefficients are not reported for either membrane. This is because there is too much error in the measurement. The Time Lag Method calculates the diffusion coefficient (D) using the following equation:

$$D = \frac{l^2}{6\theta} \qquad \text{Eq 3.a}$$

in this equation l^2 is the membrane thickness, and θ is the diffusive lag time. The diffusive lag time scales with how long a gas takes to diffuse through a membrane once a test has begun. Due to He's high permeability, this time is very short and was calculated to be less than 1 s in each run. Unfortunately, in our permeation apparatus, each gas must flow from a gas tank, and through several feet of steel tubing before it contacts the membrane. This obviously increases the time required for He to diffuse into the downstream side of the membrane, and introduces large errors. Because of the uncertainty in the true value of D for He, it was not reported. The other gases tested had much larger lag times, and any error introduced by this was negligible.

For the other gases, it becomes apparent that each gas that saw a drop in permeability also saw a drop in D. CO_2's diffusivity dropped 46%, while that of CH_4 fell 19%. Contrasting this with the molecules that saw increases in permeability, both O_2 and N_2 diffusivity coefficients increased. O_2 saw an increase of 24% while that of N_2 saw an increase of 29%. These values should be contrasted with changes in the solubility coefficients before any conclusions are drawn.

The solubility coefficients (S) were determined using the following equation:

$$S = \frac{P}{D} \qquad \text{Eq 3.b}$$

here S is the solubility coefficient, and P is the permeability. The values for the pure gases in both membranes are reported in Table 3-4. Due to the absence of a reliable value of D for He, no S could be calculated for helium.

Table 3-4. Pure gas solubility coefficients in a 6FDA-6FpDA-DABA membrane and a 20 wt % amine-functionalized ZSM-2 MMM.

Solubility Coefficient (cm^3 (STP)/cm^3 atm)

Wt % ZSM-2	He	CO_2	O_2	N_2	CH_4
0	-	4.55 ± 0.02	0.30 ± 0.02	0.15 ± 0.02	0.63 ± 0.06
20	-	6.04 ± 0.06	0.30 ± 0.02	0.13 ± 0.03	0.72 ± 0.19

These values coupled with the diffusion coefficient values can help provide some insight into the permeability changes associated with the addition of ZSM-2. CO_2 experiences a large increase in solubility with the incorporation of ZSM-2 (i.e. 33 %). This was expected after our discussion with Dr. Tsapatsis. He anticipated that CO_2 should be able to have favorable electrostatic interactions with the lithium ion that resides in the zeolite pores. Ultimately, this results in a large sorption of CO_2 in the zeolite. The drop in CO_2 diffusivity may be due to the high solubility it possesses in the zeolite. Perhaps at these pressures (i.e. 4 atm) the zeolite is not fully saturated with CO_2 and behaves more like a sponge where it sorps the gas but doesn't readily release it. This would explain both the drop in D and increase in S. Sorption experiments on the pure zeolite and polymer would have been helpful in validating or rejecting this hypothesis.

The other three gases show almost no changes in S. Methane does show an increase in S (14%), however, the standard deviations are so large that statistically they changes are not significant. These results suggest that the changes in permeability of these gases were due to restrictions (i.e. CH_4) or enhancements to diffusivity (i.e. O_2, N_2). The increases in permeability were largest for O_2 which is the smallest of these gases, while the only decrease came to the largest gas molecule (i.e. methane). Dr. Tsapatsis believed that a small fraction of the pores of the ZSM-2 were not clogged during the synthesis, and perhaps this could offer some avenue to increase the permeation of certain gases below a size threshold. These open pores would also allow CO_2 to sorp into them, and account for its high solubility.

To gauge the separation performance of these membranes, the ideal selectivities were determined by ratioing the pure gas permeabilities. The results for industrially significant gas separations are shown below in Table 3-5.

Table 3-5. Ideal selectivities for industrially significant gas separations for the pure 6FDA-6FpDA-DABA membrane and the 20 wt % ZSM-2 MMM.

Ideal Selectivities

Wt % ZSM-2	O_2 / N_2	N_2 / CH_4	He / CO_2
0	4.81 ± 0.14	1.32 ± 0.03	1.66 ± 0.06
20	5.11 ± 0.37	1.78 ± 0.03	1.96 + 0.09

While these results are encouraging, one must remember that these ratios were determined from pure gas data. When separating a mixed gas feed, the true selectivity can be measured, and this would likely be different from the ideal selectivity. ZSM-2 separates based on a selective adsorption mechanism, so it requires a mixed feed to truly show its selectivity performance.

3.5 Conclusions

In this study mixed matrix membranes were fabricated from a 6FDA-6FpDA-DABA polyimide (M_w = 93, 000g/mol) and amine-functionalized ZSM-2 zeolite. The ZSM-2 zeolites were functionalized with amine groups by reacting them with aminopropyltrimethoxysilane in toluene. Mixed matrix membranes were fabricated at 20% weight zeolite and 50% weight zeolite successfully, however the latter was too brittle to be used to gather data.

The amine tethered zeolites interacted through secondary forces with the carboxylic groups along the polymer backbone as documented by FTIR studies. Band shifts associated with hydrogen bonding of the carbonyl and amine groups were observed in the spectra. These interactions promoted adhesion between the two components.

The morphology of the MMM was documented by SEM and TEM. Both instruments did not reveal the presence of voids around the zeolites, and portrayed a membrane in which the zeolites were randomly distributed on the surface. This

suggested that the zeolite and polymer had an affinity for each other. Additionally, cross-sectional SEM images revealed that the MMMs had two phases: a polymer-rich section, and a zeolite-rich section. It was presumed this occurred due to the large differences in density between the zeolite and the casting solvent (i.e. THF).

Permeation data of He, CO_2, O_2, N_2, and CH_4 were collected and analyzed. The permeabilities of He, CO_2 and CH_4 all decreased, while O_2 and N_2 increased. The solubility coefficients for O_2, N_2, and CH_4 were roughly unchanged, while polar CO_2 saw a large increase in solubility. The changes in permeability for each gas correlated well with the change in its diffusion coefficient. Ideal selectivities improved or worsened depending on the gas pair selected.

3.6 References

1 Robeson, L. M. *Journal of Membranes Science* 1991, *61*, 165-185.

2 Koros, W. J.; Mahajan, R. *Journal of Membranes Science* 2000, *175*, 181-196.

3 Koros, W. J.; Mahajan, R. *Industrial Engineering and Chemistry Research* 2000, *39*, 2692-2696.

4 Koros, W. J.; Zimmerman, C. M.; Singh, A. *Journal of Membranes Science* 1997, *137*, 145-154.

5 Tantekin-Ersolmaz, S. B.; Atalay-Oral, C.; Tather, M.; Erdem-Senatalar, A.; Schoeman, B.; Sterte, J. *Journal of Membrane Science* 2000, *175*, 285-288.

6 Duval, J.-M.; Folkers, B.; Mulder, M. H. V.; Desgrandchamps, G.; Smolders, C. A. *Journal of Membrane Science* 1993, *80*, 189-198.

7 Gur, T. M. *Journal of Membranes Science* 1994, *93*, 283-239.

8 Suer, M. G.; Bac, N.; Yilmaz, L. *Journal of Membranes Science* 1994, *91*, 77.

9 Park, H. C.; Yong, H. H.; Kang, Y. S.; Won, J.; Kim, W. N. *Journal of Membranes Science* 2001, *188*, 151-163.

10 Nikolakis, V.; Xomeritakis, G.; Abibi, A.; Dickson, M.; Tsapatsis, M.; Vlachos, D. *Journal of Membrane Science* 2001, *184*, 209-219.

11 Crank, J. *The Mathematics of Diffusion*, 2 ed.; Oxford Press: London, 1990.

12 Alpert, N. K., W.E.; Szymanski, H.A.;. *Ir-Theory and Practice of Infrared Spectroscopy*; Plenum Publishing Corporation: New York, 1970.

13 Silverstein, R.; Webster, F. *Spectrometric Indentification of Organic Compounds*, 6 ed.; John Wiley & Sons, Inc: New York, 1998.

14 Becker, K. H.; Schmidt, H. W. *Macromolecules* 1992, *25*, 6784-6790.

15 Husk, G.; Cassidy, P.; Gebert, K. *Macromolecules* 1988, *21*, 1234-1238.

16 Kim, J. H.; Lee, S. B.; S.Y., K. *Journal of Applied Polymer Science* 2000, *77*, 2756-2767.

17 Bessonov, M.; Koton, M.; Kudryavtsev, V. V.; Laius, L. *Polyimides: Thermally Stable Polymers*; Pleneum Publishing Corp: New York, 1987.

18 Cornelius, C. J. In *Chemical Engineering*; Virginia Tech: Blacksburgh, 2000.

19 Bekkum, H. V.; Flanigen, E.; Jansen, J. C. *Introduction to Zeolite Science & Practice*; Elsevier: New York, 1991.

20 Ruthven, D. *Chemical Engineering Progress* 1988, 42-50.

Chapter 4: Preparation and Characterization of Polyimide-Zeolite L Mixed Matrix Membranes for Gas Separations

4.1 Abstract

The fabrication and characterization of a polyimide and amine-functionalized zeolite mixed matrix membrane are described. The polyimide employed in this study is 6FDA-6FpDA-DABA, and the zeolite employed is zeolite L. Zeolite L was chosen because it was synthesized without the aid of an organic template which would clog its pores. The zeolite was amine-functionalized in order for it to react with the carboxylic acid group of the polyimide and form amide-linkages. These linkages would be used to prevent dewetting of the polymer from the zeolite. Pure gas permeabilities for He, O_2, N_2, CH_4 and CO_2 are presented and high pressure permeabilities for CH_4 and CO_2 are presented. The components of the membrane are characterized using FTIR, XPS, zeta potential, and FESEM.

4.2 Introduction

The performance of polymeric membranes has been shown to follow a trade-off curve between gas permeability and selectivity illustrated by Robeson's upper bound.[1] In the past several years efforts aimed to surpass this upper bound trade off curve have focused on the development of mixed matrix membranes (MMMs) composed of polymers and zeolites. Zeolites offer excellent gas separation performance as well as

chemical and thermal stability, however, they are expensive and have poor mechanical properties. In contrast polymers are relatively inexpensive, can be processed into hollow fibers, and possess good mechanical properties, but lack high separation performance as well as chemical and thermal stability. The goal of MMMs is to combine the separation properties of the zeolites with the low cost and processability of the polymer into one membrane. Potential applications of these new membranes have been discussed elsewhere.[2]

Previous attempts at fabricating MMMs using glassy polymers and zeolites resulted in voids between the polymer and the zeolite.[3,4] This reduced the separation performance of the composite membrane relative to the pure polymer, because the gas molecules taking the path of least resistance by-passed the zeolites altogether when diffusing across the membrane. Several different silane coupling agents were successfully employed to improve adhesion between the polymer and zeolite. However, the resulting permeabilities were slightly lower, and ideal selectivities were largely unchanged, when compared to the pure polymer.[5]

Other attempts at developing glassy polymer-zeolite composite membranes have focused on fabrication methods without modifying the zeolite surface. Gür combined zeolite 13X and polyethersulfone (PES) through a melt extrusion process.[6] The two components were dried and extruded through a thin slit die to produce defect free membranes. However, the resulting permeation properties did not change significantly relative to the pure PES membrane. Süer et al. mixed polyethersulfone with either zeolite 13X or zeolite 4A and solution-cast the mixtures.[7] Three different drying and annealing procedures were used to fabricate the membranes. One method resulted in improved permeability and selectivity relative to the pure PES; This was attributed to the relatively slow drying process which allowed the polymer chains to pack better leading to a better membrane. Yong et al. developed void free polyimide-zeolite MMMs by adding 2, 4, 6-triaminopryimidine capable of hydrogen bonding with both the polymer and zeolite.[8] This additive enhanced the contact between the two components. The resulting membranes displayed increased permeability without much change in the selectivity. Koros et al. blended plasticizers with high glass transition temperature (T_g) polymers to lower their T_g 's and increase their flexibility.[9] The polymeric blends were mixed with

zeolite 4A (15% by volume) and cast to form membranes. Each MMM offered improved selectivity, but lower permeability compared to its polymer-plasticizer counterpart. Unfortunately, none of the membranes with plasticizers succeeded in surpassing Robeson's upper bound.

Mahajan et al. also investigated the addition of covalent linkages between Matrimid®, a high T_g polymer, and zeolite 4A using aminopropyltriethoxysilane as the coupling agent.[10] SEM images indicated that covalently bound MMMs displayed improved adhesion. These MMMs offered lower selectivity and slightly higher permeability than both the pure Matrimid® and the Matrimid® – unmodified zeolite 4A composite for the O_2/N_2 separation. It was proposed that this approach reduced the size of the interfacial voids, but did not eliminate them.

Mahajan et al. also investigated lower T_g polyimides which were anticipated to interact favorably with the zeolite 4A.[10] SEM images showed that some of the polyimides displayed good contact with the zeolite without the use of coupling agents. All polyimide-zeolite 4A combinations possessed good dispersion of the zeolite throughout the matrix. The permeation results for the more flexible polyimide – zeolite 4A MMMs varied depending on the polymer chosen. When coupling agents were used, decreasing permeability and increasing selectivity were observed as the volume fraction of zeolite was increased.

The authors also investigated polymers containing carboxylic groups capable of bonding directly to zeolite 4A, eliminating the need for coupling agents. At 15% by volume of zeolite the MMM had lower permeability with a small increase in selectivity, and did not surpass Robeson's upper bound.

In this chapter we expand upon our previous research on mixed matrix membranes containing zeolites, amino-functional silane coupling agents, and glassy polyimides with hydrogen bonding acidic groups incorporated into their backbone.[11] This investigation focuses on the incorporation of zeolite L instead of ZSM-2. Zeolite L differs from other zeolites employed in recent investigations used by others due to its ability to separate by selective adsorption rather than by size discrimination.[6,12-14] Also, it was synthesized without the aid of an organic template as outlined in the Experimental

section, thus there was no template clogging the pores. Additionally, zeolite characterization will be presented confirming the functionalization of the zeolite surface.

4.3 Experimental

4.3.1 Materials

The polyimide used in this study was synthesized using a step growth reaction. Step growth reactions require very pure monomers and very dry solvents in order to achieve high molecular weights with narrow polydispersities. All glassware was rinsed with acetone and flame dried before use. This section lists the solvents and monomers used in the study, and outlines the steps taken to prepare them for use in the step growth reaction synthesis.

4.3.1.1 Solvents

1-Methyl-2-Pyrrolidinone (NMP)

NMP was used as the solvent in the synthesis of the 6FDA-6FpDA-DABA polyimide. This solvent was purchased from Fisher Scientific. The solvent was dried over phosphorus pentoxide (P_2O_5) for 24 hours. Because NMP is hydroscopic, it was vacuum distilled immediately before use.

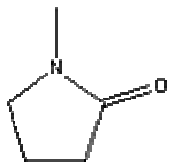

O-Dichlorobenzene (DCB)

DCB was purchased from Fisher Scientific and used in the synthesis of the 6FDA-6FpDA-DABA polyimide. It was added for the purpose of forming an azeotrope with the water produced during the step growth reaction. This azeotrope could be boiled off and help the synthesis achieve a higher molecular weight. DCB was mixed with P_2O_5 for 24 hours and then vacuum distilled immediately before use to avoid exposure to moisture.

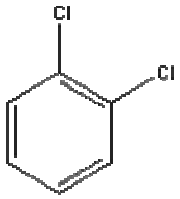

Methanol (MeOH)

Low grade MeOH was purchased from the Virginia Tech Chemistry Stockroom and used as received. This solvent was used to precipitate the polyimide from the NMP and DCB following the synthesis.

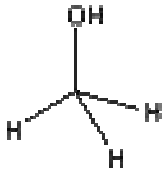

Tetrahydrofuran (THF)

Tetrahydrofuran was purchased from Fisher Scientific and was used as received. The grade purchased was high purity liquid chromatography. It was used in the fabrication of the membranes.

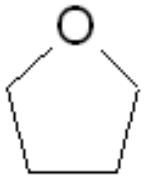

Toluene

Toluene was purchased from Fisher Scientific and used as received. The grade purchased was high purity liquid chromatography. It was used as the solvent in the reaction which covalently added amine groups to the zeolite surfaces.

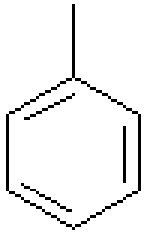

4.3.1.2 Monomers

4,4'-(Hexafluoroisopropylidene)diphthalic Anhydride (6FDA)

6FDA was purchased from Clariant with a purity >99.95%. Prior to use the material was placed under vacuum at a temperature of 150 ^{o}C to ensure compete cyclic anhydride cyclization immediately prior to use.

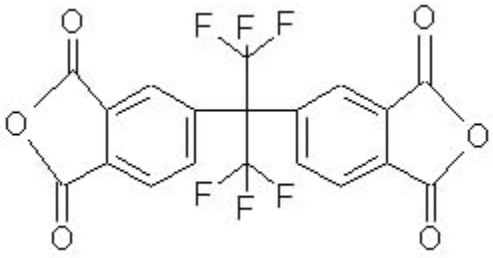

4,4'(Hexafluoroisopropylidene)dianiline (6FpDA)

6FpDA was purchased from SynQuest labs with a purity of >98%. The monomer was sublimed for further purification. After sublimation 6FpDA was kept in a dry box to avoid moisture contact.

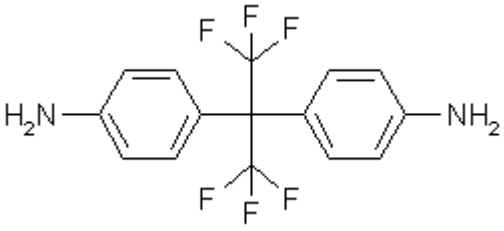

3, 5-Diaminobenzoic Acid (DABA)

DABA was purchased from Aldrich with a purity of >98% and used as received. It was dried under vacuum near 100 ^{o}C prior to use.

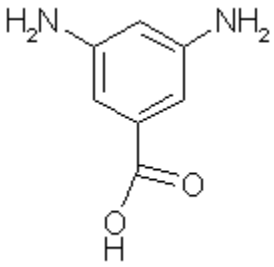

Aminopropyltriethoxysilane (APTES)

APTES was purchased from Gelest with a purity of 99%. It was used as received.

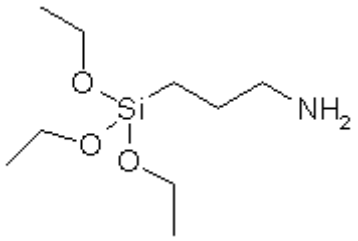

4.3.2 Synthesis of 6FDA-6FpDA-DABA

A flame dried 1000 mL 3-neck round bottom flask was used as the reaction vessel in this synthesis. The right neck was used as a N_2 inlet and held a thermometer. The center neck of the round bottom was connected to a mechanical stirrer. The left neck led to the condenser and trap to gather condensed DCB and return it round bottom flask. A diagram of the reaction setup is shown below in Figure 4-1.

4,4'–Hexafluoroisopropylidene dianiline , 4,4'–hexafluoroisopropylidenediphthalic anhydride and 3,5–diaminobenzoic acid were placed under vacuum near 100 ^{o}C to remove water prior to use. 1-Methyl-2-pyrrolidinone and *o*-dichlorobenzene were dried over phosphorous pentoxide and vacuum distilled.

NMP (485 mL) and DCB (76 mL) were added to a round bottom flask in a 4:1 molar ratio. 6FDA (74.9 g) was added under N_2 flow and allowed to completely dissolved. Following this, the 6FpDA (28 g) was added to the solution and the components were mixed at room temperature for 24 h to form a low molecular weight polyamic acid which was targeted to be end capped with anhydride groups. After 24 h the solution was heated to 180 ^{o}C for an additional 24 h to imidize the polyamic acid leading to a low molecular weight polyimide. Once the solution cooled to room temperature, DABA (12.7 g) was added, and the mixture was stirred at room temperature for 24 h to form a high molecular weight polyamic acid. After this time, it was heated to 180 ^{o}C for 24 h to imidize the polyamic acid. Following this step, the polymer solution was allowed to cool to room temperature.

After the synthesis the polyimide solution was purified using 5 μm filters. The filtered solution was poured into a methanol bath to remove the NMP and DCB from the

polymer. The precipitated polymer remained in the methanol bath for four days, during which the methanol was changed daily. After the four days, the polymer was removed and allowed to air dry overnight. Once dry, the material was then heated at 110 ^{o}C for 12 h under vacuum to remove any residual methanol.

The polyimide was then stored in a dessicator until needed.

4.3.3 Synthesis of Zeolite L

The zeolite L used in this study was synthesized by Dr. Michael Tsapatsis group at the University of Minnesota. The procedure for synthesizing zeolite L has been taken from one of his group's publications.[17]

Aluminum foil (0.05 mm thick, 99.8+%, Aldrich) and fumed silica (Grade M-5, Cabosil) were used to prepare aluminate solutions and silicate solutions, respectively. The alkali-metal ion source was potassium hydroxide (A.C.S. grade, Fisher)

A clear potassium aluminate solution was prepared by the addition of 3.6 g of aluminum foil to 150 mL of 3 M aqueous KOH solution. The solution was filtered to remove the iron impurities of the aluminum foil that remained undissolved.

Fumed silica (80 g) was dissolved in 300 mL of the KOH solution. This solution was stirred and heated at 80 ^{o}C for 12 h. After cooling to room temperature, slow addition of the clear aluminate solution to the clear silicate solution with vigorous stirring resulted in a clear homogenous solution. Subsequent adjustments of the concentrations were performed with the addition of water or aqueous KOH. Preweighed amounts of the synthesis solution were placed in Teflon lined stainless steel vessels, and placed in a rotating oven at 30 rpm and 180 ^{o}C for 8 h. Following this, the aqueous zeolite suspension was poured into centrifuge tubes, and centrifuged several times. After each centrifuge, the solution was replaced with de-ionized water. This was repeated until the pH was neutral, after which the suspension was dried at 110 ^{o}C for 12 h leaving only a zeolite powder. Samples were taken to be analyzed using WAXS for the purpose of verifying the structure of zeolites.

4.3.4 Amine Functionalization of Zeolite L

Once received from Dr. Tsapatsis' lab, zeolite L was heat treated at ~ 150 ^{o}C under vacuum for 24 h to remove any presence of water. After this time, the vacuum oven was flooded with Ar and the glass vial containing the zeolite powder was immediately sealed.

The zeolite powder was immediately added to toluene, which was purchased from Fisher and used as received. The mixture was added to a 125 mL round bottom flask, and more toluene was added to provide a zeolite concentration of approximately 6.0 mg/ml toluene. Aminopropyltriethoxysiliane (APTES), purchased from Gilest and used as received, was then added in an amount such that a ratio 0.07 ml APTES/ ml toluene was present in the flask before the reaction began. The mixture was then refluxed under an Argon purge for 3 h at a temperature near 110 ^{o}C to add amine groups to the zeolite surface.

Upon completion of the reaction, the mixture was centrifuged several times. After each centrifuge the solvent was replaced with fresh tetrahydrofuran.

4.3.5 Membrane Preparation

An amount of 6FDA-6FpDA-DABA required to produce a 20% weight zeolite - 80% weight polyimide mixed matrix membrane was added to the zeolite-THF mixture and allowed to mix for 24 h. The solution was then cast onto a Teflon coated surface, smoothed using doctor blade, and allowed to evaporate over several hours. Pure 6FDA-6FpDA-DABA membranes were produced using the same procedure.

The 20% weight zeolite L MMM and the pure polyimide membrane were both sub-T_g annealed in order to remove excess solvent. Both membranes were placed under vacuum at a temperature of 50 ^{o}C for 5 h, 150 ^{o}C for 5 h, 220 ^{o}C for 12 h, then allowed to cool to room temperature over a 9 h period.

4.3.6. Membrane Characterization

The gas permeabilities of the pure polyimide and mixed matrix membrane were measured in a constant volume – variable pressure system. Using the time lag method,[18] the permeability, diffusion coefficient, solubility coefficient, and diffusive lag time for the membranes were determined for He, O_2, N_2, CH_4 and CO_2. The gases were tested in that order for both membranes. The ideal selectivities were calculated using the pure gas permeabilities. The feed pressure for all permeation experiments was 4 atm, and the temperature was kept at 35 ^oC. In addition to this CH_4 and CO_2 permeabilities were measured at 8 and 12 atm at 35 ^oC.

The changes in the chemical environment among the pure polyimide, the polyimide and untethered zeolite, and the mixed matrix solution were investigated by analyzing transmission FTIR spectra. The spectrometer used was a BIO-RAD model FTS-40A. The samples were prepared by casting a portion of each mixture onto a CaF_2 plate. A pipette was used to transfer a repeatable amount among the different samples. The presence of hydrogen bonding between the zeolite and polymer were determined by observing shifts of characteristic absorption bands to lower wavenumbers and noting changes in peak intensities.

The molecular weight of the polyimide was determined using a Waters 150C GPC/ALC chromatograph equipped with a differential refractometer and viscometer detector. This also provided the polydispersity of the polymer solution. Samples of the polyimide were dissolved into NMP at a concentration of 3.2 mg polyimide/ml NMP. A calibration curve for the GPC was generated using narrow molecular weight polystyrene standards.

X-ray photoelectron spectroscopy (XPS) was used to determine the atomic concentrations at the surface regions of the zeolites. The system used was a Perkin Elmer-5400 Series. This system used a Mg anode operating at 300 W as the source of the x-rays. An area of 1 x 1 mm was analyzed for each sample, and experiments were performed at pressures below 5 x 10^{-6} Pa. Take-off angles of 45^o were used to probe up to a depth of ~ 3.5 nm.

Surface and cross sectional images of the composite membrane were gathered using a field emission scanning electron microscope (LEO 1550). Cross sectional samples were embedded in epoxy and microtomed.

Zeta potential measurements were obtained using a Malvern Zetasizer 3000HS. Samples consisted of aqueous zeolites suspensions of controlled pH. The pH was controlled by the addition of HCl or NaOH. The concentration of the samples was 0.39 mg zeolite per ml de-ionized water.

4.4 Results and Discussion

4.4.1 Polymer Synthesis

6FDA-6FpDA-DABA was synthesized using the approach in Figure 4-1. The details of the synthesis have been outlined in the Experimental sections. The reaction is outlined below, and has been used extensively by others.[19-21] In Figure 4-1 the aromatic dianhydride and diamine react to form a low molecular weight polyamic acid. The stoichiometry is controlled such that the ends should be anhydride groups. This polyamic acid is heated to cyclodehydrate the amic acid into a polyimide known as 6FDA-6FpDA. The low molecular weight 6FDA-6FpDA is reacted with 3,5-diaminobenzoic acid. The DABA essentially acts as a linker between the low molecular weight chains to combine them into a high molecular weight polyamic acid. This high molecular weight polyamic acid is heated to cyclodehydrate into a polyimide. The results a high molecular weight polyimide with carboxylic groups incorporated into its backbone. This polyimide is referred to as 6FDA-6FpDA-DABA.

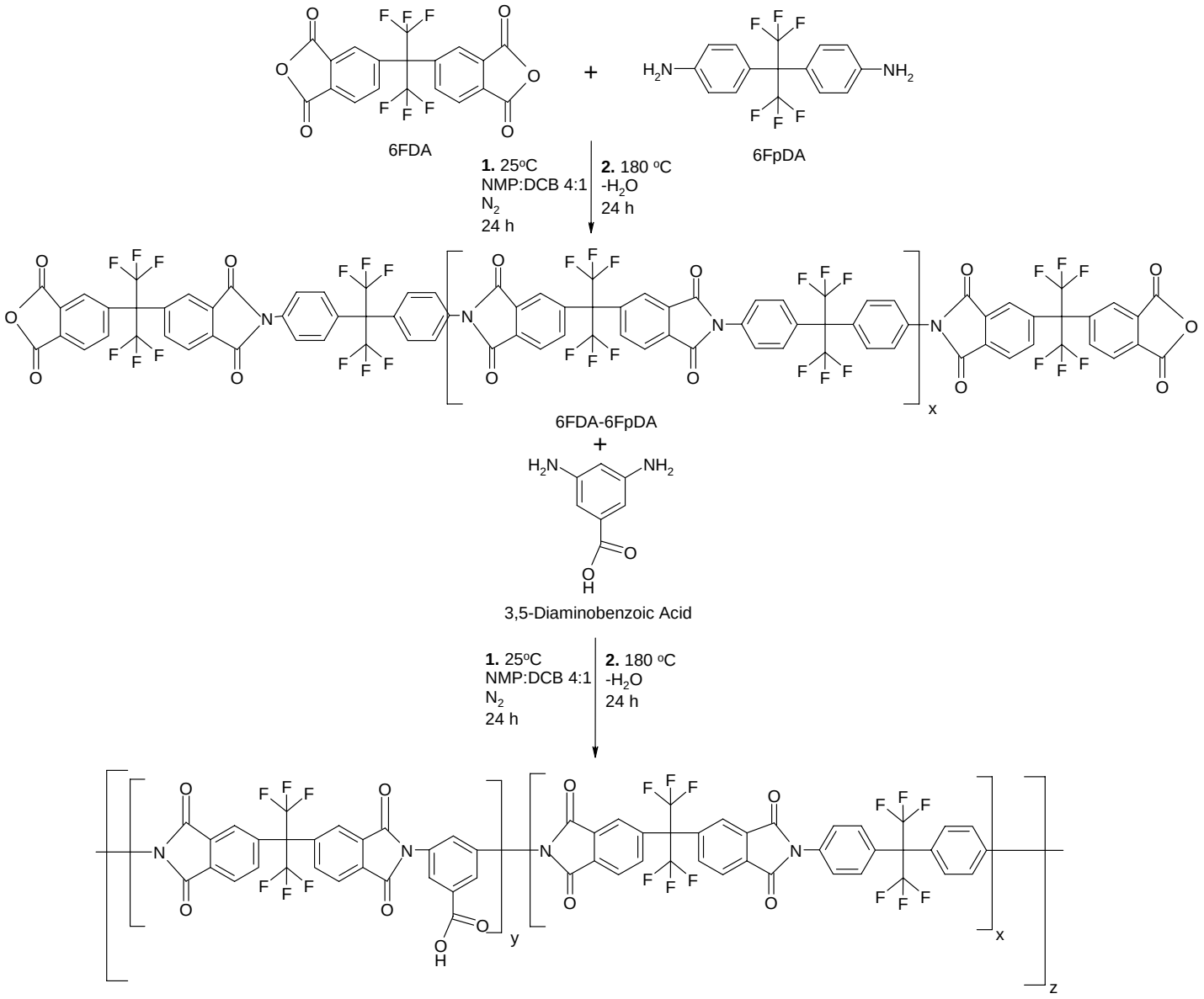

Figure 4-1. Synthesis of 6FDA-6FpDA-DABA.

Its number average molecular weight was determined using GPC to be 26,600 g mol^{-1} with a polydispersity of 2.523.

4.4.2 Zeolite L

Zeolite L was chosen as the zeolite component for the membranes. It was synthesized for us by Dr. Michael Tsapatsis' group at the University of Minnesota. Unlike the zeolite chosen for our previous work,[11] zeolite L was not synthesized using an organic template that would require calcination at a high temperature (e.g. 600 ^{o}C).

Zeolite L is zeolite with one a one dimensional pore structure which runs along its c-axis. The minimum constricting ring in its channels measures 0.71 nm, however, because of the presence of aluminum in its framework, potassium cations reside in its pores to balance the negative framework charge. This reduces the size of the pore. The unit cell has 36 tetrahedrally coordinated T-atoms (i.e. Si and Al). Zeolite L's has a Si/Al ratio of 3 and a composition of $K_9[AL_9Si_{27}O_{72}]\cdot H_2O$.

Zeolite L can be synthesized in a variety of shapes and sizes. Sizes of zeolite L can range from particles as small as 30 nm to long flat plates with aspect ratios near 100. In the latter case, the channels will run through the thickness of the zeolite (i.e. its shortest dimension).[17,22] The zeolite L used in this study had a flat plate like structure. An image of a cluster of zeolite L particles is shown in Figure 4-2.[23]

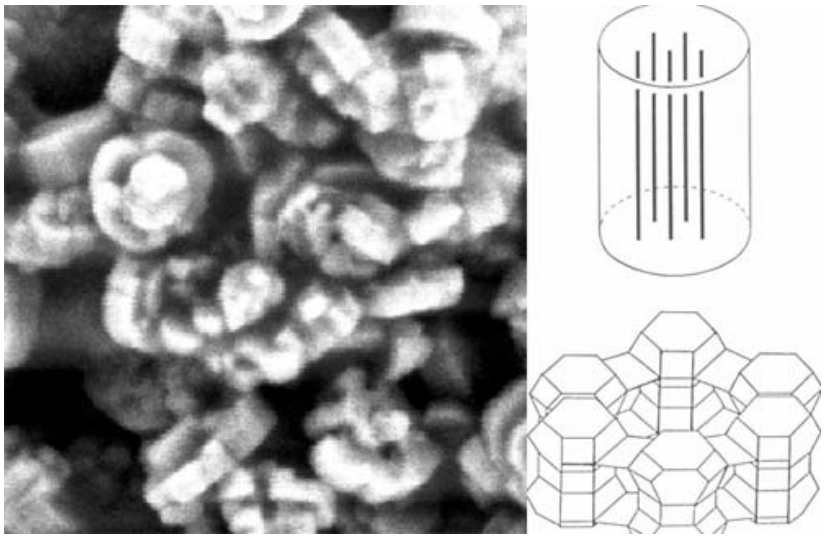

Figure 4-2. FESEM image of a cluster of zeolite L crystals (left), and an illustration of the pore direction relative to the crystal (top right) and a zeolite L pore cage (bottom right). The illustration was taken from Bekkum et al [23].

Due to the presence of cations within the channel of zeolite L, it can separate using a selective adsorption mechanism. Molecules that more strongly adsorb onto the pore walls will receive enhanced transport through access to surface diffusion rather than being limited to Knudsen diffusion. Furthermore, the selective adsorption will enhance the selectivity of the zeolite. When one component sorps to the pore wall the channel size is reduced, thus making it inaccessible to other nonadsorbing species. Species that sorb onto the zeolite pore walls are typically polar molecules (e.g. H_2O, ammonia), quadrupolar (e.g. CO_2, N_2), or are capable of π-layer interactions (e.g. aromatic hydrocarbons).[24] Because of this, zeolite L is typically targeted to remove CO_2 or unsaturated hydrocarbons from mixtures.

4.4.3 Amine-functionalizing zeolite L

Zeolite L was amine-functionalized by reacting it with aminopropyltriethoxysilane (APTES) in toluene Figure 4-3. This approach has been used by others.[25] Amine groups were added to the zeolite surfaces with the intent to react them with the carboxylic groups of the polyimide. This would create an amide linkage which would covalently attach the two components and prevent phase separation.

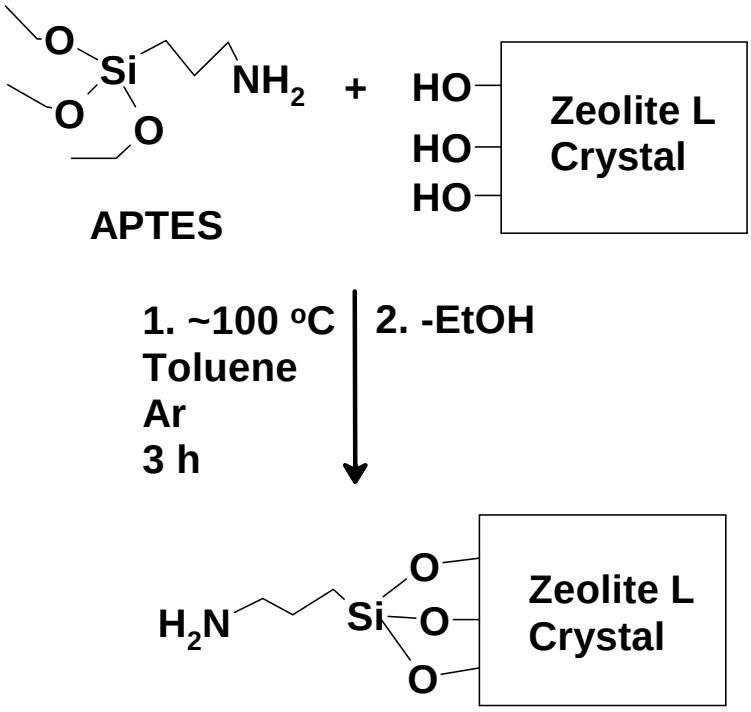

Figure 4-3. Reaction scheme in which zeolite L is amine-functionalized through a reaction with APTES.

Zeta potentials of these zeolites were gathered as a function of pH to verify the presence of the amine groups on the zeolite surface. The measured values have been plotted in Figure 4-4. The untreated zeolites exhibit the same negative zeta potentials across the pH range. The isoelectric point (IEP) of the untreated zeolites was not within the range of pH values tested (i.e. 4 - 10). However, because the surface of the untreated zeolites is chemically similar to quartz with an IEP of 2.0, it is expected that the untreated zeolite L IEP should be near this value.

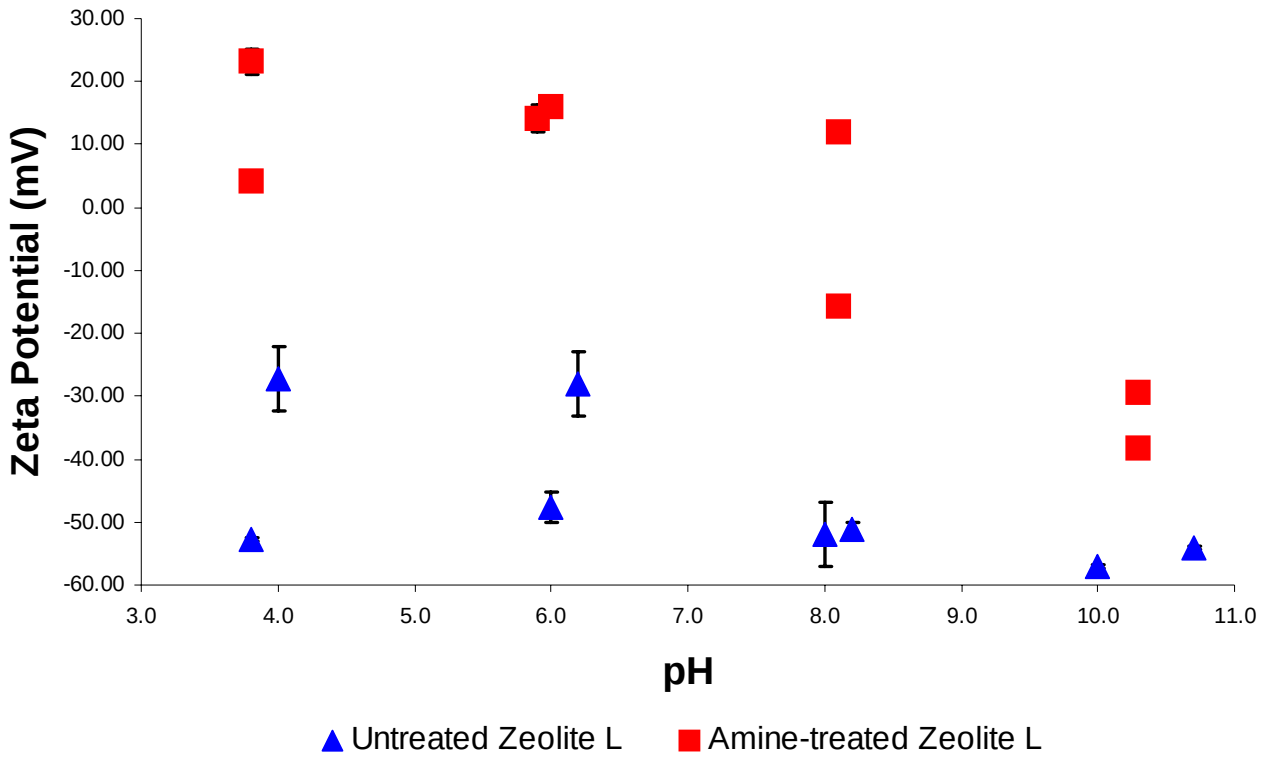

Figure 4-4. Zeta Potentials of untreated zeolite L and amine-functionalized zeolite L at varying pHs.

The amine-functionalized zeolites also display a negative zeta potential at higher pH values (i.e. 10), but deviate from the untreated zeolite values as the pH drops. The negative value at pH of 10 indicates that there were some unreacted –OH groups on the zeolite surface after the reaction. These groups lose a proton in the basic solution, leading to the negative zeta potential. As the pH drops the $–NH_2$ groups gain a proton to become $–NH_3^+$ and the zeta potential becomes positive. The functionalized zeolites appeared to reach their (IEP) between a pH of 8 and 9.

XPS was used to provide further evidence of the presence of amine groups on the surfaces of the zeolites. Samples of untreated and amine-functionalized zeolites were examined to determine their individual atomic concentrations. As a control to account

for contamination, quartz was analyzed using the same procedure. The XPS scans for the three samples are shown in Figure 4-5.

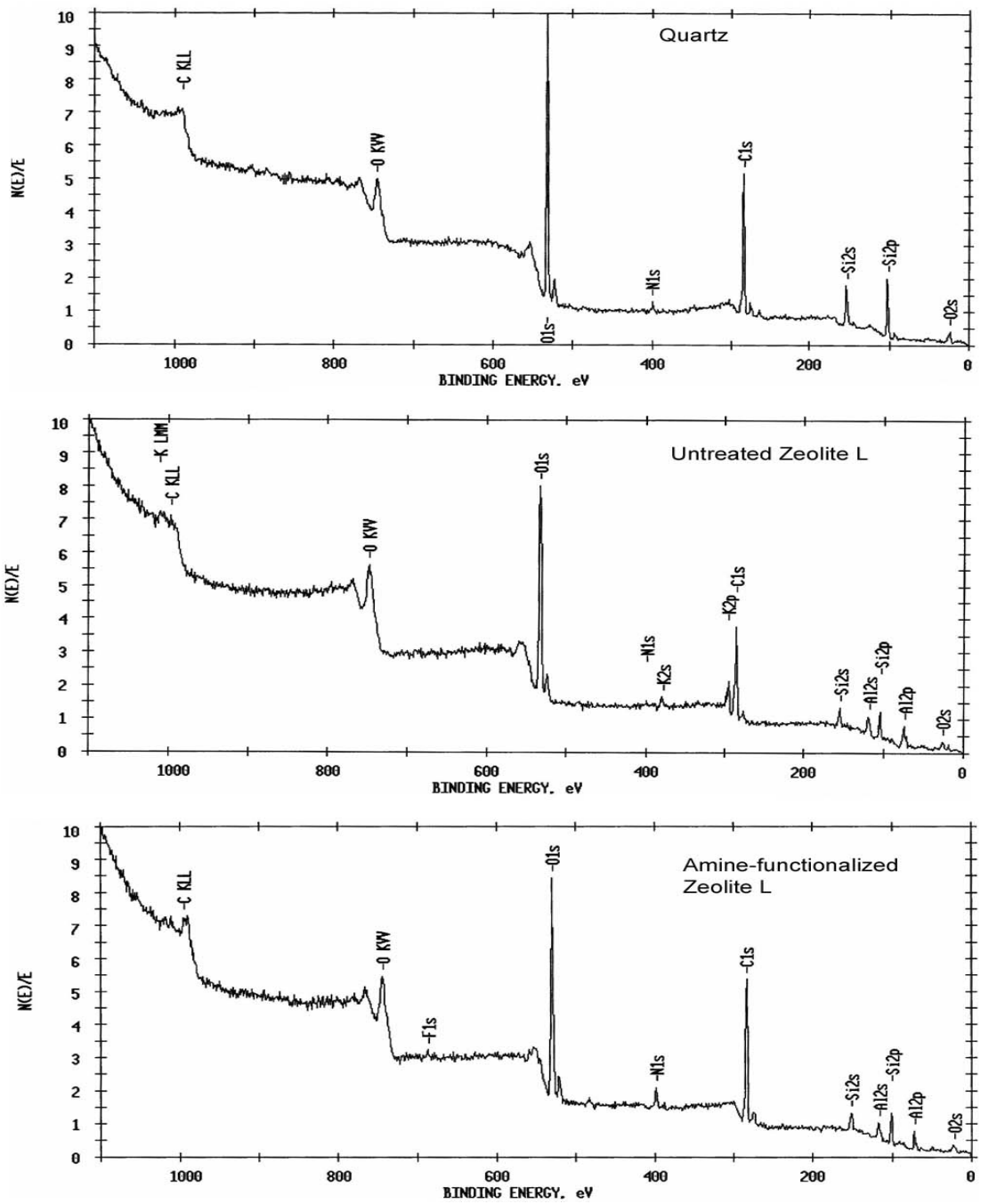

Figure 4-5. XPS scans of the samples taken at a 45^{o} take-off angle. The three XPS scans include quartz (top) which was used as a control, untreated zeolite L (middle), and amine-functionalized zeolite L (bottom).

The atomic concentrations for each of the three sample are shown in Table 4-1. The atomic percents were obtained from the peak areas of the XPS scans, and were gathered using a 45^{o} take-off angle.

Table 4-1. Atomic concentrations of quartz, untreated zeolite L, and amine-functionalized zeolite L determined via XPS.

Atomic Concentration (%)

Sample	C_{1s}	O_{1s}	N_{1s}	Si_{2p}	K_{2p}
Quartz	41.99	37.98	1.63	18.39	0
Untreated zeolite L	41.70	45.46	0.99	8.74	3.11
Amine-functionalized zeolite L	52.79	34.67	4.49	8.05	0

This data clearly verifies the presence of amine groups on the zeolite surface.

4.4.4 FTIR Spectroscopy Results

Transmission FTIR spectra were collected in order to investigate molecular interactions between the polymer and the amine-functionalized zeolites. Samples containing 20 wt % zeolite and 80 wt % polyimide were cast from THF onto CaF_2 plates and dried under vacuum at room temperature. Two samples were prepared, one containing untreated zeolite L and polyimide, and the other containing amine-functionalized zeolite L and polyimide.

Figure 4-6 shows the spectra of the two samples in the 3600 – 3000 cm^{-1} region. Both spectra show the free –OH peak of the –COOH group of the polymer at 3494 cm^{-1}. The untreated zeolite-polyimide mixture has a large increase in absorbance between 3475 – 3200 cm^{-1} peaking at 3330 cm^{-1}. These regions contain the Si-OH bands and the hydrogen bonded –OH groups from the polymer's carboxylic group. This same region in

the amine-functionalized zeolite L-polyimide spectrum peaks at 3240 cm^{-1}. Although this regions consist of several overlapping bands (i.e. –OH, Si-OH, N-H), qualitatively, the shift in the maximum intensity to lower wavenumbers indicates that there was hydrogen bonding present with the addition of amine groups into the system. The polyimide-amine-functionalized zeolite L spectrum also appears to have lower absorbance in the Si-OH region as a result of the functionalization reaction Figure 4-3 in which Si-OH groups react with the APTES to form Si-O-C linkages.

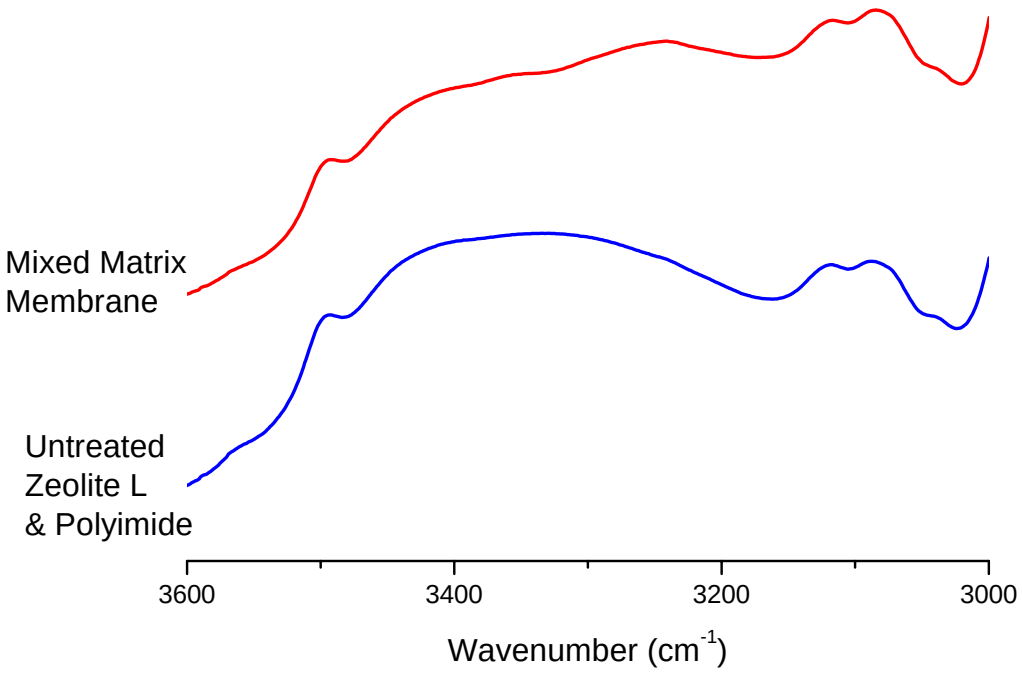

Figure 4-6. FTIR spectra of a untreated zeolite L-polyimide mixture and an amine-functionalized zeolite L MMM.

The part of the IR spectrum between 1800 and 1500 cm^{-1} is the best area to investigate for the presence of amide bands, because the strongly IR-active C=O groups

appear in this region. Figure 4-7 shows the spectra of a 20 wt % amine-functionalized zeolite L MMM in the lower frequency range.

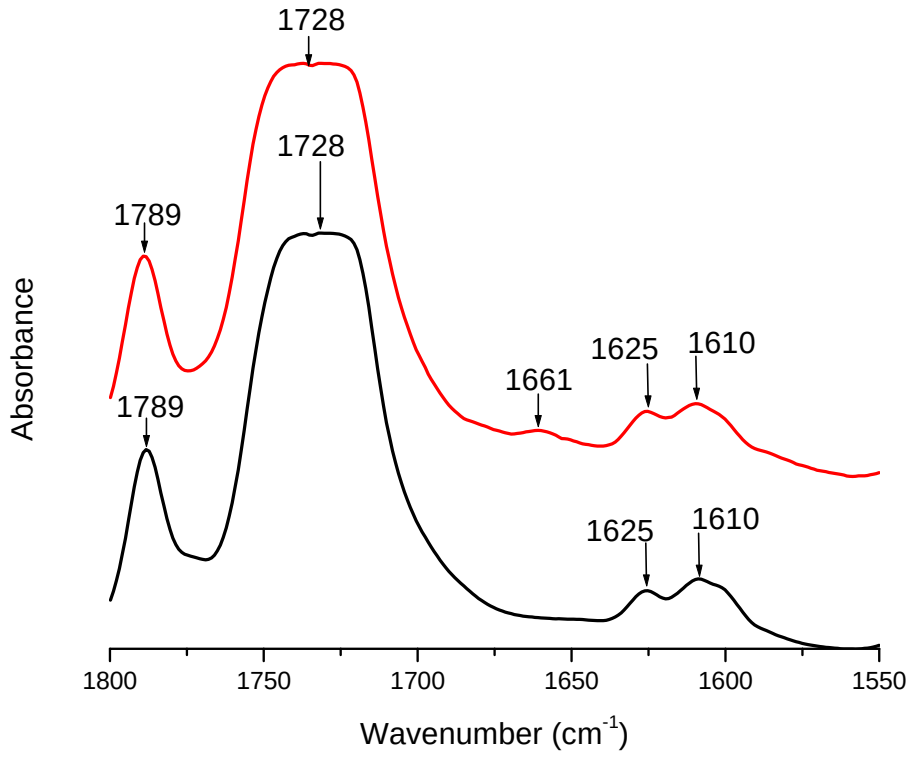

Figure 4-7. IR spectra for a 20 wt % zeolite L mixed matrix membrane before (bottom) and after (top) the annealing steps. The presence of a new band at 1661 cm-1 suggests the formation of amide linkages between the zeolite and the polyimide.

The bottom spectrum was taken from the sample before the annealing process, and the top spectrum was taken from the same sample after the annealing process. Both spectra show the 1789 cm^{-1} peak corresponding to the anhydride ends of the polyimide. The broad peak near 1728 cm^{-1} in both spectra was assigned to the carbonyl peak. The post annealed sample shows a peak at 1661 cm^{-1} that was not present in the pre annealed sample. This peak may be attributed to the C=O groups of the secondary amide linkages

created during the annealing procedure as show in Figure 4-8. Spectra of both the pure polyimide and the non-modified zeolite L - polyimide mixture were taken before and after annealing for comparison. None of the spectra possessed a peak near 1661 cm^{-1}. Furthermore, the pre and post annealing spectra of both samples were very similar suggesting that the amine functionalized zeolite was necessary for the production of the band observed in the MMM spectrum.

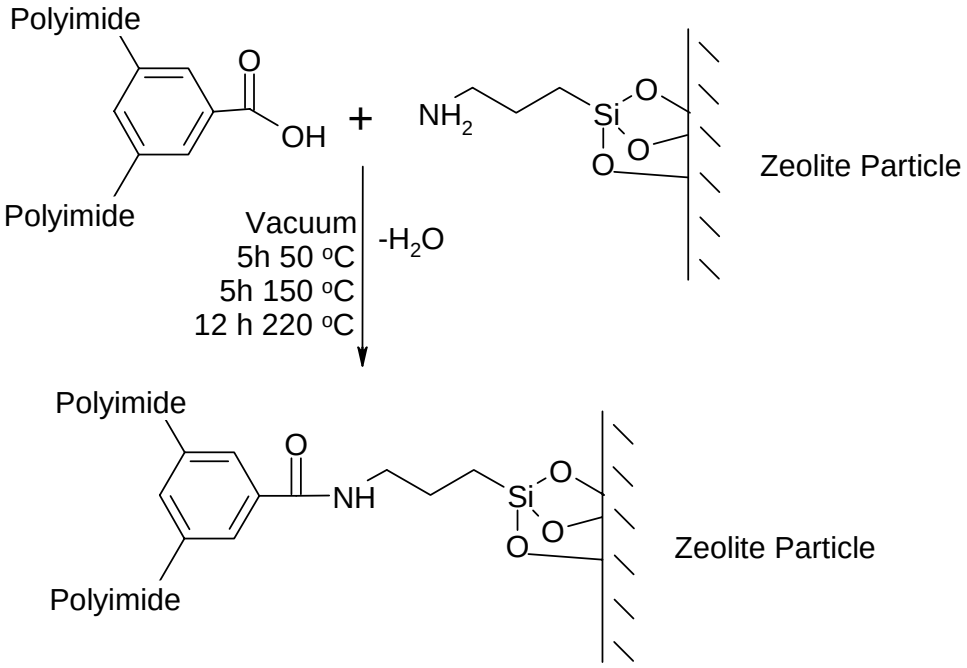

Figure 4-8. Reaction between the polyimide's carboxylic acid and the zeolite's amine group during the annealing procedure.

4.4.5 Microscopy Results

FESEM images were taken of the interior and the surface of the MMMs. Cross sectional images revealed the zeolites were well distributed throughout the membrane with a few areas of agglomeration Figure 4-9. These small regions of agglomeration were removed when the membrane was cast from a less viscous solution. However, the

resulting membranes possessed a zeolite rich region and a polymeric rich region as seen before by others.[5,11] The two phased MMMs suffered from poor mechanical properties and curling whereas the MMMs cast from a viscous solution did not encounter these difficulties.

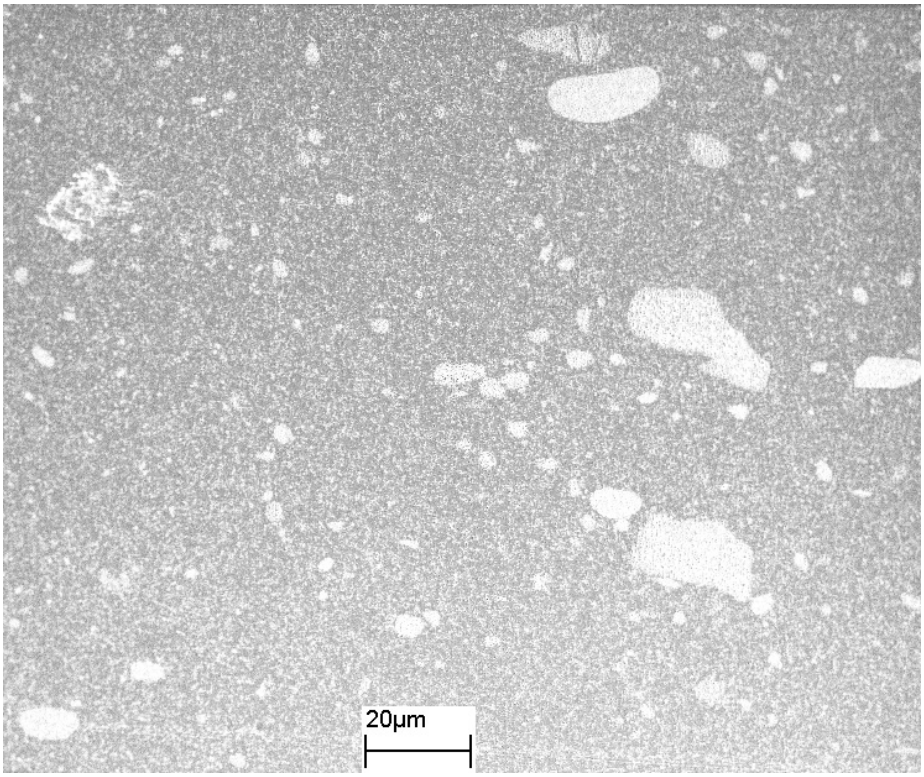

Figure 4-9. Cross-sectional FESEM image of a 20 wt % amine-functionalized zeolite L MMM.

Higher magnification images were taken in order to verify the presence or lack of unselective voids between the two components. A high powered image is shown in Figure 4-10. At this level of magnification, there is no visible evidence of the polymer dewetting from the zeolite.

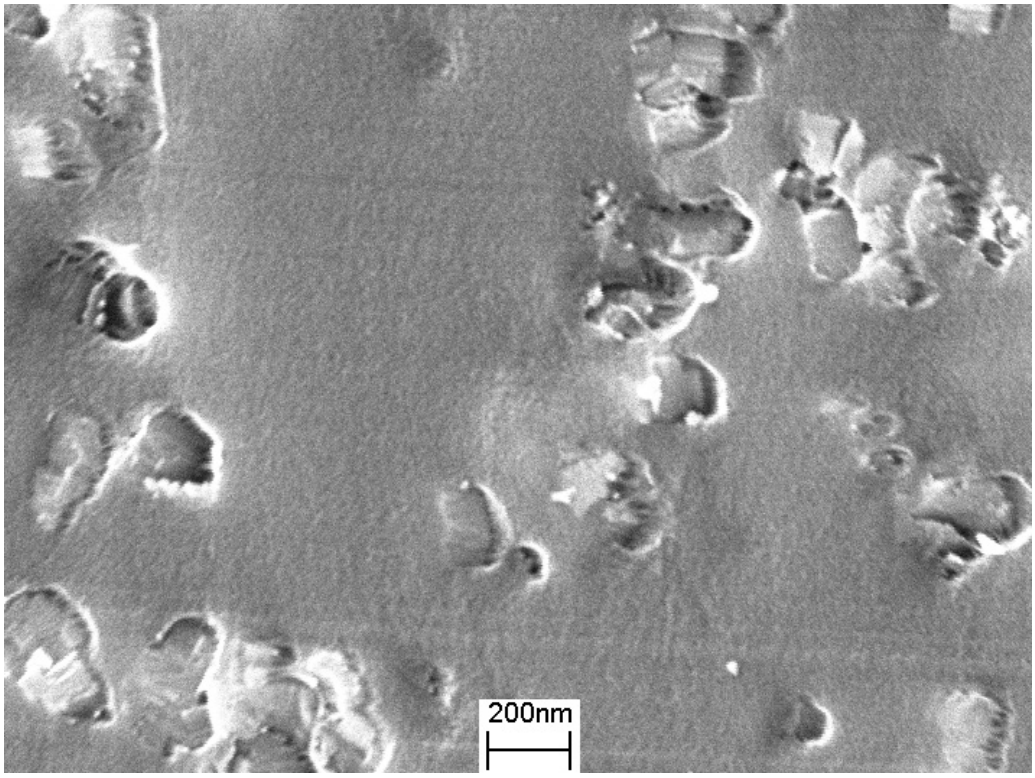

Figure 4-10. High powered FESEM cross-sectional image of a 20 wt % amine-functionalized zeolite L MMM.

Surface images of the same MMM showed that the zeolite was not agglomerated, rather more evenly distributed along the surface of the polymer Figure 4-11. When the untreated zeolites were blended with the polyimide, the resulting MMM contained agglomerated sections of zeolite which were easily visible to the human eye.

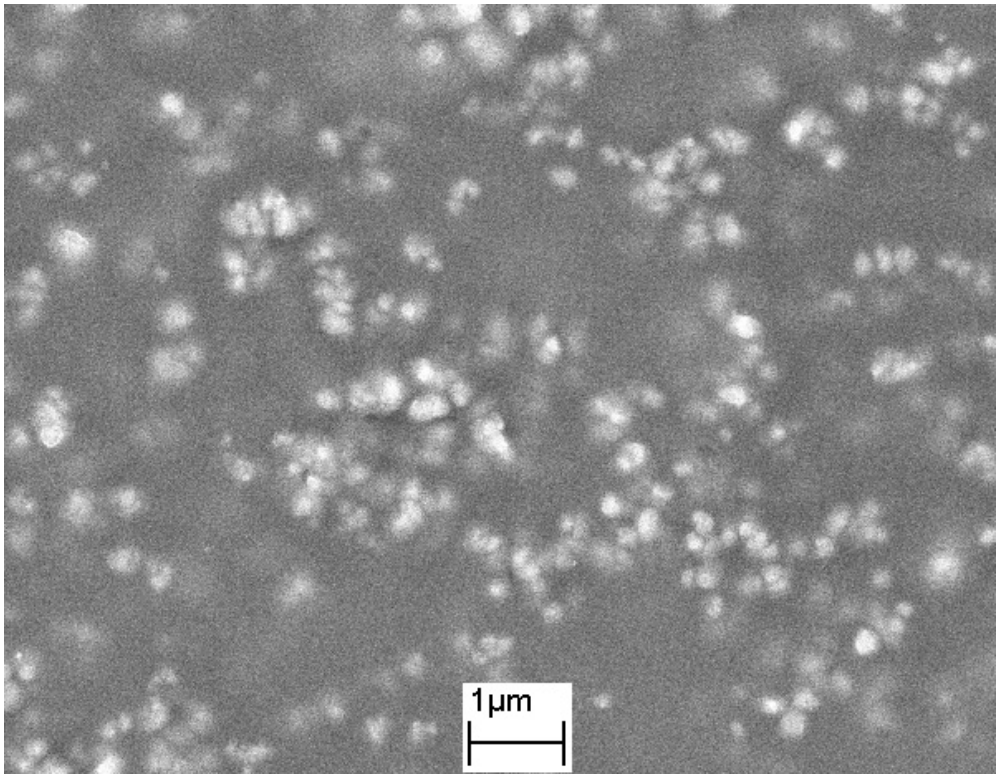

Figure 4-11. FESEM surface image of a 20 wt % amine-functionalized zeolite L MMM.

When using amine-functionalized zeolite, there was no evidence of voids between the polyimide and zeolite at higher levels of magnification as seen in Figure 4-12. This suggested that covalent linkages between the polymer and zeolite were successful in promoting adhesion between the two components.

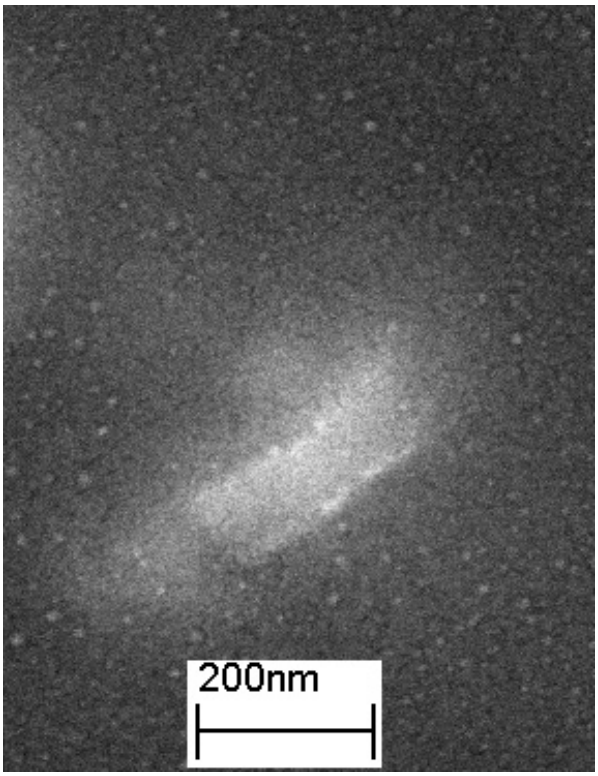

Figure 4-12. High powered FESEM surface image of a 20 wt % amine-functionalized zeolite L MMM.

4.4.6 Permeation Data

The permeation properties for the pure polyimide and a 20 wt % amine-functionalized MMM have been listed in Table 4-2. The polyimide membrane had a thickness of 86 micrometers and the MMMs thickness ranged from 110 to 130 micrometers.

Table 4-2. Pure gas permeabilities of the pure polyimide and the 20 wt % zeolite L MMM. The gases are listed in order of increasing kinetic diameter.

Pure Gas Permeability (Barrer)					
Wt % Zeolite L	**He**	**CO_2**	**O_2**	**N_2**	**CH_4**
0	99.77 ± 3.43	21.21 ± 0.14	8.88 ± 0.12	1.83 ± 0.01	0.55 ± 0.05
20	97.64 ± 13.0	20.12 ± 0.02	10.07 ± 1.39	2.26 ± 0.35	0.72 ± 0.05

The average helium permeability through the MMM decreased by less than 2% compared to the pure polyimide membrane. In addition the standard deviations overlapped for these two membranes. This was strong evidence that no voids were present between the polymer and zeolite. The presence of voids would have resulted in a large increase in the permeability of He. The nearly identical helium permeability values between the two types of membranes maybe surprising considering one system contains filler with pore sizes roughly twice the size of a helium atom. A possible explanation could be that the permeability within the pure polyimide membrane is already very high, and as a result, helium may not readily distinguish between the two phases when zeolite is introduced into the system.

Carbon dioxide showed little change between the two systems. The addition of zeolite resulted in a loss of permeability near 5%. This was surprising, as CO_2 was expected to see a boost in permeability with the addition of zeolite due to its ability to interact with the pore walls of the zeolite. This would provide it with two modes for transport: Knudsen diffusion (which is available to all of the gases), and surface diffusion. While the addition of zeolite did not enhance the permeability, it does not appear to have inhibited either. Further permeation experiments were performed on CO_2 as discussed below to provide insight into its behavior.

Oxygen permeability and nitrogen permeability both rose 13% and 23%, respectively, through the MMM when compared to the pure polyimide membrane. An increase in permeation was also observed for methane (i.e. 31%). Not knowing the pure gas permeabilities in zeolite L makes analysis difficult. However, using models adopted

by Zimmerman et al to predict the performance of MMMs, a qualitative analysis can be made. Zimmerman et al used Maxwell's model to simulate the performances of MMMs. Maxwell's model is shown below:

$$P_{eff} = \frac{P_1 P_2}{\phi_1 P_2 + \phi_2 P_1} \qquad \text{Eq 4.1}$$

in this equation P_{eff} is the permeability through the MMM, P_1 is the permeability of a gas through the pure polymer, P_2 is the permeability of the same gas through the zeolite, and φ is the corresponding volume fractions of those components. Through discussions with Dr. Tsapatsis, it is expected that the permeability of O_2, N_2 and CH_4 in the zeolite will be much higher than that of the polymer. If it is assumed that $P_2 >> P_1$, then Eq 4.1 reduces to:

$$P_{eff} = \frac{P_1}{\phi_1} \qquad \text{Eq 4.2}$$

As φ_1 will be less than 1, P_{eff} must be greater than that of the pure polyimide. In this case, the results of the 20 wt % zeolite L MMM are consistent with the predictions using Maxwell's model.

Methane and carbon dioxide permeabilities through the MMM and pure polymer membrane were recorded at several feed pressures (i.e. 4, 8, and 12 atm). These gases were chosen to study the differences in permeation behavior between a nonpolar gas (CH_4) and a polar gas (CO_2). The results have been listed in Table 4-3.

Table 4-3. Elevated feed pressure permeabilities for CO2 and CH4 for the pure polyimide and the 20 wt % zeolite L MMM.

Elevated Pressure Pure Gas Permeabilities (Barrer)

Wt % Zeolite L	4 atm		8 atm		12 atm	
	CO_2	CH_4	CO_2	CH_4	CO_2	CH_4
0	21.21 ± 0.14	0.55 ± 0.05	20.40 ± 0.03	0.53 ± 0.02	19.04 ± 0.07	0.52 ± 0.02
20	20.12 ± 0.81	0.72 ± 0.02	19.61 ± 0.33	0.59 ± 0.03	18.32 ± 0.20	0.26 ± 0.01

Carbon dioxide's permeability through the MMM began at 20.1 barrer at 4 atm, and continued to drop with each increase in feed pressure, until at 12 atm the permeability was 18.3 barrer. This decline in permeability was mirrored in the pure polyimide, and the two values were roughly within 5% of each other at each pressure level. This indicates that the CO_2 did not encounter significant transport resistance with the addition of zeolite L. This was expected, but surprisingly CO_2 permeability was not enhanced by the addition of zeolite L.

Despite the lack of enhancement, the behavior of the MMM under pure gas feeds showed promise. The MMM CH_4 permeability experienced a larger percent drop with increasing feed pressure when compared to the pure polyimide leading to an increase in ideal selectivity for the MMM. The highest methane permeability through the MMM was 0.72 barrers at 4 atm. The permeability then dropped with each increase in feed pressure. At 12 atm it had decreased to half of its value at 4 atm. One possible explanation is that the sorption capacity of methane in zeolite L is much less than that of CO_2. This difference would become more pronounced at higher pressures, and could lead to the differences in permeability behavior with pressure that were observed.

To provide an idea of how the membranes developed in this study compare against membranes developed by others, the data for the CO_2/CH_4 separation was plotted on a Robeson diagram. The diagram is shown in Figure 4-13.

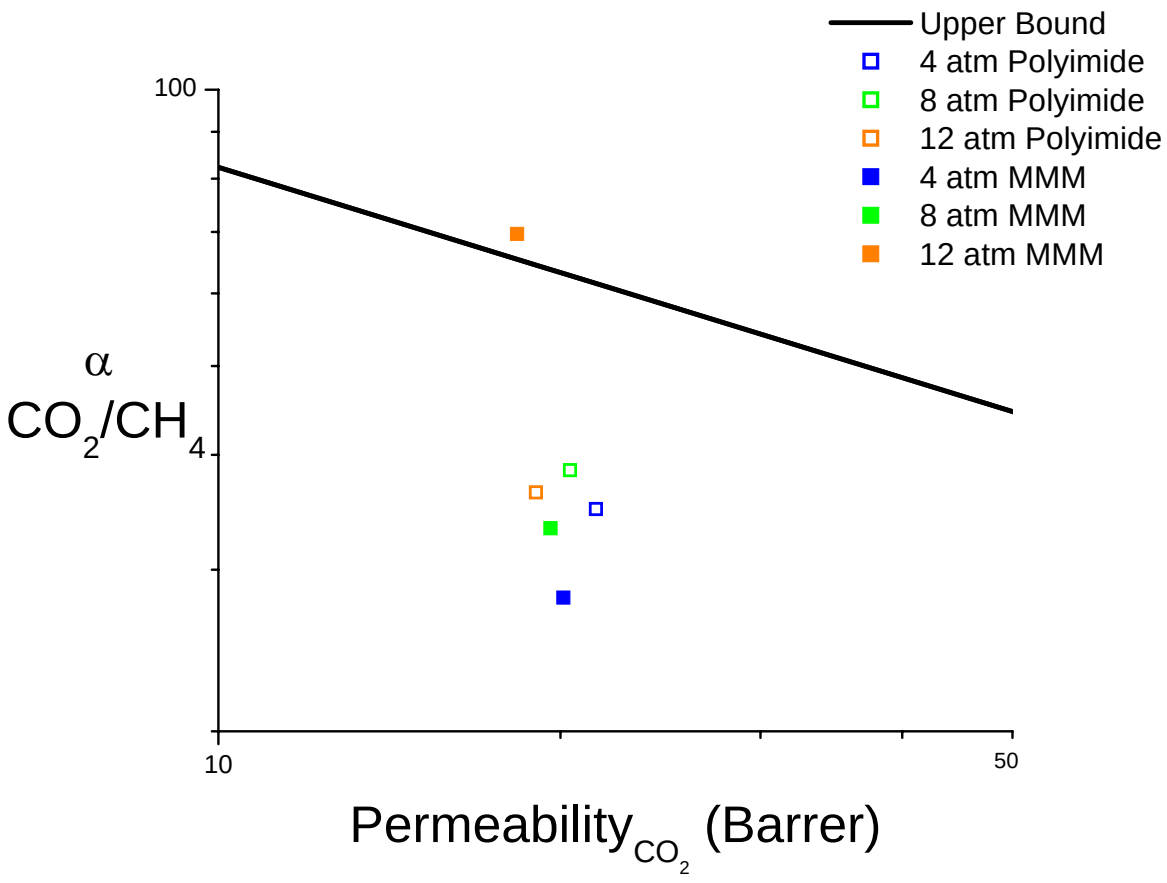

Figure 4-13. Trade-off diagram for the CO_2 / CH_4 separation.

The trade-off diagram illustrates some encouraging results. The MMMs showed a trend of small losses in permeability and larger increases in selectivity as the feed pressure was increased. At 12 atm it even broke the upper bound. The pure polyimide showed drops in permeability with increasing feed pressure, while the selectivity showed mixed results. Despite these good results, one must keep in mind that the selectivities were determined by ratioing the pure gas permeabilities, and the true selectivities of these membranes are likely different from this. It would be interesting to know the true selectivities of the MMMs to accurately determine if these membranes truly operate above the upper bound. Furthermore, if the selectivities were extrodinarly high, one

might suspect they broke the asymptotic limit of the upper bound proposed by Freemen, however, because Freemen's work for purely polymeric systems only, it can not be applied to these MMMs.[26]

The separation ability of these MMMs for mixed gas feeds is expected to be greater than what was determined using pure gas feeds, due to the selective adsorption of zeolite L. Using a mixed gas feed would let the zeolite discriminate between the species, effectively acting as a barrier to one component while allowing another to diffuse through it. This selective adsorption process of some zeolites has been shown in previous work.[27] Furthermore, the optimal permeability values of this MMM may differ from what was presented here. Zeolite L possesses a one dimensional channel. There is no method available to orient the zeolites such that their pores lie parallel to the direction of diffusion in MMMs, and thus provide the maximum increase in permeability. The enhancement in permeability offered by these zeolites may not be realized when a portion of the pores are pointed perpendicular or nearly perpendicular to the direction of diffusion. Using a zeolite with a three dimensional pore structure may overcome this limitation.

4.5 Conclusions

Mixed matrix membranes composed of 6FDA-6FpDA-DABA and amine-functionalized zeolite L were fabricated without defects. Delamination of the polymer from the zeolite was not present, and was believed to be prevented by incorporating carboxylic acid groups into the backbone of the polyimide that hydrogen bonded with the amine groups of the zeolites. FTIR spectra of the mixed matrix membrane confirmed the presence of amide linkages after the membranes were heat treated. FESEM images of the surface and the cross-section showed good contact between the two components. Furthermore, the lack of an increase in permeability of helium through the MMM as compared to the pure polyimide membrane suggested that there were no voids at the polymer-zeolite interface. Oxygen, nitrogen and methane permeabilities through the MMM increased, while those of He and CO_2 decreased. The permeabilities of CH_4 and

CO_2 were measured at 4, 8, and 12 atm. For both gases the permeability dropped with increasing pressure, though the drop was much more significant for CH_4.

The results discussed here indicate that an expanded study needs to be performed on these membranes. Using a mixed gas feed would reveal the MMMs true ability to separate gases. Zeolite L selectively adsorbs some components over others, and a mixed gas feed must be present to take advantage of this preference. Sorption studies of pure gases with zeolite L would also offer some insight into understanding this behavior.

4.6 References

1 Robeson, L. M. *Journal of Membranes Science* 1991, *61*, 165-185.

2 Koros, W. J.; Mahajan, R. *Journal of Membranes Science* 2000, *175*, 181-196.

3 Koros, W. J.; Mahajan, R. *Industrial Engineering and Chemistry Research* 2000, *39*, 2692-2696.

4 Koros, W. J.; Zimmerman, C. M.; Singh, A. *Journal of Membranes Science* 1997, *137*, 145-154.

5 Duval, J.-M.; Folkers, B.; Mulder, M. H. V.; Desgrandchamps, G.; Smolders, C. A. *Journal of Membrane Science* 1993, *80*, 189-198.

6 Gur, T. M. *Journal of Membranes Science* 1994, *93*, 283-239.

7 Suer, M. G.; Bac, N.; Yilmaz, L. *Journal of Membranes Science* 1994, *91*, 77.

8 Park, H. C.; Yong, H. H.; Kang, Y. S.; Won, J.; Kim, W. N. *Journal of Membranes Science* 2001, *188*, 151-163.

9 Koros, W. J.; Mahajan, R.; Burns, R.; Schaeffer, M. *Journal of Applied Polymer Science* 2002, *86*, 881-890.

10 Koros, W. J.; Mahajan, R. *Polymer Engineering and Science* 2002, *42*, 1420-1431.

11 Pechar, T.; Marand, E.; Davis, R.; Tsapatsis, M. *Desalination* 2002, *146*, 3-9.

12 Mahajan, R.; Koros, W. J. *Industrial Engineering and Chemical Research* 2000, *39*, 2692-2696.

13 Mahajan, R. B., R.; Schaeffer, M.; Koros, W.J. *Journal of Applied Polymer Science* 2001, *86*, 881-890.

14 Mahajan, R. K., W.J.; Polymer Engineering and Science, 2002.

15 Mahajan, R. K., W.J.; Zeolite-Function-Koros.jpg, Ed.; Polymer Engineering and Science, 2002.

16 Tantekin-Ersolmaz, S. B.; Atalay-Oral, C.; Tather, M.; Erdem-Senatalar, A.; Schoeman, B.; Sterte, J. *Journal of Membrane Science* 2000, *175*, 285-288.

17 Tsapatsis, M.; Lovallo, M.; Okubo, T.; Davis, M.; Sadakata, M. *Chem. Mater.* 1995, *7*, 1734-1741.

18 Crank, J. *The Mathematics of Diffusion*, 2 ed.; Oxford Press: London, 1990.

19 Husk, G.; Cassidy, P.; Gebert, K. *Macromolecules* 1988, *21*, 1234-1238.

20 Bessonov, M.; Koton, M.; Kudryavtsev, V. V.; Laius, L. *Polyimides: Thermally Stable Polymers*; Pleneum Publishing Corp: New York, 1987.

21 Cornelius, C. J. In *Chemical Engineering*; Virginia Tech: Blacksburgh, 2000.

22 Tsapatsis, M.; Lovallo, M.; Davis, M. *Microporous Materials* 1996, *5*, 381-388.

23 Bekkum, H. V.; Flanigen, E.; Jansen, J. C. *Introduction to Zeolite Science & Practice*; Elsevier: New York, 1991.

24 Ruthven, D. *Chemical Engineering Progress* 1988, 42-50.

25 Choi, S.; Lee, Y.; Yong, P.; Ha, K.; Yoon, K. *Journal of the American Chemical Society* 2000, *122*, 5201-5209.

26 Freeman, B. *Macromolecules* 1999, *32*, 375-380.

27 Nikolakis, V.; Xomeritakis, G.; Abibi, A.; Dickson, M.; Tsapatsis, M.; Vlachos, D. *Journal of Membrane Science* 2001, *184*, 209-219.

Chapter 5 Preparation and Characterization of a Poly(imide siloxane) and Unmodified Zeolite L Mixed Matrix Membrane

5.1 Abstract

A glassy polyimide, 6FDA-6FpDA, and block copolymers composed of 6FDA-6FpDA and amine-terminated polydimethylsiloxane were synthesized at varying weight-percents of PDMS using a bulk imidization technique. Qualitative confirmation of imidization was performed via FTIR, and the weight-percent PDMS of each copolymer was determined using ^{1}H-NMR. Polymeric membranes and mixed matrix membranes composed of copolymer and zeolite L were prepared by solution casting using the procedure outlined in this chapter. Zeolite L was chosen because it is synthesized without the aid of an organic template which could reside in its pores after the synthesis and clog them. This procedure lead to defect-free mixed matrix membranes suitable for gas separations. Pure gas permeability tests were performed using He, O_2, N_2, CH_4 and CO_2 for each membrane. Permeability trends were noted for changes in siloxane loading, and changes in zeolite loading. SEM, TEM, SAXS, and AFM were employed to characterize the morphology of the membranes as well as verify the presence of phase separation.

5.2 Introduction

Efforts to improve the separation performance of polymeric membranes have been shown a trade-off between permeability and selectivity, which was best illustrated

in 1991 by Robeson.[1] In his work Robeson was able to define an upper bound in polymeric membrane performance for several gas separations, which has very seldom been surpassed since its inception. These trade-off curves became the standard for comparing performance among different membranes, but due to their empirical development, no theoretical justification was given for them.

Later work by Freeman provided a theoretical basis for Robeson's curves.[2] Freemen combined the equations describing the upper bound developed by Robeson with the activation energy model of Brandt[3]. This allowed him to develop a new equation describing the location of the upper bound for particular gas pairs. The upper bound equation was a function of the diffusion coefficient of the most permeable component, the solubility selectivity, other properties of the polymer (e.g. backbone stiffness, and packing), and the size ratio of the gas molecules being separated. From this equation it was noted that the slope of the upper bound is strictly a function of the penetrant size ratio, and the polymer's structure has no influence upon it. The polymer structure will dictate the absolute location of the curve on the Robeson's plot. Furthermore, it was shown that the polymers with high solubility selectivity, high backbone stiffness, and increasing interchain spacing should offer the best separation performance. However, Freeman noted that solubility selectivity varies very little among polymers. Additionally, he noted that increasing the interchain spacing could lead to deleterious effects. If the spacing became too large, the penetrant diffusion coefficients would no longer be governed by thermally stimulated polymer segmental motions leading to a selectivity loss. Ultimately, Freeman remarked that unless significant enhancements in solubility selectivity could be achieved, there is an asymptotic limit to the performance of purely polymeric membranes.

Due to the anticipated limits on polymeric membrane performance, many research efforts have been focused on developing membranes with selective inorganic fillers. One such system is a mixed matrix membrane (MMM) which incorporates a polymer with inorganic zeolites. The intent of this type of membrane is to incorporate the low cost and good processability of the polymer with the excellent separation performance of the zeolite. It is believed that these types of membranes can still offer the low initial

investment cost of polymeric membranes while providing better permeability and selectivity.

Mixed matrix membranes were first developed using rubbery polymers and zeolites with the goal of improving membranes for pervaporation applications. Te Hennepe et al., mixed polydimethylsiloxane (PDMS) with silicalite-1 leading to an improved separation of ethanol from water.[4] The separation factor increased almost six fold, and the permeation rates doubled as the zeolite loading approached 70%. Jia et al., studied the same system, but for gas separation performance.[5] Their membranes showed increased permeability for He, H_2, O_2 and CO_2, while the permeabilities of N_2, CH_4, n-butane, iso-butane, and 1-butene decreased. Furthermore, the PDMS-Silicalite-1 membranes offered better O_2/N_2 selectivity than any organic membrane at the time of the publication. The authors claimed that the silicalite-1 only allowed molecules of a specific dimension or smaller to pass through. Because their membranes were up to 70% in weight zeolite (i.e. over 50% by volume zeolite), molecules too large to enter the silicalite-1 were essentially limited to diffusion through a membrane with less than half of its volume being permeable to the gas.

Later work by these authors aimed at determining ideal fabrication methods for PDMS-silicalite membranes.[6] Common problems encountered when making MMMs were the precipitation of the zeolite from solution (zeolites are not soluble in any organic solvent), and the agglomeration of zeolites in the solution leading to pin hole defects in the final membrane. Furthermore, MMMs in which the zeolites were not thoroughly dispersed did not show improvements relative to the pure polymer membrane. To overcome these problems, the authors fabricated PDMS-silicalite membranes from a suspension of ultra-fine silicalite crystals (i.e. 0.2 – 0.5 μm) and partially polymerized PDMS, which increased the viscosity of the suspension preventing the zeolites from precipitating or settling. A series of membranes of varying thicknesses, PDMS to solvent (i.e. iso-octane) ratio, and silicalite to PDMS ratio were made to find the optimum parameters. MMMs of 3.5-4.0 PDMS to solvent ratio and silicalite to PDMS ratios of 1.5-3.3 delivered the highest selectivity reproducibly of the combinations.

With rubbery MMMs showing promise in the gas separation field Duval et al., broadened the scope of research by investigating the effects of different zeolites on the

performance of rubbery MMMs.[7] Using silicalite-1 (S1), zeolite 13X (13X), zeolite KY (KY), and zeolite 5A (5A) four variables of zeolites were considered: pore size, direction of pores (1-d, 2-d, or 3-d), Si/Al ratio, which controls hydrophilicity and adsorption, and the type of cation (its size and valence). Their results indicate that the permeability and selectivity of a component can be enhanced in a membrane if the added zeolite possesses a large sorption capacity for that component. These effects were seen for the CO_2/CH_4 separation for S1, KY, and 13X in ethylene-propylene rubber (EPDM), and the effects were more pronounced until an optimum loading was reached, typically between 45 and 55 percent. The greatest enhancement of performance came from the incorporation of 13X whose pores are about twice the size of CO_2 and CH_4. The 13X-EPDM MMM offered better permeability and selectivity for all loadings relative to its S1 counterpart, despite S1 having a smaller pore size than 13X. The authors believe this indicated that size exclusion is not the only mechanism involved in separating gases, rather the affinity of the gas for the zeolite greatly influenced the MMMs properties.

Tantekin-Ersolmaz et al, investigated the relation between particle size and MMM performance for silicalite-PDMS systems.[8] Silicalite sizes were varied from 0.1 μm up to 8 μm, and the resulting MMMs were tested for O_2, N_2 and CO_2 permeability. The data indicated that as the particle size of the zeolite increased, the permeability of the membrane correspondingly increased, while the ideal selectivities remained unchanged. Furthermore, at the same loading differences in permeability were observed between MMMs with well dispersed zeolites and MMMs with agglomerated zeolites; the latter showing a higher permeability. The authors believed this phenomenon could be explained by considering the resistance at the zeolite-polymer interface. There were more interfaces and more interfacial area in the well dispersed systems. Due to this the mass transfer resistance became more pronounced. However, they did not account for the variation in fabrication methods necessary to achieve size variation, which could lead to differences in the inherent separation properties of the zeolites.

More systems were investigated by Mahajan et al.[9] Poly(vinyl acetate) (PVAC) and zeolite 4A (4A) were combined into a MMM leading to improved ideal separation values for air, but lower permeability values at a loading of 15% by volume. However, when the loading was increased to 25%, the membranes became defective; the authors

believed this was due to agglomeration of the zeolites. To overcome this, the zeolites were first primed with a polymer coating. This was achieved by dispersing 4A and "a small amount of polymer" into toluene. Toluene was not a good solvent for the polymer forcing it to coil-up thereby reducing its dimensions and allowing more of it to be adsorbed onto the zeolite surfaces. The coated zeolites were mixed with PVAC to make a MMM. At 25% and 40% volume, the MMMs offered roughly the same permeability for the air separation, but almost double the ideal selectivity.

With the improvements in separation performance associated with adding zeolites to rubber polymers, focus began to shift to mixing zeolites with glassy polymers. Initial attempts at fabricating MMM using glassy polymers and zeolites resulted in the presence of voids between the polymer and zeolite, thus reducing the separation performance of the composite membrane relative to the pure polymer.[7,9,10] Duval et al, simply mixed several glassy organic polymers with varying glass transition temperatures (T_g's), and one rubbery inorganic polymer all of which resulted in poor adhesion between the two phases. To overcome these defects, several different silane coupling agents were successfully employed to improve adhesion between the polymer and zeolite, however, the resulting permeabilities were slightly lower, and ideal selectivities were largely unchanged when compared to the pure polymer. The authors also fabricated a Poly(4-methyl-1-pentene) - Z-6032 (30% vol) MMM which was solution cast at a temperature of 60^{o}C, well above its T_g of 36^{o}C. They postulated that this would relieve any stress introduced into the membrane when the solvent evaporates. According to the SEM images of the membrane, the structure of this membrane was improved, but the membranes were still found to be defective from a "separations" perspective.

Other research efforts have been made using silane coupling agents or other means to prevent voids between the polymer-zeolite interface. Mahajan et al mixed poly(vinyl acetate) and zeolite 4A to form MMMs.[9] While they were able to create successful membranes at 15 vol % of zeolite, higher zeolite loadings resulted in defective membranes due to poor polymer-zeolite contact. To overcome these deficiencies at higher loadings the authors proposed priming the zeolites with a thin coating of polymer to aid in phase contact and dispersal. A mixture of toluene, zeolites 4A and PVAC was used for the priming. Toluene was chosen because it provided an environment where the

polymer has a stronger attraction to the zeolites than the solvent, as well as the zeolites possessing a stronger attraction to the polymer than the zeolites. Furthermore, toluene is not a strong solvent for PVAC, leading it to retract its coil size and allowing more polymer to adsorb onto the zeolites surfaces. Based on the amount of polymer and zeolites added and the surface area of the components, the calculated layer thickness was 400Å. This technique allowed the authors to fabricate MMMs with higher zeolite loadings. A trend of lower permeability and higher selectivity with increasing vol % zeolite was observed.

Yong et al developed interfacial void free polyimide mixed matrix membranes by using a low molecular weight chain capable of hydrogen bonding with both the polymer and zeolite.[11] This chain essentially enhanced the contact between the two components. The resulting membranes displayed increased permeability without much change in the selectivity. The authors mixed a commercial polyimide (i.e. Matrimid 5218 CH) (PI), 2,4,6-triaminopyrimidine (TAP) as the low molecular weight chain, and one of many zeolites (i.e. 4A, 5A, 13X, NaY) in dimethylsulfoxide, then cast onto a glass plate and leveled the solution with a casting knife. SEM images revealed that there were no voids between the polymer and zeolites with the inclusion of TAP; voids were present without the presence of TAP. IR spectra taken of the pure PI, the pure TAP, and the mixtures of the two showed the presence of hydrogen bonding between the PI's carbonyl group and the amine groups of TAP. Permeation results indicated that the addition of zeolites to the PI-TAP membrane could alter the permeation rate or selectivity depending on the nature of the zeolites added. When zeolite 4A was added, permeation rates dropped for all gases studied (i.e. He, CO_2, O_2, N_2, CH_4), however the selectivities often improved. The addition of zeolite 13X resulted in much higher permeation rates for the same gases with little, if any, loss in selectivity. Zeolite 13X has a much larger pore size than zeolites 4A (i.e. 7.4Å versus 3.8 Å) allowing a less restricted passage for gas transport through the membrane.

Work by Burns et al. researched adding plasticizers to lower the T_g of Matrimide® and increase its flexibility.[12] Polymeric blends of Matrimide® and plasticizer were cast in low volatility solvents (i.e. 1-methyl-2-pyrrolidinone, 2-pyrrolidinone) with boiling temperatures above the blend's T_g. The blends were composed of 75% weight Matrimid®

and 25 % weight plasticizer, and all displayed a single T_g indicating good compatibility. The polymer blends were mixed with zeolite 4A and cast at a temperature above the T_g of the blend. The resulting MMMs offered higher selectivity but lower permeability than the pure Matrimide-plasticizer membranes.

Mahajan et al. investigated the use of covalent linkages between the polymer and zeolite for the fabrication of a mixed matrix membrane.[13] The authors reacted aminopropylsilane with zeolite 4A to amine-functionalize the zeolite surface. These amine groups were reacted with the Matrimide®'s imide-linkage to covalently attach the two and prevent voids. SEM images showed much better adhesion between the components than when using unmodified zeolite 4A. MMMs fabricated using this procedure offered higher permeability and lower selectivity than the pure polymer. The authors believed that while they might have reduced the size of unselective voids, they had not been entirely eliminated.

Mahajan et al. expanded their research to consider chemical coupling between the polymer and zeolite.[14] Three polymers were chosen based on exhibiting intermediate T_g's and the belief they would have some attractive interaction with Zeolite 4A. These polymers contained carboxylic acid groups in their backbone which were capable of reacting with the zeolite surface to covalently attach the two components. MMMs made using this approach offered slightly improved selectivity, but a very large drop in permeability. The authors believed their approach could be used to make an attractive MMM if they had chosen a more permeable polymer.

In this chapter we present a new fabrication method for MMMs which does not require the aide of coupling agents or chemically linking the polymer to the zeolite. In this method the two components are simply mixed together and solution cast to form a defect-free MMM. This is accomplished by using a block copolymer with PDMS segments in it to provide flexibility and good contact with the zeolite. However, a polyimide block is included to improve the polymer's selectivity relative to pure PDMS, and provide more thermal stability.

5.3 Experimental

5.3.1 Solvents

Tetrahydrofuran (THF)

THF was purchased from E.M. Sciences (99.5%) and was refluxed over sodium (Aldrich) with a nitrogen purge using benzophenone as an indicator until dark purple. It was then distilled immediately before use.

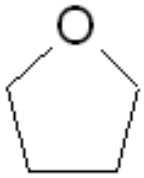

Hexane

Hexane from EMD (98.5%, HPLC grade) was purchased and used as received. It was used to extract unreacted PDMS from the copolymer after imidization.

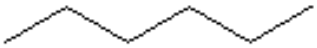

5.3.2 Monomers

4,4'-(Hexafluoroisopropylidene)diphthalic Anhydride (6FDA)

6FDA was purchased from Clariant with a purity >99.95. Prior to use the material was placed under vacuum at a temperature of 150 ^{o}C to ensure compete anhydride cyclization immediately prior to use.

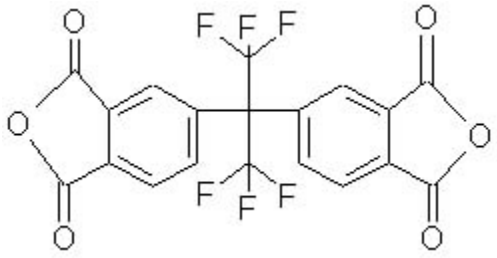

4,4'(Hexafluoroisopropylidene)dianiline (6FpDA)

6FpDA was purchased from SynQuest labs with a purity of >98. The monomer was sublimed near 180 ^{o}C for further purification. After sublimation 6FpDA was kept in a dry box to avoid moisture contact.

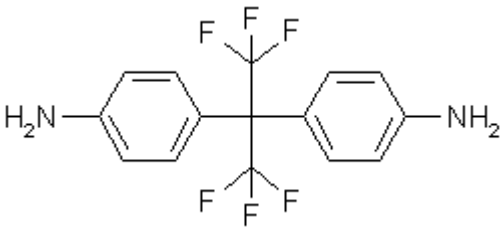

Aminopropyl Terminated Polydimethylsiloxane (PDMS)

PDMS was purchased from Gelest and used as received. Its M_n was determined using ^{1}H-NMR to be 886 g/mol.

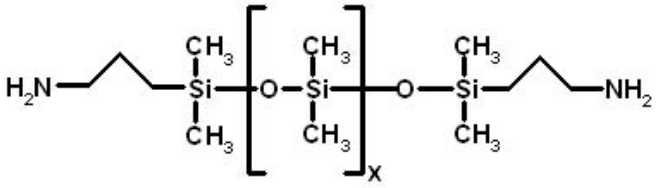

5.3.3 Synthesis of 6FDA-6FpDA

A flame-dried 125 mL 3-neck round bottom flask was used as the reaction vessel for this reaction. The right neck was fitted with a septum and pierced with a needle which was connected to an argon tank. The center neck was connected to a mechanical

stirrer and the left neck was connected to a flow indicator to monitor the flow of gas through the system.

Under Ar flow 6FDA (5.9839 g) was charged into the vessel. To this 40 mL of dry THF was added and the solution was allowed to mix for 3 hours. After this time 6FpDA was added (4.4056 g) and the solution turned a bright yellow. The solution was mixed under Ar flow for 24 hours following this step.

After 24 h, the solution was cast onto a circular Teflon coated pan with a diameter of 8.25" and allowed to dry overnight. The dried solution left a poly(amic acid film). This film was placed under vacuum at a temperature of ~300 ^{o}C for 5 h in order to imidize it.

The resulting polymer was redissolved in THF and filtered using a 5 μm filter. This filtered solution was cast into a 8.25" diameter Teflon coated pan and allowed to evaporate for 24 h. The resulting film was stored in a dessicator until needed.

5.3.4 Synthesis of 6FDA-6FpDA-PDMS Copolymer

Poly(imide siloxane) films were synthesized with targeted PDMS wt %s of 20 and 40. For both cases the steps of the synthesis were identical, and only the masses of reactants differed. The masses for all three reactants and the volume of solvent used in the reaction are listed in Table 5-1.

Table 5-1. Masses of reactants used in the synthesis of the poly(imide siloxane)s.

Targeted wt % PDMS	6FDA (g)	Amine-terminated PDMS (g)	6FpDA (g)	THF (mL)
20	5.2673	2.108	3.1665	35
40	4.287	4	1.7128	35

6FDA was added to a 100 mL three necked round bottom under argon flow. THF was added immediately after. The solution was mechanically stirred (40 rpm) for 2 hours to allow the 6FDA to dissolve and disperse well.

Amine terminated PDMS was added to the solution at an average rate of 0.5406 mL/h at room temperature. This was to ensure that the dianhydride was always in excess and immediately endcapped the PDMS monomer. After the addition of PDMS the solution was allowed to react for 24 hours.

6FpDA was added to the solution, and the solution was mixed for 24 hours. After this time it was cast onto a 8.5" diameter Teflon coated pan. The pan was covered with a glass plate to help slow evaporation. The solution was given 24 hours to dry at room temperature.

Once dry, the film was placed under vacuum and the temperature was raised to its expected T_g for 6 hours. During this time, the polyamic acid thermally imidized to become a polyimide. The film was then allowed to cool to room temperature under vacuum.

Imidized films were dissolved in THF, and cast into a hexane bath for 3 days to remove unreacted PDMS monomer. During this time the hexane was changed daily. After the three days the polymer was allowed to air-dry and placed under vacuum overnight to remove any residual solvent.

The polyimide film was redissolved in THF and filtered using a 5 μm filter. The filtered solution was immediately cast onto a Teflon plate and allowed to dry. The resulting films were mostly clear with a slight yellow tint to them. Following this, it was stored in a dessicator until needed.

5.3.5 Synthesis of Zeolite L

The zeolite L used in this study was synthesized by Dr. Michael Tsapatsis group at the University of Minnesota. The procedure for synthesizing zeolite L has been taken from one of his group's publications.[15]

Aluminum foil (0.05 mm thick, 99.8+%, Aldrich) and fumed silica (Grade M-5, Cabosil) were used to prepare aluminate solutions and silicate solutions, respectively. The alkali-metal ion source was potassium hydroxide (A.C.S. grade, Fisher)

A clear potassium aluminate solution was prepared by the addition of 3.6 g of aluminum foil to 150 mL of 3 M aqueous KOH solution. The solution was filtered to remove the iron impurities of the aluminum foil that remained undissolved.

Fumed silica (80 g) was dissolved in 300 mL of the KOH solution. This solution was stirred and heated at 80 ^{o}C for 12 h. After cooling to room temperature, slow addition of the clear aluminate solution to the clear silicate solution with vigorous stirring resulted in a clear homogenous solution. Subsequent adjustments of the concentrations were performed with the addition of water or aqueous KOH. Preweighed amounts of the synthesis solution were placed in Teflon lined stainless steel vessels, and placed in a rotating oven at 30 rpm and 180 ^{o}C for 8 h. Following this, the aqueous zeolite suspension was poured into centrifuge tubes, and centrifuged several times. After each centrifuge, the solution was replaced with de-ionized water. This was repeated until the pH was neutral, after which the suspension was dried at 110 ^{o}C for 12 h leaving only a zeolite powder. Samples were taken to be analyzed using WAXS for the purpose of verifying the structure of zeolites.

5.3.6 Fabrication of 6FDA-6FpDA and 6FDA-6FpDA-PDMS membranes

The fabrication procedures for the pure 6FDA-6FpDA membrane and the pure 6FDA-6FpDA-PDMS membranes were identical.

1.25 grams of the pure polymer were dissolved in 20 mL of THF and stirred for two days. The volume of solution was evaporated to 10 mL over this time, leading to a viscous solution. The solution was cast into a 2.5” diameter Teflon coated pan. The pan was covered with a glass plate to slow the evaporation of solvent allowing for a film with a uniform thickness without curling. The solutions were given 2 days to dry.

Once dry, the films were placed under vacuum and the temperature was raised to 100 ^{o}C for 12 hours. After this period the films were allowed to cool to room temperature under vacuum over a 6 hour period.

A 2.5" diameter circular sample was cut from the film and used for permeation tests.

5.3.7 Fabrication of 6FDA-6FpDA+20 wt % Zeolite L and 6FDA-6FpDA-*block*-PDMS+20 wt % Zeolite L Mixed Matrix Membranes

The fabrication procedures for the 20 wt % zeolite L-6FDA-6FpDA mixed matrix membranes and the 20 wt % zeolite L-6FDA-6FpDA-*block*-PDMS mixed matrix membranes were identical.

Approximately 1.3 grams of the pure polymer was dissolved into 20 mL of THF and mixed for 24 hours.

Approximately 400 mg of zeolite L were placed into a 20 mL glass vial under vacuum. The temperature of the vacuum oven was raised to 175 ^{o}C for 12 hours to remove any moisture residing in the zeolites' pores. After the 12 hours, the vacuum was flooded with argon and the glass vial was capped. The zeolite was then immediately poured into polymer-THF solution.

The mixture was allowed to mix for 24 hours. During this time the volume of the mixture reduced to roughly 10 mL and became viscous. The mixture was cast into a 2.5" diameter Teflon coated pan and was immediately covered with a glass plate to ensure a slow evaporation of the solvent. A slow evaporation of the solvent would reduce solvent concentrations within the film, and lead to more uniformly thick film without curling. The mixture was allowed to dry over a 2 day period.

After drying the film was placed under vacuum and the temperature was raised to 100 ^{o}C for 12 hours. Following this the film was allowed to cool to room temperature under vacuum over a 6 hour period.

A 2.5" diameter circular sample was cut from the film and used for permeation tests.

5.3.8 Polymer and Membrane Characterization

Fourier Transform Infrared Spectroscopy was used for the purposes of identifying functional groups of the synthesized polymers and studying the interactions between the components of each membrane (e.g. hydrogen bonding). The FTIR used in this study was a BIO-RAD FTS-40A. This model was equipped with a liquid nitrogen cooled MCT detector and was capable of gathering spectra in the 4000 – 400 cm^{-1} region. The FTIR was set with a wave number resolution of 1 cm^{-1} and an aperture of 2 cm. The computer software which ran the FTIR was BIO-RAD WinIR Ver. 3.0.

Transmission spectroscopy was used for gathering the spectra of the samples. Samples were prepared from solutions. A pipette was used to transfer a small repeatable amount of solution to the CaF_2 plate or KBr plate which would dry as a thin film. The films would be allowed to air dry, and then placed in the vacuum oven at room temperature to remove any residual solvent.

CaF_2 plates were used for investigating the region between 4000 and 1100 cm^{-1} and KBr plates were used when investigating the region between 1100 and 400 cm^{-1}. The sample compartment was continually purged with dry air during the time a spectrum was being gathered from it.

Spectral peaks were numbered automatically by the software, and when necessary the software was used to make a baseline to a spectrum. Peaks were assigned to specific groups using two separate books by Alpert and Silverstein.[16,17] Evidence of hydrogen bonding between components was taken as shifts to lower wavenumbers.

Molecular weights were determined using a Waters SEC apparatus equipped with an autosampler, a 410 refractive index detector, and an in-line miniDawn multiangle laser light scattering detector with 690 nm laser. The GPC was operated by Ann Fornoff of Dr. Long's group in the Chemistry Department. Samples were run in THF (ACS grade) at 40 ^{o}C using polystyrene standards. Three samples from each batch of polymer were analyzed to provide a statistical distribution.

400 MHz ^{1}H-NMR was employed for determining the weight percent of PDMS incorporated into the copolymer. A Varian INOVA spectrometer was the model used.

Samples were prepared from 15 -20mg of polymer in 0.7 mL of d6-acetone. The solution was held in a 5 mm diameter and 8" long NMR tube from Ace Glass Inc.

FESEM was used in this research for the purpose of studying the morphology of the materials, to look for delamination of the organics from the inorganics, and to verify if phase separation existed in the block copolymers. The FESEM used in this study was a LEO 1550 which was equipped with two secondary electron detectors, and a five axis (i.e. x, y, z, θ, φ) sample stage.

Samples used to gather surface images were cut from cast films. These samples were mounted onto a sample holder using a conductive double stick tape. Due to polymers being poor conductors, the samples were coated with a 7 nm gold coating using a Crussington 208HR Sputter Coater. Mounted samples were placed into the sputter coater which was pumped down and flushed with argon several times. The samples would then be put under vacuum and the gold coating was applied.

Atomic force microscopy was used for mapping the topology of membrane surfaces as well as determining if any phase separation was present in the block copolymer membranes. The AFM used in this research was a Digital Instruments Dimension 3000. Samples were cut from cast films and applied to mount using double-stick tape. The sample was left underneath a anti-static device for 5 minutes to remove any static charge it may possess.

The AFM was operated in tapping mode using tips purchased from Nanodevices (TAP300) and used as received. The tips had a resonant frequency of 300 kHz and a spring constant of 40 N/m.

TEM was used for gathering high magnification and high resolution images of the bulk of the membranes. Samples were prepared as follows. From cast films, samples approximately 2 x 5 mm were taken and embedded were epoxy embedded. The epoxy was allowed to cure at room temperature. The embedded samples were ultramicrotoned with a diamond knife, and pieces with thicknesses of 50 – 70 nm were captured on a 300 mesh copper grid.

SAXS was utilized to verify the presence of phase separation. A Phillips Model PW1729 was used that operated at 40 kV and 20 mA. A slit collimated (0.03 x 5 mm^2)

Kratky camera with nickel filtered CuKα radiation with a wavelength of 1.542 A was used. The detector was a Braun OED 50 position sensitive platinum wire detector.

Permeabilities of polymeric membranes and composite membranes were measured using a constant volume varying pressure apparatus. Permeability was measured directly, and the Time Lag Method was applied to the recorded data to determine the diffusivity coefficient as outlined in the Literature Review.[18] The solubility coefficient was taken as the ratio of the permeability to diffusivity coefficient. A schematic of the permeation system is shown in Figure 5-1.

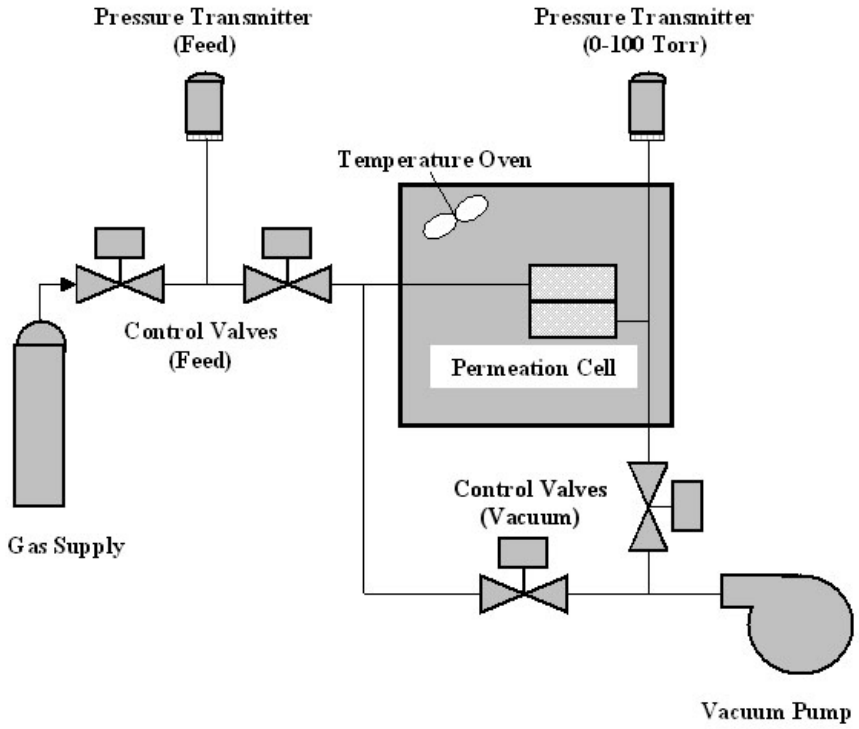

Figure 5-1. Diagram of the permeation system used in this study.

Gas pressures of the permeation setup were monitored using two pressure transducers. The gas feed pressure was measured using a pressure transducer from Omega. The model number was PX621-300G10V, and it had a range of 0 - 300 psig. The permeate pressure was measured using a MKS Instruments pressure transducer (model number 722A12TCE2FA). This pressure transducer had a range of 0 – 100 torr.

The permeation cell was isolated from its surroundings using an insulated box. The temperature within the box was controlled using an Omegalux silicone rubber flexible heater whose output was regulated by an electronic digital. An Omega resistance thermal detector with a resistance of 100 ohms was used to measure the temperature of the cell and feed gas. Air was circulated within the box using a computer fan.

The gases used in this research were He, CO_2, O_2, N_2, and CH_4. Each gas possessed a purity of 99.99% and was used as received from Air Products. The feed pressure was kept constant at 4 atm for all experiments. The temperature was kept constant at 35 ^oC for all experiments in this research. Each gas was run through a membrane six times and the average results and the standard deviations were reported.

Membranes samples were cut into 2.0" diameter circles and placed into a permeation cell. The samples were placed onto a microporous alumina support and sealed within the cell. A picture of the permeation cell is listed in Figure 5-2. The cell was custom manufactured, composed of stainless steel, and fitted with three separate gaskets to prevent leaks. The two sides were connected using six ¼" hex bolts.

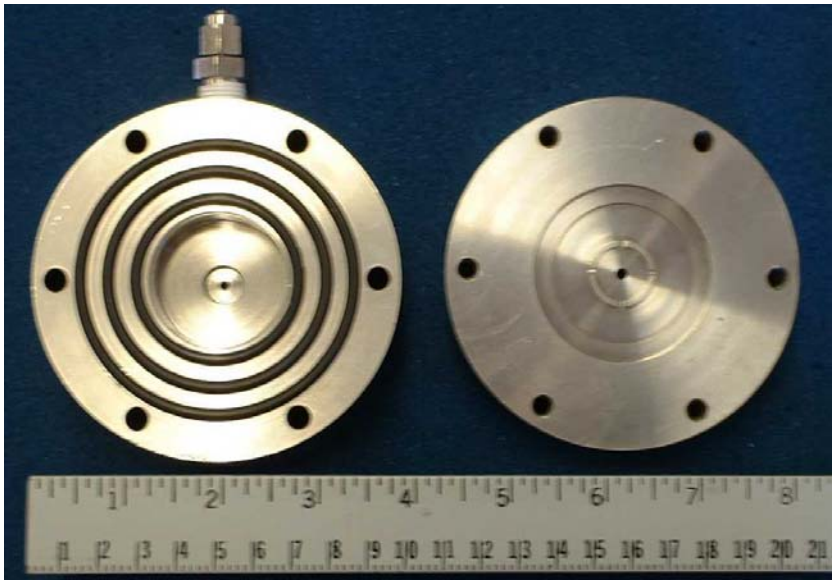

Figure 5-2. Image of the permeation cell used in this study. The left half of the cell is the feed side and contains the three gaskets used to prevent leaks. The center of the left piece is a hallow cavity. The right piece is the permeate side and hold the membrane and microporous alumina support (not shown).

Recorded data was analyzed using the Time Lag method with the aide of the software programs Microcal Origin (v6.0) and MS Excel (Office 2000). Background noise contributions to the permeate pressure were accounted for by adjusting the permeation pressure values at the very beginning of each test to a value of zero. The adjusted permeation data was plotted against time, and the slope was determined using the *Linear Fit* function in Microcal Origin. Data from a typical run is shown below in Figure 5-3.

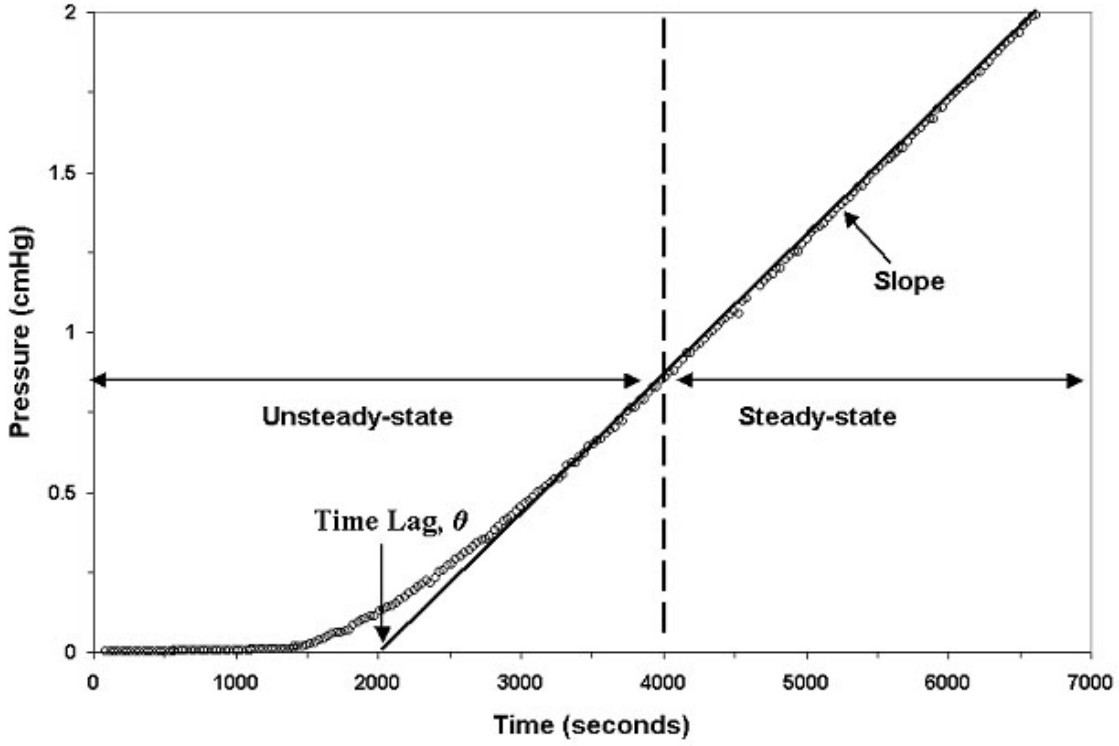

Figure 5-3. Typical permeation experiment data analyzed using Time Lag Method.

Ideal selectivities were calculated by ratioing the pure gas permeabilities.

5.4 Results and Discussion

5.4.1 Polyimide Synthesis

Using the procedure outlined in the Experimental section, 6FDA-6FpDA was synthesized using a step growth reaction. The stoichiometry of the reaction was controlled so that the 6FDA monomer was in slight excess of the 6FpDA monomer. The reaction scheme is outlined below Figure 5-4.

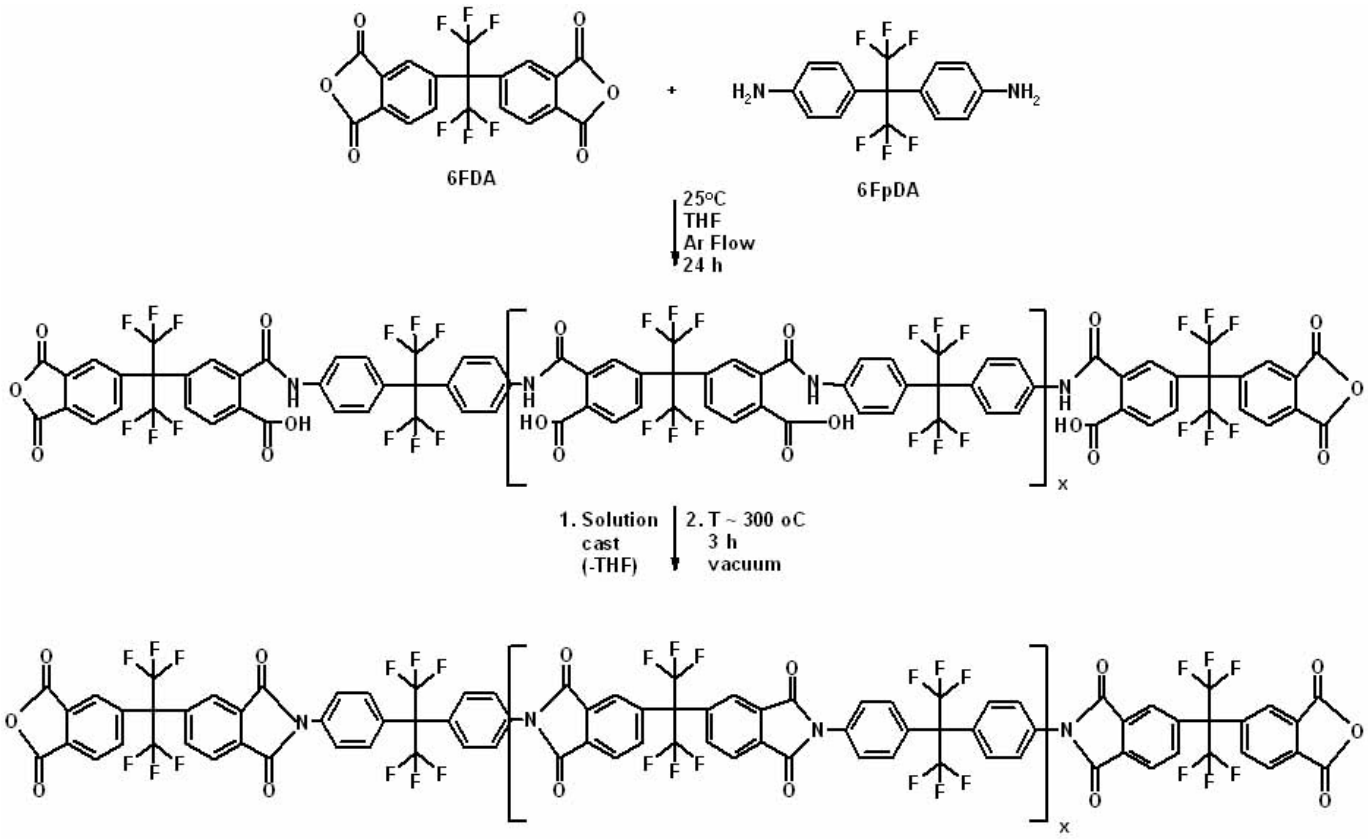

Figure 5-4. Synthesis route employed for 6FDA-6FpDA.

In the synthesis 6FDA was first charged into the 3-neck round bottom flask to ensure it was in excess of 6FpDA. This was done in an effort to ensure the polyimide chains' ends were anhydride groups. After 24 hours the two monomers reacted to form a

poly(amic acid). The reaction solution was cast onto a teflon coated plate, and allowed to dry. It was then placed under vacuum and treated at a temperature above its T_g (~300 ^oC) in order to imidize it. The film changed from a largely clear before the imidization to a yellow color after the imidization.

The molecular weights for this synthesis have been reported in the Gel Permeation Chromatography Results section.

5.4.2 Verification of Imidization of 6FDA-6FpDA via FTIR

FTIR was employed to qualitatively verify that the poly(amic acid) was imidized. The poly(amic acid) and polyimide spectra between 3600 and 2600 cm^{-1} are shown below in Figure 5-5.

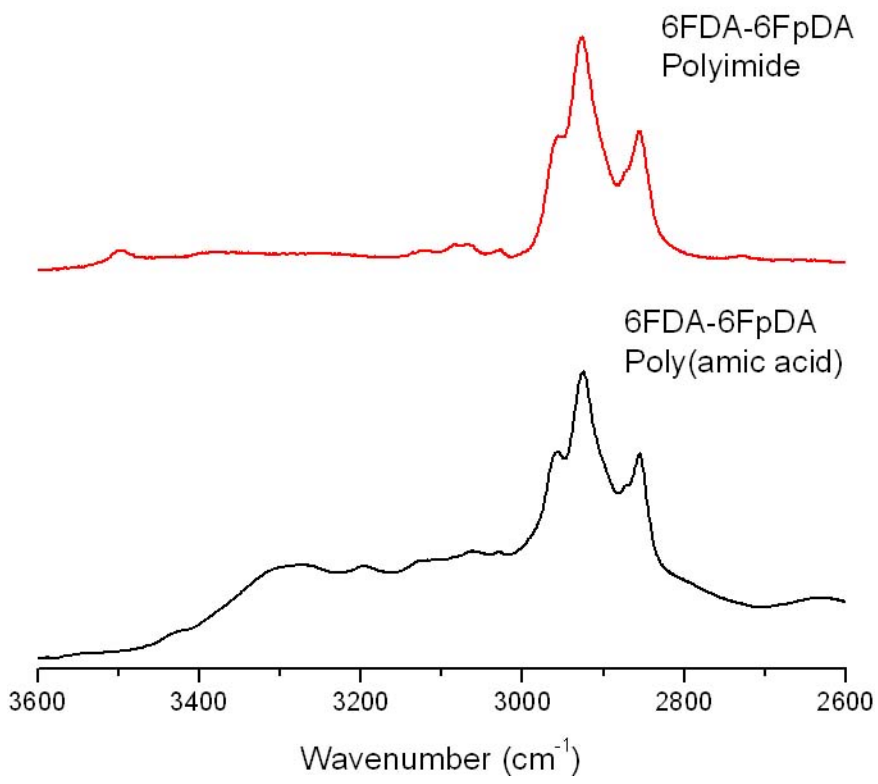

Figure 5-5. FTIR spectra of the 6FDA-6FpDA polyamic acid and the 6FDA-6FpDA polyimide between 3600-2600 cm-1.

In this region $-NH_2$ and –OH groups are IR active. These groups both contribute to the absorbance between 3450 and 3000 cm^{-1} in the poly(amic acid) spectrum. Once the poly(amic acid) was heated above its T_g for several hours, the absorbance in this region dwindles to almost nothing, as shown in the polyimide spectrum. The polyimide spectrum shows a small peak at 3500 cm^{-1} which is a result of free –COOH groups. This could be attributed to a few factors. First, it could indicate that there was not 100% imidization, however, the large decrease in IR activity in this region qualitatively indicates that a high degree of imidization was obtained. Secondly, it could be residual 6FDA that never reacted as a result of not having its rings closed during the presynthesis heat treatment. If a 6FDA monomer's rings were opened due to moisture contact, and did not close during the heat treatment, it would not react with the diamine monomers, and could show up in the spectrum.

The small peaks in the polyimide spectrum between 3100 and 3000 cm^{-1} are from aromatic C-H stretches. The IR bands below 3000 cm^{-1} are alkyl C-H stretches likely due to residual THF.

Polyamides and polyimides are also IR active at lower wavenumbers. Figure 5-6 shows the spectra of the poly(amic acid) and the polyimide.

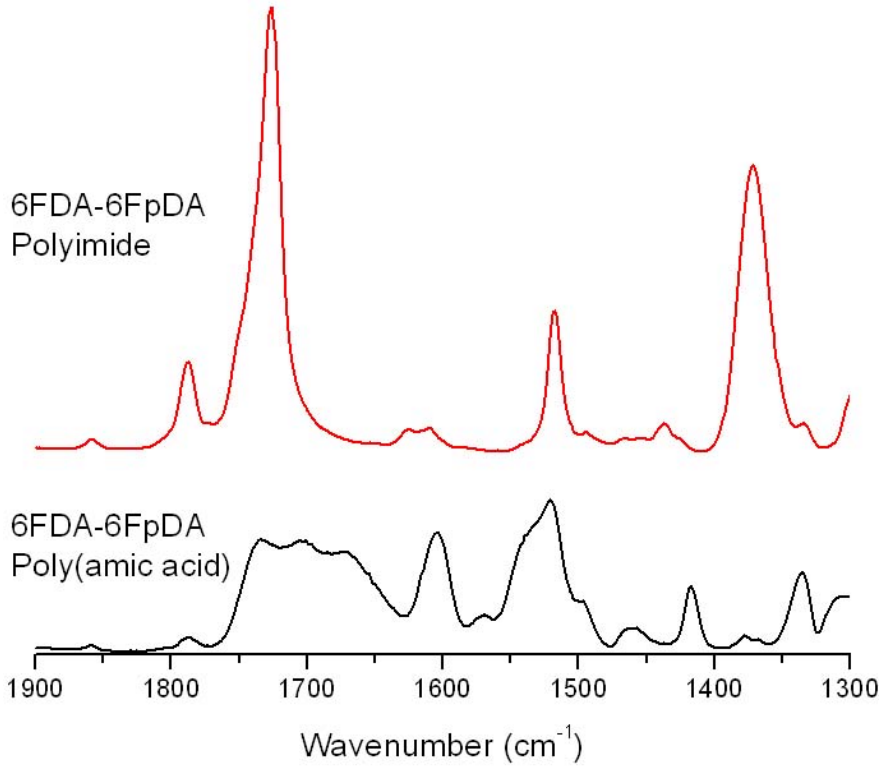

Figure 5-6. FTIR spectra of 6FDA-6FpDA poly(amic acid) and 6FDA-6FpDA polyimide between 1900 and 1300 cm^{-1}.

The polyimide spectrum clearly displays some sharply absorbing peaks which are not present in the poly(amic acid) spectrum. The poly(amic acid) spectrum has a broad band stretching from 1750 – 1600 cm^{-1}. This region contains the stretches associated with amide groups. After the heat treatment this broad band develops into two sharp peaks at 1787 and 1728 cm^{-1}. Both of these peaks are from the C=O stretches of the polyimide. The band at 1787 cm^{-1} is associated with the carbonyl groups near the anhydride ends, and the peak at 1728 cm^{-1} is associated with the carbonyl groups in the polyimide repeat unit.[19-21] The peak which develops at 1373 cm^{-1} is associated with the C-N-C linkages of the polyimide repeat unit.[22]

5.4.3 Synthesis of Poly(imide siloxane)s

5.4.3.1 Molecular weight determination of PDMS monomer

Amine-terminated PDMS was purchased from Gelest and used as received. The supplier only offers a range of 800 – 1000 g/mol for the M_n of the monomer. ^{1}H-NMR was employed to more accurately determine the M_n of the PDMS monomer. The ^{1}H-NMR spectrum of the PDMS monomer is shown in Figure 5-7.

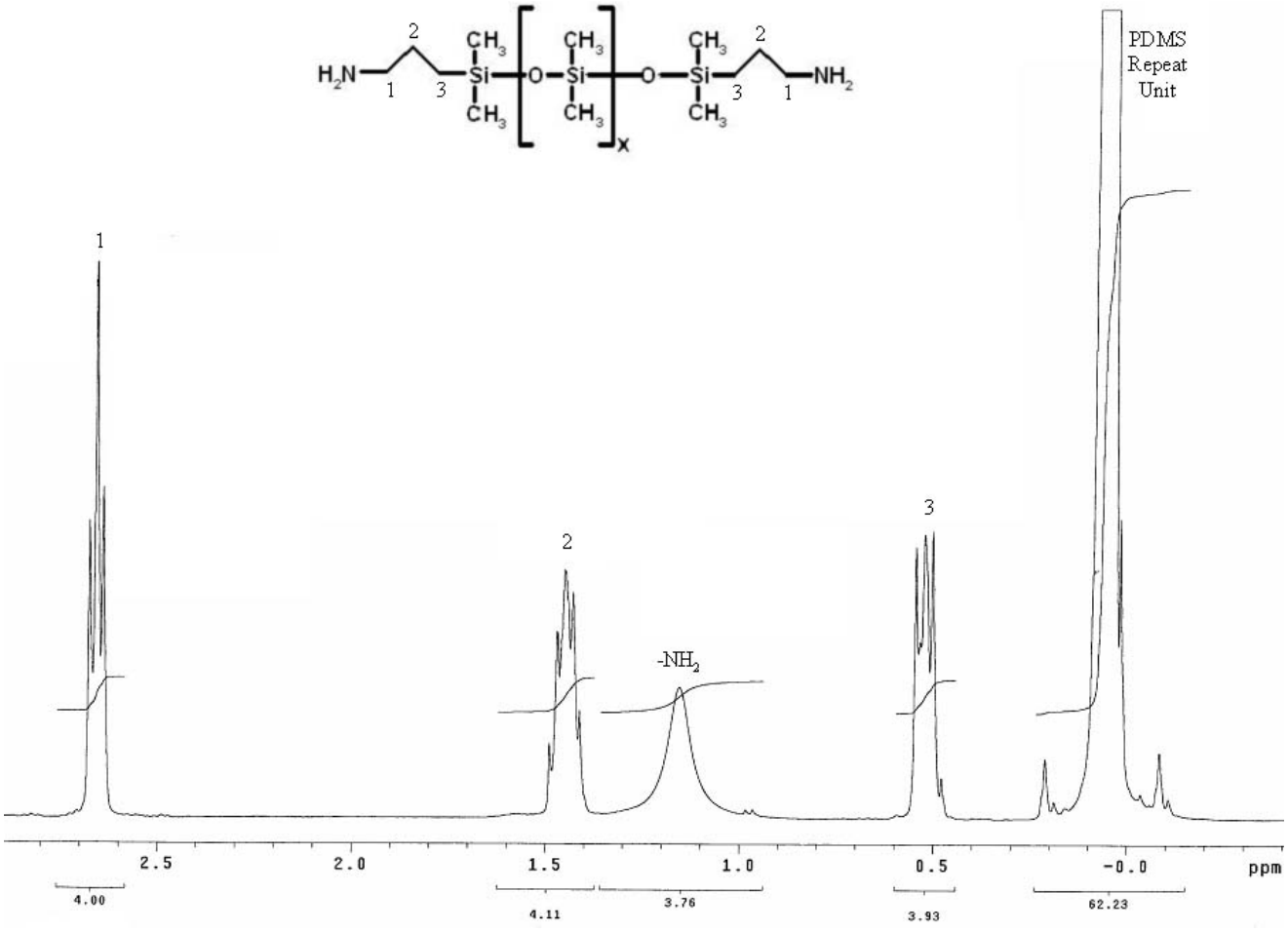

Figure 5-7. 400 MHz 1H-NMR spectrum for the amine-terminated PDMS monomer used in this study.

Our peak assignments agreed with those of McGrath et al.[23]

Using the area under the assigned peaks the molecular weight was determined. The peak assigned to the repeat unit of PDMS (i.e. Si-$(CH_3)_2$) near 0.05 ppm has an area of 62.23. Using this and the number of H atoms per repeat unit (i.e. 6), the M_n can be determined as follows:

$$\frac{62.23}{6\,\text{H atoms}} = 10.37\ \text{Repeat Units}$$

The molecular weight of the repeat units is

$$10.37\ \text{RU}\,\frac{74.17\ \text{g/mol}}{\text{RU}} = 769.3\ \text{g/mol}$$

Add on M_n of the two aminopropyl groups

$$M_n = 769.3 + 2\cdot(14.01 + 12.01\cdot 3 + 1.01\cdot 8)$$

$$M_n = 885.5\ \text{g/mol}$$

This result is in agreement with the manufacturer's label.

5.4.3.2 Synthesis of Poly(imide siloxane)s

Using the procedure outlined in the Experimental section, 6FDA-6FpDA-PDMS was synthesized using a step growth reaction.[24] The copolymer was synthesized at two different weight percents of PDMS. In both cases the synthesis was the same, and only the masses of monomer used differed. The first step of the reaction scheme to synthesize 6FDA-6FpDA-PDMS is shown below in Figure 5-8.

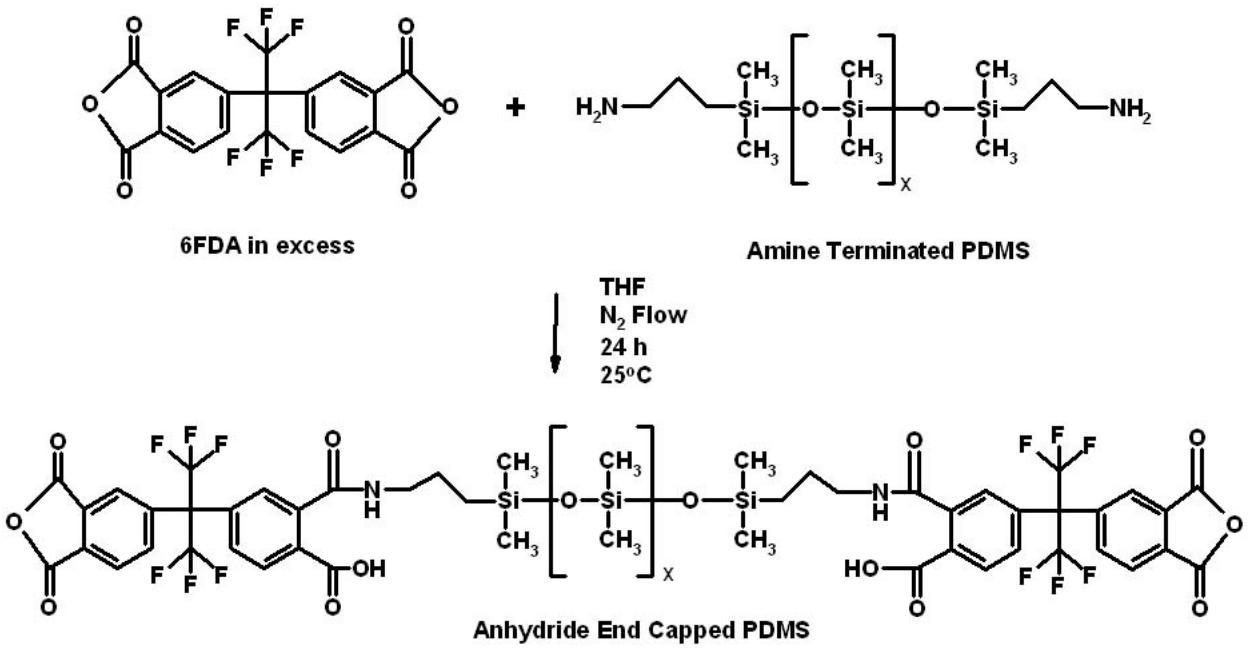

Figure 5-8. End capping amine-terminated PDMS with dianhydride groups. This step is performed with excess 6FDA to ensure complete end-capping.

The above step was performed in excess 6FDA to ensure end-capping of the PDMS monomer. The endcapping of PDMS with anhydride would prevent blocks of 6FDA-PDMS from occurring.

After 24 hours, the aromatic diamine 6FpDA was added to the reaction. The addition of 6FpDa would build a poly(amic acid) block which would later be converted into a polyimide block. The reaction scheme for this step is shown below in Figure 5-9.

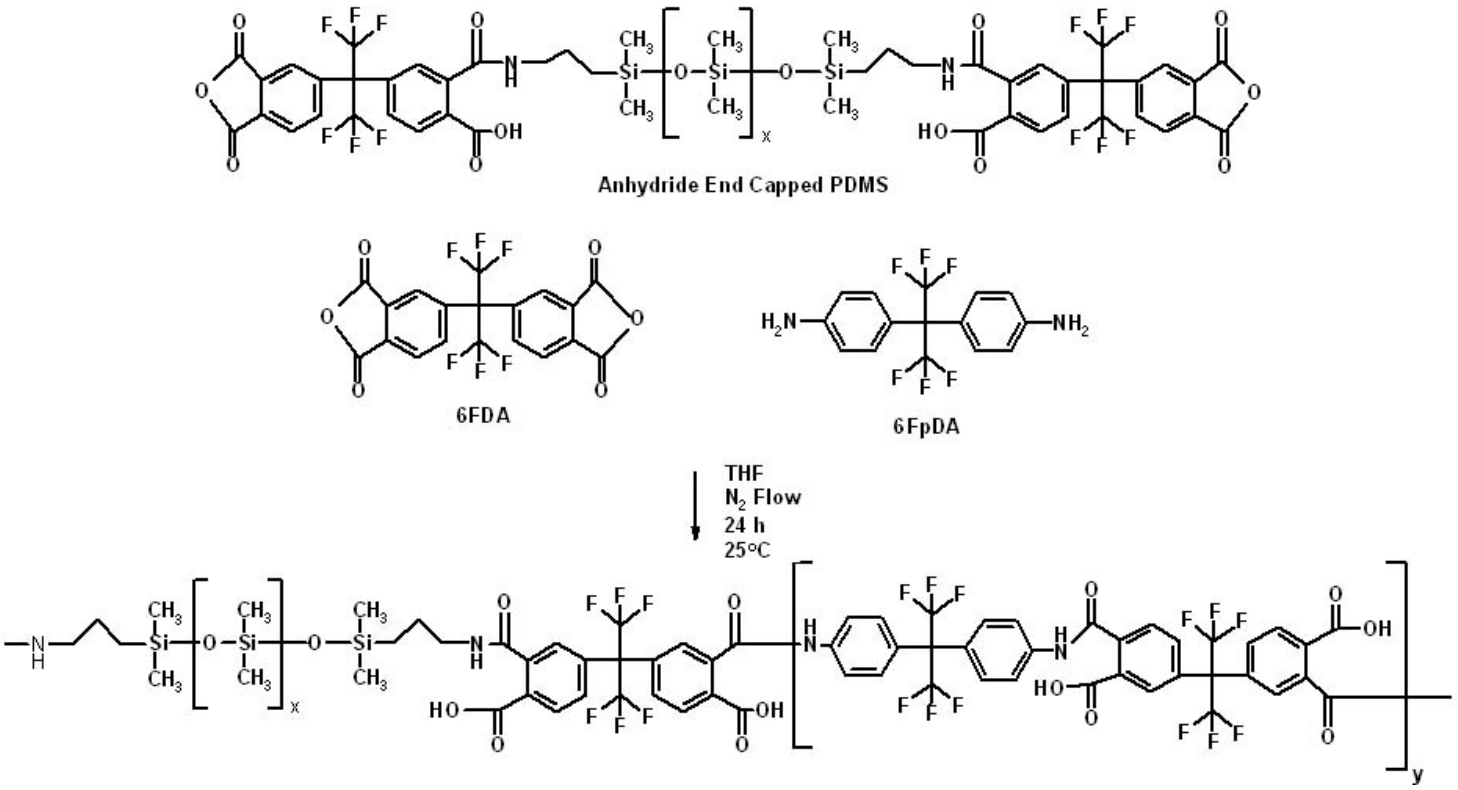

Figure 5-9. Step 2 of the poly(imide siloxane) synthesis. In this step 6FpDA is added to the anhydride end-capped PDMS.

After 24 hours, the reaction solution was cast onto a Teflon coated pan. The solvent was allowed to evaporate overnight, leaving a mostly clear poly(amic acid) film. This film was placed under vacuum at a temperature higher than the film's T_g to imidize it. After imidization the film turned a yellowish color. This step is shown in Figure 5-10.

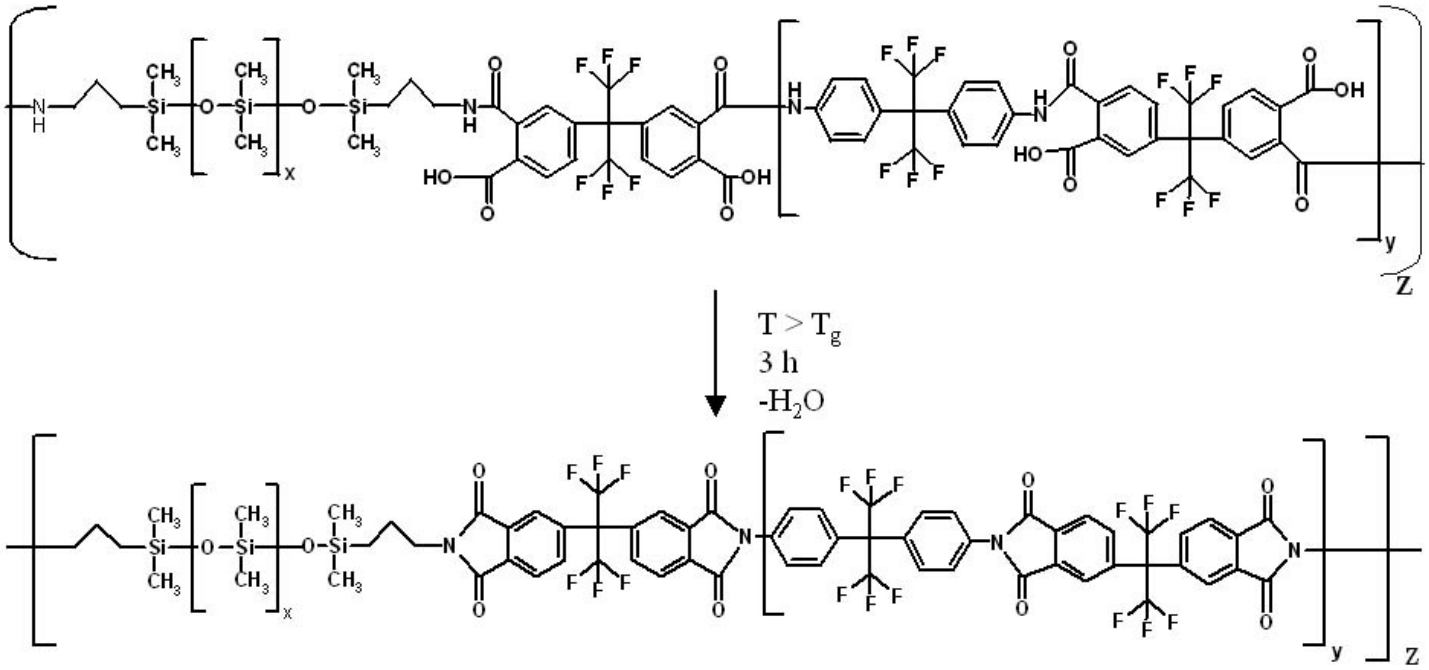

Figure 5-10. Imidization step of the synthesis of the 6FDA-6FpDA-PDMS block copolymer.

The molecular weights for the copolymers are listed in the Gel Permeation Chromatography Results section later.

5.4.3.3 Determining the weight percent of PDMS via ^{1}H-NMR

The weight percent incorporated into the polyimide's backbone was determined using ^{1}H-NMR. After the imidization step, the copolymers were redissolved in THF and extracted in hexane bath for the purpose of removing any unreacted PDMS monomer as described in the Experimental section. After the hexane bath, the polymers were again dried in a vacuum oven at 100 ^{o}C. NMR samples consisted of 15 – 20 mg of polymer dissolved in 0.7 mL of d6-acetone.

Below is the 400 MHz ^{1}H-NMR spectrum for the synthesized poly(imide siloxane) at 41 wt % PDMS (Figure 5-11).

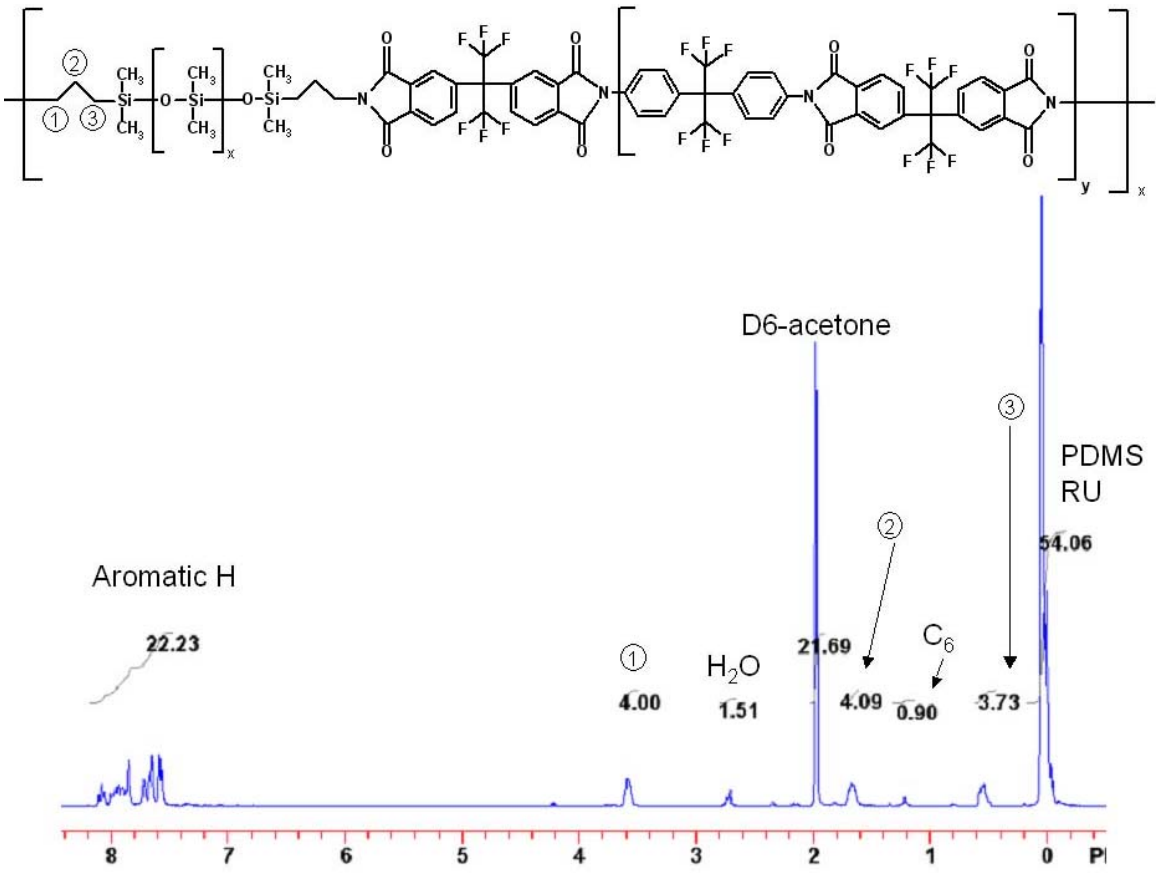

Figure 5-11. 400 MHz ^{1}H-NMR spectrum of the 41 wt % PDMS poly(imide siloxane).

The weight percent for the 41 % PDMS copolymer was determined using the procedure outlined below. NUTS software was used to Fourier Transform, baseline, and integrate the area of the peaks in the NMR spectrum. The integrate values for the peaks are shown on the spectrum. The aromatic protons of the polyimide block appear downfield between 8.25 – 7.5 ppm due to deshielding, while the protons of the PDMS repeat unit appear upfield at 0.1 ppm.[25] The protons associated with the propyl group of the PDMS block have three peaks. The protons on the carbon adjacent to the nitrogen atom appear at 3.6 ppm, while the protons on the center carbon appear at 1.7 ppm, and the protons on the carbon next to the Si atom appear at 3.73 ppm. Additionally, some sample contamination is present represented by the other peaks (e.g. water, hexane, acetone).[26] The corresponding integrated area values are listed above each peak.

The weight percens of PDMS was determined by using the number of aromatic protons per repeat unit, the number of protons per α-carbon (i.e. the carbon on the PDMS propyl chain which is covalently bonded to the nitrogen atom), their corresponding areas, and each segments molecular weight.

The molecular weight of the hard block (i.e. polyimide) and the soft block (i.e. PDMS) in the copolymer are listed below:

$$\text{6FDA - 6FpDA}: \quad M_n = 742 \frac{g}{mol}$$

$$\text{PDMS}: \quad M_n = 881.5 \frac{g}{mol}$$

Using the peak areas for the aromatic hydrogens and the alpha-carbon hydrogens, the hard-soft block ratio can be determined.

$$\text{6FDA - 6FpDA}: \quad \frac{14\ \text{H}}{\text{Repeat Unit}}$$

$$\text{PDMS}: \quad \frac{4\ \text{H}}{\text{Repeat Unit}}$$

$$\frac{\text{Hard Segments}}{\text{Soft Segments}} = \frac{\dfrac{(\text{Aromatic H Peak Area})}{\#\ \text{H per Hard Segment}}}{\dfrac{(\alpha\text{ - H Peak Area})}{\#\ \text{H per Soft Segment}}}$$

$$= \frac{\text{Hard Segment}}{\text{Soft Segment}}$$

$$= \frac{\dfrac{23.59}{14}}{\dfrac{4}{4}}$$

$$\frac{\text{Hard Segments}}{\text{Soft Segments}} = 1.685$$

The weight % PDMS can now be calculated using the ratio of hard to soft segments. The calculation is shown below:

$$\text{WT \% PDMS} = \frac{M_n \text{ PDMS}}{\frac{\text{Hard Segment}}{\text{Soft Segment}} \cdot \left(M_n \text{ 6FDA - 6FpDA}\right) + M_n \text{ PDMS}} \cdot 100\%$$

$$= \frac{881.5}{1.685 \cdot 742 + 881.5} \cdot 100\%$$

$$\text{WT \% PDMS} = 41\%$$

The same procedure was used to determine the weight percent in the other copolymer. It was synthesized with a target of 20 wt % PDMS. According to the ^{1}H-NMR spectrum analysis, it was determined to be 22 wt % PDMS .

In all the ^{1}H-NMR spectra gathered, there were no peaks above 10 ppm. Aromatic darboxylic acid structures show proton peaks in this area, and the lack of peaks above 10 ppm provided quantitative verification of imidization.[24,27]

5.4.3.4 Verification of Imidization via FTIR

FTIR spectroscopy was employed to qualitatively verify the successful imidization of both copolymers. The spectrum between 3600 and 2600 cm^{-1} for the 22 wt % PDMS copolymer is shown below in Figure 5-12.

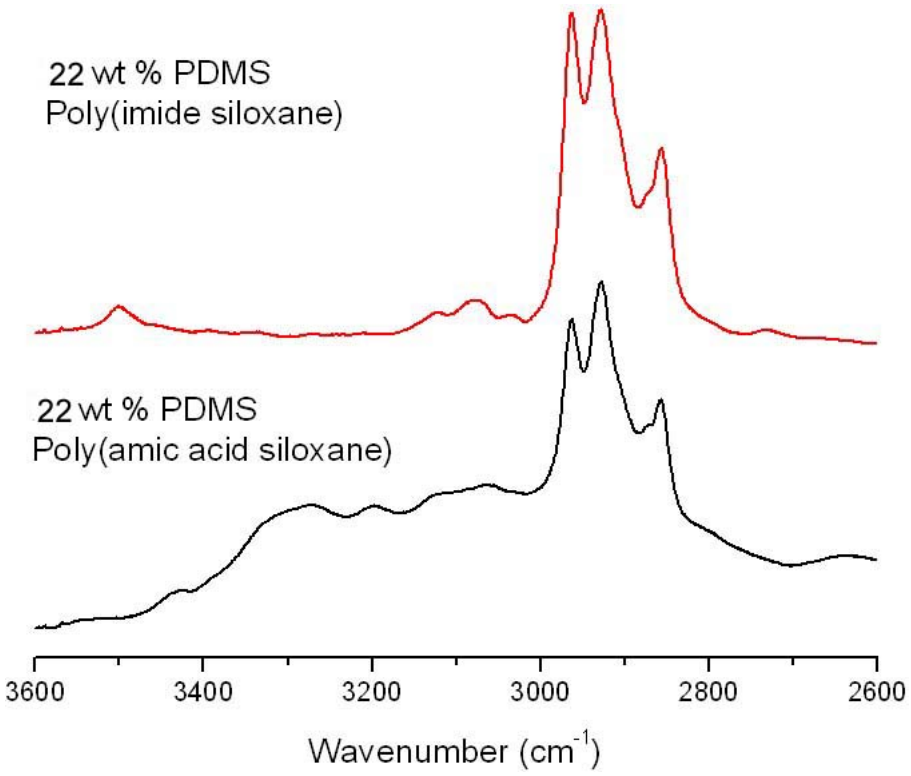

Figure 5-12. FTIR spectra for the 22 wt% PDMS poly(amic acid siloxane) and its corresponding poly(imide siloxane) between 3600 and 2600 cm-1.

In this region of the IR spectrum $-NH_2$ and –OH groups are active. These groups both contribute to the absorbance between 3450 and 3000 cm^{-1} in the poly(amic acid) spectrum. Once the poly(amic acid) was heated above its T_g for several hours, the absorbance in this region dwindles to almost nothing, as shown in the polyimide spectrum. This is a result of the cyclodehydration of the poly(amic acid) into a polyimide in which the –COOH and –CONH groups react to form an imide ring. The polyimide spectrum shows a small peak at 3500 cm^{-1} which is a result of free –COOH groups. There are a few possible explanations for this. First, this could indicate that there was not 100% imidization, however, the large decrease in IR activity in this region qualitatively indicates that a high degree of imidization was obtained. This explanation would also be inconsistent with the ^{1}H-NMR results which did not display any aromatic carboxylic acid proton peaks.

A more likely explanation is that the some of the 6FDA monomer was not successfully heat treated. As mentioned in the Experimental section, the 6FDA monomer is heated under vacuum to ensure its ends are closed; the anhydride ends can react with moisture to form –COOH groups. If indeed they were open prior to the synthesis, they should not have reacted, and could show up in the FTIR spectrum in this area.

The small peaks in the polyimide spectrum between 3100 and 3000 cm^{-1} are from aromatic C-H stretches. The IR bands below 3000 cm^{-1} are alkyl C-H stretches due the PDMS repeat units, the propyl units, and perhaps some residual THF.

Imide rings have their own characteristic IR active bands at lower wavenumbers. In Figure 5-13 the IR spectrum between 1900 and 1300 cm^{-1} are shown for both polymers.

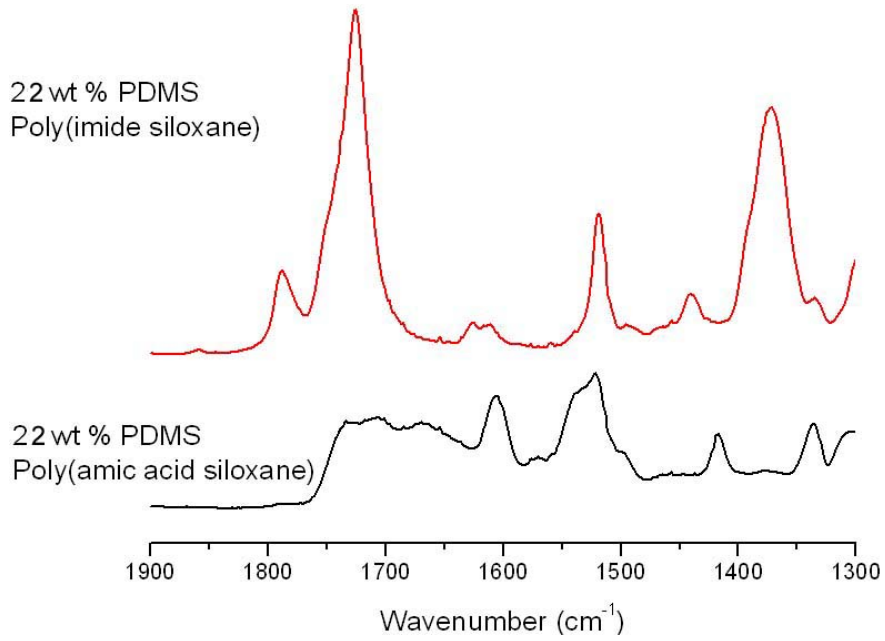

Figure 5-13. FTIR spectra for the 22 wt% PDMS poly(amic acid siloxane) and its corresponding poly(imide siloxane) between 1900 and 1300 cm-1.

The polyimide spectrum clearly displays some sharply absorbing peaks which are not present in the poly(amic acid siloxane) spectrum. The poly(amic acid siloxane) spectrum has a broad band stretching from 1750 – 1600 cm^{-1}. This region contains the

stretches associated with amide groups. After the heat treatment this broad band develops into two sharp peaks at 1787 and 1728 cm^{-1}. Both of these peaks are from the C=O stretches of the polyimide. The one at 1787 cm-1 is associated with the carbonyl groups near the anhydride ends and the peak at 1728 cm-1 is associated with the carbonyl groups in the polyimide repeat unit. [19-21] The peak which develops at 1373 cm^{-1} also is associated with the C-N-C linkages of the polyimide repeat unit.[22]

The same analysis is applicable to the 41 wt %. Below is the spectrum for the 41 wt % PDMS copolymer between 3600 and 2600 cm^{-1} (Figure 5-14).

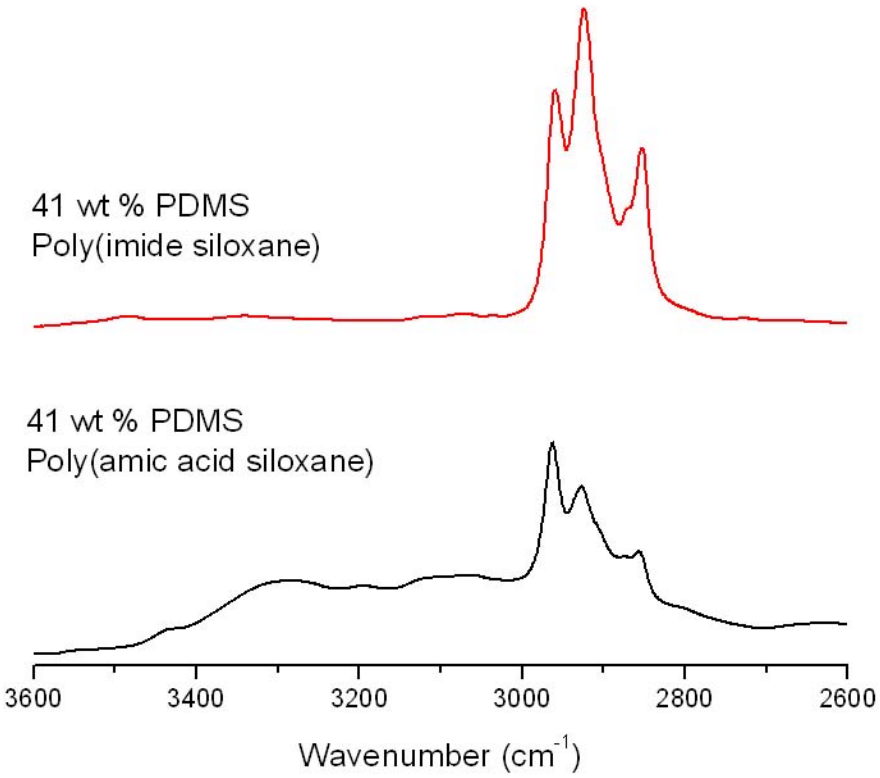

Figure 5-14. FTIR spectra for the 41 wt% PDMS poly(amic acid siloxane) and its corresponding poly(imide siloxane) between 3600 and 2600 cm-1.

The same analysis given to the 22 wt % PDMS copolymer can be applied here, because the same monomers and solvent were used in the synthesis; only their masses differed. This holds true for the region between 1900 -1300 cm^{-1} which is shown below for the two copolymers at 41 wt % PDMS (Figure 5-15).

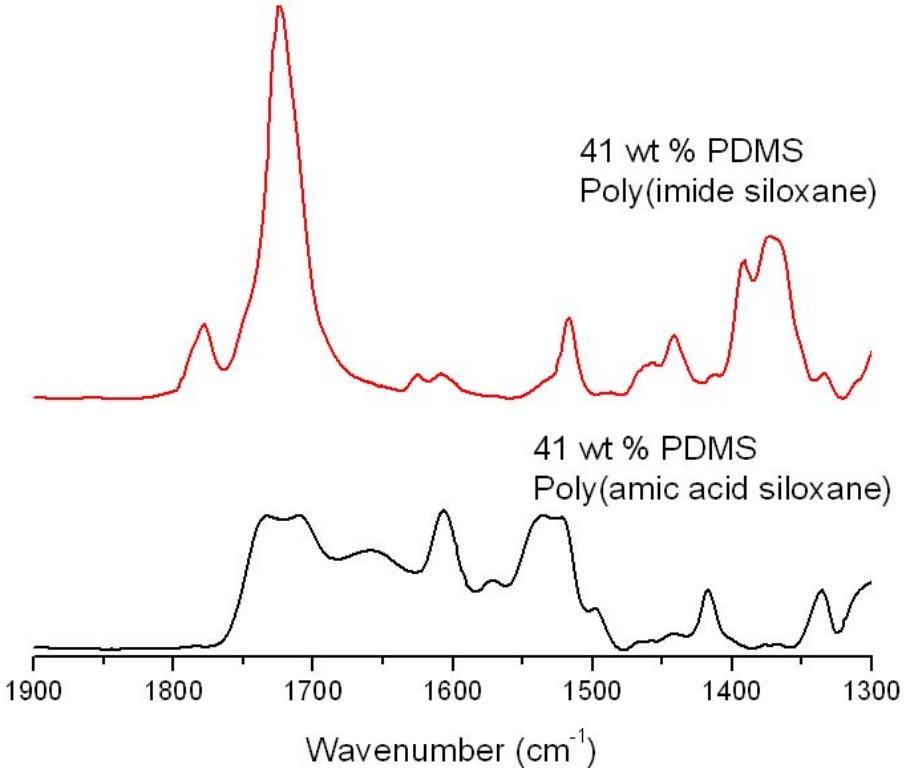

Figure 5-15. FTIR spectra for the 41 wt% PDMS poly(amic acid siloxane) and its corresponding poly(imide siloxane) between 1900 and 1300 cm^{-1}.

5.4.4 Gel Permeation Chromatography Results

GPC experiments were employed to determine the molecular weights of the polymers synthesized in this study. The results are summarized below in Table 5-2.

Table 5-2. GPC results for the synthesis of 6FDA-6FpDA and 6FDA-6FpDA-PDMS.

Wt % PDMS	M_n (g/mol)	M_w (g/mol)	Polydispersity
0	18150 ± 1220	38570 ± 1610	2.13 ± 0.08
25	35890 ± 1320	79910 ± 1490	2.23 ± 0.04
41	62330 ± 4000	131300 ± 30120	2.10 ± 0.43

5.4.5 Microscopy Results

5.4.5.1 Field Emission Scanning Electron Microscopy (FESEM)

FESEM was utilized to provide surface images of the mixed matrix membranes. Below is a surface image of a 20 wt % zeolite L 6FDA-6FpDA MMM (Figure 5-16).

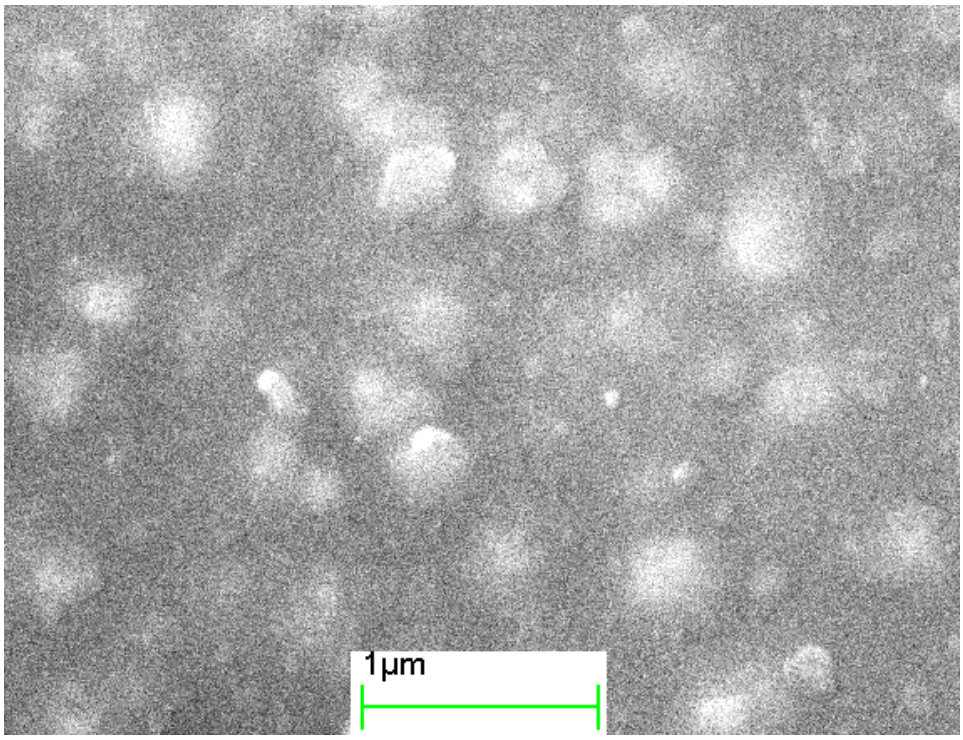

Figure 5-16. FESEM surface image of a 20 wt % zeolite L 6FDA-6FpDA mixed matrix membrane.

At this level of magnification there is no evidence of the polyimide delaminating from the zeolite. This is contrary to the observations of others who mixed untreated zeolites with rigid polymers, and comparable adhesion to the samples discussed in Chapters 3 and 4 in which we amine-functionalized the zeolite surfaces.[7,11,28,29] However, there are several factors which could explain this difference. First, the lack of visual confirmation of voids at this level of magnification does not rule out presence of voids. If there were voids in this membrane, they could be too small to be visible at this

magnification. A higher level of magnification could reveal voids between the two components. Secondly, when comparing our work to that of others, it must be recognized that our study used different zeolites. Most of the studies we refer to used zeolites which were made commercially. Our zeolite L was synthesized for us by Dr. Michael Tsapatsis group at the University of Minnesota. These synthesize zeolites crystals had sizes on the order of a hundred nanometers or less, which is much smaller than the sizes of zeolites which are made commercially. Commercially available zeolites have sizes ranging from 600 to a few thousand nanometers. Currently, no studies have been performed which focus on the adhesion between a glassy polymer polymer and zeolite as a function of zeolite size.

When we compare this result to our own work in Chapter 3 and 4 we must consider that this polymer is different than the 6FDA-6FpDA-DABA used in those studies. The addition of DABA groups (i.e. 3,5-diaminobenzoic acid) comes at the expense of 6FpDA, as they are both diamines which react with the dianhydride 6FDA. This lowers the content of 6FpDA within the polymer and reduces its flexibility by two routes. First, because DABA contains –COOH groups which are capable of hydrogen bonding, the chains are likely to become more rigid due to interchain interactions. Secondly, 6FpDA contains a sp^3 carbon in its backbone whereas DABA does not. Therefore, as one removes 6FpDA linkages are replaces them with DABA linkages, the backbone should lose flexibility.

The copolymer mixed matrix membranes were studied as well using FESEM. Below is a picture of a 20 wt % zeolite MMM, which uses the 22 wt % PDMS poly(imide siloxane) copolymer as the matrix (Figure 5-17).

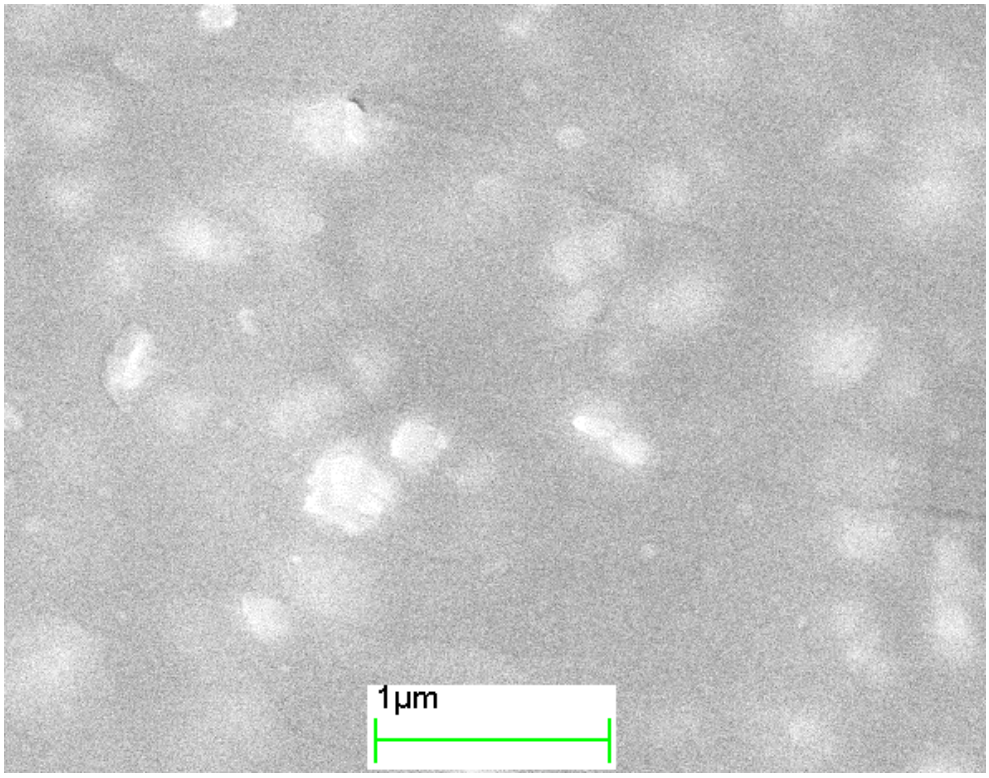

Figure 5-17. FESEM surface image of a 20 wt % zeolite L mixed matrix membrane with a 22 wt % PDMS poly(imide siloxane) copolymer matrix.

Like the pure polyimide FESEM image, at this level of magnification there is no evidence of the copolymer dewetting from the zeolite. Additionally, this image like the others taken of it does not show any evidence of agglomeration of the zeolite.

A surface image of the 20 wt % zeolite L MMM using the 41 wt % PDMS poly(imide siloxane) is shown below in Figure 5-18.

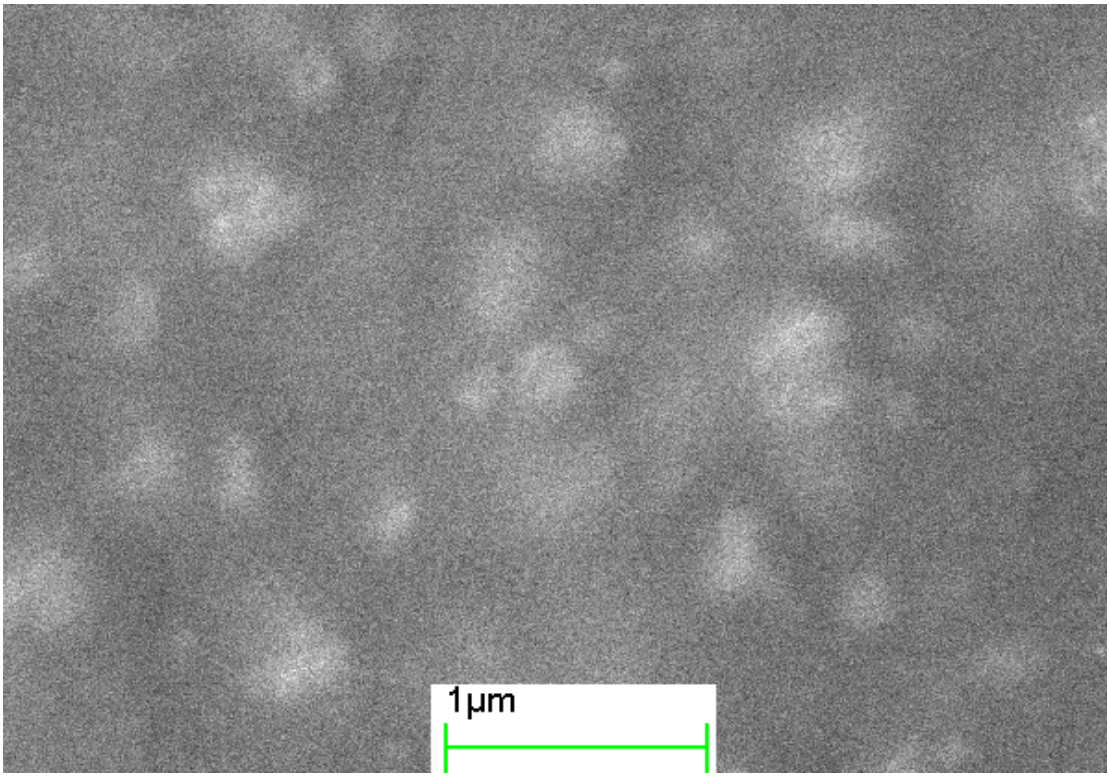

Figure 5-18. FESEM surface image of a 20 wt % zeolite L mixed matrix membrane with a 41 wt % PDMS poly(imide siloxane) copolymer matrix.

Like the others there is no evidence of the copolymer delaminating from the zeolite at this level of magnification. Furthermore, the zeolite did not show any signs of agglomeration in this membrane in any of the SEM images taken of it.

To monitor the effects of the zeolite loading, images were taken of a 30 wt % zeolite L MMM using the 41 wt % PDMS poly(imide siloxane) as the polymer matrix. A surface image of the of the MMM is shown below in Figure 5-19.

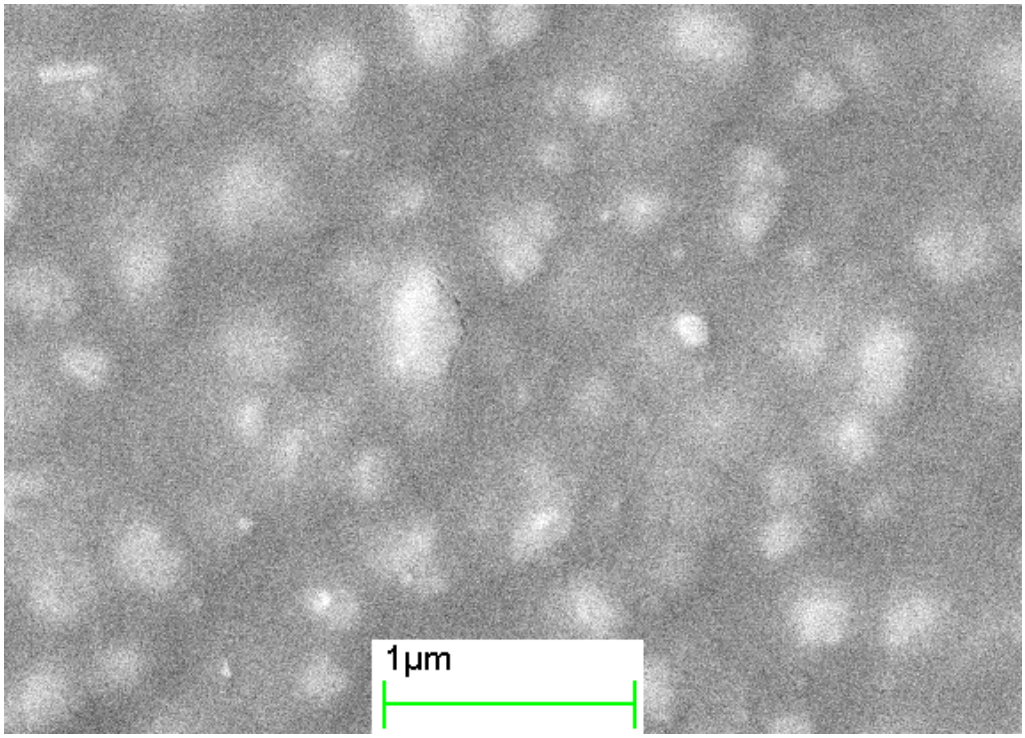

Figure 5-19. FESEM surface image of a 30 wt % zeolite L mixed matrix membrane with a 41 wt % PDMS poly(imide siloxane) copolymer matrix.

Again, at this level of magnification there is no evidence of the polymer dewetting from the zeolite, despite a 50 % increase in zeolite loading. Also, the zeolites still do not show signs of agglomeration in any of the SEM images taken of this membrane.

Finally, it should be noted that higher levels of zeolite incorporation can be achieved in these copolymer systems in comparison to the 6FDA-6FpDA-DABA MMMs presented in Chapter 3.

5.4.5.2 Transmission Electron Microscopy (TEM)

TEM images were taken of the pure 6FDA-6FpDA polymer, and the 22 and 41 wt % PDMS poly(imide siloxane) copolymers. The images were taken to verify the presence of phase separation of the hard segments from the soft segments in the copolymers. The pure polyimide images were used as a control sample. The images are shown below in Figure 5-20.

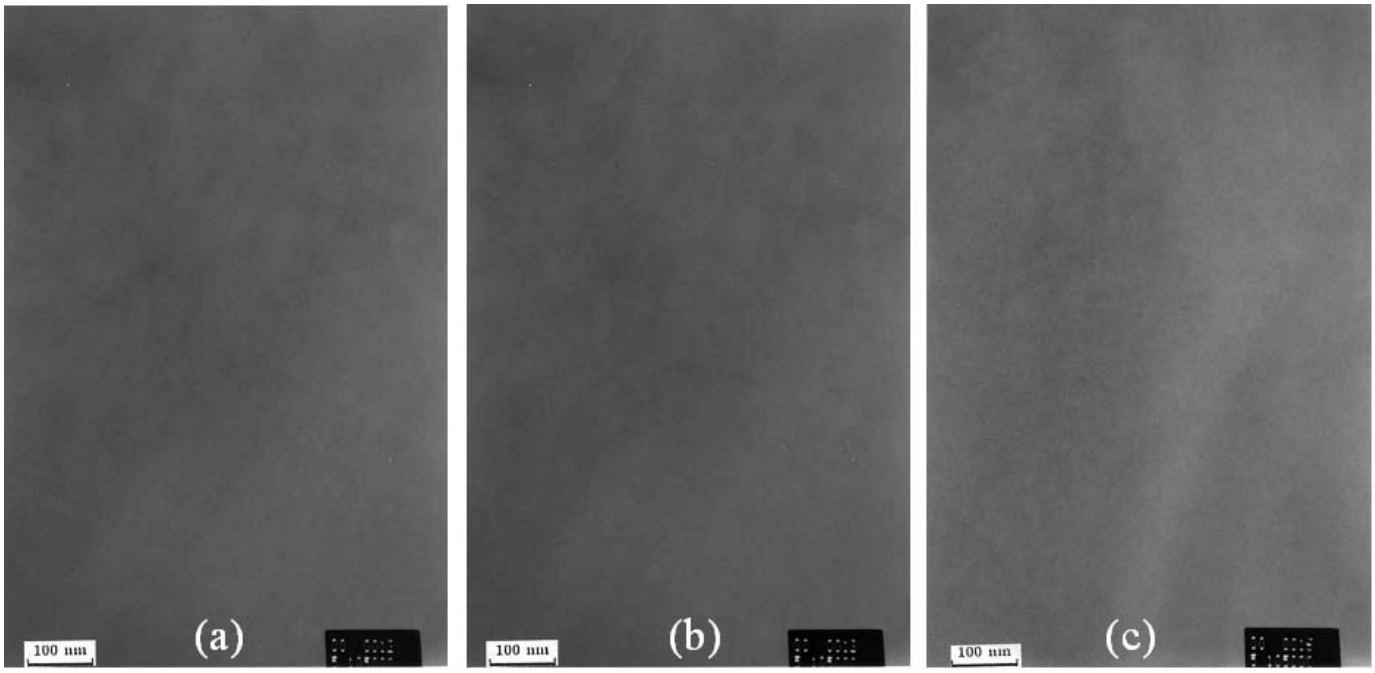

Figure 5-20. TEM images of (a) 6FDA-6FpDA, (b) 22 wt % PDMS poly(imide siloxane), and (c) 41 wt % PDMS poly(imide siloxane). The bar on the lower left of each image represents 100 nm.

From the images above, there is no indication of phase separation in the copolymers. However, this does not prove there is no phase separation present within the copolymer systems. It is possible that the sizes of the domains are too small to be distinguished from each other using TEM. One must recall that the block sizes of these copolymers are relatively small (i.e. PDMS M_n = 881 g/mol). Work by Bowens and work by Rogers et al. studying poly(imide siloxane)s with TEM showed readily distinguishable phases.[24,30] This is because the siloxane phase has a much higher electron density than the polyimide phase, which leads to a large difference in contrast between the two. However, in both cases the PDMS monomers used in the synthesis possessed at least a M_n of 2000 g/mol. Later work by McGrath et al. would show that when the siloxane moiety exceeded 1000 g/mol, phase separation would occur.[23]

The PDMS monomer used in our copolymer possessed a M_n of 885 g/mol. While this is below the threshold discovered by McGrath et al, our copolymers have different structures, which could alter the threshold Because of this, there are three possible TEM

results: 1) there is no phase separation, or 2) there is phase separation, but the sizes of the domains are too small to be detected using TEM, or 3) there is phase separation, but there is not enough contrast between the two phases for them to become visible using this method. This makes the TEM results inconclusive. In order to determine if phase separation is present, other techniques must be employed.

5.4.5.3 Atomic Force Microscopy (AFM)

Atomic force microscopy was used in tapping mode to map the surface of the polymers. Additionally, phase imaging provided some insight into the presence of phase separation between the siloxane segments and the polyimide segments of the copolymers.

Height and phase images of all three polymers are shown below in Figure 5-21. For each image a 1 x 1 μm^2 section of polymer was investigated. The z-range for the left height image is 10 nm, and the range for the right phase image is 5^o.

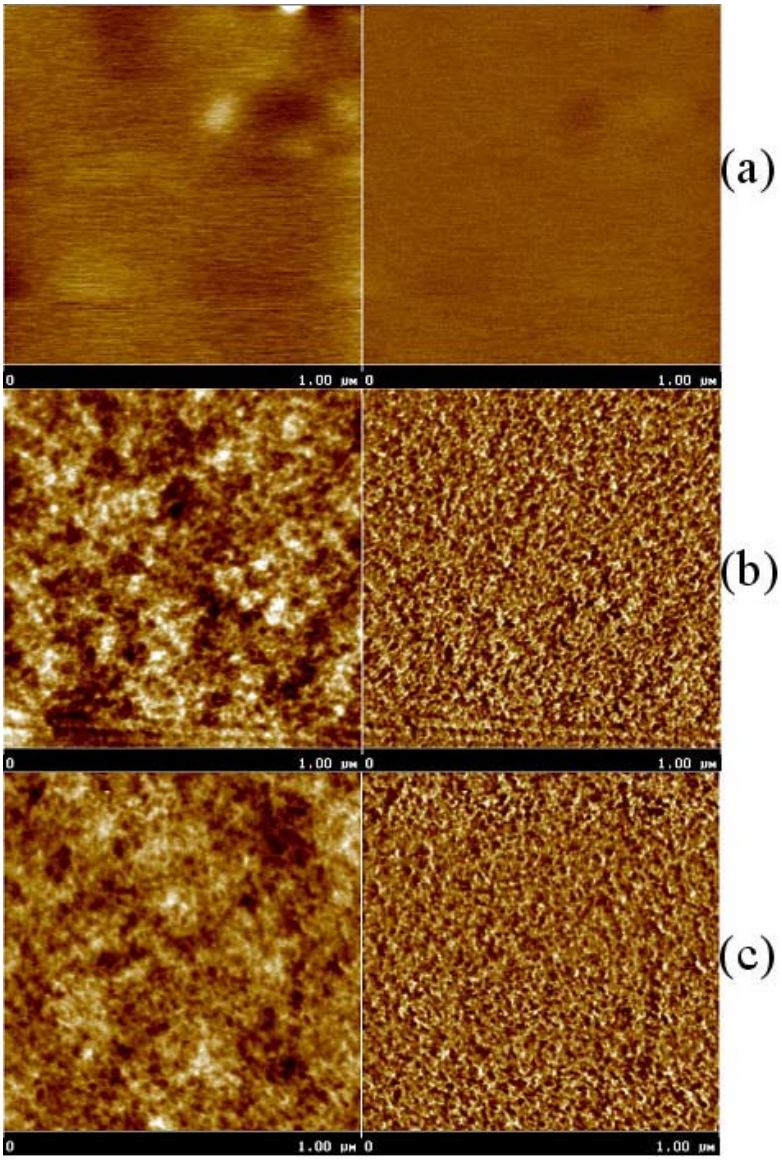

Figure 5-21. AFM height (left) and phase (right) images of (a) the 6FDA-6FpDA polyimide, (b) the 22 wt % PDMS poly(imide siloxane), and (c) the 41 wt % PDMS poly(imide siloxane).

There is a clearly visible change in the phase images between the polyimide and the copolymers. The phase images distinguish between hard and soft segments, due to their differences in modulus (i.e. hard segments have a higher modulus). The softer segments, in this case the siloxane segments, show up as darker regions in the image, while the harder segments (i.e. polyimide) show up as brighter regions. From the phase

images, it is evident that there appears to be the formation of hard and soft domains with the addition of PDMS. This could indicate phase separation within the copolymers.

One must recall that AFM only maps the surface of the sample, and does not investigate the bulk. It has been established that PDMS has low surface tension and surface energies due to their very large molar volumes, low intermolecular interactions, and high flexibilities.[31] PDMS' values for surface tension are typically much lower than that of other polymers.[32] As a result, the air-polymer surfaces of siloxane containing copolymers are enriched in the lower surface energy siloxane. This is a result of an effort to minimize the interfacial or surface energy.[32] Because of this, merely looking at the surface should be considered insufficient for characterizing the bulk of the polymer.

The height images can also show some evidence of phase separation due to the roughness. It is more easily visible in a 3-D view, as shown below in Figure 5-22.

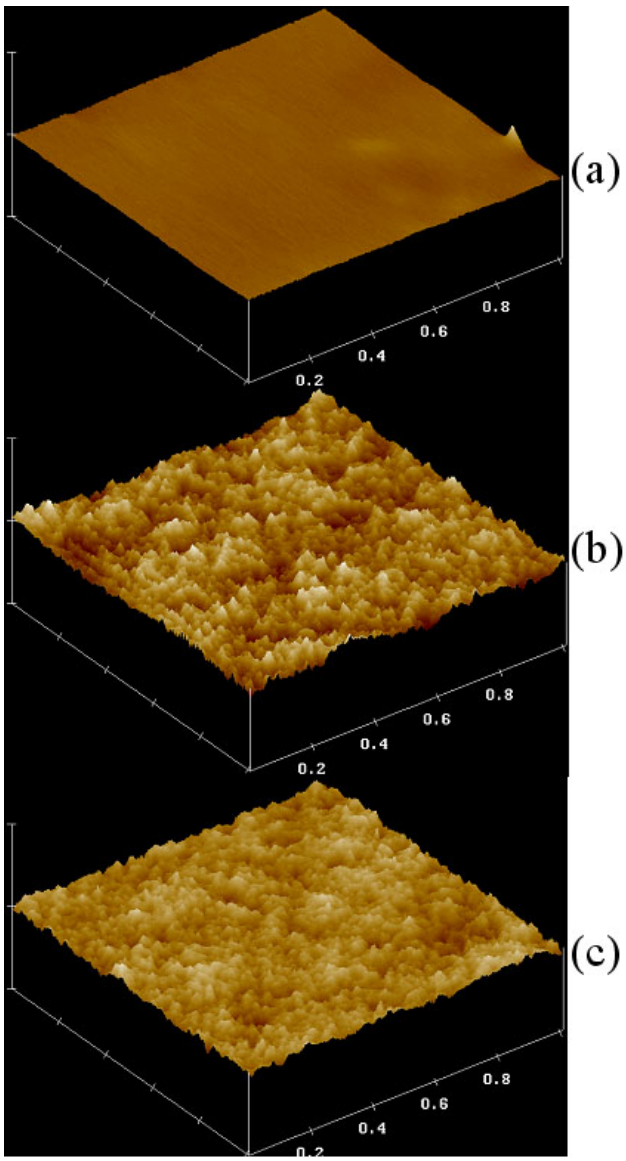

Figure 5-22. AFM topographical images of (a) the 6FDA-6FpDA polyimide, (b) the 22 wt % PDMS poly(imide siloxane), and (c) the 41 wt % PDMS poly(imide siloxane). The z-axis is 30 nm for each image.

These images show that the poly(imide siloxane) surfaces are much more rough than the surface of the pure polyimide. This would be consistent with our phase images and with the surface images of others studying poly(imide siloxane)s.[24,33]

These AFM images appear to show a phase separated copolymeric system on the surface. However, due to AFM's limitation to only study the surface of the samples, one should not conclude that the bulk is phase separated.

5.4.5.4 Small Angle X-ray Scattering (SAXS)

SAXS was utilized to determine if phase separation was present within the copolymer samples. This method analyzes the bulk of the sample, and serves as an excellent tool for determining the presence of microphase separation. The SAXS patterns of the three polymers are shown in Figure 5-23. . In the figure, s is the scattering vector and is defined as $s = (2/\lambda)\sin(\theta/2)$, where λ is the wavelength and θ is the scattering angle.

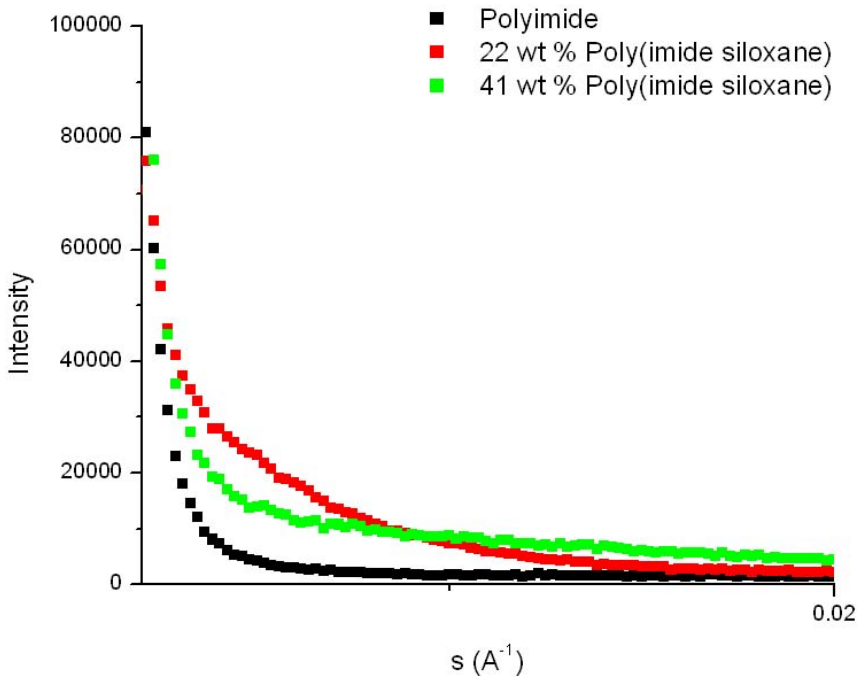

Figure 5-23. SAXS patterns of the pure polyimide, the 22 wt % poly(imide siloxane), and the 41 wt % poly(imide siloxane).

If any of the copolymers were microphase separated, there would be a shoulder in its SAXS pattern. As is evident from these patterns, there are no shoulders present for

any pattern suggesting there is no phase separation in the copolymers. However, one must consider that there must be a discrepancy in the scattering power between the two phases. If the scattering power of the PDMS phase is similar to that of the polyimide, it is possible SAXS would not reveal the presence of phase separation.

5.4.6 Permeability Measurements

5.4.6.1 Pure Polymer Membranes

Permeability measurements were gathered for the three pure polymer membranes. The procedure followed to prepare the membranes is listed in the Experimental section.

The permeability results for the pure polymers are listed in Table 5-3. The gases are listed in order of increasing kinetic diameter. The thicknesses of the pure polymer membranes tested ranged from 0.0035 ± 0.0006" for 6FDA-6FpDA to 0.0060 ± 0.0005" for the 41 wt % PDMS poly(imide siloxane).

Table 5-3. Pure gas permeabilities of the pure polyimide (0 wt % PDMS), the 22 wt % PDMS poly(imide siloxane), and the 41 wt % PDMS poly(imide siloxane).

	Permeability (Barrer)				
Wt % PDMS	**He**	**CO_2**	**O_2**	**N_2**	**CH_4**
0	45.78 ± 1.45	17.30 ± 0.49	4.17 ± 0.18	0.91 ± 0.01	0.58 ± 0.01
22	66.19 ± 7.82	76.76 ± 1.39	14.61 ± 0.43	4.60 ± 0.03	5.76 ± 0.57
41	85.85 ± 0.55	229.34 ± 1.78	48.17 ± 0.58	18.07 ± 0.36	41.91 ± 1.48

The permeability results followed the expected trend. Specifically, increased permeability with the addition of the highly permeable PDMS moiety was observed. The increases in permeability for each gas with the addition of PDMS roughly follow a relationship with size; the larger the gas the larger the increase in permeability. The

smallest molecule, He, increased about 1.9 fold, while the largest molecule (CH_4) experienced a 72-fold increase in permeability. The other gas permeabilities fell in between the two, but CO_2 saw a slightly larger increase in permeability than O_2 despite having a smaller kinetic diameter.

To determine what factors lead to these changes in permeability, the diffusion and solubility coefficients were determined using the Time Lag Method which is described in detail in the Literature Review. The diffusion coefficients (D) for the polymeric membranes are listed below in Table 5-4.

Table 5-4. Pure gas diffusion coefficients of the pure polyimide (0 wt % PDMS), the 22 wt % PDMS poly(imide siloxane), and the 41 wt % PDMS poly(imide siloxane).

	Diffusion Coefficient (cm^2 s^{-1})				
Wt % PDMS	**He**	**CO_2**	**O_2**	**N_2**	**CH_4**
0	-	2.43 ± 0.05	5.46 ±1.26	1.74 ± 0.02	0.39 ± 0.03
22	-	13.09 ± 0.21	27.82 ± 5.75	10.89 ± 0.47	4.88 ± 0.55
41	-	98.18 ± 2.76	144.44 ± 47.45	134.46 ± 59.25	75.75 ± 12.61

Helium diffusion coefficients are not reported for any of the membranes. This is because there is too much error in the measurement to make an accurate calculation. The Time Lag Method calculates the diffusion coefficient (D) using the following equation:

$$D = \frac{l^2}{6\theta} \qquad \text{Eq 5.1}$$

in this equation l^2 is the membrane thickness, and θ is the diffusive lag time. The diffusive lag time scales with how long a gas takes to diffuse through a membrane once a test has begun. Due to He's high permeability, this time is very short and was calculated to be approximately 1s in each run. Unfortunately, in our permeation apparatus, each gas

must flow from a gas tank and through several feet of steel tubing before it contacts the membrane. This obviously increases the time required for He to diffuse into the downstream side of the membrane, and introduces large errors. Because of the uncertainty in the true value of D for He, it was not reported. The other gases tested had much larger lag times, and any error introduced by this was negligible.

Over the range of PDMS content, the increases in diffusion coefficients for these gases is $CH_4 > N_2 > CO_2 > O_2$. Like the permeability, the largest increases are seen for the largest gases, and carbon dioxide and oxygen are reversed in this trend. The backbone of PDMS is more flexible than that of the polyimide at this temperature, as the T_g of PDMS is -123 ^oC.[34] This allows larger molecules to diffuse more easily than in a rigid polyimide, and leads to a higher diffusion coefficient.

The larger increase of D for carbon dioxide compared to oxygen is not easy to explain. One possible explanation is the already relatively large D of O_2 in the pure polyimide membrane. Because it is already twice that of CO_2, and even more when compared to N_2 and CH_4, oxygen may not benefit as much from the addition of PDMS as the others.

The solubility coefficients for the gases are shown below in Table 5-5.

Table 5-5. Pure gas solubility coefficients of the pure polyimide (0 wt % PDMS), the 22 wt % PDMS poly(imide siloxane), and the 41 wt % PDMS poly(imide siloxane).

Solubility Coefficient (cm^3_{gas} @ STP $cm^{-3}_{polymer}$ atm^{-1})

Wt % PDMS	He	CO_2	O_2	N_2	CH_4
0	-	5.42 ± 0.04	0.61 ± 0.19	0.39 ± 0.01	1.14 ± 0.07
22	-	4.46 ± 0.15	0.41 ± 0.09	0.32 ± 0.02	0.91 ± 0.18
41	-	1.78 ± 0.06	0.27 ± 0.08	0.12 ± 0.07	0.43 ± 0.06

The solubility coefficients (S) were determined using the following equation:

$$S = \frac{P}{D} \qquad \text{Eq 5.2}$$

here S is the solubility coefficient, and P is the permeability. Due to the absence of a reliable value of D for He, no S could be calculated for helium.

For the entire set of polymers the trend in solubility is $CO_2 > CH_4 > O_2 > N_2$. This trend is consistent with the factors which are known to determine solubility. The most influential parameter which determines a gas molecule's solubility is its ease of condensation. This can best be quantified by the molecule's critical temperature (T_C), which is the temperature below which the gas can liquefy by simply raising the pressure. The T_C's of the gases above are listed in Table 5-6.[35]

Table 5-6. Critical temperature of gases used in this study.

Gas	T_C (K)
CO_2	304.2
O_2	154.4
N_2	126.1
CH_4	190.7

As is evident from Table 5-6, the trend in T_C is the same as that for S, specifically, $CO_2 > CH_4 > O_2 > N_2$. This offers some explanation of why some gases have higher solubilities than others regardless of the polymer type.

Regardless of which gas is considered, in each case the solubility of the gas decreases as the PDMS loading increases. This is consistent with the work of others working with poly(imide siloxane)s.[36-38] Additionally, this is consistent with the Dual Mode Sorption model.[39] The Dual Mode Sorption (DMS) model was introduced in 1981, and since then has become the primary model for analysis of permeation through glassy membranes.[39] This model takes into account the two modes of sorption in glassy

polymers: sorption in between the polymer chains called the dissolved mode (C_D), and sorption in the free volume (i.e. Langmuir sites) referred to as the hole-filling mode (C_H).

The total concentration of penetrant (C) within a glassy amorphous polymer can be expressed as:

$$C = C_D + C_H \qquad \text{Eq 5.3}$$

C_D can be expressed using Henry's law, and C_H can be expressed using the equation below:

$$C_H = \frac{C_H' \cdot b \cdot P}{1 + b \cdot P} \qquad \text{Eq 5.4}$$

Substituting those equations into Eq (5.3) leads to the DMS model:

$$C = k_d P + \frac{C_H' \cdot b \cdot P}{1 + b \cdot P} \qquad \text{Eq 5.5}$$

typically, C is the concentration of gas within the polymer and carries units of cm^3 (STP)/$cm^3_{polymer}$, k_d is Henry's constant and has units of cm^3 (STP)/$cm^3_{polymer}$ atm, C_H' is the hole saturation constant and has units of cm^3 (STP)/$cm^3_{polymer}$, b is the affinity constant for the gas molecules to the Langmuir sites and has units of atm^{-1}, and P is the feed pressure in atm.

Tsujita et al were able to show that the changes in k_d relative to the changes in C_H' for a series of poly(imide siloxane)s was small. This suggests that the changes in solubility upon the addition of PDMS to a polyimide are more strongly associated with the loss of unrelaxed volume which serves as adsorption sites for gas molecules, than changes in the Henry's constant.

C_H' has been related to the excess volume through the following equation:[39]

$$C_H' = \left(\frac{V_g - V_l}{V_g} \right) \rho^* \qquad \text{Eq (5.6)}$$

where V_g is the specific volume of the glassy polymer, V_l is the specific volume of the hypothetical rubbery polymer, and ρ^* is the molar density of the penetrant.

The hole saturation constant is temperature dependant, because the unrelaxed volume in a glassy polymer can be reduced, if not eliminated by increasing the

temperature. As a glassy polymer is heated to its T_g, the polymer chains acquire more thermal energy to overcome rotational restrictions, and thus can adopt more conformations. When at or above its T_g, the chains have enough energy to pack differently, specifically, more efficiently, and reduce the excess volume within the polymer matrix. From Eq (5.6), it is evident that this phenomenon will force the value of V_g to approach that of V_l, and thus, C_H' will go to zero. Work by Koros et. al examined this concept in a study of poly(ethylene terephthalate) (PET) and CO_2.[40] The group determined the hole saturation constant of PET at different temperatures above and below PET's T_g. Their results showed a clear inverse relationship between C_H' and temperature; C_H' would go to zero as T_g was reached. A sample of their results is shown in Figure 5-24.[40] Studies by Toi et al. have verified that the relationship between C_H' and T_g is linear with an intercept at zero at a temperature equal to the T_g.[41] Tsujita et al verified the same trend for their poly(imide siloxanes).[37,38]

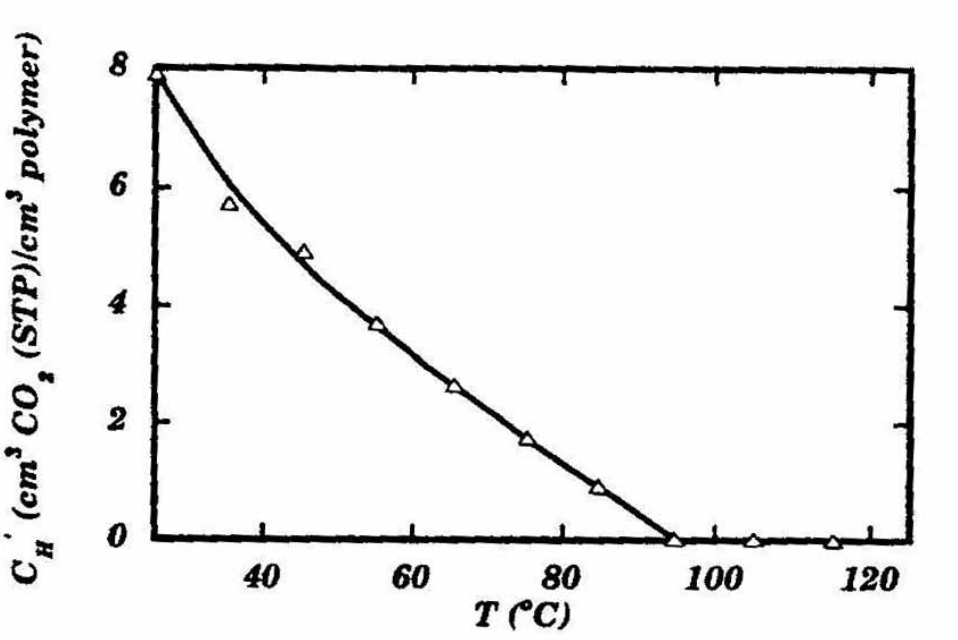

Figure 5-24. The effect of temperature on the Langmuir capacity constant for CO_2 in PET. Image taken from reference 40.

Perhaps a simpler way to explain the above idea is that the addition of PDMS lowers the number of Langmuir sites. The amount of PDMS in the copolymer comes at the expense of the glassy polyimide whose rigid nature creates the free volume which acts as sorption sites. Therefore, as the weight percent of PDMS increases, the weight percent of polyimide decreases, resulting in less sorption sites. This would lower the solubility as by lowering and eventually eliminating the second term in Eq (5.5).

The addition of PDMS also affects the solubility in a second way. S is a function of the interactions between the penetrant and the polymer. Some gases can have favorable interactions with polymer functional groups. CO_2 and N_2 have quadrupole moments which increase their solubility in polar polymers.[42] As the PDMS content increases at the expense of the polyimide content, functional groups such as C=O are reduced. This reduces the number of interactive sites of the polymer. Koros et al, performed a study in which the solubilities of CO_2 to CH_4 were reported for a series of polymers.[43] These polymers contained different amounts of polar functional groups. Their results showed that the solubilities of the gases were the highest in the polymers with the largest number of polar functional groups.[43] As the number of polar groups was decreased, the solubility decreased.

5.4.6.2 Mixed Matrix Membranes

Permeability measurements were gathered for the copolymer mixed matrix membranes. The procedure followed to prepare the membranes is listed in the Experimental section. Attempts at fabricating a 6FDA-6FpDA MMM with 20 wt % zeolite L were unsuccessful, as the membrane was too brittle to work with and fractured easily.

The permeability results for the mixed matrix membranes and their corresponding copolymers are listed in the tables in this section. The gases are listed in order of increasing kinetic diameter. The thicknesses of the mixed matrix membranes tested ranged from 0.0128 ± 0.0013” for the 20 wt % PDMS poly(imide siloxane) MMM to 0.0156 ± 0.0021” for the 40 wt % PDMS poly(imide siloxane).

5.4.6.2.1 20 wt % Zeolite L Mixed Matrix Membranes with 22 wt % PDMS Poly(imide siloxane) as the Polymer Matrix

The permeability results of the 20 wt % zeolite L MMM with 22 wt % PDMS poly(imide siloxane) as the polymer matrix are shown below in Table 5-7. The permeability for its corresponding pure polymer membrane has been listed as well for comparison. The gases are listed in order of increasing kinetic diameter.

Table 5-7. Pure gas permeabilities of the 22 wt % PDMS poly(imide siloxane) and the 20 wt % zeolite L MMM with 22 wt % PDMS poly(imide siloxane) as the polymer matrix.

22 wt % PDMS Poly(imide siloxane)

Membrane Permeabilities (Barrer)

Wt % Zeolite L	He	CO_2	O_2	N_2	CH_4
0	66.19 ± 7.82	76.76 ± 1.39	14.61 ± 0.43	4.60 ± 0.03	5.76 ± 0.57
20	47.11 ± 0.96	59.04 ± 0.40	10.78 ± 0.94	3.64 ± 0.11	4.98 ± 0.07
% Change	-28.83	-23.08	-26.22	-20.91	-13.55

As the table indicates, the permeability of each gas is less through the MMM relative to the pure polymer. The magnitude of the change in permeability closely mirrors that of the kinetic diameter with only O_2 and CO_2 reversed. Specifically, smaller gases experience a larger drop with the introduction of zeolite. To understand what may be leading to these results, the diffusion coefficients and solubility coefficients were determined using the Time Lag Method.

The diffusion coefficients for the same pair of membranes are listed below in Table 5-8. As mentioned in the Pure Polymer Membranes section, the diffusion coefficient of helium can not be calculated.

Table 5-8. Pure gas diffusion coefficients of the 22 wt % PDMS poly(imide siloxane) and the 20 wt % zeolite L MMM with 22 wt % PDMS poly(imide siloxane) as the polymer matrix.

22 wt % PDMS Poly(imide siloxane) Membrane

Diffusion Coefficients (cm^2 s^{-1})

Wt % Zeolite L	He	CO_2	O_2	N_2	CH_4
0	-	13.09 ± 0.21	27.82 ± 5.75	10.89 ± 0.47	4.88 ± 0.55
20	-	14.39 ± 0.33	27.28 ± 3.04	13.17 ± 3.25	6.51 ± 0.22
% Change	-	9.94	-0.14	20.96	33.37

Each gas saw no change in, or an increase in its diffusion coefficient with the introduction of zeolite L. Like the permeability, the two largest molecules (i.e. N_2 and CH_4) experienced the largest increases, while the smaller molecules (CO_2 and O_2) experienced a smaller increase or no increase. From this data, it appears as if the drops in permeability were not due to the diffusion coefficient, rather due to changes in the solubility.

The solubility coefficients for the same pair of membranes are listed below in Table 5-9. As mentioned in the Pure Polymer Membranes section, the diffusion coefficient of helium can not be calculated, therefore, the solubility coefficient of helium can not be calculated.

Table 5-9. Pure gas solubility coefficients of the 22 wt % PDMS poly(imide siloxane) and the 20 wt % zeolite L MMM with 22 wt % PDMS poly(imide siloxane) as the polymer matrix.

22 wt % PDMS Poly(imide siloxane) Membrane

Solubility Coefficients (cm^3_{gas}@STP $cm^{-3}_{polymer}$ atm^{-1})

Wt % Zeolite L	He	CO_2	O_2	N_2	CH_4
0	-	4.46 ± 0.15	0.41 ± 0.09	0.32 ± 0.02	0.91 ± 0.18
20	-	3.12 ± 0.05	0.30 ± 0.04	0.22 ± 0.07	0.58 ± 0.03
% Change	-	-30.04	-27.69	-31.05	-36.02

From this data it is evident that the drops in permeability with the addition of zeolite L were due to large drops in gas solubility. Interestingly, the range of % change in solubility (-27.7 – -36.0) is much smaller than that of the diffusion coefficient (0 – 33.7) and permeability (-28.8 - -13.6), though the reason for this is not yet understood. The addition of zeolite L was expected to lower the solubility of noninteracting gases such as methane and oxygen. However, it was expected to increase the solubility of gases such as CO_2 and N_2 which possess quadrupole moments. These gases should have electrostatic interactions with the cations residing in the zeolite pores. The intrinsic permeabilities, diffusivities and solubilities of these gases in zeolite L are not available as of this writing; this makes drawing conclusions difficult. A possible explanation is that the assumption that the sorption capacity of zeolite L is greater than that of the polyimide is incorrect. If the assumption were incorrect, the addition of zeolite merely added a less sorptive filler and would explain the drop in solubility. Additionally, the addition of zeolite L with its 0.71 nm pore would allow an easier diffusion should the gas molecules encounter a pore channel. If the increases in diffusion were overtaken by the losses in solubility, this could account for the drops in permeability.

5.4.6.2.2 20 wt % Zeolite L Mixed Matrix Membranes with 41 wt % PDMS Poly(imide siloxane) as the Polymer Matrix

The permeability results of the 20 wt % zeolite L MMM with 41 wt % PDMS poly(imide siloxane) as the polymer matrix are shown below in Table 5-10. The permeability for its corresponding pure polymer membrane have been listed as well for comparison. The gases are listed in order of increasing kinetic diameter.

Table 5-10. Pure gas permeabilities of the 41 wt % PDMS poly(imide siloxane) and the 20 wt % zeolite L MMM with 41 wt % PDMS poly(imide siloxane) as the polymer matrix.

41 wt % PDMS Poly(imide siloxane) Membrane Permeabilities (Barrer)

Wt % Zeolite L	He	CO_2	O_2	N_2	CH_4
0	85.85 ± 0.55	229.34 ± 1.78	48.17 ± 0.58	18.07 ± 0.36	41.91 ± 1.48
20	75.78 ± 1.3	199.41 ± 0.40	44.19 ± 1.19	17.57 ± 0.17	41.61 ± 0.10
% Change	-11.74	-13.05	-8.27	-2.78	-0.73

Like the 22 % PDMS poly(imide siloxane), the 41 wt % PDMS poly(imide siloxane) MMM has a lower permeability than its pure copolymer counterpart. There is a general trend with size as the larger gases have a smaller drop in permeability. When compared to the 22 % PDMS poly(imide siloxane) membranes, there is a smaller drop in permeability for each gas in the 41 % PDMSpoly(imide siloxane) membranes. To help explain these trends the diffusivity and solubility coefficients were determined.

The diffusion coefficients for the same pair of membranes are listed below in Table 5-11. As mentioned in the Pure Polymer Membranes section, the diffusion coefficient of helium can not be calculated.

Table 5-11. Pure gas diffusion coefficients of the 41 wt % PDMS poly(imide siloxane) and the 20 wt % zeolite L MMM with 41 wt % PDMS poly(imide siloxane) as the polymer matrix.

41 wt % PDMS Poly(imide siloxane) Membrane

Diffusion Coefficients (cm^2 s^{-1})

Wt % Zeolite L	He	CO_2	O_2	N_2	CH_4
0	-	98.18 ± 2.76	144.44 ± 47.75	134.46 ± 59.25	75.75 ± 12.61
20	-	66.20 ± 0.54	188.47 ± 3.91	110.03 ± 2.26	80.64 ± 0.97
% Change	-	-32.57	30.48	-18.16	6.46

As shown in the table, there does not appear to be a trend in the diffusion coefficient among the gases with respect to size.

The solubility coefficients for this pair of membranes are shown in Table 5-12. As mentioned in the Pure Polymer Membranes section, the diffusion coefficient of helium can not be calculated, therefore, the solubility coefficient of helium can not be calculated.

Table 5-12. Pure gas solubility coefficients of the 41 wt % PDMS poly(imide siloxane) and the 20 wt % zeolite L MMM with 41 wt % PDMS poly(imide siloxane) as the polymer matrix.

41 wt % PDMS Poly(imide siloxane) Membrane

Solubility Coefficients (cm^3_{gas}@STP $cm^{-3}_{polymer}$ atm^{-1})

Wt % Zeolite L	He	CO_2	O_2	N_2	CH_4
0	-	1.78 ± 0.06	0.27 ± 0.08	0.12 ± 0.07	0.43 ± 0.06
20	-	2.29 ± 0.01	0.18 ± 0.01	0.12 ± 0.01	0.39 ± 0.01
% Change	-	28.86	-34.14	-1.61	-8.24

Again there does not appear to be a trend between size and solubility with the addition of zeolite. The addition of zeolite L did result in a large increase solubility of CO_2 as was anticipated due to its quadrupole moment. Nitrogen, which also possesses a quadrupole moment, still has a very low T_C and saw essentially no change in it solubility. The two noninteracting gases, O_2 and CH_4, both saw drops in solubility; O_2 more so presumably due to its low T_C.

When we compare the MMMs with the same zeolite loading but different wt %s of PDMS, some insight into the drops in permeability can be made. Each gas has a lower solubility in the 41 wt % PDMS copolymer than in the 22 wt % PDMS copolymer for the reasons outlined in the Pure Polymer Membrane section. However, the addition of zeolite L in the 22 wt % PDMS copolymer resulted in a large loss of solubility regardless of the gas. This was not reciprocated in the 41 wt % PDMS copolymer, as it showed mixed results concerning changes in solubility. One possible explanation is that the solubility of some interactive gases in the zeolite is between that of PDMS and 6FDA-6FpDA. The addition of zeolite L essentially provided a more sorptive medium than the pure PDMS, and thus raised the solubility of some gases. This phenomenon would be more evident at larger PDMS loadings, where the zeolite could recover some of the

losses in S due to the PDMS. At higher polyimide loadings, the zeolite may actually appear more like nonsorping filler (or less sorping filler), and thus lower the solubility.

Comparing the diffusion coefficient of a gas in the different membranes is difficult. There does not appear to be any trend associated with the addition of zeolite. Perhaps these results would be better understood if the diffusion coefficients of these gases in zeolite L were available.

5.4.6.2.3 Mixed Matrix Membrane Properties as a Function of Zeolite L Loading

Mixed matrix membranes using 41 wt % PDMS poly(imide siloxane) as the polymer matrix were fabricated at different zeolite loadings. The zeolite loadings were 0, 20, and 30 % wt zeolite L. The pure copolymer membrane had a thickness of 0.0060 ± 0.0005", the 20 wt % zeolite L MMM had a thickness of 0.0156 ± 0.0021", and the 30 wt % zeolite L MMM had a thickness of 0.0111 ± 0.0010. The permeabilities of these membranes have been listed in Table 5-13.

Table 5-13. Pure gas permeabilities of the 41 wt % PDMS poly(imide siloxane) membranes at different zeolite L loadings.

41 wt % PDMS Poly(imide siloxane) Membrane Permeabilities (Barrer)

Wt % Zeolite L	He	CO_2	O_2	N_2	CH_4
0	85.85 ± 0.55	229.34 ± 1.78	48.17 ± 0.58	18.07 ± 0.36	41.91 ± 1.48
20	75.78 ± 1.3	199.41 ± 0.40	44.19 ± 1.19	17.57 ± 0.17	41.61 ± 0.10
30	81.2 ± 0.5	219.38 ± 0.99	47.57 ± 0.34	19.29 ± 0.13	47.15 ± 0.21

Except for methane, each gas has a lower permeability in the MMMs when compared to the pure copolymer. There does appear to be a small increase in

permeability when the zeolite loading is increased from 20 to 30 wt % zeolite. To provide some insight into causes of the changes, both the diffusivity coefficient and the solubility coefficient were determined.

The diffusion coefficients for each gas in the series of membranes are shown below in Table 5-14. As stated before, the diffusivity and solubility coefficients for helium could not be calculated.

Table 5-14. Pure gas diffusion coefficients of the 41 wt % PDMS poly(imide siloxane) membranes at different zeolite L loadings.

41 wt % PDMS Poly(imide siloxane) Membrane

Diffusion Coefficients (cm^2 s^{-1})

Wt % Zeolite L	He	CO_2	O_2	N_2	CH_4
0	-	98.18 ± 2.76	144.44 ± 47.75	134.46 ± 59.25	75.75 ± 12.61
20	-	66.20 ± 0.54	188.47 ± 3.91	110.03 ± 2.26	80.64 ± 0.97
30	-	65.25 ± 0.58	222.29 ± 0.16	122.43 ± 0.12	88.23 ± 0.18

As stated previously, once D has been calculated for a gas, S can be calculated from D and the permeability. The solubility coefficients for each gas in the series of membranes are shown in Table 5-15.

Table 5-15. Pure gas solubility coefficients of the 41 wt % PDMS poly(imide siloxane) membranes at different zeolite L loadings.

41 wt % PDMS Poly(imide siloxane) Membrane

Solubility Coefficients (cm^3_{gas}@STP $cm^{-3}_{polymer}$ atm^{-1})

Wt % Zeolite L	He	CO_2	O_2	N_2	CH_4
0	-	1.78 ± 0.06	0.27 ± 0.08	0.12 ± 0.07	0.43 ± 0.06
20	-	2.29 ± 0.01	0.18 ± 0.01	0.12 ± 0.01	0.39 ± 0.01
30	-	2.56 ± 0.03	0.16 ± 0.01	0.12 ± 0.01	0.41 ± 0.01

The solubility trends largely agree with what was expected. Carbon dioxide saw a large increase in solubility, while the others saw no change or decreases in solubility. The diffusion coefficients again make it difficult to draw conclusions. The changes do not correlate with size. Until the permeability properties of pure zeolite L are obtained, no conclusions about the relation between zeolite L loading and D should be made.

5.4.7 Robeson Diagram for all Membranes

A Robeson diagram, or upper bound plot, provides a visual description of the separation performance of a membrane. Additionally, it acts as a method to quickly compare the performance of several membranes at once.

Each membrane's separation performance for the CO_2/CH_4 separation is shown below on a Robeson diagram Figure 5-25. A MMM composed of only zeolite L and the pure polyimide is not shown, because it was never successfully fabricated.

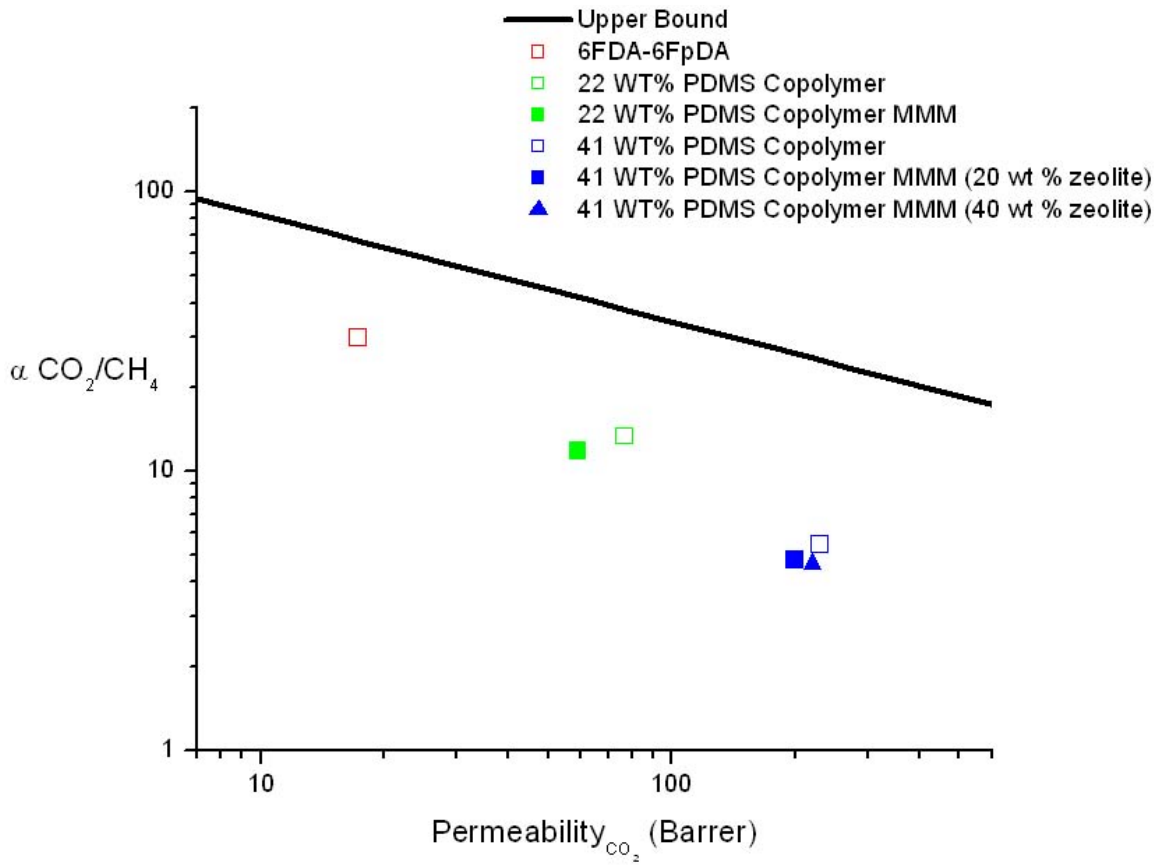

Figure 5-25. Trade-off diagram for the CO_2/CH_4 separation for all membranes included in this study.

As is evident from the figure, the addition of zeolite L to the copolymers did not improve their separation performance. In each case a drop in both selectivity and permeability was observed. However, one must use caution in concluding that these MMM systems do not offer better performance relative to the pure polymer. As mentioned before, zeolite L separates based on a selective adsorption method, in which molecules such as CO_2 which can interact with the cations in the pores are adsorbed to the exclusion of another noninteracting gas (e.g. CH_4). The selectivities shown in the figure were determined by ratioing the pure gas permeabilities. Zeolite L needs a mixed gas feed to truly display its separation capabilities. While mixed gas permeation experiments would likely slightly lower the permeability values of the gases, it could

reveal much better selectivity values than what we determined. It would be interesting to know the true selectivities of the MMMs to accurately determine if these membranes truly operate above the upper bound. Furthermore, if the selectivities were extrodinarly high, one might suspect they broke the asymptotic limit of the upper bound proposed by Freemen, however, because Freemen's work for purely polymeric systems only, it can not be applied to these MMMs.[2]

5.5 Conclusions

A glassy polyimide, 6FDA-6FpDA, and block copolymers composed of 6FDA-6FpDA and amine-terminated polydimethylsiloxane were synthesized at varying weight-percents of PDMS using a bulk imidization technique. Qualitative confirmation of imidization was performed via FTIR, and the weight-percent PDMS of each copolymer was determined using ^{1}H-NMR to be 22 and 41 wt %. Each polymer was used to fabricate gas separation membranes. Additionally, mixed matrix membranes composed of copolymer and zeolite L were prepared by solution casting using the procedure outlined in this chapter. This procedure lead to defect-free mixed matrix membranes suitable for gas separations. Attempts at preparing a MMM using the pure polyimide failed due to the membranes brittle nature.

TEM, SAXS, and AFM were employed to characterize the morphology of the membranes as well as verify the presence of phase separation. While TEM and SAXS did not provide any indication of phase separation in the copolymers, phase images taken using AFM showed a phase separated system on the surface. Additionally, it was noted using 3-D height images obtained using AFM that the addition of PDMS in the polymer backbone lead to a rougher surface.

SEM images were taken of the MMMs. In each case there was no evidence of the polymer delaminating from the zeolite surfaces. Additionally, there was no evidence of the zeolite agglomerating, suggesting a good dispersion.

Pure gas permeability tests were performed using He, O_2, N_2, CH_4 and CO_2 for each polymeric membrane and its corresponding MMMs. In the pure polymer systems, the addition of PDMS to the polyimide backbone leads to increased permeability and

decreased selectivity. Evaluation of the diffusion and solubility coefficients showed the addition of siloxane segments drastically increased D, while lowering S for each gas.

The addition of zeolites to the copolymer systems resulted in a loss of both permeability and selectivity for each system. The permeability of He dropped with the addition of zeolite, suggesting that the incorporation of PDMS into the polyimide's backbone was sufficient to prevent unselective voids at the polymer-zeolite interface. While the 22 wt % PDMS poly(imide siloxane) MMM showed increases in D and losses in S with the addition of zeolite L, the 41 wt % PDMS poly(imide siloxane) MMM did not reveal a strong trend with the addition of zeolite L for either coefficient.

A series of membranes with different zeolite L loadings was made using 41 wt % PDMS poly(imide siloxane) as the polymer matrix. Zeolite L loadings were made at 0, 20, and 30 wt%. While the permeability dropped relative to the pure polymer for every gas at 20 wt % zeolite L, the permeabilities of the gases began to approach and in some cases surpass that of the pure polymer at 30 wt % zeolite L. The diffusion coefficients trends depended on the gas, and did not correlate with the size of the gas. Carbon dioxide saw a large increase in solubility with each increase in zeolite loading as was expected. Nitrogen and methane did not experience a change in their solubilities, while the weakest sorbing gas oxygen saw a drop in solubility with each increase in zeolite loading.

None of the MMMs offered an increase in ideal selectivity, however, to gauge the true separation performance of these materials, mixed gas experiments need to be performed.

5.6 References

1 Robeson, L. M. *Journal of Membranes Science* 1991, *61*, 165-185.

2 Freeman, B. *Macromolecules* 1999, *32*, 375-380.

3 Brandt, W. W. *Journal of Physics and Chemistry* 1959, *63*, 1080.

4 Te Hennepe, H.; Bargeman, D.; Mulder, M.; Smolders, C. *Journal of Membrane Science* 1987, *35*, 39-55.

5 Jia, M.; Peinemann, K.-V.; Behling, R.-D. *Journal of Membrane Science* 1991, *57*, 289-292.

6 Jia, M.-D.; Pleinemann, K.-V.; Behling, R.-D. *Journal of Membrane Science* 1992, *73*, 119-128.

7 Duval, J.-M.; Folkers, B.; Mulder, M. H. V.; Desgrandchamps, G.; Smolders, C. A. *Journal of Membrane Science* 1993, *80*, 189-198.

8 Tantekin-Ersolmaz, S. B.; Atalay-Oral, C.; Tather, M.; Erdem-Senatalar, A.; Schoeman, B.; Sterte, J. *Journal of Membrane Science* 2000, *175*, 285-288.

9 Koros, W. J.; Mahajan, R. *Industrial Engineering and Chemistry Research* 2000, *39*, 2692-2696.

10 Koros, W. J.; Zimmerman, C. M.; Singh, A. *Journal of Membranes Science* 1997, *137*, 145-154.

11 Park, H. C.; Yong, H. H.; Kang, Y. S.; Won, J.; Kim, W. N. *Journal of Membranes Science* 2001, *188*, 151-163.

12 Koros, W. J.; Mahajan, R.; Burns, R.; Schaeffer, M. *Journal of Applied Polymer Science* 2002, *86*, 881-890.

13 Koros, W. J.; Mahajan, R. *Polymer Engineering and Science* 2002, *42*, 1420-1431.

14 Koros, W. J.; Mahajan, R. *Polymer Engineering and Science* 2002, *42*, 1432-1441.

15 Tsapatsis, M.; Lovallo, M.; Okubo, T.; Davis, M.; Sadakata, M. *Chem. Mater.* 1995, *7*, 1734-1741.

16 Alpert, N. K., W.E.; Szymanski, H.A.;. *Ir-Theory and Practice of Infrared Spectroscopy*; Plenum Publishing Corporation: New York, 1970.

17 Silverstein, R.; Webster, F. *Spectrometric Indentification of Organic Compounds*, 6 ed.; John Wiley & Sons, Inc: New York, 1998.

18 Crank, J. *The Mathematics of Diffusion*, 2 ed.; Oxford Press: London, 1990.

19 Husk, G.; Cassidy, P.; Gebert, K. *Macromolecules* 1988, *21*, 1234-1238.

20 Becker, K. H.; Schmidt, H. W. *Macromolecules* 1992, *25*, 6784-6790.

21 Kim, J. H.; Lee, S. B.; S.Y., K. *Journal of Applied Polymer Science* 2000, *77*, 2756-2767.

22 Park, H.; Kim, J.; Nam, S.; Y, L. *Journal of Membrane Science* 2003, *220*, 59-73.

23 McGrath, J.; Dunson, D.; Mecham, S.; Hedrick, J. *Advances in Polymer Science* 1999, *140*, 61-105.

24 Bowens, A. In *Synthesis and characterization of poly(siloxane imide) block copolymers and end-functional polyimides for interphase applications*; Virginia Tech: Blacksburg, 1999.

25 Solomons, T. *Organic Chemistry*, 5 ed.; John Wiley & Sons, Inc: New York, 1992.

26 Gottlieb, H. E.; Kotlyar, V.; Nudelman, A. *Journal of Organic Chemistry* 1997, *62*, 7512-7515.

27 McGrath, J. E.; Arnold, C. A.; Summers, J. D.; Chen, Y. P.; Bott, R. H.; Chen, D. 1989.

28 Suer, M. G.; Bac, N.; Yilmaz, L. *Journal of Membranes Science* 1994, *91*, 77.

29 Gur, T. M. *Journal of Membranes Science* 1994, *93*, 283-239.

30 Rogers, M. E.; Glass, T. E.; Mecham, S. J.; Rodrigues, D.; Wilkes, G. L.; McGrath, J. *Journal of Applied Polymer Science Part A: Polymer Chemistry* 1994, *32*, 2663.

31 Shafrin, E. G. In *Polymer Handbook*; Brandrup, J.; Immergut, E. H., Eds.; John Wiley: New York, 1975; pp 111-221.

32 Yilgor, I.; McGrath, J. In *Advancees in Polymer Science*; Benoit, H.; Fujita, H., Eds.; Springer-Verlag: New York, 1988; Vol. 86, pp 1-86.

33 Furukawa N, Y. Y., Furukawa M, Yuasa M, Kimura Y. *JOURNAL OF POLYMER SCIENCE PART A-POLYMER CHEMISTRY* 1997, *35*, 2239-2251.

34 Sperling, L. *Introduction to Physical Polymer Science*, 2 ed.; John Wiley & Sons, Inc.: New York, 1992.

35 Mulder, M. *Basic Principles of Membrane Technology*, 1 ed.; Kluwer Academic Publishers: Boston, 1991.

36 Chen, S. H.; Lee, M.-H.; Lai, J.-Y. *European Polymer Journal* 1996, *12*, 1403-1408.

37 Nakagawa, T.; Nishimura, T.; Higuchi, A. *Journal of Membrane Science* 2002, *206*, 149-163.

38 Tsujita, Y.; Yoshimura, K.; Yoshimuzu, A.; Kinoshita, T. *Polymer* 1993, *34*, 2597-2601.

39 Koros, W. J.; Chern, R. T.; Stannett, V. T.; Hopfenberg, H. B. *Journal of Polymer Science: Physics Edition* 1981, *19*, 1513-1530.

40 Koros, W. J.; Paul, D. R. *Journal of Polymer Science: Polymer Physics Edition* 1978, *16*, 1947-1963.

41 Toi, K.; Morel, G.; Paul, D. R. *Journal of Applied Polymer Science* 1982, *27*, 2997.

42 Freeman, B. D.; Ghosal, K. *Polymers for Advanced Technologies* 1994, *5*, 673-697.

43 Koros, W. J.; Paul, D. R. In *Synthetic Membranes*; Chenoweth, M. B., Ed.; Harwood Academic Publishers: New York, 1986.

Chapter 6 Preparation and Characterization of Poly(imide siloxane) and Carbon Nanotube Mixed Matrix Membranes

6.1 Abstract

Mixed matrix membranes composed of a poly(imide siloxane) copolymer and carbon nanotubes were fabricated. The copolymer contained 41 wt % PDMS as determined using ^{1}H-NMR. Mixed matrix membranes were prepared using both open-ended and close-ended carbon nanotubes. SEM images were taken of the surface and cross section of the membranes to search for voids between the two components as well as investigate the degree of nanotubes dispersion in the membrane. Pure gas permeation experiments were performed using He and N_2.

6.2 Introduction

Polymeric membranes designed for gas separations have been known to have a trade-off between permeability and selectivity as shown in upper bound curves developed by Robeson.[1] Attempts at merely altering the chemical structure of the polymer have begun to offer diminishing returns in improved performance. Recent theoretical work by Freemen concluded that there is an asymptotic limit to the separation capabilities of polymeric membranes.[2] Unless new systems are developed to improve membrane performance, membranes will continue to be limited to a few niche applications.[3]

Recent work focused on developing the membranes capable of operating above the upper bound have focused on mixed matrix membranes (MMMs). These membranes combine polymer with a filler, usually zeolite. Early attempts at fabricating MMMs used rubbery polymers and zeolites.[4-7] These membranes proved to be successful at pervaporation applications such as separating ethanol from water. Later work would involve using glassy polymers and zeolites to prepare MMMs suitable for gas separation applications.[5,8-11] While some of the glassy MMMs did offer improvements in selectivity, they often were accompanied with losses in selectivity. However, it should be noted that research on glassy MMMs is still in its early stages as the first publication on this topic appeared in 1993. [11]

A potential filler which has not received any attention for use in MMMs for gas separations is carbon nanotubes (CNTs). In depth reviews of this type of material are available elsewhere.[16] Briefly stated, carbon nanotubes are graphite sheets rolled into circular bundles. They can be synthesized to have diameters of several angstroms or tens of nanometers, and their lengths can be up to several micrometers. Additionally, these tubes can be synthesized as singular tubes called single walled nanotubes (SWNTs) or as a series of shells of different diameters spaced around a common axis called multiwalled nanotubes. In both cases the ends of the CNTs can be open or closed. Some of the attractive characteristics of CNTs are their outstanding mechanical properties, their high strength-to-weight ratio, and their excellent thermal stability.

Simulations predicting the diffusivity properties of simple gases in CNTs show that these materials may be suitable filler for a polymer to make MMMs. Ackerman et al performed atomistic simulations of diffusion of pure Ar and Ne through SWNT's.[17] For comparison, they also predicted the diffusion of these gases through the zeolite silicalite. Their results predicted that the self diffusivity of Ar in SWNT's was orders of magnitude larger than in silicalite. At low pressures the self diffusivity in the CNTs was predicted to be on the order of 10^{-1} $cm^{-2}s^{-1}$ which was much higher than the 10^{-4} $cm^{-2}s^{-1}$ of silicalite. However, as the pressure was increased to 80 bar, the self diffusivity of Ar in the SWNT's dropped to 10^{-3} $cm^{-2}s^{-1}$ while that of Ar in zeolite was relatively unchanged. This was attributed to the very smooth surface of the interior of the CNT's. At low pressures the adsorbed Ar molecules are well separated from each other, but as the

pressure increases this is no longer true. Therefore, the diffusivity begins to become affected by atom-atom collisions. This same trend was predicted for Ne.

To date there is only one publication in which a CNT-polymer MMM was fabricated. In that study, Hinds et al developed a MWNT-polystyrene MMM and measured N_2 permeation as well as the transport of $Ru(NH_3)_6^{3+}$ across the membrane in aqueous solution.[18] The tubes within this membrane were well aligned during their synthesis using vapor deposition on a quartz substrate, and a toluene-polystyrene solution was spin coated over the grown MWNT's. The tubes had diameters ranging from 5-10 nm. To remove the film from the quartz after the solution was dried, hydrofluoric acid was employed. This technique resulted in a MWNT-polystyrene membrane film of 5 to 10 μm in thickness. These films were then put under a plasma oxidation treatment to etch away the surfaces of films. Because polystyrene etches faster the CNT's, this process effectively removed any polymer film covering the pores of the MWNT's.

Permeation experiments of pure N_2 and aqueous $Ru(NH_3)_6^{3+}$ were gathered at room temperature. Nitrogen permeance showed a linear relation with pressure drop across the membrane, with a value of 2.6 μmol $m^{-2}s^{-1}Pa^{-1}$. For an aqueous solution of $Ru(NH_3)_6^{3+}$, another linear relationship with pressure across the membrane was observed. The flux was measured to be 0.9 μmol $cm^{-2}h^{-1}$. In an attempt to control the flow rate of the ion through the CNT membrane, the authors coated that tip of the membranes with carboxylic groups, intending the slow the transport of the positive ion through interactions with the anion of the carboxylic groups. This method reduced the flux by a factor of 5.5, suggesting that fluxes of molecules could be controlled through these types of membranes.

In this chapter the preliminary work on developing mixed matrix membranes using a poly(imide siloxane) and carbon nanotubes is presented. Based on the work outlined above, the intent of this investigation was to add CNTs to a polymer matrix to improve its permeability properties. While no improvements in selectivity were anticipated with the addition of the CNTs, it was believed that the increases in permeability would be so large that they would offset any selectivity losses. This method could lead to membranes which would operate above the upper bound as shown below in Figure 6-1.

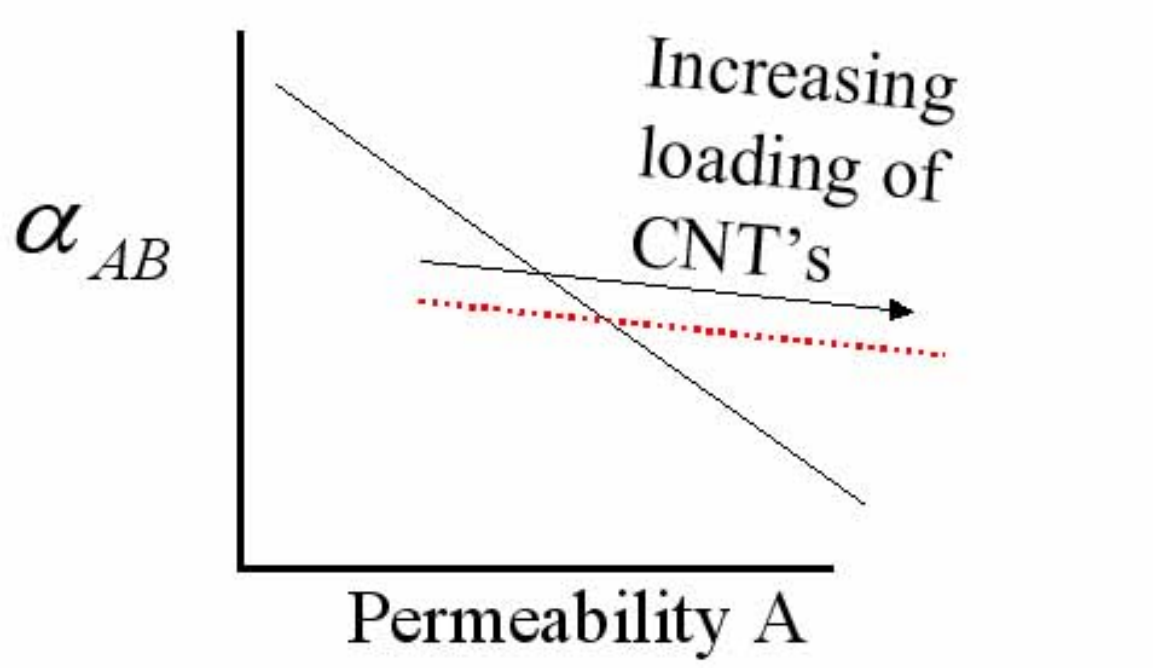

Figure 6-1. Proposed poly(imide siloxane) and carbon nanotube mixed matrix membrane performance as a function of nanotube loading.

A fabrication method as well as SEM images of the membranes are discussed. The permeation properties of the pure poly(imide siloxane) and the MMMs using open-ended and closed-ended single walled nanotubes are listed as well.

6.3 Experimental

6.3.1 Materials

6.3.1.1 Solvents

Tetrahydrofuran (THF)

THF was purchased from E.M. Sciences (99.5%) and was refluxed over sodium (Aldrich) with a nitrogen purge using benzophenone as an indicator until dark purple. It was then distilled immediately before use.

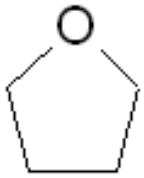

Hexane

Hexane from EMD (98.5%, HPLC grade) was purchased and used as received. It was used to extract unreacted PDMS from the copolymer after imidization.

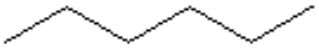

6.3.1.2 Monomers

4,4'-(Hexafluoroisopropylidene)diphthalic Anhydride (6FDA)

6FDA was purchased from Clariant with a purity >99.95. Prior to use the material was placed under vacuum at a temperature of 150 ^{o}C to ensure compete anhydride cyclization immediately prior to use.

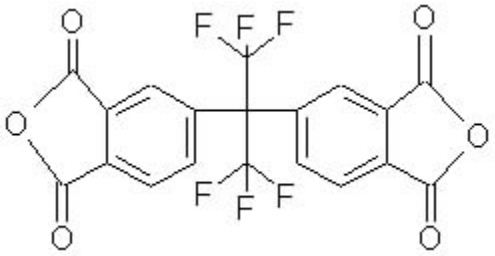

4,4'(Hexafluoroisopropylidene)dianiline (6FpDA)

6FpDA was purchased from SynQuest labs with a purity of >98. The monomer was sublimed near 180 ^{o}C for further purification. After sublimation 6FpDA was kept in a dry box to avoid moisture contact.

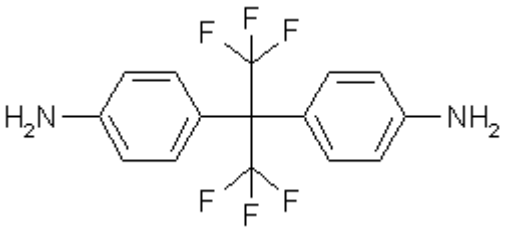

Aminopropyl Terminated Polydimethylsiloxane (PDMS)

PDMS was purchased from Gelest and used as received. Its M_n was determined using ^{1}H-NMR to be 886 g/mol.

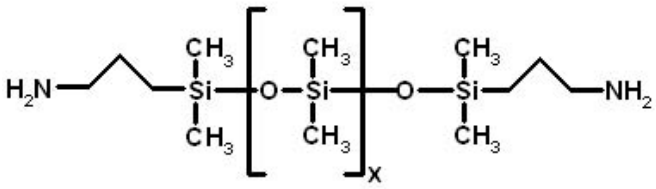

6.3.1.3 Carbon Nanotubes

Both closed-ended and open-ended single walled carbon nanotubes were purchased from Carbon Solutions, Inc. and used as received. The closed-ended nanotubes had a purity from 70-90 %, and the open-ended had a purity from 60-80%. The average diameter of individual anotubes was 1.4 ± 0.2 nm and the range of lengths for individual nanotubes was 50 - 500 nm. These individual tubes are typically in bundles of tubes with lengths of 0.5 – 1.5 microns.

6.3.2 Synthesis of 6FDA-6FpDA-PDMS Copolymer

A poly(imide siloxane) was synthesized with a targeted PDMS wt % of 40.

6FDA (4.287 g) was added to a 100 mL three necked round bottom under argon flow. THF was added immediately after. The solution was mechanically stirred (40 rpm) for 2 hours to allow the 6FDA to dissolve and disperse well.

Amine terminated PDMS (4.000 g) was added to the solution at an average rate of 0.5406 mL/h at room temperature. This was to ensure that the dianhydride was always in

excess and immediately endcapped the PDMS monomer. After the addition of PDMS the solution was allowed to react for 24 hours.

6FpDA (1.7128 g) was added to the solution, and the solution was mixed for 24 hours at room temperature. After this time it was cast onto a 8.5" diameter Teflon coated pan. The pan was covered with a glass plate to help slow evaporation. The solution was given 24 hours to dry at room temperature.

Once dry, the film was placed under vacuum and the temperature was raised to its expected T_g for 6 hours. During this time, the polyamic acid thermally imidized to become a polyimide. The film was then allowed to cool to room temperature under vacuum.

Imidized films were dissolved in THF, and cast into a hexane bath for 3 days to remove unreacted PDMS monomer. During this time the hexane was changed daily. After the three days the polymer was allowed to air-dry and placed under vacuum overnight to remove any residual solvent.

The polyimide film was redissolved in THF and filtered using a 5 μm filter. The filtered solution was immediately cast onto a Teflon plate and allowed to dry. This procedure gave mostly clear films with a dark yellow shade. Following this, it was stored in a dessicator until needed.

6.3.3 Fabrication 6FDA-6FpDA-PDMS Copolymer Membranes

1.25 grams of the copolymer were dissolved in 20 mL of THF and stirred for two days. The volume of solution was evaporated to 10 mL over this time, leading to a viscous solution. The solution was cast into a 2.5" diameter Teflon coated pan. The pan was covered with a glass plate to slow the evaporation of solvent allowing for a film with a uniform thickness without curling. The solutions were given 2 days to dry at room tempreature.

Once dry, the films were placed under vacuum and the temperature was raised to 100 ^{o}C for 12 hours. After this period the films were allowed to cool to room temperature under vacuum over a 6 hour period.

A 2.5” diameter circular sample was cut from the film and used for permeation tests.

6.3.4 Fabrication of Poly(imide siloxane)-Carbon Nanotube Mixed MatrixMembranes

The fabrication procedures for the mixed matrix membranes were identical, regardless of the type of nanotubes employed. The only difference was the amount of nanotubes added to make a 1 or 10 wt % CNT MMM.

Approximately 1.3 grams of the pure polymer was dissolved into 20 mL of THF and mixed for 24 hours. After this time a predetermined mass to make a desired loading of CNT was added to the polymer solution. The mixture was allowed to mix for 24 hours at room temperature.

Following this time period, the mixture was sonicated for 15 minutes, after which it was allowed to mix for 15 minutes. This process was repeated for several hours.

During this time the volume of the mixture reduced to roughly 10 mL and became viscous. The mixture was cast into a 2.5” diameter Teflon coated pan and was immediately covered with a glass plate to ensure a slow evaporation of the solvent. A slow evaporation of the solvent would reduce solvent concentrations within the film, and lead to more uniformly thick film without curling. The mixture was allowed to dry over a 2 day period at room temperature.

After drying the film was placed under vacuum and the temperature was raised to 100 ^{o}C for 12 hours. Following this the film was allowed to cool to room temperature under vacuum over a 6 hour period.

A 2.5” diameter circular sample was cut from the film and used for permeation tests.

6.3.5 Membrane Characterization

Fourier Transform Infrared Spectroscopy was used for the purposes of identifying functional groups of the synthesized polymers and studying the interactions between the

components of each membrane (e.g. hydrogen bonding). The FTIR used in this study was a BIO-RAD FTS-40A. This model was equipped with a liquid nitrogen cooled MCT detector and was capable of gathering spectra in the 4000 – 400 cm^{-1} region. The FTIR was set with a wave number resolution of 1 cm^{-1} and an aperture of 2 cm. The computer software which ran the FTIR was BIO-RAD WinIR Ver. 3.0.

Transmission spectroscopy was used for gathering the spectra of the samples. Samples were prepared from solutions. A pipette was used to transfer a small repeatable amount of solution to the CaF_2 plate or KBr plate which would dry as a thin film. The films would be allowed to air dry, and then placed in the vacuum oven at room temperature to remove any residual solvent.

CaF_2 plates were used for investigating the region between 4000 and 1100 cm^{-1} and KBr plates were used when investigating the region between 1100 and 400 cm^{-1}. The sample compartment was continually purged with dry air during the time a spectrum was being gathered from it.

Spectral peaks were numbered automatically by the software, and when necessary the software was used to make a baseline to a spectrum. Peaks were assigned to specific groups using two separate books by Alpert and Silverstein.[19,20] Evidence of hydrogen bonding between components was taken as shifts to lower wavenumbers.

Molecular weights were determined using a Waters SEC apparatus equipped with an autosampler, a 410 refractive index detector, and an in-line miniDawn multiangle laser light scattering detector with 690 nm laser. The GPC was operated by Ann Fornoff of Dr. Long's group in the Chemistry Department. Samples were run in THF (ACS grade) at 40 ^{o}C using polystyrene standards. Three samples from each batch of polymer were analyzed to provide a statistical distribution.

400 MHz ^{1}H-NMR was employed for determining the weight percent of PDMS incorporated into the copolymer. A Varian INOVA spectrometer was the model used. Samples were prepared from 15 -20mg of polymer in 0.7 mL of d6-acetone. The solution was held in a 5 mm diameter and 8" long NMR tube from Ace Glass Inc.

FESEM was used in this research for the purpose of studying the morphology of the materials, to look for delamination of the organics from the inorganics, and to verify if phase separation existed in the block copolymers. The FESEM used in this study was a

LEO 1550 which was equipped with two secondary electron detectors, and a five axis (i.e. x, y, z, θ, φ) sample stage.

Samples used to gather surface images were cut from cast films. These samples were mounted onto a sample holder using a conductive double stick tape. Sample used for cross sectional images were first immersed in liquid nitrogen, and then snapped in half before mounting. Due to polymers being poor conductors, the samples were coated with a 7 nm gold coating using a Crussington 208HR Sputter Coater. Mounted samples were placed into the sputter coater which was pumped down and flushed with argon several times. The samples would then be put under vacuum and the gold coating was applied.

Permeabilities of polymeric membranes and composite membranes were measured using a constant volume varying pressure apparatus. Permeability was measured directly, and the Time Lag Method was applied to the recorded data to determine the diffusivity coefficient as outlined in the Literature Review.[21] The solubility coefficient was taken as the ratio of the permeability to diffusivity coefficient. A schematic of the permeation system is shown in Figure 6-2.

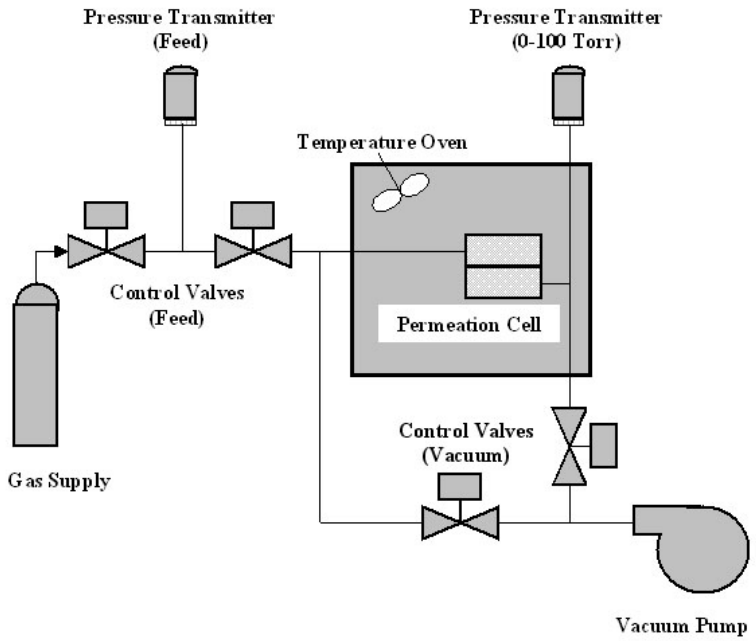

Figure 6-2. Schematic of the system used to perform permeation experiments.

Gas pressures of the permeation setup were monitored using two pressure transducers. The gas feed pressure was measured using a pressure transducer from Omega. The model number was PX621-300G10V, and it had a range of 0 - 300 psig. The permeate pressure was measured using a MKS Instruments pressure transducer (model number 722A12TCE2FA). This pressure transducer had a range of 0 – 100 torr.

The permeation cell was isolated from its surroundings using an insulated box. The temperature within the box was controlled using an Omegalux silicone rubber flexible heater whose output was regulated by an electronic digital. An Omega resistance thermal detector with a resistance of 100 ohms was used to measure the temperature of the cell and feed gas. Air was circulated within the box using a computer fan.

The gases used in this research were He, CO_2, O_2, N_2, and CH_4. Each gas possessed a purity of 99.99% and was used as received from Air Products. The feed pressure was kept constant at 4 atm for all experiments. The temperature was kept constant at 35 ^oC for all experiments in this research. Each gas was run through a membrane six times and the average results and the standard deviations were reported.

Membranes samples were cut into 2.0" diameter circles and placed into a permeation cell. The samples were placed onto a microporous alumina support and sealed within the cell. A picture of the permeation cell is listed in Figure 6-3. The cell was custom manufactured, composed of stainless steel, and fitted with three separate gaskets to prevent leaks. The two sides were connected using six ¼" hex bolts.

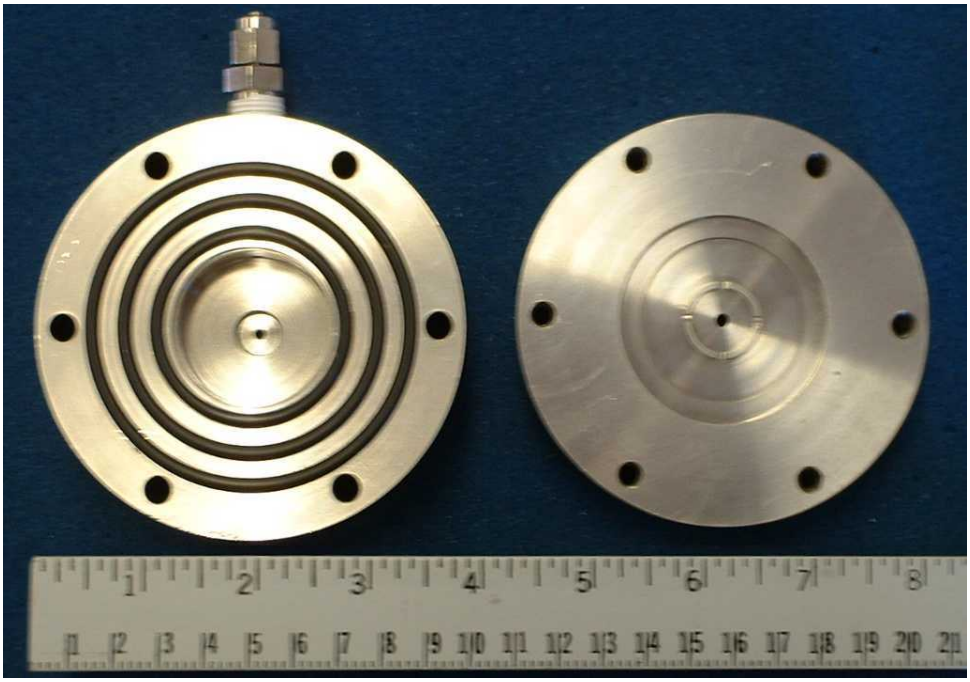

Figure 6-3. Image of the permeation cell used in this study. The left half of the cell is the feed side and contains the three gaskets used to prevent leaks. The center of the left piece is a hallow cavity. The right piece is the permeate side and hold the membrene and microporous alumina support (not shown).

Recorded data was analyzed using the Time Lag method with the aide of the software programs Microcal Origin (v6.0) and MS Excel (Office 2000). Background noise contributions to the permeate pressure were accounted for by adjusting the permeation pressure values at the very beginning of each test to a value of zero. The adjusted permeation data was plotted against time, and the slope was determined using the *Linear Fit* function in Microcal Origin. Data from a typical run is shown below in Figure 6-4.

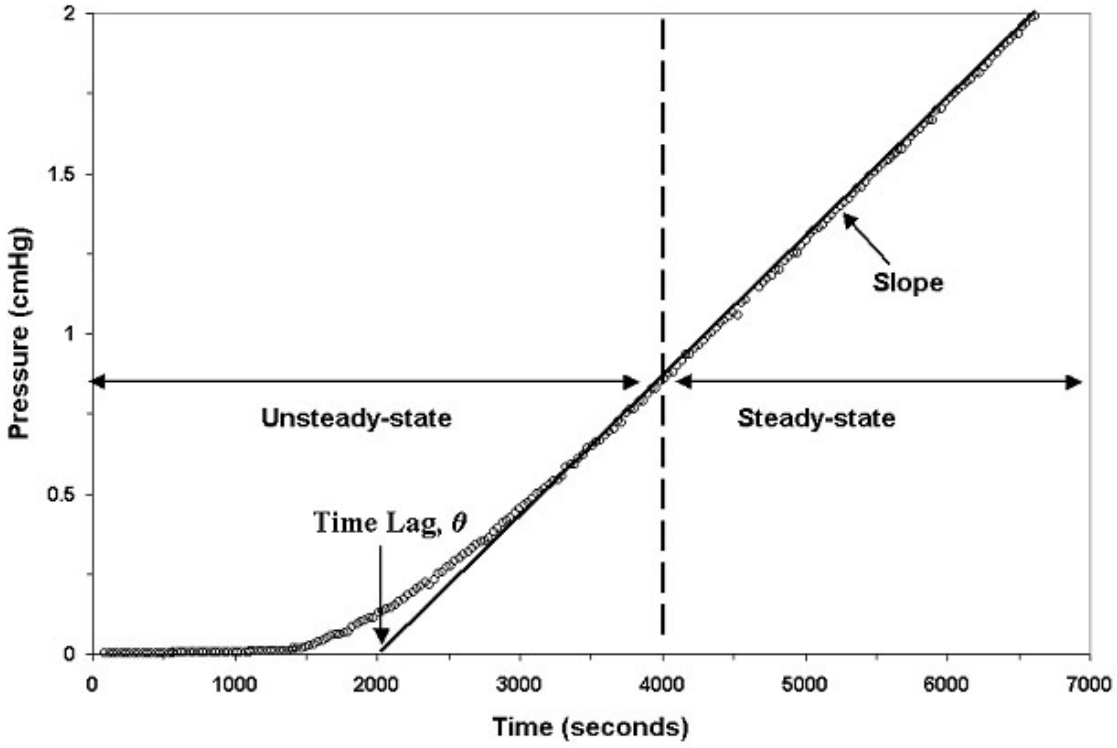

Figure 6-4. Typical permeation experiment data analyzed using Time Lag Method.

Ideal selectivities were calculated by ratioing the pure gas permeabilities.

6.4 Results and Discussion

6.4.1 Copolymer Synthesis

Using the procedure outlined in the Experimental section, 6FDA-6FpDA-PDMS was synthesized using a step growth reaction.[22] The copolymer was synthesized with a targeted PDMS weight % of 40. The first step of the reaction scheme to synthesize 6FDA-6FpDA-PDMS is shown below in Figure 6-5.

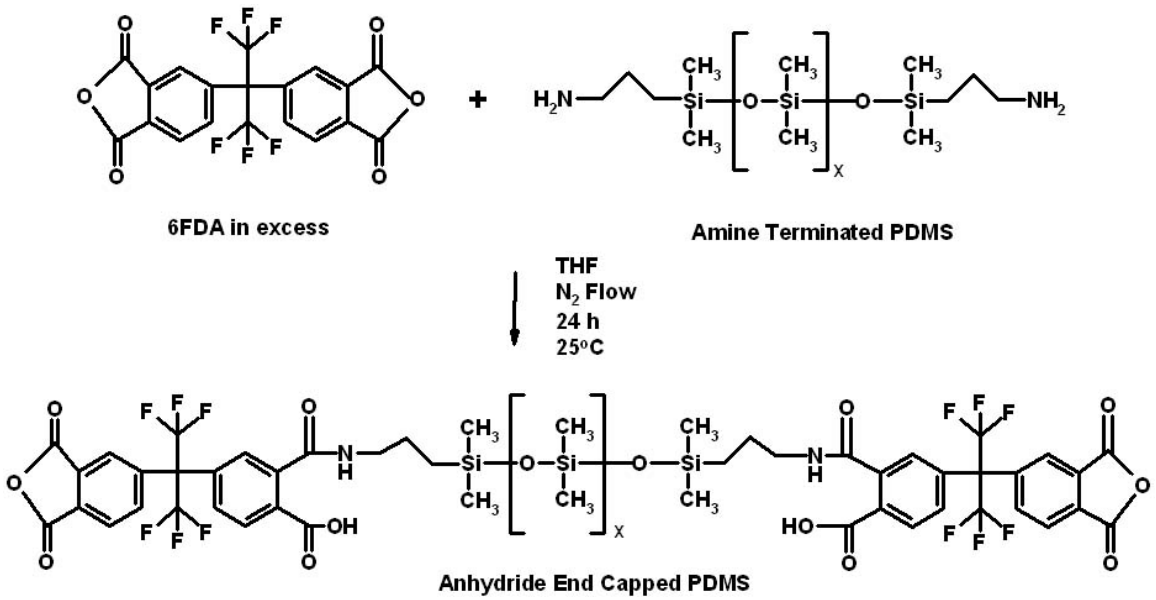

Figure 6-5. End capping amine-terminated PDMS with dianhydride groups. This step is performed with excess 6FDA to ensure complete endcapping.

The above step was performed in excess 6FDA to ensure end-capping of the PDMS monomer. The endcapping of PDMS with anhydride would prevent blocks of 6FDA-PDMS from occurring.

After 24 hours, the aromatic diamine 6FpDA was added to the reaction. The addition of 6FpDa would build a poly(amic acid) block which would later be converted into a polyimide block. The reaction scheme for this step is shown below in Figure 6-6.

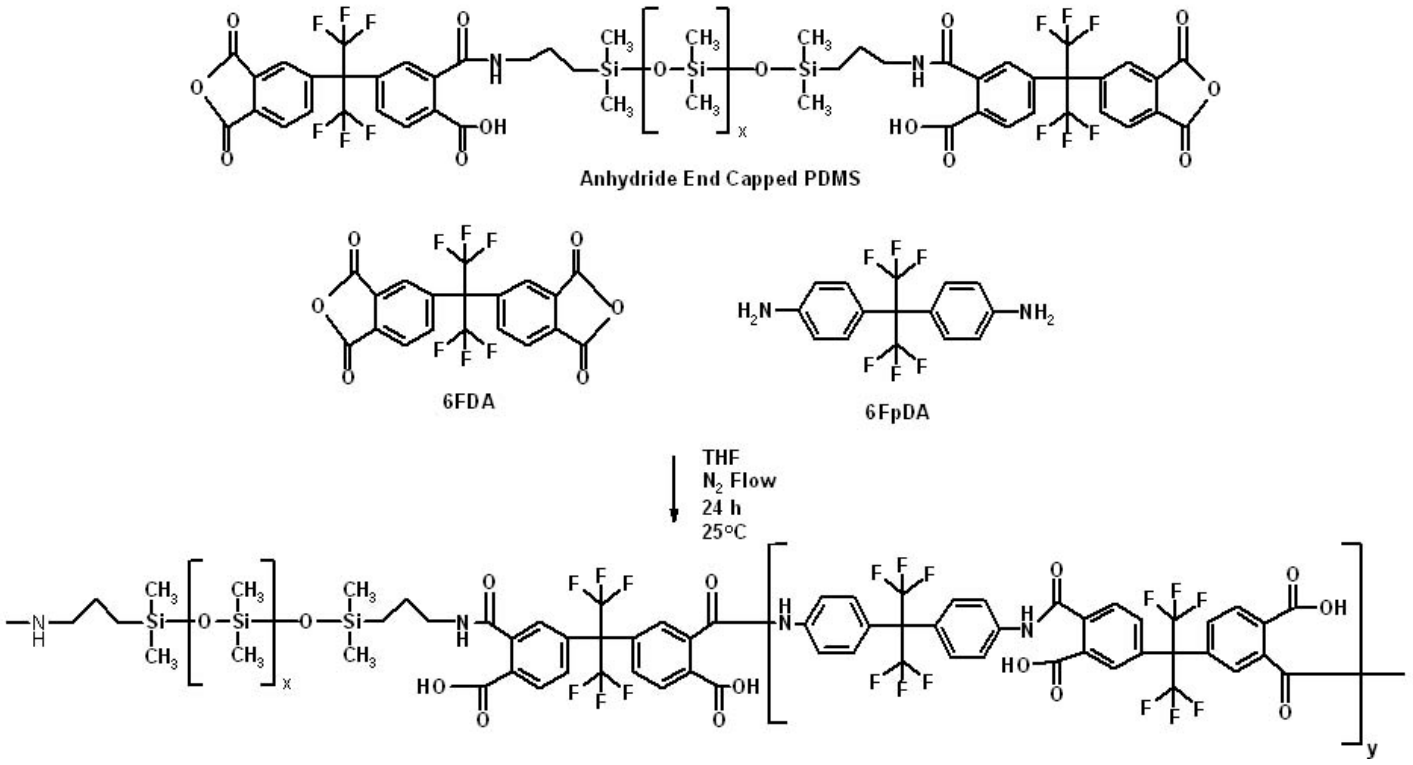

Figure 6-6. Step 2 of the poly(imide siloxane) synthesis. In this step 6FpDA is added to the anhydride end-capped PDMS.

After 24 hours, the reaction solution was cast onto a Teflon coated pan. The solvent was allowed to evaporate overnight, leaving a mostly clear poly(amic acid) film. This film was placed under vacuum at a temperature higher than the film's T_g to imidize it. After imidization the film turned a yellowish color. This step is shown in Figure 6-7.

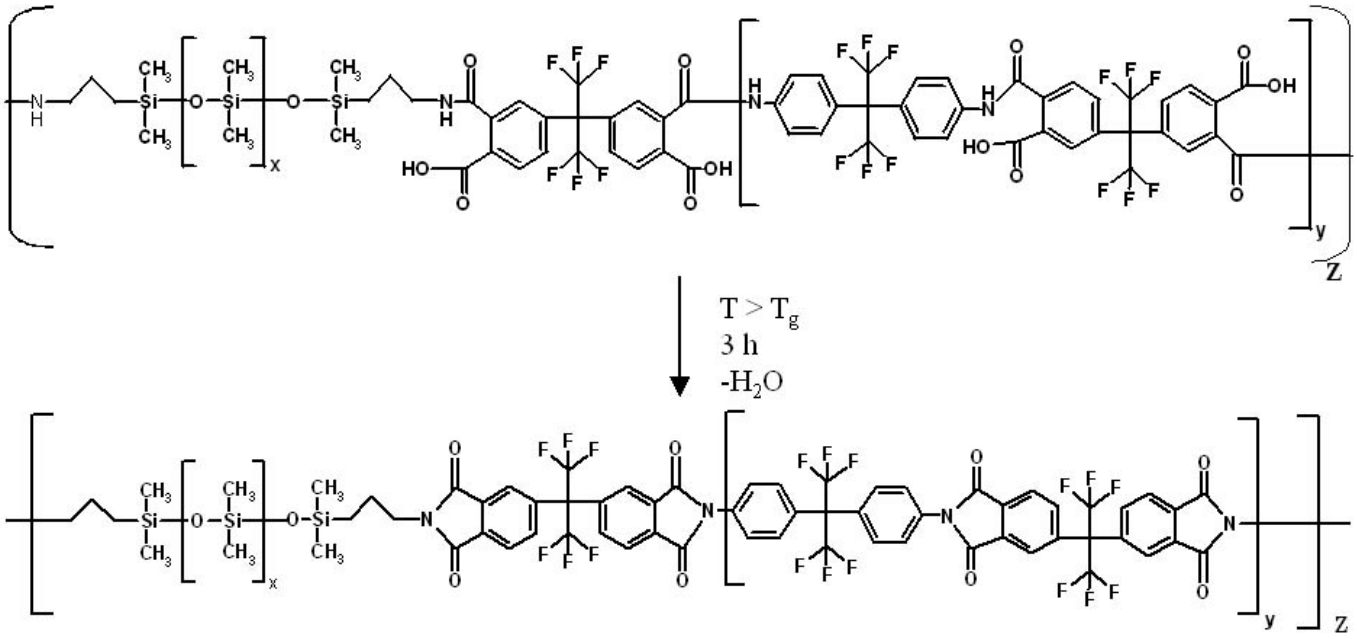

Figure 6-7. Imidization step of the synthesis of the 6FDA-6FpDA-PDMS block copolymer.

The molecular weights for the copolymers were determined via gel permeation chromatography. The results were M_n = 62,330 ± 4000 g/mol with a M_w of 131,300 ± 30,120 g/mol.

6.4.2 Determining the Weight Percent of PDMS via ^{1}H-NMR

6.4.2.1 Molecular Weight Determination of PDMS Monomer

Amine-terminated PDMS was purchased from Gelest and used as received. The supplier only offers a range of 800 – 1000 g/mol for the M_n of the monomer. ^{1}H-NMR was employed to more accurately determine the M_n of the PDMS monomer. The ^{1}H-NMR spectrum of the PDMS monomer is shown in Figure 6-8.

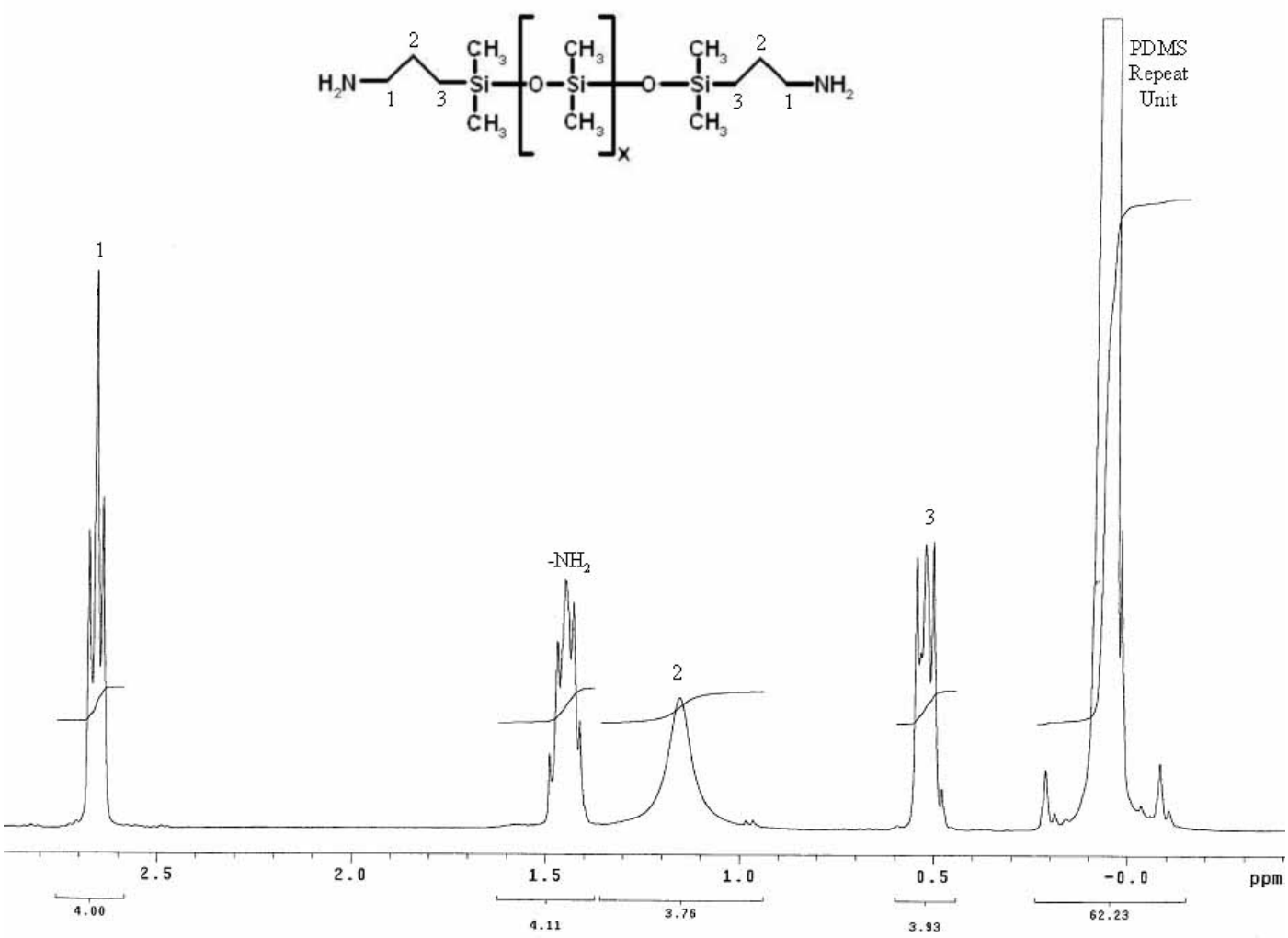

Figure 6-8. 400 MHz 1H-NMR spectrum for the amine-terminated PDMS monomer used in this study.

Peaks were assigned based on previous assignments by McGrath et al.[23]

Using the area under the assigned peaks the molecular weight was determined. The peak assigned to the repeat unit of PDMS (i.e. Si-$(CH_3)_2$) near 0.05 ppm has an area of 62.23. Using this and the number of H atoms per repeat unit the M_n can be determined as follows:

$$\frac{62.23}{6\,\text{H atoms}} = 10.37\ \text{Repeat Units}$$

with the number of repeat untis and the molecular weight
of a repeat unit, we can determine the Mn of the PDMS block

$$10.37\ \text{RU}\,\frac{74.17\ \text{g/mol}}{\text{RU}} = 769.3\ \text{g/mol}$$

Add on M_n of the two aminopropyl groups

$$M_n = 769.3 + 2\cdot(14.01 + 12.01\cdot 3 + 1.01\cdot 8)$$

$$M_n = 885.5\ \text{g/mol}$$

6.4.2.2 Determination of Weight Percent of PDMS

The weight percent incorporated into the polyimide's backbone was determined using ^{1}H-NMR. After the imidization step, the copolymers were redissolved in THF and extracted in a hexane bath for the purpose of removing any unreacted PDMS monomer as described in the Experimental section. After the hexane bath, the polymers were again dried in a vacuum oven at 100 ^{o}C. NMR samples consisted of 15 – 20 mg of polymer dissolved in 0.7 mL of d6-acetone.

Below is the 400 MHz ^{1}H-NMR spectrum for the synthesized poly(imide siloxane) at 41 wt % PDMS (Figure 6-9).

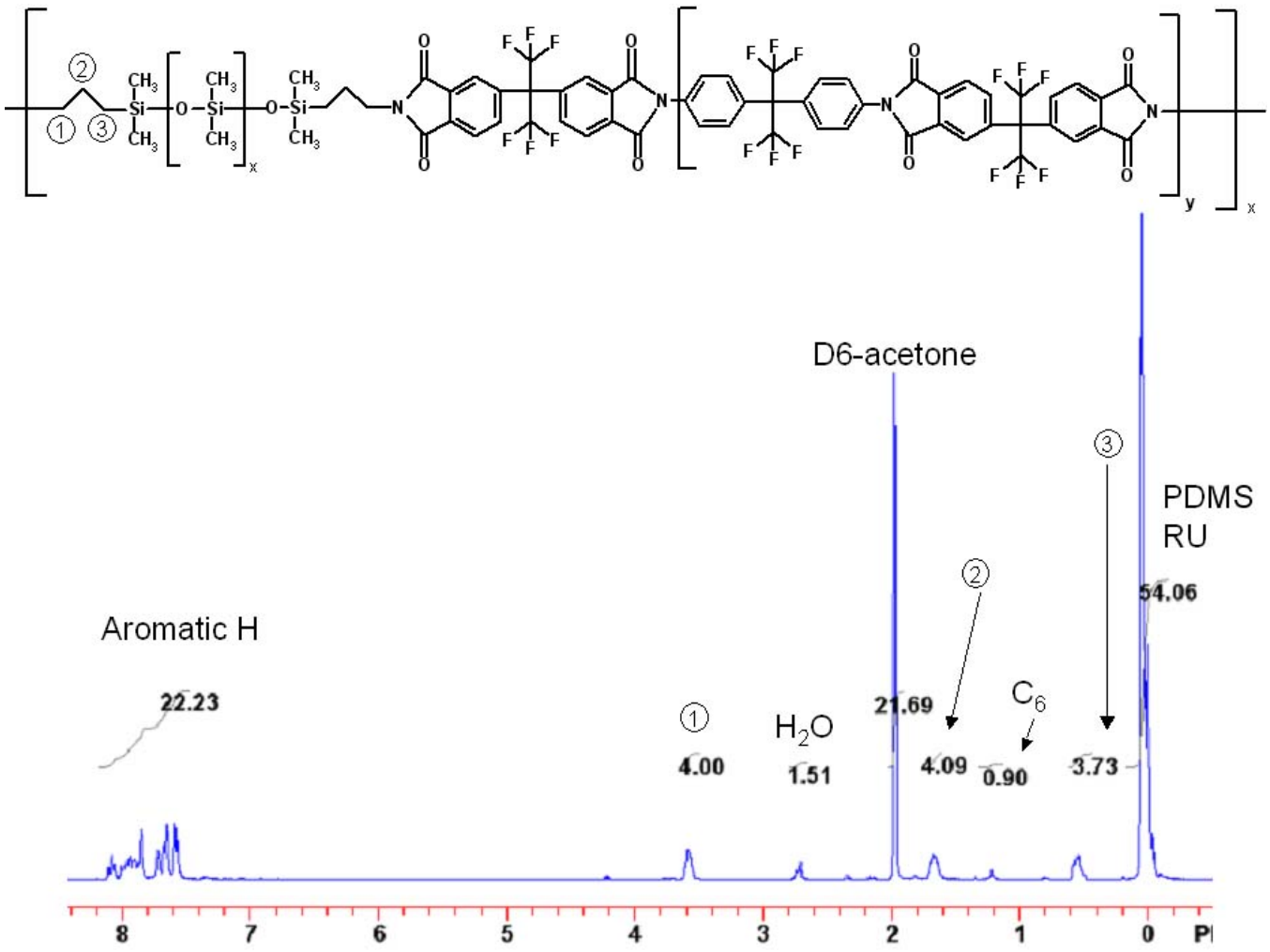

Figure 6-9. 400 MHz 1H-NMR spectrum of the 41 wt % PDMS poly(imide siloxane).

The weight percent for the 41 % PDMS copolymer was determined using the procedure outlined below. NUTS software was used to Fourier Transform, baseline, and integrate the area of the peaks in the NMR spectrum. The integrate values for the peaks are shown on the spectrum. The aromatic protons of the polyimide block appear downfield between 8.25 – 7.5 ppm due to deshielding, while the protons of the PDMS repeat unit appear upfield at 0.1 ppm.[24] The protons associated with the propyl group of the PDMS block have three peaks. The protons on the carbon adjacent to the nitrogen atom appear at 3.6 ppm, while the protons on the center carbon appear at 1.7 ppm, and the protons on the carbon next to the Si atom appear at 3.73 ppm. Additionally, some

sample contamination is present represented by the other peaks (e.g. water, hexane, acetone).[25] The corresponding integrated area values are listed above each peak.

The weight percens of PDMS was determined by using the number of aromatic protons per repeat unit, the number of protons per α-carbon (i.e. the carbon on the PDMS propyl chain which is covalently bonded to the nitrogen atom), their corresponding areas, and each segments molecular weight.

The molecular weight of the hard block (i.e. polyimide) and the soft block (i.e. PDMS) in the copolymer are listed below:

$$\text{6FDA - 6FpDA}: \quad M_n = 742 \frac{g}{mol}$$

$$\text{PDMS}: \quad M_n = 881.5 \frac{g}{mol}$$

Using the peak areas for the aromatic hydrogens and the alpha-carbon hydrogens, the hard-soft block ratio can be determined.

$$\text{6FDA - 6FpDA}: \quad \frac{14\ \text{H}}{\text{Repeat Unit}}$$

$$\text{PDMS}: \quad \frac{4\ \text{H}}{\text{Repeat Unit}}$$

$$\frac{\text{Hard Segments}}{\text{Soft Segments}} = \frac{\dfrac{(\text{Aromatic H Peak Area})}{\#\ \text{H per Hard Segment}}}{\dfrac{(\alpha\text{ - H Peak Area})}{\#\ \text{H per Soft Segment}}}$$

$$= \frac{\text{Hard Segment}}{\text{Soft Segment}}$$

$$= \frac{\dfrac{23.59}{14}}{\dfrac{4}{4}}$$

$$\frac{\text{Hard Segments}}{\text{Soft Segments}} = 1.685$$

The weight % PDMS can now be calculated using the ratio of hard to soft segments. The calculation is shown below:

$$WT\,\%\,PDMS = \frac{M_n\ PDMS}{\frac{Hard\ Segment}{Soft\ Segment}\cdot\left(M_n\ 6FDA\text{-}6FpDA\right)+M_n\ PDMS}\cdot 100\%$$

$$= \frac{881.5}{1.685\cdot 742+881.5}\cdot 100\%$$

$$WT\,\%\,PDMS = 41\%$$

In the ^{1}H-NMR spectrum gathered, there were no peaks above 10 ppm. Aromatic carboxylic acid structures show proton peaks in this area, and the lack of peaks above 10 ppm provided quantitative verification of imidization.[22,26]

6.4.3 Verification of Imidization via FTIR Spectroscopy

FTIR spectroscopy was employed to qualitatively verify the successful imidization for the copolymer. The spectrum between 3600 and 2600 cm^{-1} for the 22 wt % PDMS copolymer is shown below in Figure 6-10.

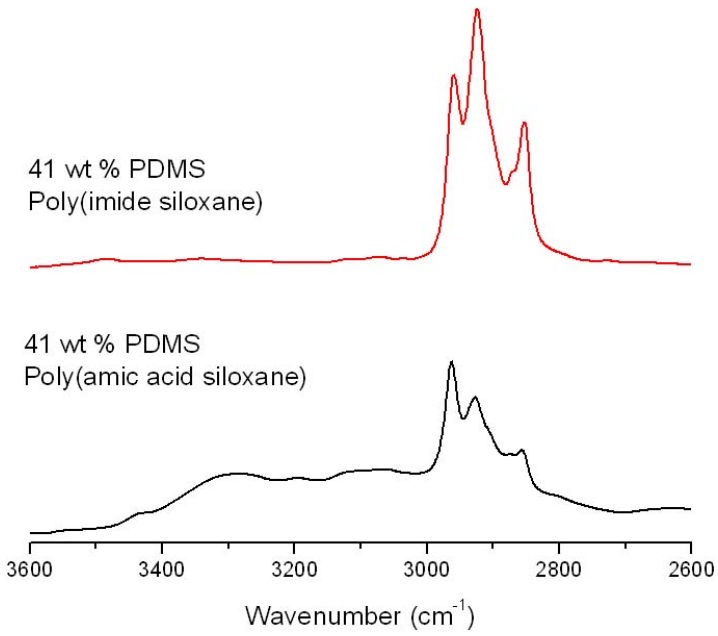

Figure 6-10. FTIR spectra for the 41 wt% PDMS poly(amic acid siloxane) and its corresponding poly(imide siloxane) between 3600 and 2600 cm^{-1}.

In this region of the IR spectrum $-NH_2$ and –OH groups are active. These groups both contribute to the absorbance between 3450 and 3000 cm^{-1} in the poly(amic acid) spectrum. Once the poly(amic acid) was heated above its T_g for several hours, the absorbance in this region dwindles to almost nothing, as shown in the polyimide spectrum. This is a result of the cyclodehydration of the poly(amic acid) into a polyimide in which the –COOH and –CONH groups react to form an imide ring. The polyimide spectrum shows a small peak at 3500 cm^{-1} which is a result of free –COOH groups. Ther are a few possible explanations for this. First, this could indicate that there was not 100% imidization, however, the large decrease in IR activity in this region qualitatively indicates that a high degree of imidization was obtained. This explanation would also be inconsistent with the ^{1}H-NMR results which did not display any aromatic carboxylic acid proton peaks.

A more likely explanation is that the some of the 6FDA monomer was not successfully heat treated. As mentioned in the Experimental section, the 6FDA monomer is heated under vacuum to ensure its ends are closed; the anhydride ends can react with moisture to form –COOH groups. If indeed they were open prior to the synthesis, they should not have reacted, and could show up in the FTIR spectrum in this area.

The small peaks in the polyimide spectrum between 3100 and 3000 cm^{-1} are from aromatic C-H stretches. The IR bands below 3000 cm^{-1} are alkyl C-H stretches due the PDMS repeat units, the propyl units, and perhaps some residual THF.

Imide rings have their own characteristic IR active bands at lower wavenumbers. In Figure 6-11 the IR spectrum between 1900 and 1300 cm^{-1} are shown for both imidized and preimidized copolymer

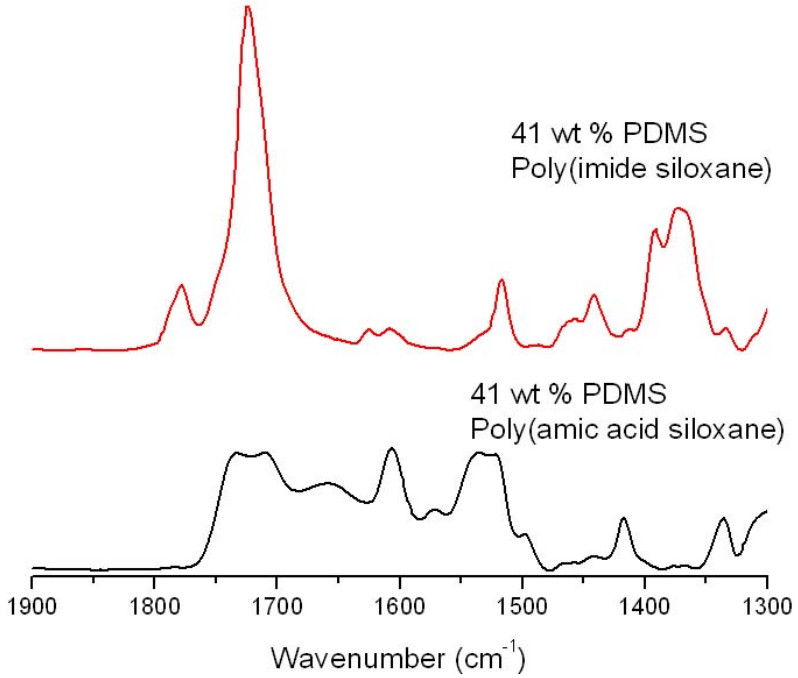

Figure 6-11. FTIR spectra for the 41 wt% PDMS poly(amic acid siloxane) and its corresponding poly(imide siloxane) between 1900 and 1300 cm^{-1}.

The polyimide spectrum clearly displays some sharply absorbing peaks which are not present in the poly(amic acid siloxane) spectrum. The poly(amic acid siloxane) spectrum has a broad band stretching from 1750 – 1600 cm^{-1}. This region contains the stretches associated with amide groups. After the heat treatment this broad band develops into two sharp peaks at 1787 and 1728 cm^{-1}. Both of these peaks are from the C=O stretches of the polyimide. The one at 1787 cm^{-1} is associated with the carbonyl groups near the anhydride ends and the peak at 1728 cm^{-1} is associated with the carbonyl groups in the polyimide repeat unit. [27-29] The peak which develops at 1373 cm^{-1} also is associated with the C-N-C linkages of the polyimide repeat unit.[30]

6.4.4 Microscopy Results

The pure copolymer and MMM films were analyzed using FESEM. Cross sectional images were taken of each membrane to determine the extent of nanotubes

dispersion within the polymer matrix. An image of the pure copolymer with no CNTs is shown below in Figure 6-12.

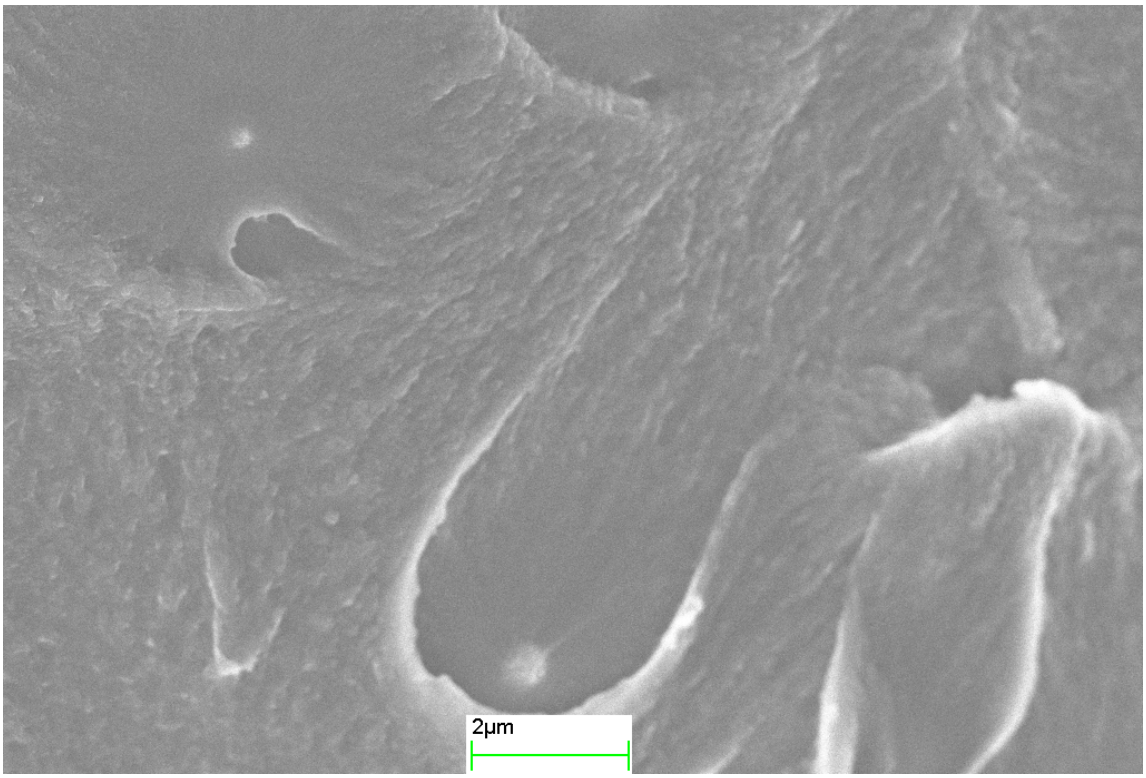

Figure 6-12. FESEM cross-sectional image of the pure poly(imide siloxane).

The cross-section of a 10 wt % closed-ended CNT MMM is shown below in Figure 6-13.

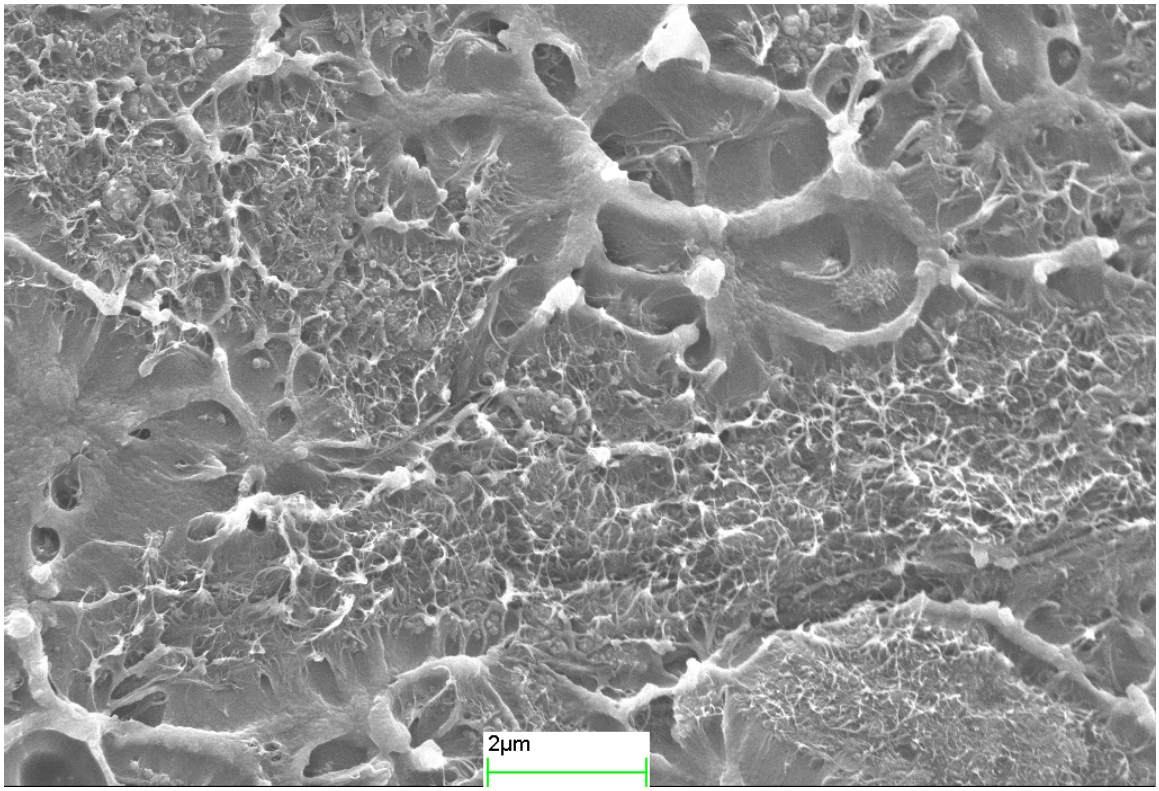

Figure 6-13. FESEM cross-sectional image of the a 10 wt % close-ended carbon nanotube MMM.

At this level of CNT loading, there is clearly agglomeration of the nanotubes within the matrix. Even without any visual aid, agglomerations were readily visible on the surface of the 10 wt % MMM.

Attempts at eliminating or reducing this were made by lowering the wt % of CNTs. Below are images of 1 wt % CNT MMMs Figure 6-14. The top image is a cross sectional image of MMM using close-ended CNTs, while the bottom image is a cross-sectional image of MMM using open-ended CNTs in the copolymer.

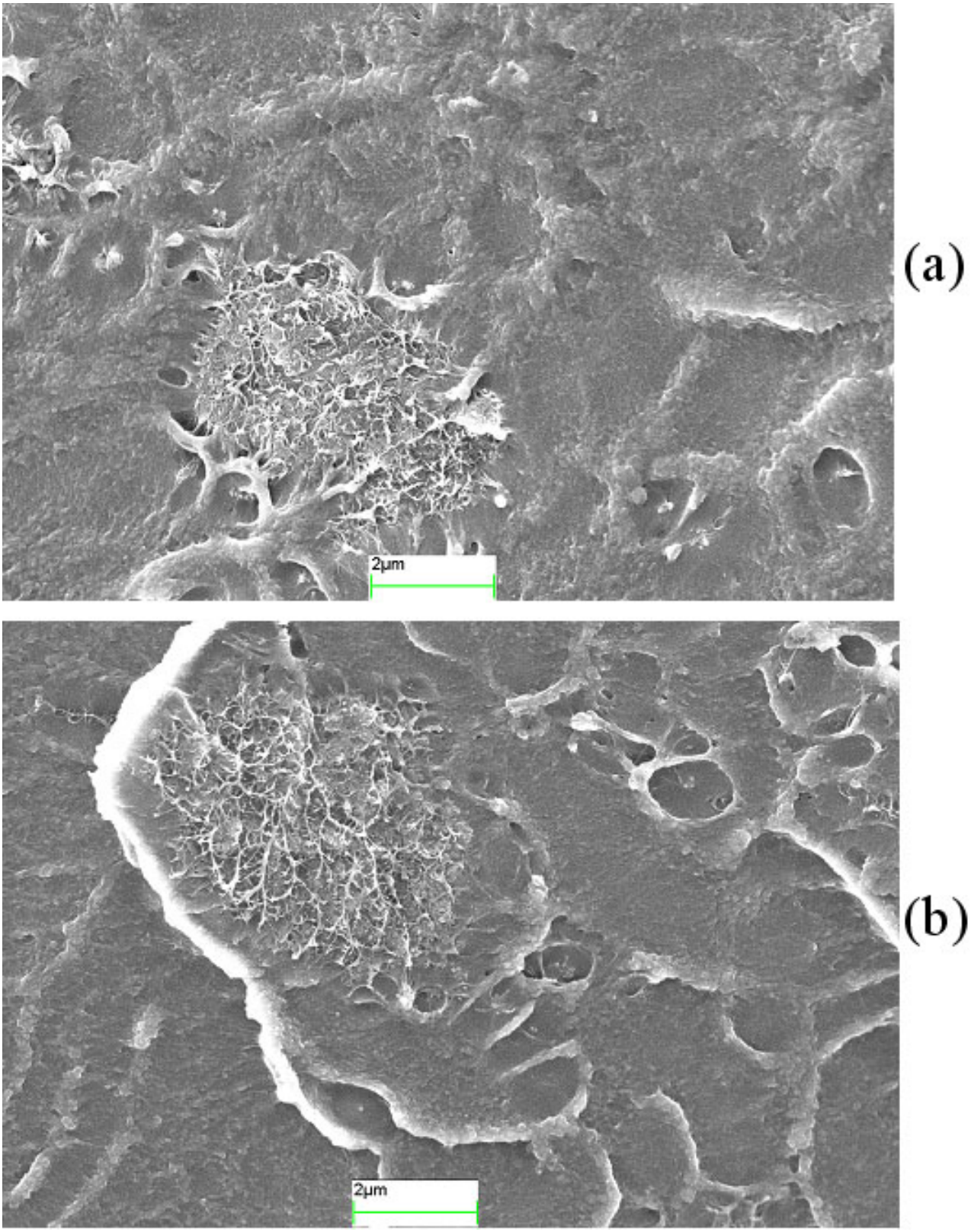

Figure 6-14. FESEM cross-sectional images of MMMs with 1 wt % carbon nanotube using (a) close-ended CNTs and (b) open-ended CNTs.

Even at this lower loading of CNTs, the tubes remain agglomerated regardless which type of nanotubes is employed. While the close-ended CNT MMM did not show signs of agglomeration until it was viewed under the SEM, the open-ended CNT MMM did show signs of agglomeration without visual aid. The reason for this is not yet understood. Studies by others attempting to disperse CNTs into a polymer matrix have encountered similar difficulties.[31-33] Difficulties in dispersion have been attributed to van der Waals attractions among the tubes in combination with their high surface area and high aspect ratio. Usually, when solution casting polymer-CNT composite films, dispersion of the CNTs is achieved using high-energy sonication or the using an ultrasonic head.[34-36] Other methods have focused on using in situ polymerization of the monomers in a CNT dispersed solution.[33,37,38] In situ polymerization appears to be the most promising approach at this time. In order to break-up the CNT agglomerations, techniques like in situ polymerization, or high-energy sonication will likely need to be employed.

6.4.5 Permeability Measurements

6.4.5.1 Closed-ended Carbon Nanotube Mixed Matrix Membranes

Permeability measurements for He and N_2 were gathered from the pure 40 wt % PDMS poly(imide siloxane), a 1 wt % closed-ended CNT poly(imide siloxane) MMM, and a 1 wt % open-ended CNT MMM. The gases were chosen with specific tasks in mind. Due to its small size He serves as an excellent probing gas for identifying the presence of voids. The presence of unselective voids at the interface between the polymer and nanotubes should offer sites of high permeability for He. Nitrogen was chosen because it permeates the slowest through the pure copolymer of all the gases we had available to us. Because of this, enhancements in transport with the addition of nanotubes would likely be the most pronounced for this gas.

The permeability results for the pure poly(imide siloxane) and the 1 wt % close-ended CNT MMM are show below in Table 6-1. The procedure used to prepare the membranes is outlined in the Experimental section of this chapter. The thickness of the

pure copolymer membrane was 0.0060 ± 0.0005" and the thickness of the MMM was 0.0091 ± 0.0002".

Table 6-1. Pure gas permeabilities of the 41 wt % PDMS poly(imide siloxane) and the 1 wt % closed-ended carbon nanotube MMM with 41 wt % PDMS poly(imide siloxane) as the polymer matrix.

Pure Gas Permeability (Barrer)

Wt % Closed CNT	He	N_2
0	85.85 ± 0.55	18.48 ± 1.56
1	63.80 ± 0.70	19.51 ± 0.24
Percent Change	-25.68	5.57

The large drop in permeability of He suggests that the copolymer adhered well to the nanotubes. The average permeability of nitrogen increased roughly 6%, but the standard deviations of the runs overlap each other. Therefore, statistically there was no change in nitrogen's permeability. To explain help explain these trends the diffusion and solubility coefficients of nitrogen were calculated.

Table 6-2 below lists the diffusion and solubility coefficients for nitrogen.

Table 6-2. Diffusivity and solubility coefficients of nitrogen for the 41 wt % PDMS poly(imide siloxane) and the 1 wt % close-ended carbon nanotube MMM with 41 wt % PDMS poly(imide siloxane) as the polymer matrix.

Diffusion and Solubility Coefficients for Nitrogen

Wt % Closed CNT	D (cm^2 s^{-1})	S (cm^3 @ STP $cm^{-3}_{polymer}$ atm)
0	175.92 ± 10.48	0.08 ± 0.01
1	127.04 ± 22.24	0.12 ± 0.03
Percent Change	-27.76	50.00

Helium diffusion coefficients are not reported for any of the membranes in this chapter. This is because there is too much error in the measurement to make an accurate calculation. The Time Lag Method calculates the diffusion coefficient (D) using the following equation:

$$D = \frac{l^2}{6\theta} \qquad \text{Eq 6.1}$$

in this equation l^2 is the membrane thickness, and θ is the diffusive lag time. The diffusive lag time scales with how long a gas takes to diffuse through a membrane once a test has begun. Due to He's high permeability, this time is very short and was calculated to be approximately 1s in each run. Unfortunately, in our permeation apparatus, each gas must flow from a gas tank and through several feet of steel tubing before it contacts the membrane. This obviously increases the time required for He to diffuse into the downstream side of the membrane, and introduces large errors. Because of the uncertainty in the true value of D for He, it was not reported. The solubility coefficient is calculated using D, therefore it can not be determined for He as well. The other gases tested had much larger lag times, and any error introduced by this was negligible.

From the table it is evident that nitrogen experiences a large drop in the diffusion coefficient. This would be consistent if the closed-ended CNTs behaved as impermeable filler as was expected. Making inferences from the changes in the solubility coefficient is

more difficult due to the overlap in the variance of the measurement. While the average permeability of the MMM exceeds that of the pure copolymer implying that S must have increased to overcome the losses in D, the standard deviations of the permeability measurements overlap each other. This prevents one concluding that S must have increased.

Based on these results, it is believed that the addition of closed-ended CNTs to the copolymer adds an impermeable filler. This lowers the permeability of He, and hinders the diffusion of nitrogen.

6.4.5.2 Open-ended Carbon Nanotube Mixed Matrix Membranes

The permeability results for the pure poly(imide siloxane) and the 1 wt % close-ended CNT MMM are show below in Table 6-3. The procedure used to prepare the membranes is outlined in the Experimental section of this chapter. The thickness of the pure copolymer membrane was 0.0112 ± .0018" and the thickness of the MMM was 0.0085 ± .0009".

A different batch of copolymer was used for these membranes, therefore, there are differences in the pure polymer data in this chapter.

Table 6-3. Pure gas permeabilities of the 41 wt % PDMS poly(imide siloxane) and the 1 wt % open-ended carbon nanotube MMM with 41 wt % PDMS poly(imide siloxane) as the polymer matrix.

Pure Gas Permeability (Barrer)

Wt % Open CNT	He	N_2
0	87.10 ± 1.60	20.40 ± 0.28
1	77.20 ± 1.80	18.70 ± 0.11
Percent Change	-11.37	-8.33

As in the closed-ended CNT MMM, the open-ended CNT MMM sees a drop in He permeability. However, it is a much smaller drop. Nitrogen sees a drop as well, which is different from the close-ended CNT MMM. In both cases this may seem surprising, as the polymer essentially contains filler with an average pore diameter of 1.4 nm. However, it must be noted that no effort was put into orienting the nanotubes within the matrix. Aligned nanotubes with their pores running parallel to the direction of diffusion would be optimal. These nanotubes are likely randomly oriented.

The diffusivity and solubility coefficients for nitrogen were calculated to help explain this trend. As mentioned earlier, this is not possible for He.

The diffusivity and solubility coefficients for nitrogen are shown below in Table 6-4.

Table 6-4. Diffusivity and solubility coefficients of nitrogen for the 41 wt % PDMS poly(imide siloxane) and the 1 wt % open-ended carbon nanotube MMM with 41 wt % PDMS poly(imide siloxane) as the polymer matrix.

Diffusion and Solubility Coefficients for Nitrogen

Wt % Open CNT	D (cm^2 s^{-1})	S (cm^3 @ STP $cm^{-3}_{polymer}$ atm)
0	139.05 ± 3.73	0.11 ± 0.00
1	138.93 ± 0.10	0.10 ± 0.00
Percent Change	-0.08	-9.09

From the table we see there is essentially no change in nitrogen's diffusion coefficient upon the addition of open-ended CNTs, while its solubility dropped 9%. The lack of a drop in D when compared to the closed-ended nanotubes MMM suggests that these tubes do not impede diffusion. In this MMM there is a drop in solubility relative to the pure copolymer. The reason for this is not yet known. Nitrogen has been shown to adsorp more in open-ended CNTs than closed ended CNTs.[39] However, the measurements in these experiments were made at very low temperatures (e.g. 77 K).

Additionally, the experiments were made on pure single walled CNTs, and our work involves polymer-CNT mixtures. Sorption experiments on all of the membranes in this study at 35 ^{o}C would be helpful in explaining these results.

6.5 Conclusions

A poly(imide siloxane) was synthesized using an aromatic dianhydride, an aromatic diamine and amine-terminated PDMS for the siloxane block. The weight percent of PDMS was determined to be 41 using ^{1}H-NMR. Successful imidization was verified using FTIR. This copolymer was mixed with carbon nanotubes, both open-ended and closed-ended, for the purpose of fabricating mixed matrix membranes suitable for gas separations. SEM images showed that both types of nanotubes were agglomerated within the polymer matrix. Permeability measurements of He showed drops in permeability with the addition on CNTs, regardless of which type. Additionally, N_2 showed a small drop in permeability with the addition of open-ended CNTs, and no change relative to the pure copolymer for closed-ended CNT MMMs. The drop in permeability in the open-ended CNT MMM appears to be due to losses in solubility, as the diffusion coefficient was unchanged. This is in contrast to the closed-ended CNT MMM which saw a large drop in the diffusion coefficient of nitrogen, and no change in solubility. The drop in permeability of He suggests good contact between the polymer and the nanotubes, while the lack of changes in permeability of N_2 could mean that these tubes are not aligned well in the matrix and act more as impermeable filler.

6.6 References

1 Robeson, L. M. *Journal of Membranes Science* 1991, *61*, 165-185.

2 Freeman, B. *Macromolecules* 1999, *32*, 375-380.

3 Scott, K. *Handbook of Industrial Membranes*, 2 ed.; Elsevier Science Publishers, 1998.

4 Fraenkel, D.; Levin, G.; Goldman, M. *Journal of Applied Polymer Science* 1989, *37*, 1791-1800.

5 Koros, W. J.; Mahajan, R. *Industrial Engineering and Chemistry Research* 2000, *39*, 2692-2696.

6 Smolders, C. A.; Duval, J. M.; Folkers, B.; Mulder, M. H. V.; Desgrandchamps, G. *Journal of Membrane Science* 1993, *80*, 189-198.

7 Tantekin-Ersolmaz, S. B.; Atalay-Oral, C.; Tather, M.; Erdem-Senatalar, A.; Schoeman, B.; Sterte, J. *Journal of Membrane Science* 2000, *175*, 285-288.

8 Koros, W. J.; Mahajan, R. *Polymer Engineering and Science* 2002, *42*, 1420-1431.

9 Koros, W. J.; Mahajan, R. *Polymer Engineering and Science* 2002, *42*, 1432-1441.

10 Koros, W. J.; Mahajan, R. *Polymer Engineering and Science* 2002, *42*, 1432-1441.

11 Mahajan, R. K., W.J.; Polymer Engineering and Science, 2002.

12 Mahajan, R. K., W.J.; Zeolite-Function-Koros.jpg, Ed.; Polymer Engineering and Science, 2002.

13 Mulder, M. H.; Duval, J. M.; J. B. Kemperman; Folkers, B.; Desgrandchamps, G.; Smolders, C. A. *Journal of Applied Polymer Science* 1994, *54*, 409-418.

14 Pechar, T.; Marand, E.; Davis, R.; Tsapatsis, M. *Desalination* 2002, *146*, 3-9.

15 Duval, J.-M.; Folkers, B.; Mulder, M. H. V.; Desgrandchamps, G.; Smolders, C. A. *Journal of Membrane Science* 1993, *80*, 189-198.

16 Popov, V. *Materials Science and Engineering* 2004, *43*, 61-102.

17 Ackerman, D. M.; Skoulidas, A. I.; Sholl, D. S.; Johnson, J. K. *Molecular Simulation* 2003, *29*, 677-684.

18 Hinds, B.; Chopra, N.; Rantell, T.; Andrews, R.; Gavalas, V.; Bachas, L. *Science* 2004, *303*.

19 Alpert, N. K., W.E.; Szymanski, H.A.;. *Ir-Theory and Practice of Infrared Spectroscopy*; Plenum Publishing Corporation: New York, 1970.

20 Silverstein, R.; Webster, F. *Spectrometric Indentification of Organic Compounds*, 6 ed.; John Wiley & Sons, Inc: New York, 1998.

21 Crank, J. *The Mathematics of Diffusion*, 2 ed.; Oxford Press: London, 1990.

22 Bowens, A. In *Synthesis and characterization of poly(siloxane imide) block copolymers and end-functional polyimides for interphase applications*; Virginia Tech: Blacksburg, 1999.

23 McGrath, J.; Dunson, D.; Mecham, S.; Hedrick, J. *Advances in Polymer Science* 1999, *140*, 61-105.

24 Solomons, T. *Organic Chemistry*, 5 ed.; John Wiley & Sons, Inc: New York, 1992.

25 Gottlieb, H. E.; Kotlyar, V.; Nudelman, A. *Journal of Organic Chemistry* 1997, *62*, 7512-7515.

26 McGrath, J. E.; Arnold, C. A.; Summers, J. D.; Chen, Y. P.; Bott, R. H.; Chen, D. 1989.

27 Husk, G.; Cassidy, P.; Gebert, K. *Macromolecules* 1988, *21*, 1234-1238.

28 Becker, K. H.; Schmidt, H. W. *Macromolecules* 1992, *25*, 6784-6790.

29 Kim, J. H.; Lee, S. B.; S.Y., K. *Journal of Applied Polymer Science* 2000, *77*, 2756-2767.

30 Park, H.; Kim, J.; Nam, S.; Y, L. *Journal of Membrane Science* 2003, *220*, 59-73.

31 Wong, M.; Paramsothy, M.; Xu, X.; Ren, Y.; Li, S.; Liao, K. *Polymer* 2003, *44*, 7757-7764.

32 Zhang, W. D.; Shen, L.; Phang, I. Y.; Liu, T. *Macromolecules* 2004, *37*, 256-259.

33 Park, C.; Ounaies, Z.; Watson, K.; Crooks, R. E.; Smith, J.; Lowther, S.; Connell, J.; Siochi, E. J.; Harrison, J. S.; St. Clair, T. *Chemical Physics Letters* 2002, *364*, 303-308.

34 Qian, D.; Dickey, E. C.; Andrews, R.; Rantell, T. *Applied Physics Letters* 2000, *76*, 2868-2870.

35 Safadi, B.; Andrews, R.; Grulke, E. *Journal of Applied Polymer Science* 2002, *84*, 2660-2669.

36 Pirlot, C.; Willems, I.; Fonseca, A.; Nagy, J. B.; Delhalle, J. *Advanced Engineering Materials* 2002, *4*, 109-114.

37 Velasco-Santos, C.; Martinez-Hernandez, A. L.; Fisher, F. T.; Ruoff, R.; Castano, V. M. *Chem. Mater.* 2003, *15*, 4470-4475.

38 Park, C.; Crooks, R. E.; Siochi, E. J.; Harrison, J. S.; Evans, N.; Kenik, E. *Nanotechnology* 2003, *14*, L11-L14.

39 Fujiwara A, I. K., Suematsu H, Kataura H, Maniwa Y, Suzuki S, Achiba Y. *CHEMICAL PHYSICS LETTERS* 2001, *336*, 205-211.

Chapter 7 Conclusions and Future Work

The primary goal of this research was to determine if mixed matrix membranes (MMMs) composed of polymer and zeolite could be created without the presence of unselective voids at their interfaces. For each combination of zeolite (i.e. ZSM-2 or zeolite L) and polymer (i.e. 6FDA-6FpDA-DABA or 6FDA-6FpDA-PDMS) this appears to have been achieved. The evidence that supports this conclusion comes from several experiments. Permeability measurements of He showed drops in permeability for every membrane to which zeolite was added. If there were voids in the MMMs, the He permeability would have increased sharply. SEM images did not reveal any dewetting of the polymer from the zeolite. Finally, high powered TEM images of the 6FDA-6FpDA-DABA membranes failed to reveal the presence of voids.

A second goal of this research was to determine the nature of the interactions between the polymer and amine-functionalized zeolites. FTIR data gathered from the 6FDA-6FpDA-DABA and amine-functionalized ZSM-2 MMM indicated the presence of hydrogen bonding that was not present in either the pure polyimide or the polyimide-unfunctionalized ZSM-2 spectra. FTIR data gathered from the 6FDA-6FpDA-DABA and amine-functionalized zeolite L MMM indicated the presence of amide-linkages. This MMM was put through an annealing procedure at temperatures up to 220 ^{o}C; this was not done in the 6FDA-6FpDA-DABA and amine-functionalized ZSM-2 MMM. The pure polyimide spectrum and the polyimide-untethered zeolite L spectrum were put through the same treatment, and in both cases, there was no evidence of amide-linkages in the spectra. From this it appears that amine groups covalently attached to the zeolite can be

used to interact with carboxylic groups of the polyimide either through secondary forces or covalent bonds, depending on the heat treatment the MMM receives.

High pressure permeability studies were performed for CO_2 and CH_4 using the 6FDA-6FpDA-DABA and amine-functionalized zeolite L MMM and its corresponding pure polyimide membrane. There was less than a 5% drop in CO_2 permeability between the pure polyimide and the MMM across the pressure range tested (i.e. 4, 8, and 12 atm). However, methane's permeability showed a much larger pressure dependence. In the pure polyimide, the permeability only dropped very slightly with each pressure increase. In the MMM, methane's permeability showed a large drop with each increase in pressure. It is believed that zeolite L has a much larger sorption capacity for polar molecules such as CO_2 than for nonpolar molecules such as CH_4. This difference in sorption capacity could become more pronounced at higher pressures, and account for the differences in permeation behavior.

This study also tested the possibility of employing copolymers with flexible segments as the polymer matrix. Because the flexible segment can adhere to the zeolite surface, this eliminated the time consuming and tedious steps of amine-functionalizing the zeolite. Copolymers were synthesized by incorporating PDMS segments into the 6FDA-6FpDA backbone at 22 and 41 wt % PDMS. TEM images did not reveal any distinguishable phases, suggesting there was no phase separation in the copolymers. However, AFM images did reveal a phase separated surface. SEM images did not reveal any evidence of the copolymer dewetting from the unmodified zeolite L surface. Additionally, helium's permeability dropped with the addition of unmodified zeolite L in each of the copolymer MMMs, while the 6FDA-6FpDA polyimide MMMs were too brittle to handle. Each permeability of the remaining gases decreased with the addition of zeolite L, regardless of the polymer matrix. At 20 wt % loading of zeolite L, the 22 wt % PDMS poly(imide siloxane) MMM showed small increases in D and large losses in S with the addition of zeolite L. At the same zeolite loading the 41 wt % PDMS poly(imide siloxane) MMM did not reveal a strong trend with the addition of zeolite L for either coefficient. When the zeolite loading was increased for this 41 wt % PDMS MMM, each gas received an increase in permeability relative to the 20 wt % zeolite L MMM, but

most were still below that of the pure copolymer. There did not appear to be trends in D or S with zeolite loading.

The final objective of this study was to determine if MMMs could be prepared from carbon nanotubes (CNTs) and poly(imide siloxane)s. Closed-ended CNTs were mixed with a 41 wt % PDMS poly(imide siloxane) and solution cast. SEM images indicated that the CNTs were agglomerated within the membrane. This was also observed for MMMs composed using open-ended CNTs. The permeability of He dropped for both types of membranes, but more so for the closed-ended CNTs MMM. This was taken as an indication of good contact between the copolymer and nanotubes. Permeation measurements using nitrogen brought mixed results. In the closed-ended CNT MMM, there was no change in permeability, however, in the open-ended CNT MMM there was a small drop in permeability. This drop appeared to be associated with a small decrease in solubility with the addition of CNTs. The reason for this is not yet understood, but a possible explanation is that the addition of these open-ended tubes lowers the solubility. Furthermore, the nanotubes need to be oriented to offer improvements in the diffusion coefficient.

The fundamental premise of mixed matrix membranes is that the addition of zeolite to a polymer matrix will improve the selectivity of the matrix. However, simply selecting a polymer and zeolite at random would be a poor strategy for designing a MMM. Future studies should utilize components with similar permeabilities, or utilize components in which the zeolite is more permeable and selective than the polymer. This ensures that the gas molecules will permeate through the more selective zeolite, resulting in better separation. If the polymer is more permeable than the zeolite, the gas molecules will diffuse around the zeolite, bypassing any of its selective benefits. This was seen in the poly(imide siloxane)s studied in Chapter 5. While the lack of a coupling agent in the preparation of a MMM improves the ease and time required in production, the siloxane segments appeared to be more permeable than zeolite L. The addition of zeolite L lowered the permeability of the membranes and offered no improvements in ideal selectivity. Using a lower molecular weight amine-terminated PDMS monomer may still provide a means to avoid the use of coupling agents, but improve the selectivity of the copolymer as the PDMS segments would become smaller. Another possible strategy is to

replace the poly(imide siloxane) with another polymer that has adequate flexibility to adhere to the zeolite, but has a much lower permeability.

To optimize the performance of the MMMs, the fillers should be oriented in future work. Methods (e.g. electric or magnetic fields) which would orient the zeolite or nanotubes such that their channels were aligned directly with the path of diffusion would prevent the filler becoming an impermeable "boulder" to gas molecules. For zeolites, the orientation may not even be necessary. Using a zeolite which possesses a 3-D pore structure with pore openings on each of its sides would allow a condensate to diffuse into it regardless of which face it comes into contact.

A final strategy that should be pursued in future work is choosing fillers with large aspect ratios. Using thin, flat, and long fillers would maximize the surface area per volume of the filler within the polymer matrix. Properly orienting the filler in the polymer matrix would maximize the gas-filler contact, and thus take advantage of the filler's selectivity.

There are several extensions of this work which could be done to determine whether the addition of CNTs or zeolite to polymer matrices can lead to improved gas separations. Determining the sorption of the gases in zeolite L, ZSM-2, and in carbon nanotubes would help explain the permeation results of this work, particularly the high pressure studies in Chapter 4. Performing sorption experiments using CO_2 and CH_4 in zeolite L could provide answers to the large drop in CH_4 permeability and the lack of a drop in CO_2 permeability. Dr. Marand's group will be benefiting from the addition of a sorption apparatus before the end 2004, and may address this issue. This will allow her group to measure the amount of a gas sorbed into a material (e.g. polymer, zeolite) at different pressures.

Perhaps the largest contribution to this work could be made by performing mixed gas separation experiments. Analyzing the permeation stream using a GC would allow one to know the true selectivity of the membranes. Most importantly, the mixed feed would allow the true selectivity of the MMMs to be determined, as the zeolites need a mixed feed to operate using a selective adsorption mechanism.

Vita

Todd William Pechar was born on August 24, 1975 in Suffolk County, NY. Shortly after his birth, his family moved to Slippery Rock, PA where he was raised. He graduated from Slippery Rock Area High School in 1993. Todd enrolled at the University of Pittsburgh and graduated with a B.S. in Chemical Engineering in 1997. During his stay he worked for Chelsea Building Products, The St. John's River Water Management District, and Sony Chemical Corporation of America. After graduating he accepted a position as a process engineer at Toray Plastics of America in North Kingstown, RI. In August of 1999, Todd left Toray and enrolled in the graduate program of the Chemical Engineering program at Virgina Tech. In January of 2000 he joined the research group of Dr. Eva Marand and began researching mixed matrix membrane systems. During this time he earned a M.E. and Ph.D. in chemical engineering. Todd will be working as a Postdoctoral Fellow for Dr. Garth Wilkes at Virginia Tech in August 2004. He will be researching the development and structure-property relationships of polyurethanes which are produced using more environmentally friendly processes and renewable natural resources.